Assessment of a flamelet approach to evaluating mean species mass fractions in moderately and highly turbulent premixed flames

Citation for the original published paper (version of record):
Lipatnikov, A., Nilsson, T., Yu, R. et al (2021)
Assessment of a flamelet approach to evaluating mean species mass fractions in moderately and highly turbulent premixed flames
Physics of Fluids, 33: 1-25
http://dx.doi.org/10.1063/5.0047500

(article starts on next page)

Assessment of a flamelet approach to evaluating mean species mass fractions in moderately and highly turbulent premixed flames

A.N. Lipatnikov[1,*], T. Nilsson[2], R. Yu[2], X.S. Bai[2], V.A. Sabelnikov[3,4]

[1]*Department of Mechanics and Maritime Sciences, Chalmers University of Technology, Gothenburg, 41296 Sweden*
[2]*Division of Fluid Mechanics, Department of Energy Sciences, Lund University, Lund, 22100, Sweden*
[3]*ONERA – The French Aerospace Laboratory, F-91761 Palaiseau, France*
[4]*Central Aerohydrodynamic Institute (TsAGI), 140180 Zhukovsky, Moscow Region, Russian Federation*
[*]Corresponding author, lipatn@chalmers.se

Abstract

Complex-chemistry Direct Numerical Simulation (DNS) data obtained from lean methane-air turbulent flames are analysed to perform *a priori* assessment of predictive capabilities of the flamelet approach to evaluating mean concentrations of various species in turbulent flames characterized by Karlovitz numbers $Ka = 6.0$, 74.0, and 540. Six definitions of a combustion progress variable c are probed and two types of Probability Density Functions (PDFs) are adapted: (i) actual PDFs extracted directly from the DNS data or (ii) presumed β-function PDFs obtained using the DNS data on the first two moments of the c-field. Results show that the mean density, the mean temperature, and the mean mass fractions of CH_4, O_2, H_2O, CO_2, CO, CH_2O, CH_3, and HCO are very well predicted using the temperature-based combustion progress variable c_T and the actual PDF. For other considered species, the quantitative predictions are worse, but still appear to be encouraging (with the exception of CH_3O at $Ka = 540$). The use of the flamelet library obtained from the equidiffusive laminar flame improves results for H_2, HO_2, and H_2O_2 at the highest Karlovitz number. Alternative definitions of the combustion progress variable perform worse and the reasons for this are explored. The use of the β-function PDF yields worse results for intermediate species such as OH, O, H, CH_3, and HCO, with this PDF being significantly different from the actual PDF. Application of the flamelet approach to rates of production/consumption of various species is also addressed and implications of obtained results for modeling are discussed.

Keywords: premixed turbulent combustion, complex chemistry, modeling, DNS, PDF, flamelet

NOMENCLATURE

a, b	parameters of beta function PDF
c	combustion progress variable
Da	Damköhler number
$g = \overline{c'^2}/[\bar{c}(1-\bar{c})]$	segregation factor
Ka	Karlovitz number
L_{xx}	longitudinal integral length scale of turbulence
Le	Lewis number
P	probability density function (PDF)
P_β	beta function PDF

Re_t	turbulent Reynolds number
S_{ij}	components of the rate-of-strain tensor
S_L	laminar flame speed
T	temperature
t	time
U_t	turbulent burning velocity
$\mathbf{u} = \{u_1, u_2, u_3\}$	velocity vector
u'	rms turbulent velocity
$\mathbf{W} = \{W_1, \dots, W_N\}$	rates of production/consumption of species $n = 1, \dots N$
$\mathbf{x} = \{x_1, x_2, x_3\}$	spatial coordinates
x	coordinate axis normal to the mean flame brush
$\mathbf{Y} = \{Y_1, \dots, Y_N\}$	mass fractions of species $n = 1, \dots N$
$\delta_L = (T_b - T_u)/\max\|\nabla T\|$	laminar flame thickness
ε	dissipation rate
η	Kolmogorov length scale
Λ	width of computational domain
ν	kinematic viscosity
ξ	sample variable
ρ	density
$\tau_t = L_{xx}/u'$	eddy turn over time
Φ	equivalence ratio

Subscripts

b	burned
c	combustion progress variable
F	fuel
L	laminar
T	temperature
t	turbulent
u	unburned

Operators

$\bar{\cdot}$	Reynolds-averaged quantity
$\tilde{\cdot}$	Favre-averaged quantity
$\langle\cdot\rangle$	quantity averaged over a transverse plane

I. INTRODUCTION

Turbulent burning is a highly non-linear multiscale phenomenon, which involves a number of bulk and local effects to be explored. Accordingly, several alternative methods are developed and adopted to model the influence of turbulence on combustion today. One of the most promising approaches, whose development Prof. E.E. O'Brien contributed[1-10] significantly to, deals with a transport equation for a Probability Density Function (PDF) of a single scalar characteristic of the mixture state in a flame. Significant progress made in research into the PDF transport equation is reviewed elsewhere.[11-14] In particular, this approach (i) allows researchers to easily solve the problem of averaging the rate of product creation, while this problem is the major challenge to alternative models of turbulent burning, and (ii) can directly be applied to various types of flames (premixed, non-premixed, or partially premixed). In the following, solely premixed burning is addressed and the so-called combustion progress variable c, which varies from zero in fresh reactants to unity in combustion products, is considered to be a single scalar characteristic of the mixture state in an adiabatic, iso-baric, equidiffusive, and single-step chemistry flame.

In addition to the classical problem of predicting the PDF $P(c)$, recent trends in R&D of ultra-clean and highly efficient combustion technologies pose new challenges for modeling. In particular, due to strict legislation on emissions from engines, the problem of predicting concentrations of various species (not only reactants and major products, but also intermediate species such as CO, CH_2O, O, H, OH, etc.) in turbulent flames has been attracting a growing attention. To average concentrations of various species using a PDF $P(c)$, which is either obtained by solving an appropriately closed transport equation or is modeled in another way, dependencies of the local species concentrations on c should also be invoked. For this purpose, the so-called flamelet concept[15] is widely used, e.g. see Table 4 in a review paper by Gicquel et al.[16] or Tables 5 and 6 in on a review paper by Lipatnikov.[17] The concept assumes adopting results (the so-called flamelet library) of numerical simulations of a set of laminar premixed flames (representative of local inherently laminar flamelets in a turbulent flow), performed by invoking an appropriately detailed model of molecular transport and chemical mechanism. Using an available technique such as Flamelet Prolongation of Intrinsic Low-Dimensional Manifolds[18] (FPI) or Flamelet Generation Manifold[19] (FGM), these results can be stored in a form of dependencies of temperature $T_L(c)$, density $\rho_L(c)$, mass fractions $Y_{n,L}(c)$ and mass rates $W_{n,L}(c)$ of consumption/production of $n = 1, \dots, N$ species on the combustion progress variable c.[20] Finally, the following Reynolds-averaged equations

$$\bar{\mathbf{W}}(\mathbf{x},t) = \int_0^1 \mathbf{W}_L(c)P(c,\mathbf{x},t)dc, \quad (1)$$

$$\bar{\mathbf{Y}}(\mathbf{x},t) = \int_0^1 \mathbf{Y}_L(c)P(c,\mathbf{x},t)dc, \quad (2)$$

$$\bar{T}(\mathbf{x},t) = \int_0^1 T_L(c)P(c,\mathbf{x},t)dc, \quad (3)$$

$$\bar{\rho}(\mathbf{x},t) = \int_0^1 \rho_L(c)P(c,\mathbf{x},t)dc \quad (4)$$

(or counterpart filtered equations for Large Eddy Simulation, LES) are applied to evaluate the mean (or filtered, respectively) production/consumption rates $\bar{\mathbf{W}}$, mass fractions $\bar{\mathbf{Y}}$, temperature $\bar{T}$, and density $\bar{\rho}$, respectively. Here, $\mathbf{W}$ and $\mathbf{Y}$ are N-dimensional vector-functions that encompass reaction rates W_n and mass fractions Y_n, respectively, for $1 \le n \le N$ species.

In spite of the wide use of the flamelet concept coupled with a PDF $P(c)$ in numerical research into premixed or stratified turbulent combustion,[21-45] such an approach definitely requires further study. In particular, its validation has yet been mainly performed in *a posteriori* RANS[21,26,27,30,32,40] or LES[22,24,25,28,29,31,33-37,39,41-45] studies, with the reported results showing limited capabilities of the approach for predicting mean concentrations of intermediate species such as (i) CO, e.g., see Fig. 24 in a paper by Galpin et al.,[24], Fig. 18 in a paper by Kolla and Swaminathan,[27] Figs. 9 and 13 in a paper by Lecocq er al.,[29] Fig. 10 in a paper by Darbyshire and Swaminathan,[30] Fig. 25 in a paper by Nambully et al.,[35] Fig. 9 in a paper by Nambully et al.,[36] Fig. 20 in a paper by Langella et al.,[41] or Fig. 18 in a paper by Donini et al.,[43] (ii) OH, e.g., see Fig. 11 in a paper by Langella and Swaminathan[39] or Fig. 21 in a paper by Langella et al.,[41] (iii) H_2 in hydrocarbon-air flames, e.g., see Fig. 10 in a paper by Darbyshire and Swaminathan,[30] Fig. 12 in a paper by Langella and Swaminathan,[39] or Fig. 20 in a paper by Langella et al.,[41] and (iv) CH_2O, e.g., see Fig. 5 in a paper by Galeazzo et al.[44] However, these results are not sufficient to draw the negative conclusion regarding the flamelet concept. Indeed, first, predictive capabilities of Eq. (1) and Eqs. (2)-(4) can be significantly different, as will be discussed later. Second, substantial disagreement between computed (RANS or LES) and measured or Direct Numerical Simulation (DNS) data, observed in the aforementioned figures, could stem not only from eventual limitations of the flamelet concept, but also from limitations of the invoked PDFs, as well as other models adopted in *a posteriori* study. For instance, as reviewed earlier,[46,47] capabilities of available models for predicting thermal expansion effects in premixed turbulent flames are limited and such limitations could account for the disagreement discussed here.

Therefore, there is need for *a priori* study that allows us to assess predictive capabilities of Eqs. (1)-(4) under various conditions. Such an assessment appears to be of interest, because recent experimental and DNS data reviewed by Driscoll et al.[48] indicate that the domain of the flamelet concept validity is substantially wider than it was earlier assumed. This hypothesis results from comparison of profiles of conditioned quantities extracted from highly turbulent flames with the counterpart profiles obtained from laminar flames,[48] see also recent experimental data by Skiba et al.[49] The hypothesis implies that Eqs. (1)-(4) could perform well even in sufficiently intense turbulence. However, *a priori* quantitative assessment of Eqs. (1)-(4) has so far been very limited. In particular, Domingo et al.[22] demonstrated that Eq. (2) could predict filtered mass fraction of OH, extracted from their two-dimensional DNS data obtained from a weakly turbulent (turbulent Reynolds number was as low as 55) flame at a single distance from flame-holder. Moreover, Lapointe and Blanquart[42] analyzed their DNS data to *a priori* explore Eq. (1) applied to a single rate $\bar{W}_c$ of product creation (i.e., the source term in the transport equation for $\bar{c}$).

Recently, two of the present authors[50-53] (i) analysed DNS data obtained by Dave and Chaudhuri[54] and by Im et al.[55-59] from lean complex-chemistry hydrogen-air turbulent flames characterized by different Karlovitz numbers and (ii) quantitatively validated Eqs. (2)-(4) not only for major reactants H_2 and O_2, product H_2O, temperature, and density, but also for the radicals H, O, and OH by adopting actual PDFs $P(c)$ extracted from the same DNS data. In line with other recent data reviewed by Driscoll et al.,[48] these numerical findings indicate that the flamelet approach could be useful even under highly turbulent conditions, and, therefore, call for further assessment of Eqs. (1)-(4) for other fuels and in more intense turbulence. The present work responds to this request by performing *a priori* quantitative assessment of Eqs. (1)-(4) for various species using recent DNS data[45,60,61] obtained from lean methane-air flames under conditions of moderate, intense, and very intense turbulence. This is the major goal of the present study. It is worth stressing again that, with the exception of the aforementioned papers by Domingo et al.[22] and Lipatnikov et al.,[50-53] the present authors are not aware of another investigation aimed at *a priori* quantitative assessment of Eq. (2) for intermediate species such as CO or the radicals H, O, OH, etc. in premixed or stratified turbulent flames. In particular, the present authors are not aware of *a priori* quantitative assessment of Eq. (2) for intermediate species against results of a 3D complex-chemistry DNS of a C_xH_y-air flame or a flame characterized by Ka significantly larger than 100.

The present work is not limited to exploring Eqs. (1)-(4) all together but aims also at testing each equation separately. Indeed, while both Eq. (1) and Eqs. (2)-(4) stem from the same flamelet concept, the latter equations could perform better in a turbulent flow, because variations in the mass fractions Y_n, temperature T, or density ρ in a flame are smoother than variations in the rates W_n. Accordingly, eventual errors associated with the flamelet concept, i.e. reduction of $Y_n(\mathbf{x},t)$ and $W_n(\mathbf{x},t)$ to $Y_{n,L}[c(\mathbf{x},t)]$ and $W_{n,L}[c(\mathbf{x},t)]$, respectively, and eventual errors in modeling $P(c)$ could result in significantly larger errors in averaging the rates W_n when compared to averaging the mass fractions Y_n. This was indeed shown recently.[50-53]

Note that, in spite of their apparent similarity, Eqs. (1) and (2) aim at solving basically different problems, i.e. prediction of the mean rate $\overline{W}_c$ of product creation and evaluation of mean mass fractions of various species. Accordingly, hypotheses and models developed to solve the former problem, which was also attacked in many studies that did not invoke Eq. (1), may differ significantly from hypotheses and models developed to solve the latter problem. The present focus is mainly placed on the latter problem, i.e. evaluation of mean mass fractions of various species adopting Eq. (2).

In addition to the major goal stated above, i.e. separately testing the flamelet Eq. (1) and Eqs. (2)-(4), the present work aims also at assessing the so-called presumed PDF approach. While a PDF for the combustion progress variable can be found by solving an appropriately closed transport equation[4,11-14] for $P(c,\mathbf{x},t)$, another option known as a presumed PDF approach is commonly taken in applied CFD research into turbulent flames due to its computational efficiency. That approach consists in[62-64] (i) assuming a general shape $P(c)$ of the PDF, which still involves a few unknown parameters, and (ii) evaluating these parameters by comparing values of the first moments of the $c(\mathbf{x},t)$-field, calculated using the PDF, with the values of these moments, obtained by solving appropriately closed transport equations, e.g. for the Reynolds-averaged $\bar{c}(\mathbf{x},t)$ or the Favre-averaged $\tilde{c}(\mathbf{x},t) \equiv \overline{\rho c}(\mathbf{x},t)/\bar{\rho}(\mathbf{x},t)$ and $\overline{c^2}(\mathbf{x},t)$ or $\widetilde{c^2}(\mathbf{x},t) \equiv \overline{\rho c^2}(\mathbf{x},t)/\bar{\rho}(\mathbf{x},t)$, respectively. More specifically, (i) the mean source terms $\overline{W}_c(\mathbf{x},t)$ and $\overline{cW_c}(\mathbf{x},t)$ in the transport equations for $\tilde{c}(\mathbf{x},t)$ and $\widetilde{c^2}(\mathbf{x},t)$, respectively, are closed invoking the presumed PDF, (ii) the transport equations are numerically integrated, (iii) the PDF parameters are recalculated using the obtained fields of $\tilde{c}(\mathbf{x},t)$ and $\widetilde{c^2}(\mathbf{x},t)$, and, finally, (iv) Eq. (2) is applied to evaluate mean concentrations of various species.

The PDF shape can be presumed adopting a sum of Dirac delta functions,[65] various combinations of Dirac delta functions and a flamelet PDF,[22,23,26,66-68] or the following beta function[62-64]

$$P_\beta\left(c,\bar{c},\overline{c^2}\right)=\frac{\Gamma(a+b)}{\Gamma(a)\Gamma(b)}c^{a-1}(1-c)^{b-1}, \quad (5)$$

$$a=\bar{c}\left(\frac{1}{g}-1\right), \qquad b=(1-\bar{c})\left(\frac{1}{g}-1\right). \quad (6)$$

Here, $g=\overline{c'^2}/[\bar{c}(1-\bar{c})]$ is the segregation factor, $\overline{c'^2}=\overline{c^2}-\bar{c}^2$ is the variance of c, and the gamma function $\Gamma(a)=\int_0^\infty \zeta^{a-1}\mathrm{e}^{-\zeta}d\zeta$ is required to satisfy the normalization constraint of $\int_0^1 P(c)dc=1$. Henceforth, dependencies of $\bar{c}$, $\overline{c^2}$, g, a, b, etc. on $\mathbf{x}$ and t are not specified for brevity. Equations similar to Eqs. (5) and (6) can also be written using mass-weighted PDF $\tilde{P}_\beta\left(c,\tilde{c},\widetilde{c^2}\right)=\rho(c)P_\beta\left(c,\bar{c},\overline{c^2}\right)/\bar{\rho}$ and the Favre-averaged first, $\tilde{c}$, and second, $\widetilde{c^2}$, moments. The latter option is often preferred, because, formally, transport equations for $\tilde{c}$ and $\widetilde{c^2}$ involve a smaller number of unclosed terms than those for $\bar{c}$ and $\overline{c^2}$. In the present paper, the former option is taken, because the use of direct statistics or mass-weighted statistics in Eqs. (1)-(6) is equally justified from the fundamental perspective and results reported in the following are basically similar for both statistics. In applied CFD research, the presumed beta-function PDF is widely accepted, because its shape is very flexible and, depending on the values of a and b, the PDF $P_\beta\left(c,\bar{c},\overline{c^2}\right)$ can vary from a quasi-bi-modal PDF ($g\to 1$) associated with the flamelet regime of premixed turbulent combustion[69] to a quasi-Gaussian PDF ($g\ll 1$) associated with extreme turbulence (or with a small filter size in the case of LES). Moreover, the numerical efficiency of the approach benefits from the simple algebraic relations given by Eq. (6).

Accordingly, a secondary goal of the present work consists in assessing the presumed beta-function PDF approach against the DNS data.[45,60,61] In addition to the aforementioned major and secondary goals, the work aims also at exploring different choices of combustion progress variable.

In the next section, DNS data analyzed for these purposes are briefly summarized. The test results are reported in Section III, with implications of these results for modeling being discussed in Section IV. Conclusions are drawn in Section V.

II. DIRECT NUMERICAL SIMULATION

Since the DNS are discussed in detail elsewhere,[45] see cases A1, A2, and A3 therein, we will restrict ourselves to a brief summary of the simulations. They dealt with statistically 1D, planar premixed flames that propagated from right to left along the x-axis in a rectangular box ($2\Lambda\times\Lambda\times\Lambda$) discretized on a uniform mesh of $2N\times N\times N$ nodes. The periodic and convective outflow boundary conditions were set on the transverse sides and the outlet, respectively. To keep a flame near the domain center, the mean inlet velocity was adjusted to match the flame speed. Homogeneous, isotropic, statistically stationary turbulence was pre-generated using forcing in a cube with the periodic boundary conditions. This pre-generated turbulence was used to set the initial conditions. The same (statistically) turbulence entered the computational domain through the left boundary during combustion simulations. Inside the domain, the turbulence was forced adapting a method discussed elsewhere.[70,71]

At $t=0$, a planar laminar flame (CH_4-air mixture with the equivalence ratio $\Phi=0.6$ under the atmospheric conditions, the laminar flame speed $S_L=0.12$ m/s and thickness $\delta_L=(T_b-T_u)/\max|\nabla T|=0.92$ mm) was embedded into the computational domain at $x=\Lambda$. The continuity, low-Mach-number Navier-Stokes, species and energy transport equations were numerically solved. A skeletal mechanism (16 species and 35 reactions) by Smooke and Giovangigli[72] was used. Differential diffusion effects and temperature-dependence of molecular transport coefficients were modeled using Fourier's and Fick's laws with mixture-averaged transport properties calculated following CHEMKIN. Soret and Dufour effects were neglected.

The DNS solver was described in detail and validated elsewhere.[73] A 5th order weighted essentially non-oscillatory (WENO) finite difference method was used for convective terms and a 6th order central difference scheme was used for all other terms. For unsteady terms, a second-order operator splitting scheme[74] was adopted by integrating chemical source terms between two half-time-step integrations of the diffusion term. The integration of the diffusion term was further divided into smaller explicit steps to ensure stability. The overall time step was set to get the CFL number smaller than 0.1. Reaction rates in species transport equations were integrated using the stiff DVODE solver.[75] The variable-coefficient Poisson equation for pressure differences was solved adopting a multigrid method.[76]

Table I. Simulation conditions

case	N	L_{xx}/δ_{th}	η/δ_{th}	$\delta_{th}/\Delta x$	u'/S_L	Ka	Da	Re_t
A1	256	1.3	0.105	23.5	3.7	6.0	0.38	32
A2	256	1.0	0.036	23.5	18.	74.	0.06	120
A3	512	1.0	0.021	47.0	66.	540.	0.015	390

Three cases characterized by different rms velocities u' and, hence, different Karlovitz numbers $Ka = (u'/S_L)^{3/2}(\delta_{th}/L_{xx})^{1/2}$, Damköhler numbers $Da = L_{xx}S_L/(u'\delta_{th})$, and turbulent Reynolds numbers $Re_t = u'L_{xx}/\nu_u$, see Table I, were simulated. Here, L_{xx} is the axial longitudinal integral length scale evaluated by integrating the correlation function for the axial velocity; $\eta = (\nu^3/\varepsilon)^{1/4}$ is the Kolmogorov length scale; ν_u is the kinematic viscosity of unburned mixture; $\varepsilon = 2\nu S_{ij}S_{ij}$ is the rate of dissipation of turbulent kinetic energy; $S_{ij} = \left(\partial u_i/\partial x_j + \partial u_j/\partial x_i\right)/2$ is the rate-of-strain tensor; $\Delta x = \Delta y = \Delta z$ is the grid spacing; the summation convention applies to repeated indexes; and all turbulence characteristics are averaged over the volume of a cube where the turbulence is pre-generated. The computational domain width is $\Lambda = 5$ mm.

Six different combustion progress variables are defined as follows $c_k = (\phi_k - \phi_{k,u})/(\phi_{k,b} - \phi_{k,u})$, where $\phi_1 = Y_{CH4}, \phi_2 = Y_{O2}, \phi_3 = Y_{H2O}$, and $\phi_4 = Y_{CO2}$, are the mass fractions of CH_4, O_2, H_2O, and CO_2, respectively, $\phi_5 = Y_{CO2} + Y_{CO}$, and $\phi_6 = T$. Note that the dependencies of combustion progress variables defined using sums of $Y_{H2O} + Y_{CO2} + Y_{CO}$ or $Y_{H2O} + Y_{CO2} + Y_{CO} + Y_{H2}$ on the temperature-based $c_T \equiv c_6$ are almost identical to $c_2(c_T)$ in the considered unperturbed laminar premixed flame. Accordingly, these sums were not addressed in the present study.

Mean profiles $\bar{q}(\bar{c}_k)$ of various quantities q were evaluated as follows. First, $q(\mathbf{x},t)$ and $c_k(\mathbf{x},t)$-fields were averaged over each transverse plane x =const at each instant t (25, 21 and 30 snapshots separated by $\Delta t = 0.5\tau_t = 0.5\, L_{xx}/u'$ in cases A1, A2 and A3, respectively). Second, the obtained profiles of $\langle q\rangle(x,t)$ were transformed to $\langle q\rangle(\bar{\xi})$ using the profiles of $\langle c_k\rangle(x,t)$ divided into 51 intervals. Here, $\bar{\xi}$ is a sample variable for $\langle c_k\rangle(x,t)$ and a transverse plane x =const contributes to the value of $\langle q\rangle(\bar{\xi}_j)$ if $\left|\langle c_k\rangle(x,t) - \bar{\xi}_j\right| < 0.01$ $\left(\bar{\xi}_j = 0.02j;\ j = 0, \ldots, 50.\right)$. The analyzed snapshots were stored at $t > 10\tau_t$.

To examine Eqs. (1)-(4), the DNS PDFs $P_k(\xi, x, t)$ were sampled from grid points characterized by $\left|c_k(\mathbf{x},t) - \xi_j\right| < 0.0025$ $\left(\xi_j = 0.005j;\ j = 0, \ldots, 200\right)$ in each transverse plane x =const at each instant t. Here, ξ is a sample variable for the instantaneous $c_k(\mathbf{x},t)$-fields. Subsequently, the PDFs $P_k(\xi,x,t)$ were transformed to $P_k(\xi,\bar{\xi})$ using the profiles of $\langle c_k\rangle(x,t)$, as discussed above. To assess the presumed β-function PDF approach, the first, $\langle c_k\rangle(x,t)$ or $\bar{c}_k(x)$, and second, $\langle c_k^2\rangle(x,t)$ or $\overline{c_k^2}(x)$, respectively, moments extracted from the DNS data were substituted into Eq. (6), followed by substitution of the obtained values of a and b into Eq. (5). Finally, six sets of dependencies of $\overline{\mathbf{W}}(\bar{c}_k)$, $\overline{\mathbf{Y}}(\bar{c}_k)$, $\bar{T}(\bar{c}_k)$, or $\bar{\rho}(\bar{c}_k)$ were computed for the six c_k using the two types of PDFs and Eq. (1), (2), (3), or (4), respectively.

III. RESULTS AND DISCUSSION

Figure 1 shows that, in all three cases, Eq. (3) very well predicts the mean temperature using both the actual and presumed β-function PDFs and adopting the oxygen-based combustion progress variable c_2 or, to a lesser extent, the water-based c_3 (dependencies of $\bar{T}$ on the temperature-based $\bar{c}_6$ reduce to a straight line and, therefore, are not shown). The use of the fuel-based c_1 results in underestimating the mean temperature at $\bar{c}_1 > 0.8$. Worst predictions are obtained adopting c_4 and c_5, which both are based on the mass fraction of CO_2. These differences between mean temperatures extracted from the DNS data and yielded by Eq. (3) will be discussed later. The dependencies $\bar{T}(\bar{c}_k)$ calculated using the actual and presumed β-function PDFs are hardly distinguishable in all cases.

Figure 2 also supports the flamelet concept by quantitatively validating Eq. (4) with either the actual or the presumed β-function PDF for the temperature-based c_6 or the fuel-based c_1. The use of c_2 (c_3) based on the mass fraction of O_2 (H_2O, respectively) yields slightly underestimated (overestimated, respectively) $\bar{\rho}$ in cases A1 and A2 (A2 and A3, respectively), but the differences are rather small at least for c_2. Similar to Fig. 1, worst predictions are obtained adopting c_4 and c_5. It is of interest to note that while the flamelet Eq. (4) performs well under conditions of the present study, the computed dependencies $\bar{\rho}(\bar{c}_k)$ are non-linear contrary to the well-known Bray-Moss-Libby[69] (BML) linear relation of $\bar{\rho} = \rho_u(1-\bar{c}) + \rho_b\bar{c}$. Since the BML theory relies not only on the flamelet concept, but also (and mainly) on a hypothesis that the probability of finding intermediate states of the mixture is much less than unity, the discussed observation implies that this hypothesis does not hold under conditions of the present study. This could be expected, because $Ka > 1$ in all three cases.

Figures 3 and 4 quantitatively validate the flamelet Eq. (2) for major reactants and products, including CO, provided that the combustion progress variable is defined using the temperature, see the bottom row, with both the actual and β-function PDFs yielding very good results (note that $\bar{Y}_{CO_2}$ is slightly underestimated in cases A2 and A3). For four other $\bar{c}_k$, the computed results are generally good, but Eq. (2) performs worse for some species in some cases, e.g. (i) for $\bar{Y}_{CO_2}(\bar{c}_1)$ and $\bar{Y}_{CO}(\bar{c}_1)$ in all three cases, see red lines in the first rows in Figs. 3 and 4, respectively, (ii) for $\bar{Y}_{CH_4}(\bar{c}_2)$ in cases A2 and A3 or for $\bar{Y}_{CO}(\bar{c}_2)$ in cases A1 and A2, see the second row in Fig. 4, or (iii) for $\bar{Y}_{CO_2}(\bar{c}_3)$ and $\bar{Y}_{O_2}(\bar{c}_3)$ in all three cases, see the third row in Fig. 3, or for $\bar{Y}_{CO}(\bar{c}_3)$ in cases A1 and A2 and $\bar{Y}_{CH_4}(\bar{c}_3)$ in cases A2 and A3, see the third row in Fig. 4. The use of the CO_2-based c_4 or c_5 yields the worst results for $\bar{Y}_{H_2O}(\bar{c}_k)$ in cases A2 and A3, see black lines in the fourth row in Fig. 3, and for $\bar{Y}_{CH_4}(\bar{c}_k)$ in all three cases, see black lines in the fourth row in Fig. 4 or 5, respectively. Moreover, $\bar{Y}_{CO}(\bar{c}_4)$ or $\bar{Y}_{CO}(\bar{c}_5)$ is substantially overestimated in case A3, see red lines in the fourth row in Fig. 4 or 5, respectively.

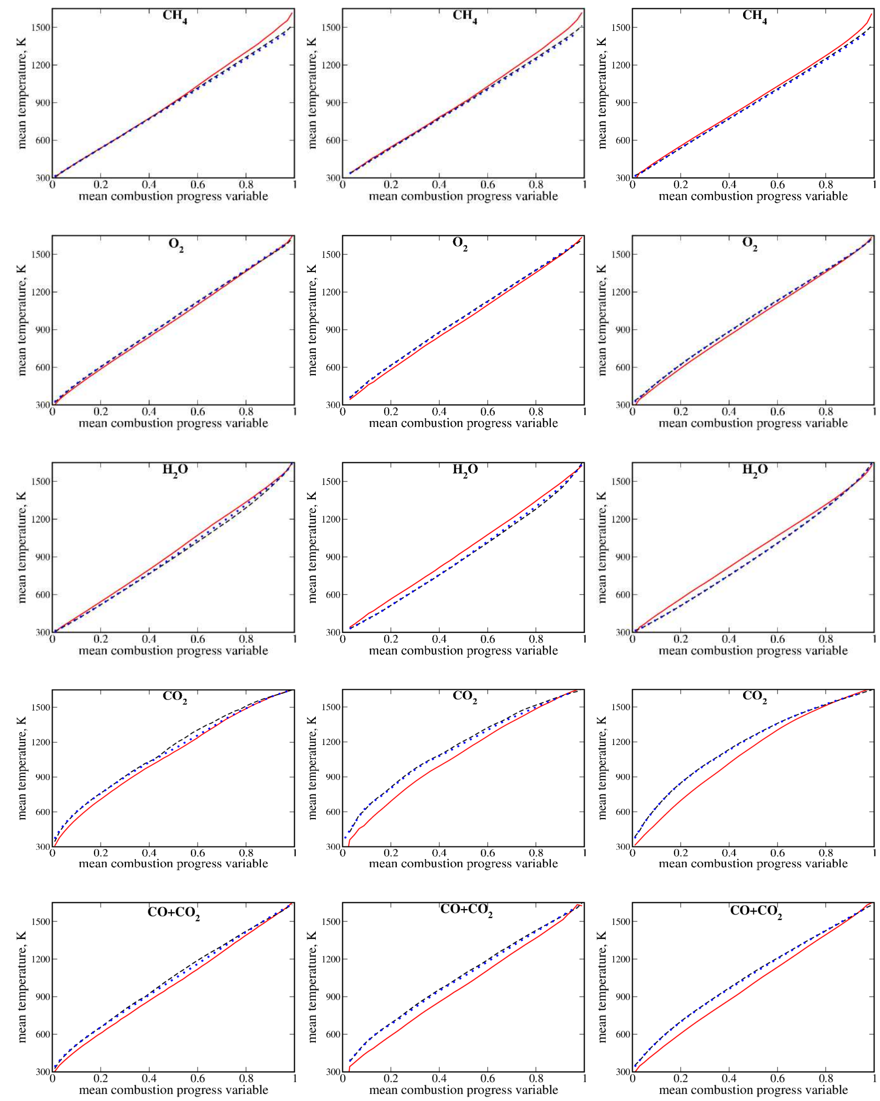

FIG. 1. Mean temperature vs. various mean combustion progress variables $\bar{c}_k$ specified in the top of each subfigure. Solid lines show $\bar{T}$ extracted from the DNS data. Dashed lines show $\bar{T}$ evaluated using the flamelet library and the PDF extracted from the DNS data. Dotted lines show $\bar{T}$ calculated invoking the β-distribution PDF. Results computed in cases A1, A2, and A3 are plotted in the left, middle, and right columns, respectively.

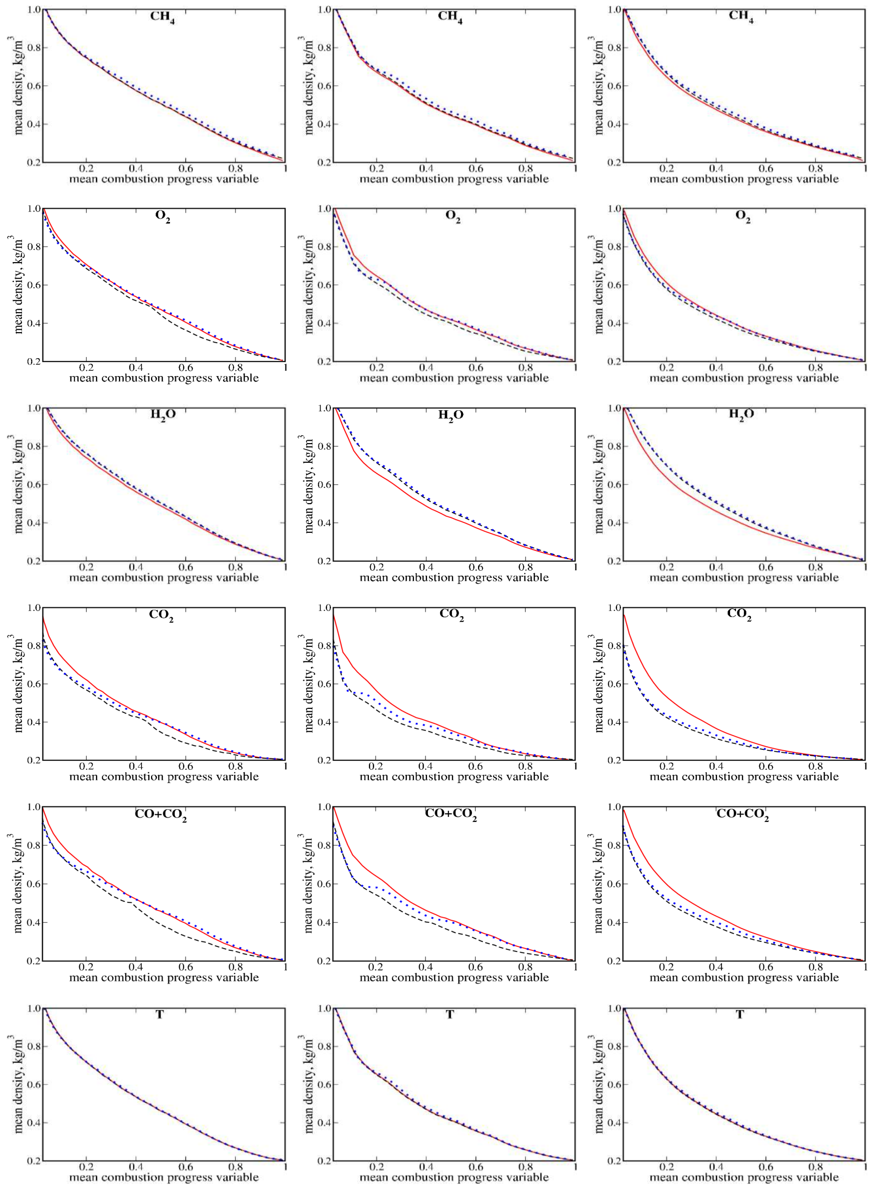

FIG. 2. Mean density vs. various mean combustion progress variables $\bar{c}_k$ specified in the top of each subfigure. Legends are explained in caption to Fig. 1.

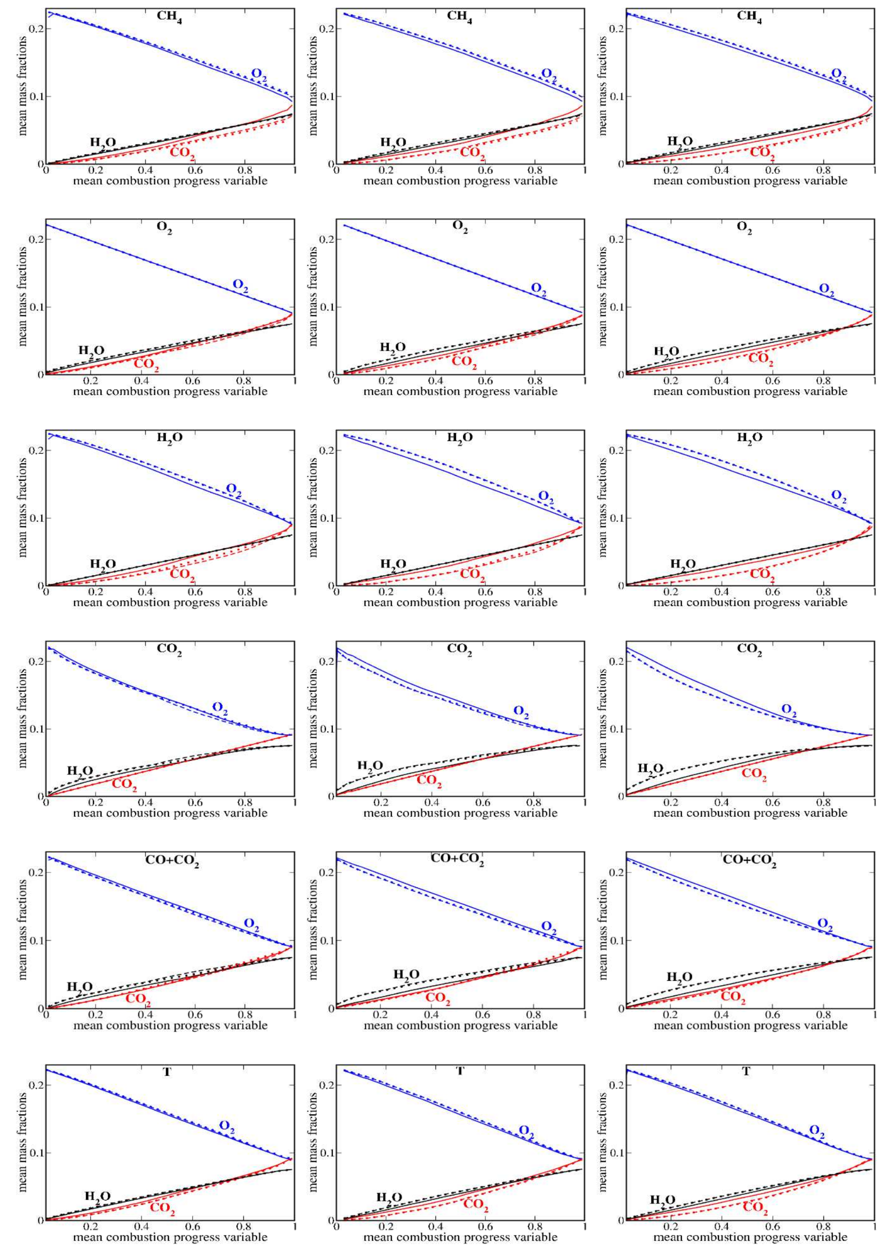

FIG. 3. Mean mass fractions of O_2, H_2O, and CO_2 vs. various mean combustion progress variables $\bar{c}_k$ specified in the top of each subfigure. Legends are explained in caption to Fig. 1.

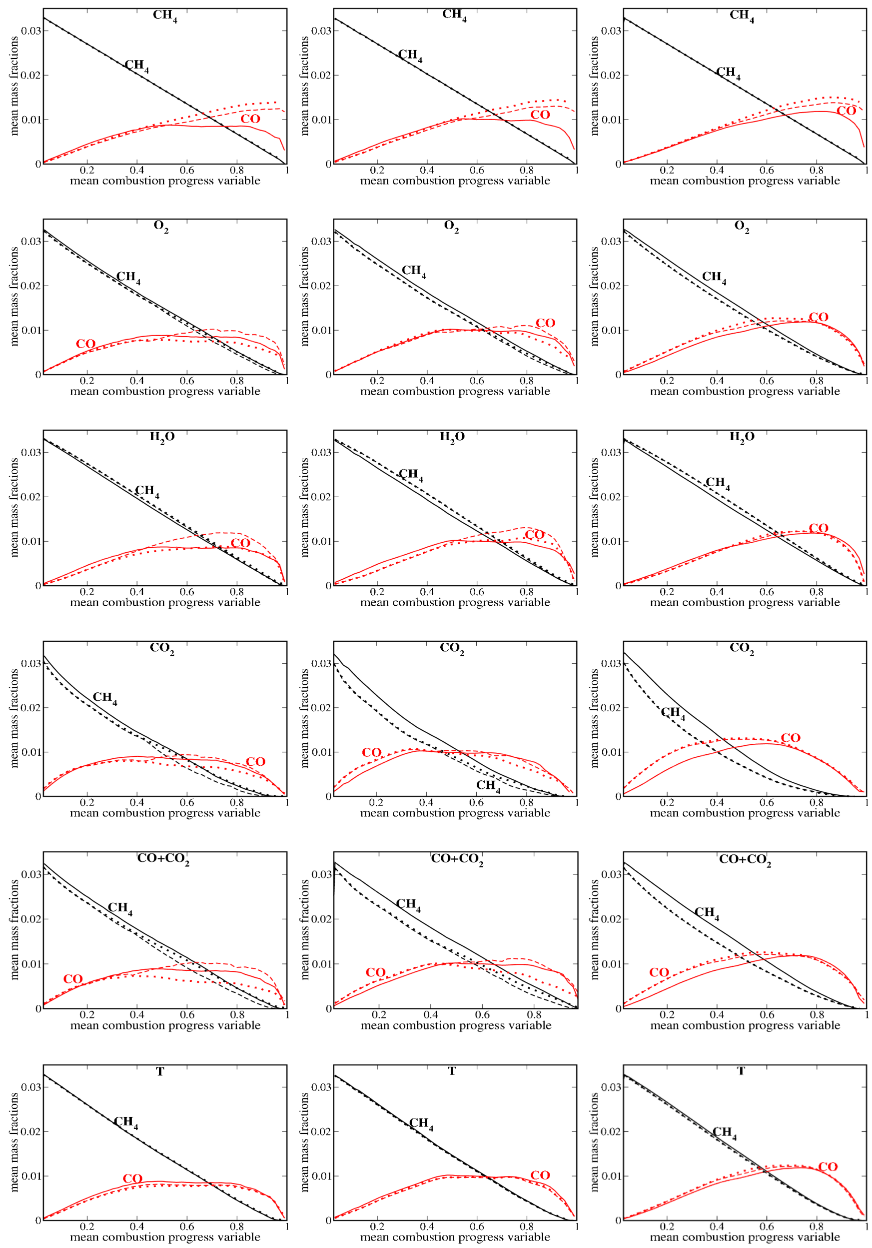

FIG. 4. Mean mass fractions of CH_4 and CO vs. various mean combustion progress variables $\bar{c}_k$ specified in the top of each subfigure. Legends are explained in caption to Fig. 1.

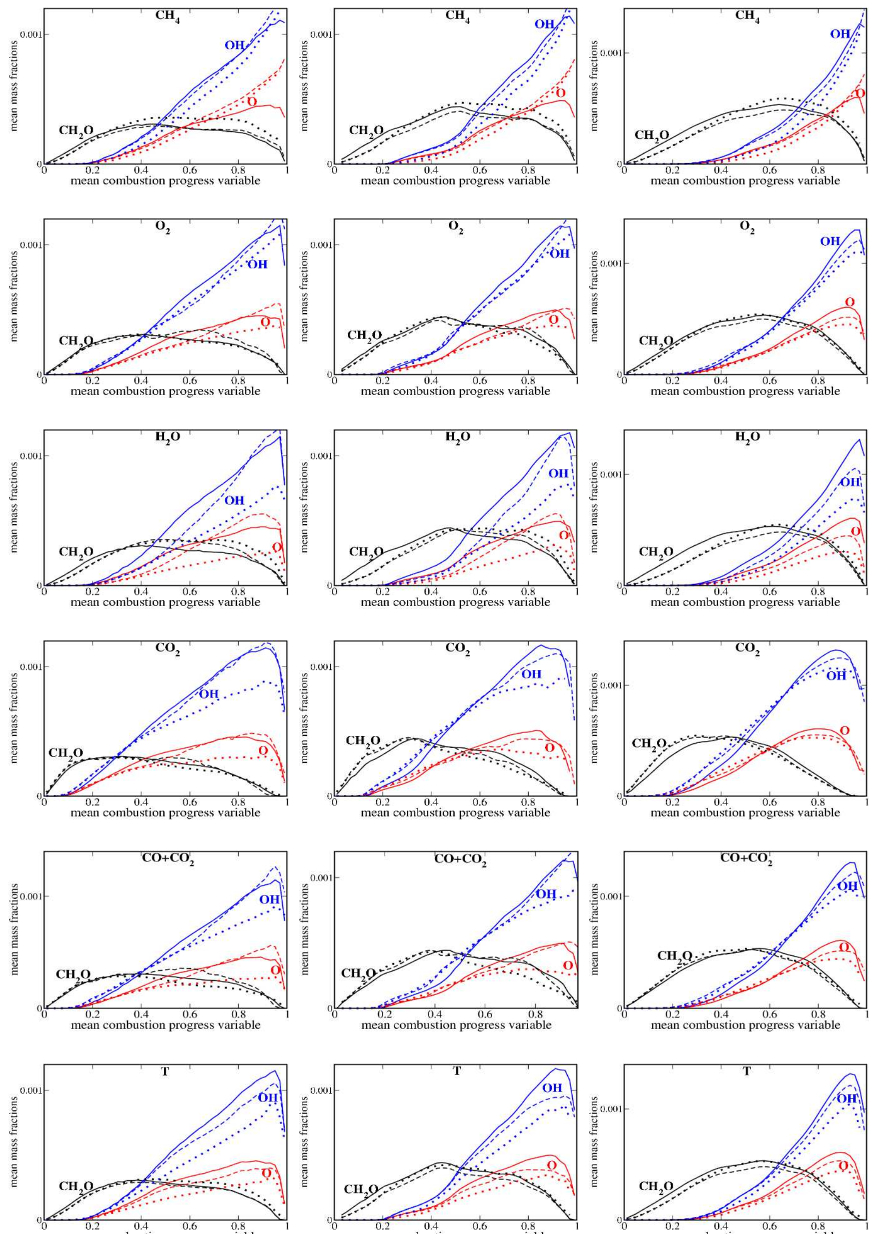

FIG. 5. Mean mass fractions of CH_2O, OH, and O vs. various mean combustion progress variables $\bar{c}_k$ specified in the top of each subfigure. Legends are explained in caption to Fig. 1.

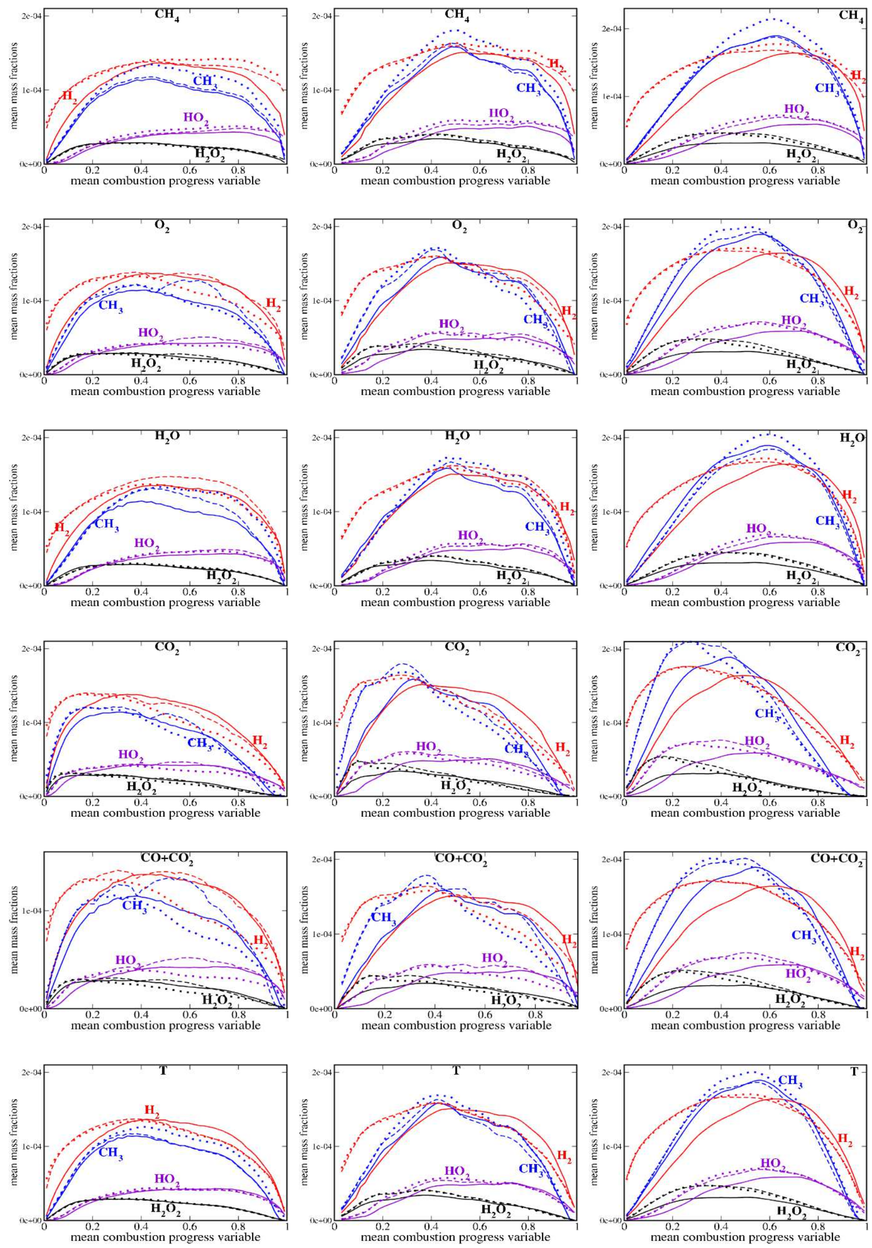

FIG. 6. Mean mass fractions of CH_3, H_2, HO_2, and H_2O_2 vs. various mean combustion progress variables $\bar{c}_k$ specified in the top of each subfigure. Legends are explained in caption to Fig. 1.

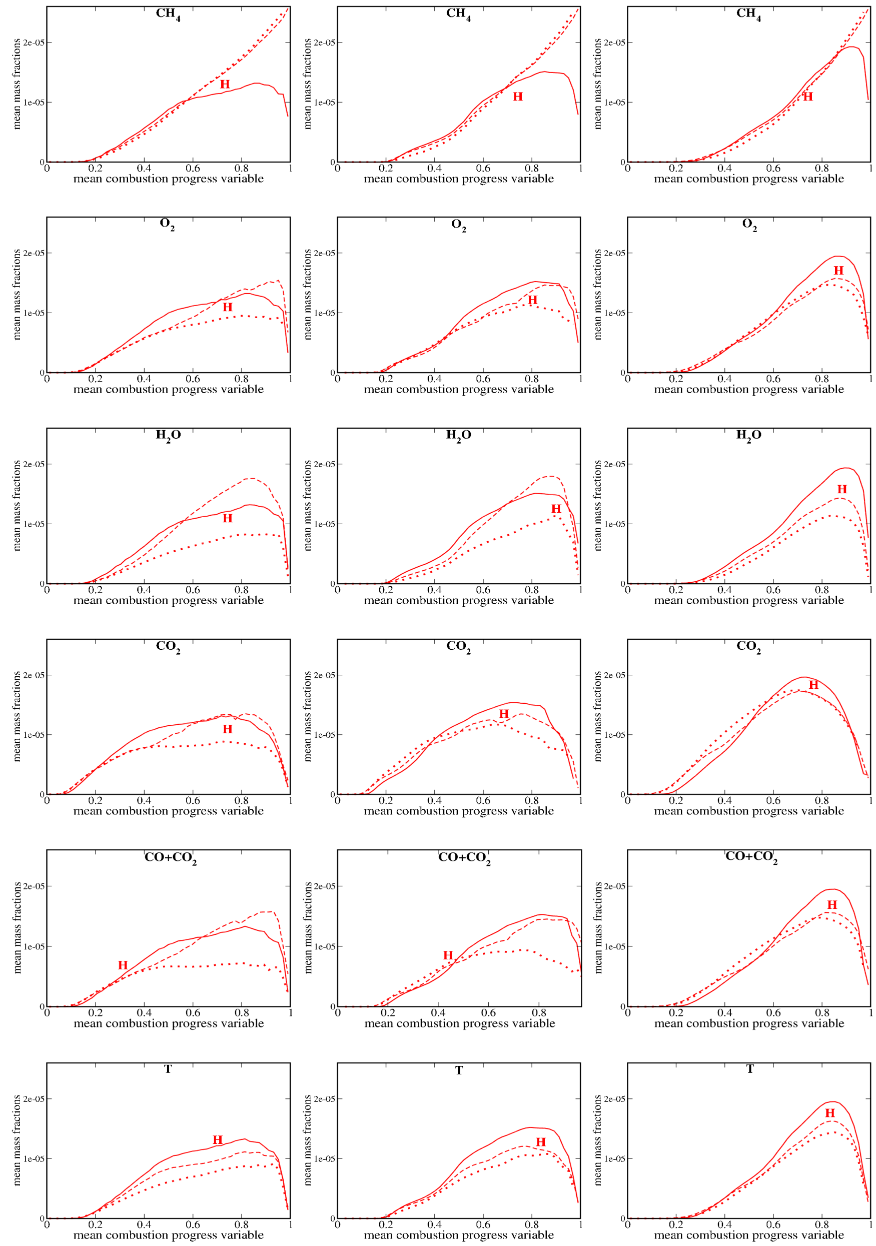

FIG. 7. Mean mass fraction of H vs. various mean combustion progress variables $\bar{c}_k$ specified in the top of each subfigure. Legends are explained in caption to Fig. 1.

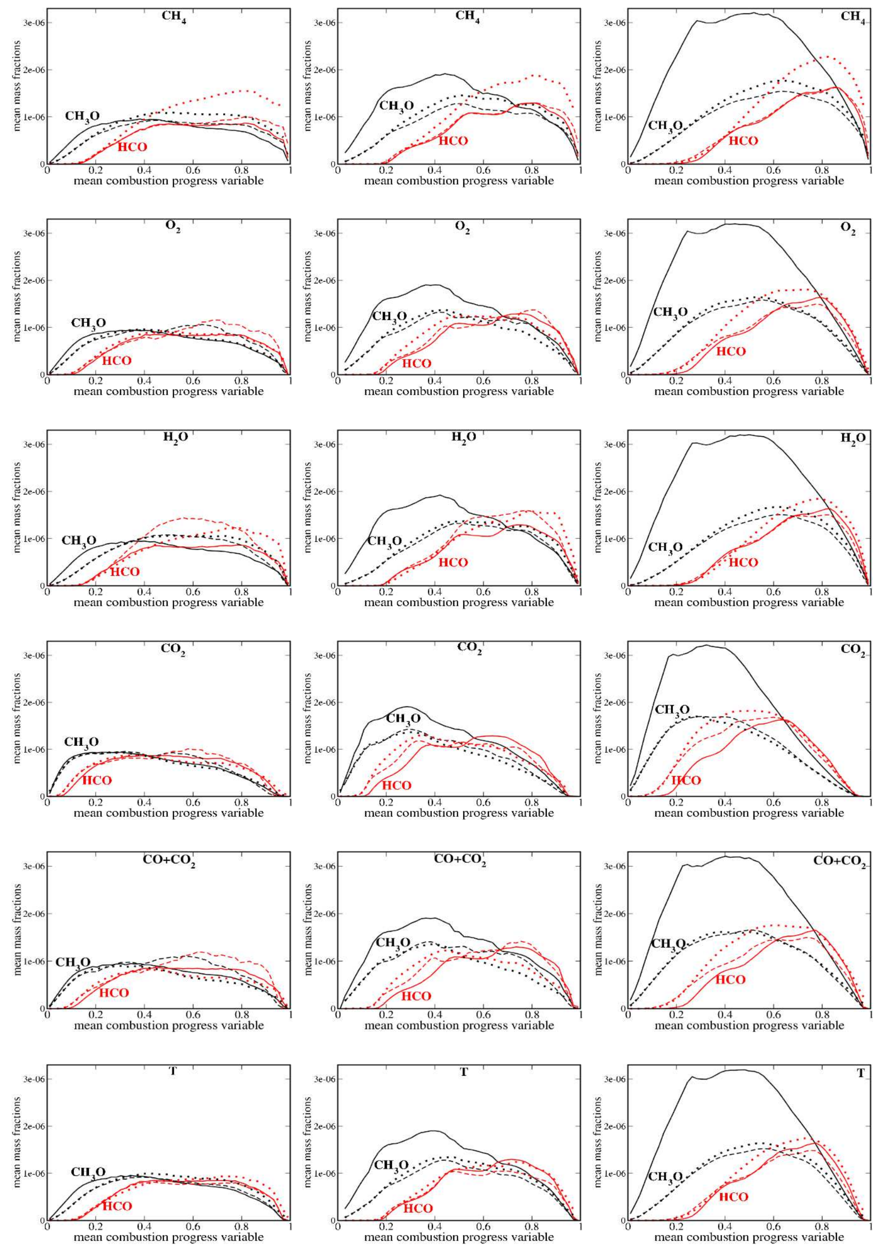

FIG. 8. Mean mass fraction of CH3O and HCO vs. various mean combustion progress variables $\bar{c}_k$ specified in the top of each subfigure. Legends are explained in caption to Fig. 1.

All in all, Figs. 1-4 quantitatively validate the flamelet Eqs. (2)-(4) at various $6 \leq Ka \leq 540$, at least if the combustion progress variable is defined using the temperature, with good results being obtained adopting not only the actual PDFs, but even the presumed β-function PDFs. However, these findings are expected, because both PDFs are built using the correct values of the first two moments of the $c(\mathbf{x}, t)$-field and spatial variations of the density, temperature, or mass fractions of major reactants and products are relatively smooth (weakly non-linear) in a flame. Prediction of mean mass fractions of intermediate species, whose spatial variations are substantially non-linear and are characterized by significantly smaller length scales, appears to be a much more difficult task, which is addressed for all 10 such species, considered within the framework of the skeletal mechanism by Smooke and Giovangigli,[72] in Figs. 5-8. The following trends are worth noting.

First, if (i) combustion progress variable is defined based on the temperature, as recommended above, and (ii) the PDF $P_6(\xi, \bar{\xi})$ is extracted from the DNS data, Eq. (2) very well predicts the mean mass fractions of CH_2O, CH_3, and HCO in all three cases, see the bottom rows in each figure and cf. black solid and dashed lines in Fig. 5, blue solid and dashed lines in Fig. 6, and red solid and dashed lines in Fig. 8. The mean mass fractions of OH and O are slightly underestimated, cf. blue or red, respectively, solid and dashed lines in Fig. 5. The mean mass fraction of HO_2 or H_2O_2 is very well predicted in case A1, cf. violet or black, respectively, solid and dashed lines in Fig. 6, but Eq. (2) performs worse with increasing Ka. The mean mass fraction of H_2 is overestimated at $\bar{c}_k < c_k^*$ and the mean mass fraction of H is underestimated at $\bar{c}_k > c_k^*$, with c_k^* being increased with increasing Ka, cf. red solid and dashed lines in Figs. 6 and 7, respectively. At a first glance, this limitation of Eq. (2) is associated with high molecular diffusivities of H_2 and H. Local phenomena caused by interaction of complex chemistry and preferential diffusion effects were already documented in DNS studies of highly turbulent lean hydrogen-air flames.[77-79] Finally, the mean mass fraction of CH_3O is significantly underpredicted in cases A2 and, especially, A3, cf. black solid and dashed lines in Fig. 8.

Second, if combustion progress variable is still defined based on the temperature, the actual and β-function PDFs yield almost the same results for CH_2O, H_2, HO_2, H_2O_2, and CH_3O. For five other intermediate species, i.e. OH, O, CH_3, H, or HCO, the two PDFs yield substantially different results. This difference implies that Eqs. (5) and (6) do not predict the PDF extracted from the DNS data. Differences between the actual PDFs extracted from the DNS data and β-function PDFs built using the first two moments of the $c_T(\mathbf{x}, t)$-field extracted from the same DNS data are clearly seen in Fig. 9.

Third, in cases A2 and A3, $\bar{Y}_n(\bar{c}_k)$ obtained by adopting the actual PDF for the oxygen-based c_2 and the temperature-based c_5, are comparable for the most intermediate species, but, in case A1, the use of c_2 yields sunstantially worse results for CO, see Fig. 4, CH_2O, see Fig. 5, CH_3, see Fig. 6, HCO and CH_3O, see Fig. 8.

Fourth, even for four other combustion progress variables, results computed using Eq. (2) seem to be encouraging. For some species, the predictions are very good: $\bar{Y}_{OH}(\bar{c}_1)$, cf. blue solid and dashed lines in the first row in Fig. 5; $\bar{Y}_O(\bar{c}_4)$, cf. red solid and dashed lines in the fourth row in Fig. 5; $\bar{Y}_{HO_2}(\bar{c}_3)$, cf. violet solid and dashed lines in the third row in Fig. 6; $\bar{Y}_{CH_3}(\bar{c}_1)$, cf. blue solid and dashed lines in the first row in Fig. 6; $\bar{Y}_H(\bar{c}_4)$ cf. solid and dashed lines in the fourth row in Fig. 7; or $\bar{Y}_{HCO}(\bar{c}_1)$, cf. red solid and dashed lines in the first row in Fig. 8.

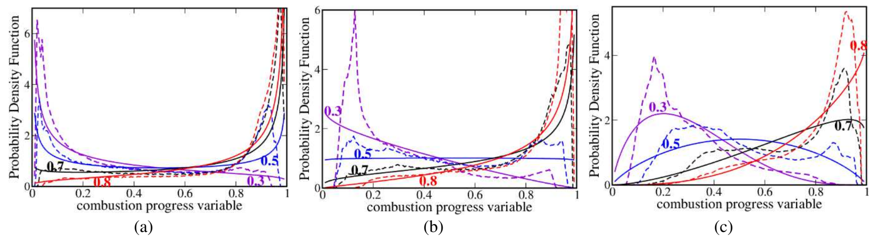

FIG. 9. Probability density functions for the temperature-based combustion progress variable $c_6 \equiv c_T$ obtained at $\bar{c}_6 = 0.3$ (violet curves), 0.5 (blue curves), 0.7 (black curves), and 0.8 (red curves) from flames (a) A1 (left cell), (b) A2 (middle cell), and (c) A3 (right cell). Solid lines show β-function PDFs built using the first two moments of the $c_6(\mathbf{x},t)$-field extracted from the DNS data. Dashed lines show actual PDFs extracted from the DNS data.

All in all, Figs. 1-8 considered all together (i) support the flamelet Eqs. (2)-(4) in a wide range of $6 \le Ka \le 540$, with certain reservations discussed above, (ii) indicate that the temperature is a better choice for defining combustion progress variable under conditions of the present study, and (iii) call for development of a better model for the combustion-progress-variable PDF. Sufficiently good quantitative agreement between the profiles of $\bar{Y}_n(\bar{c}_6)$ extracted from the DNS data and calculated using Eq. (2) with the actual PDF $P_6(\xi,\bar{\xi})$, obtained for almost all species at high Karlovitz numbers up to 540, is the major result of the above analysis. This result appears to be of significant importance for applied CFD research into premixed or stratified turbulent burning, because it supports the use of a simple Eq. (2) in unsteady multi-dimensional simulations. It is worth remembering, however, that such simulations invoke other models of various phenomena such as influence of turbulence on combustion, thermal expansion effects, heat losses, etc., as well as a model of the PDF $P(c)$. Bearing in mind good *a priori* prediction shown in Figs. 1-8, accuracy of such *a posteriori* simulation is likely to be limited by some of the aforementioned models, rather than by Eq. (2). For this reason and because the flamelet Eqs. (1)-(4) are tools for the applied CFD research, further improvement of results reported in Figs. 1-8, e.g. by invoking a flamelet library created for strained laminar premixed flames, does not seem to be of the top priority at the moment, as well as a thorough investigation of differences between the profiles of $\bar{Y}_n(\bar{c}_k)$ extracted from the DNS data and calculated using the actual PDFs $P_k(\xi,\bar{\xi})$ extracted from the same data. Nevertheless, these differences deserve some discussion.

There are three types of such differences, which are more pronounced (i) for certain $\bar{c}_k$ when compared to the temperature-based $\bar{c}_6 \equiv \bar{c}_T$, (ii) for some species even if $\bar{c}_T$ is adopted, or (iii) in the highly turbulent flame A3. To reveal the causes of these differences, Fig. 10 shows the structure of the unperturbed laminar flame calculated using the skeletal mechanism by Smooke and Giovangigli[72] (solid lines), as well as the structure of the counterpart equidiffusive flame (dashed lines). In the latter case, molecular mass diffusivities of each species are equal to the molecular heat diffusivity of the mixture or, in other words, $Le_n = 1$ for each species n. Since the use of the temperature-based combustion progress variable c_T yielded the best agreement between the DNS data and results obtained adopting Eqs. (2)-(4), Fig. 10 reports the flame structure in the c_T-space. The following trends are worth emphasizing.

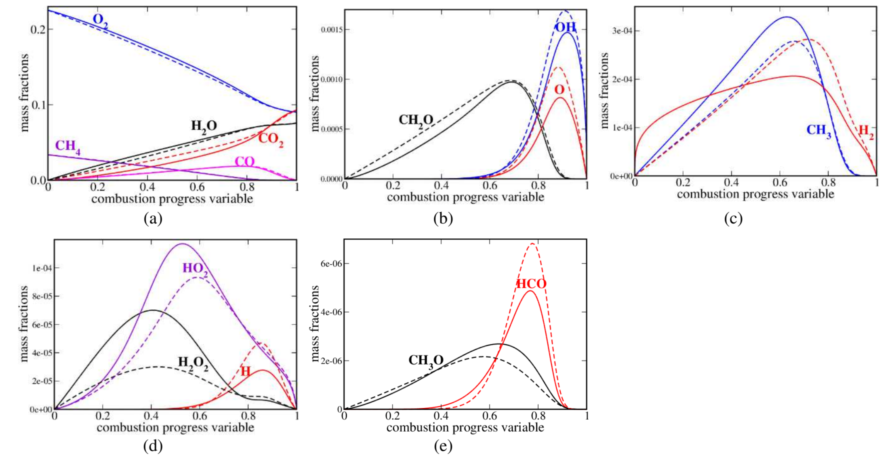

FIG. 10. Mass fractions of (a) CH_4, O_2, H_2O, CO_2, and CO, (b) CH_2O, O, and H, (c) H_2 and CH_3, (d) HO_2, H_2O_2, and H, and (e) CH_3O and HCO vs. temperature-based combustion progress variable c_T. Solid and dashed lines show mass fractions calculated for unperturbed laminar flames with $Le_n \neq 1$ and $Le_n = 1$, respectively.

First, Fig. 10a shows that, for O_2 or H_2O, dependencies of $Y_{n,L}(c_T)$ are almost linear at $c_T < 0.85$, but become weakly non-linear at larger c_T, with variations in the mass fraction of oxygen or water being less pronounced at $c_T > 0.85$. The same trends are also observed for the fuel, with the mass fraction of CH_4 almost vanishing at $c_T > 0.85$. If (i) species k is selected to define a combustion progress variable c_k and (ii) the rate of change of Y_k with c_T is decreased in a certain range of c_T, i.e. $|dY_k/dc_T|$ is small (or very small, as for CH_4 at $c_T > 0.85$); even small (very small for methane) variations in Y_k or c_k are accompanied with significant variations in other mass fractions Y_n in the considered range of c_T, i.e. the non-linearities of the dependencies of $Y_{n,L}$ on c_k are more (much more for CH_4) pronounced when compared to the non-linearity of $Y_{n,L}(c_T)$. For instance, the peak absolute value of the second derivative $|d^2Y_{CO}/dc_F^2|$ reached in the unperturbed laminar flame in an interval of $0.05 < c_T < 0.95$ is larger than the peak $|d^2Y_{CO}/dc_T^2|$ by almost six orders of magnitude and this difference is even larger at larger c_T. Furthermore, if a dependence of $Y_{n,L}(c_k)$ is highly non-linear, the use of $Y_{n,L}(c_k)$ for averaging the mass fraction $Y_n(\mathbf{x},t)$ by adopting Eq. (2) can result in significant errors. Accordingly, differences between $\bar{Y}_n(\bar{c}_1)$ extracted from the DNS data and calculated using Eq. (2) with the actual PDF (see the top rows in Figs. 3-8) are expected due to the highly non-linear dependencies $Y_{n,L}(c_1)$ at large $c_1 \equiv c_F$, i.e. in the flame zone characterized by vanishing mass fraction of CH_4 and, hence, $c_F \approx 1$. This effect is expected to be of the most importance at large $\bar{c}_F$. Such differences are well pronounced for CO (see red curves in Fig. 4), O (see red curves in Fig. 5), H_2 in case A1 (see red curves in Fig. 6), and H (see Fig. 7). For CH_2O, CH_3, H_2O_2, CH_3O, and HCO, such differences are weakly (if any) pronounced, because the mass fractions of these species almost vanish at large c_F, as shown in Fig. 10. The above discussion and Fig. 10 indicate that the fuel mass fraction is not the best choice for defining combustion progress variable for the studied lean methane-air flame.

Similar reasoning explains worse performance of the combustion progress variables c_4 and c_5, which involve the mass fraction of CO_2. In the studied unperturbed laminar flame, the non-linearities of the dependencies $c_4(c_T)$ and $c_5(c_T)$ are well pronounced, with the derivatives dc_4/dc_T and dc_5/dc_T being decreased with decreasing c_T. Accordingly, at low c_T, the same variations in Y_n are accompanied with larger variations in c_T when compared to variations in c_4 or c_5 and the dependencies of $Y_n(c_4)$ and $Y_n(c_5)$ are more non-linear when compared to $Y_n(c_T)$. For instance, the peak absolute value of the second derivative $|d^2\rho/dc_T^2|$ reached in the unperturbed laminar flame in an interval of $0.05 < c_T < 0.95$ is smaller than the peak $|d^2\rho/dc_4^2|$ or $|d^2\rho/dc_5^2|$ by a factor of about 30 and 7.2, respectively. As a result, the use of Eq. (4) jointly with c_4 or c_5 yields substantially underestimated mean density, see the fourth and fifth rows in Fig. 2. An increase in the effect magnitude with Ka may be attributed to stronger fluctuations in more intense turbulence.

Generally speaking, since the peak value of $|d^2Y_n/dc_k^2|$ obtained from an unperturbed laminar flame characterizes the degree of non-linearity of the dependence $Y_{n,L}(c_k)$ in the flame, comparison of $|d^2Y_{n,L}/dc_k^2|$ could be used for selecting the most appropriate combustion progress variable before applying Eqs. (2)-(4) to modeling premixed turbulent combustion.

Second, recent DNS data[80-84] indicate that the local flame structure (i) is less sensitive to preferential diffusion and Lewis number effects in more intense turbulence and (ii) tends to the structure of the equidiffusive laminar premixed flame with increasing Ka (note that burning velocity remains highly sensitive to the aforementioned effects even in very intense turbulence, as well documented in earlier experiments reviewed elsewhere[85,86] and in more recent measurements[87-89]). Accordingly, the profiles of $Y_{n,L,Le=1}(c_T)$, obtained from the studied unperturbed laminar premixed flame by setting Lewis numbers equal to unity for all species and reported in dashed lines in Fig. 10, were averaged adopting Eq. (2) with the actual PDF extracted from the DNS data. In Fig. 11, results obtained from flames A1 and A3 are plotted in dotted lines for some species, whereas dashed lines show $\bar{Y}_n(\bar{c}_T)$ computed for $Le_n \neq 1$, with all other things being equal. In flame A1 ($Ka = 6.0$), the use of the $Y_{n,L,Le=1}(c_T)$-profiles results in worse agreement with the DNS data (solid lines) for CH_2O, CH_3, HO_2, H_2O_2, H, and HCO, but weakly affects the agreement for H_2 and CH_3O. On the contrary, the use of the $Y_{n,L,Le=1}(c_T)$-profiles substantially (slightly) improves predictions for H_2 and HO_2 (CH_2O and H_2O_2, respectively) in flame A3 ($Ka = 540$). Nevertheless, even in flame A3, the use of the $Y_{n,L,Le=1}(c_T)$-profiles yields worse results for CH_3, H (to a lesser extent), and HCO. For other species that are not shown in Fig. 11 differences between results simulated invoking $Y_{n,L}(c_T)$ and $Y_{n,L,Le=1}(c_T)$ are small. Thus, eventual mitigation of preferential diffusion effects in highly turbulent flames could explain some differences between the profiles of $\bar{Y}_n(\bar{c}_T)$ extracted from the DNS and the profiles of $\bar{Y}_n(\bar{c}_T)$ yielded by Eq. (2) with $Y_{n,L}(c_T)$ and the actual PDF. However, such an explanation is not sufficient for all species, e.g. H or CH_3O. The above discussion and Fig. 11 imply that the boundary of utility of the laminar-flame profiles $Y_{n,L}(c_T)$ for evaluating mean species concentrations in turbulent flames is close to $Ka = O(500)$ for the studied lean methane-air mixture. Simulations at a higher Ka are required to test this hypothesis. Moreover, averaging profiles of $Y_{n,L}(c_T)$ and $Y_{n,L,Le=1}(c_T)$ obtained from strained laminar premixed flames could be performed to further explore physical mechanisms that reduce predictive capabilities of Eq. (2) and this could be a subject for future study.

The major result the present work consists in showing that Eq. (2) supplemented with the simplest version of flamelet library (a single unperturbed laminar premixed flame) works well for various intermediate species even at high Ka. This result implies also that even if strain effects play an important role locally, they significance is substantially reduced after averaging, at least for mean species concentrations. In this regard, it is worth noting that recent experimental data by Skiba et al.[49] show that the profiles of $Y_n(c_T)$ calculated for freely propagating laminar premixed flame agree well with conditioned proiles of $\langle Y_n|c_T\rangle$ extracted from highly turbulent flames for CH_2O, CH, and OH, see Figs. 2 and 3 in the cited paper.

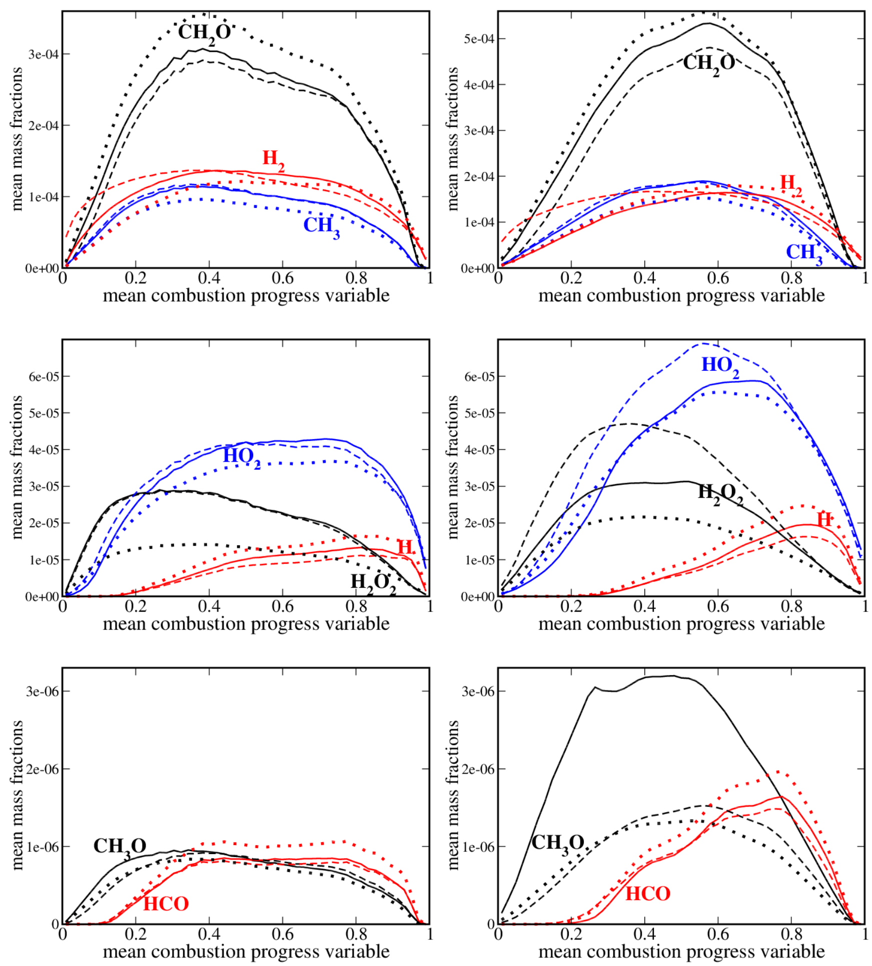

FIG. 11. Mean mass fractions of various species noted near relevant curves vs. mean temperature-based combustion progress variable $\bar{c}_T$. Solid lines show $\bar{Y}_n$ extracted from the DNS data. Dashed and dotted lines show $\bar{Y}_n$ evaluated using the PDF extracted from the DNS data and flamelet libraries calculated for $Le_n \neq 1$ and $Le_n = 1$, respectively. Results obtained from flames A1 ($Ka = 6.0$) and A3 ($Ka = 540$) are plotted in the left and right columns, respectively.

Contrary to Eqs. (2)-(4), results obtained by testing the flamelet Eq. (1) are less satisfactory. For instance, Fig. 12 (results computed using other c_k are worse and not reported here) show that, for major radicals such as O and OH, the profiles of $\overline{W}_n(\bar{c}_T)$ extracted directly from the DNS data, see solid lines, differ significantly from the profiles of $\overline{W}_n(\bar{c}_T)$ obtained by substituting the actual PDF into Eq. (1), see dashed lines. The β-function PDF yields even worse results, see dotted lines. The significant difference between the predictive capabilities of the flamelet Eqs. (1) and (2), cf. Fig. 12 with the next to the bottom row in Fig. 5, is associated with the fact that variations in a species concentration in a flame are smoother than variations in the rate of production/consumption of the same species. The significant differences between the mean rates $\overline{W}_O(\bar{c}_T)$ or $\overline{W}_{OH}(\bar{c}_T)$, computed by adopting the actual and β-function PDFs, with all other things being equal, indicate limitations of the latter PDF, which were already shown in Fig. 9.

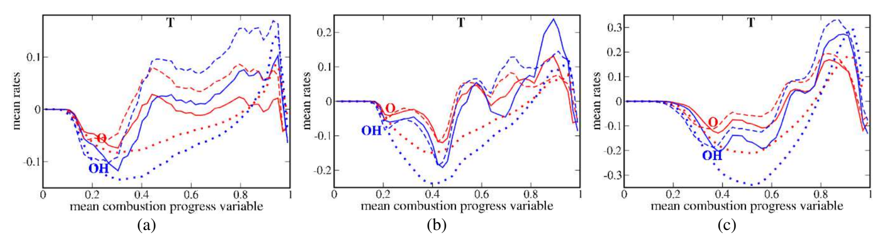

FIG. 12. Mean rates $\overline{W}_n$ [s^{-1}] of production/consumption of radicals O (red lines) and OH (blue lines) vs. mean temperature-based combustion progress variable $\bar{c}_T$. Solid lines show $\overline{W}_n$ extracted from the DNS data. Dashed lines show $\overline{W}_n$ evaluated using Eq. (1) and the PDF extracted from the DNS data. Dotted lines show $\overline{W}_n$ calculated invoking the β-distribution PDF. Results computed in cases (a) A1, (b) A2, and (c) A3 are plotted in the left, middle, and right columns, respectively.

It is worth remembering, however, that Eq. (1) is commonly applied solely to evaluating the source term $\overline{W}_c$ in the transport equation for the mean combustion progress variable,[21-45] whereas mean concentrations of various species are calculated using Eq. (2). Accordingly, the focus of assessment of Eq. (1) should be placed on its ability to predict $\overline{W}_c$ for differently defined c_k. Such results are reported in Figs. 13 and 14 for species-based and temperature-based combustion progress variables, respectively. The following trends are worth noting.

First, for all c_k and in all cases, the actual and β-function PDFs yield different results, cf. dashed and dotted lines. Nevertheless, in most such cases, with the exception of the fuel-based c_1 in all three flames, c_4 in flames A1 and A2, or c_5 in flames A2 and A3, either the mean rates obtained using the two PDFs show comparable agreement with the raw DNS data or the mean rates evaluated invoking the presumed β-function PDF agree better with the raw data, e.g. $\overline{W}_{c,2}(\bar{c}_2)$ in flame A1, $\overline{W}_{c,3}(\bar{c}_3)$ in all three flames, or $\overline{W}_{c,6}(\bar{c}_T)$ in flames A2 and A3. This observation implies that, in the discussed cases, errors due to the use of the flamelet library for the reaction rates and errors due to the use of the β-function PDF occasionally counterbalance one another and make a wrong impression that Eqs. (1), (5), and (6) are well validated. However, "validation" of Eq. (1) by adopting a wrong PDF is definitely not validation. This example shows that *a posteriori* study performed by invoking several different submodels could lead to a wrong conclusion such as "validation" of a wrong submodel.

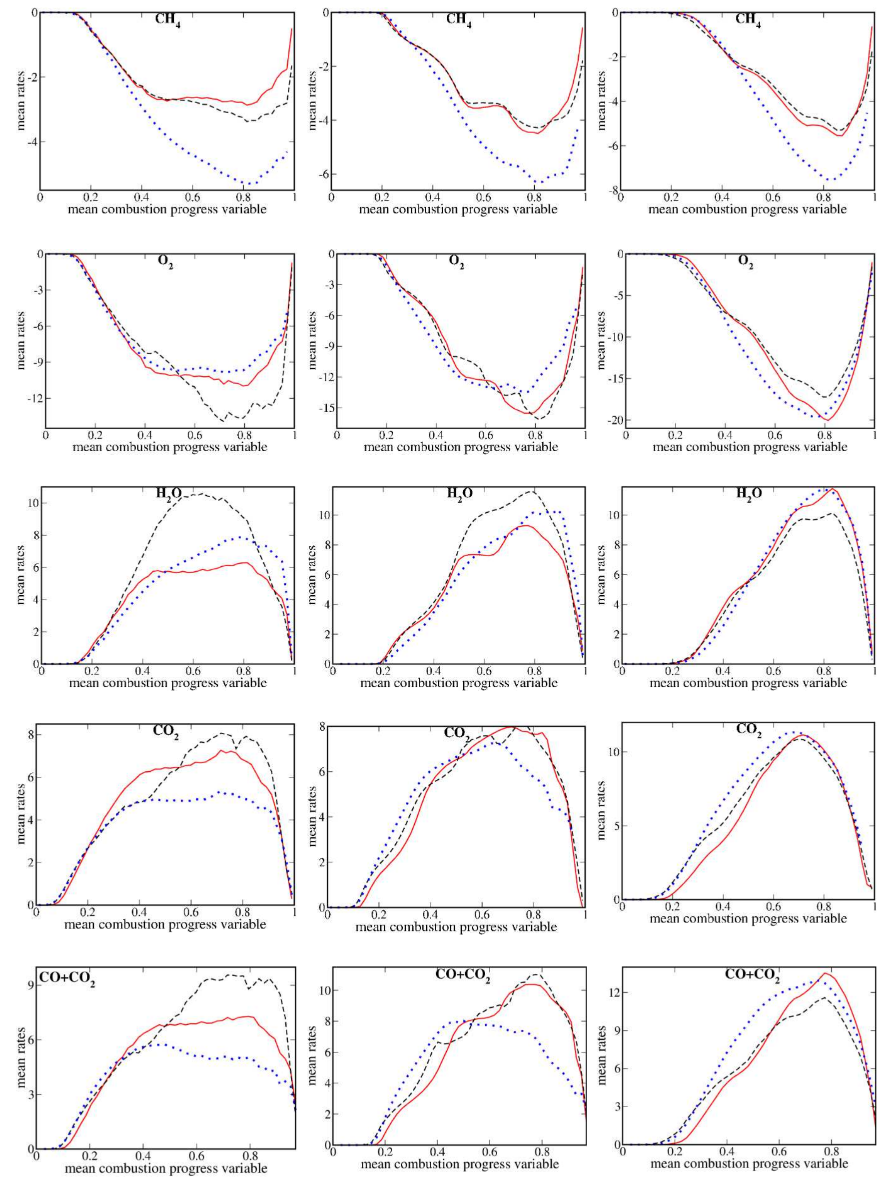

FIG. 13. Mean rates $\overline{W}_n$ [s^{-1}] of production/consumption of major products/reactants vs. mean combustion progress variables defined using the mass fraction Y_n of the same product/reactant. Legends are explained in caption to Fig. 12.

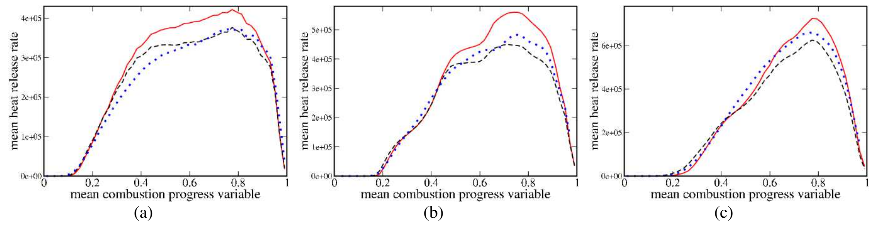

FIG. 14. Mean heat release rates $\overline{W}_T$ [K/s] vs. mean temperature-based combustion progress variable $\bar{c}_T$. Legends are explained in caption to Fig. 12.

Second, if the cases A1, A2, and A3 are considered all together, substitution of the β-function PDFs given by Eqs. (5) and (6) into Eq. (1) does not allow us to predict $\overline{W}_{c,k}$ for any c_k, cf. dotted and solid lines. In a single case, the use of certain c_k (e.g., c_2 in case A1, c_2 or c_3 in case A2, c_3 or c_T in case A3) can yield good results due to the aforementioned mutual cancellations of two types of errors. Indeed, in each of these five cases, the use of the actual PDF yields the profile of $\overline{W}_{c,k}(\bar{c}_k)$ that differs substantially from $\overline{W}_{c,k}(\bar{c}_k)$ calculated by adopting a less accurate β-function PDF.

Third, dependencies of $\overline{W}_{c,k}(\bar{c}_k)$ calculated by substituting the actual PDF into Eq. (1) differ substantially from dependencies of $\overline{W}_{c,k}(\bar{c}_k)$ extracted directly from the DNS data for $\bar{c}_2$ (with the exception of case A2), $\bar{c}_3$, $\bar{c}_4$ or $\bar{c}_5$ (in case A1), and $\bar{c}_T$. The differences (i) are less pronounced in case A3 and (ii) are small for the fuel-based $\bar{c}_1$ (with the exception of the trailing edges of the flame brushes in cases A1 and A2). Therefore, as far as modeling of the source term $\overline{W}_c$ in the transport equation for the mean combustion progress variable is concerned, Figs. 13 and 14 highlight the fuel-based c_1 and, to a lesser extent, the CO_2-based c_4. On the contrary, c_1 is not the best choice for evaluating the mean mass fraction of CO using Eq. (2), cf. red solid and dashed lines in the top row in Fig. 4, or the mean temperature using Eq. (3), cf. solid and dashed lines in the top row in Fig. 1. The CO_2-based c_4 or c_5 is the worst choice for calculating the mean temperature and density adopting Eqs. (3) and (4), respectively, cf. solid and dashed lines in the fourth rows in Figs. 1 and 2, respectively.

It is of interest to note that turbulent burning velocities obtained by integrating different $\langle W\rangle_{c,k}[\langle c\rangle_k(x,t)]$ along the normal to the mean flame brush can be substantially different even if the actual $\overline{W}_{c,k}(\bar{c}_k)$ appears to be close to $\overline{W}_{c,k}(\bar{c}_k)$ evaluated by substituting the actual PDF into Eq. (1). It is worth remembering that $\langle W\rangle_{c,k} = \langle W\rangle_k[\langle c\rangle_k(x,t)]$ and $\overline{W}_{c,k}[\bar{c}_k(x)]$ designate the rates averaged over the transverse plane at a single instant and the rates averaged over the transverse plane and various instants, respectively.

The aforementioned difference is reported in Fig. 15, which shows evolutions of turbulent burning velocities defined as follows

$$U_{T,k}(t) = \frac{1}{\rho_u\left(Y_{k,b} - Y_{k,u}\right)} \int_{-\infty}^{\infty} \langle\rho\rangle(x,t)\langle W\rangle_k[\langle c\rangle_k(x,t)]dx \quad (7)$$

for species-based combustion progress variables c_1 (CH_4), c_2 (O_2), c_3 (H_2O), and c_4 (CO_2) or

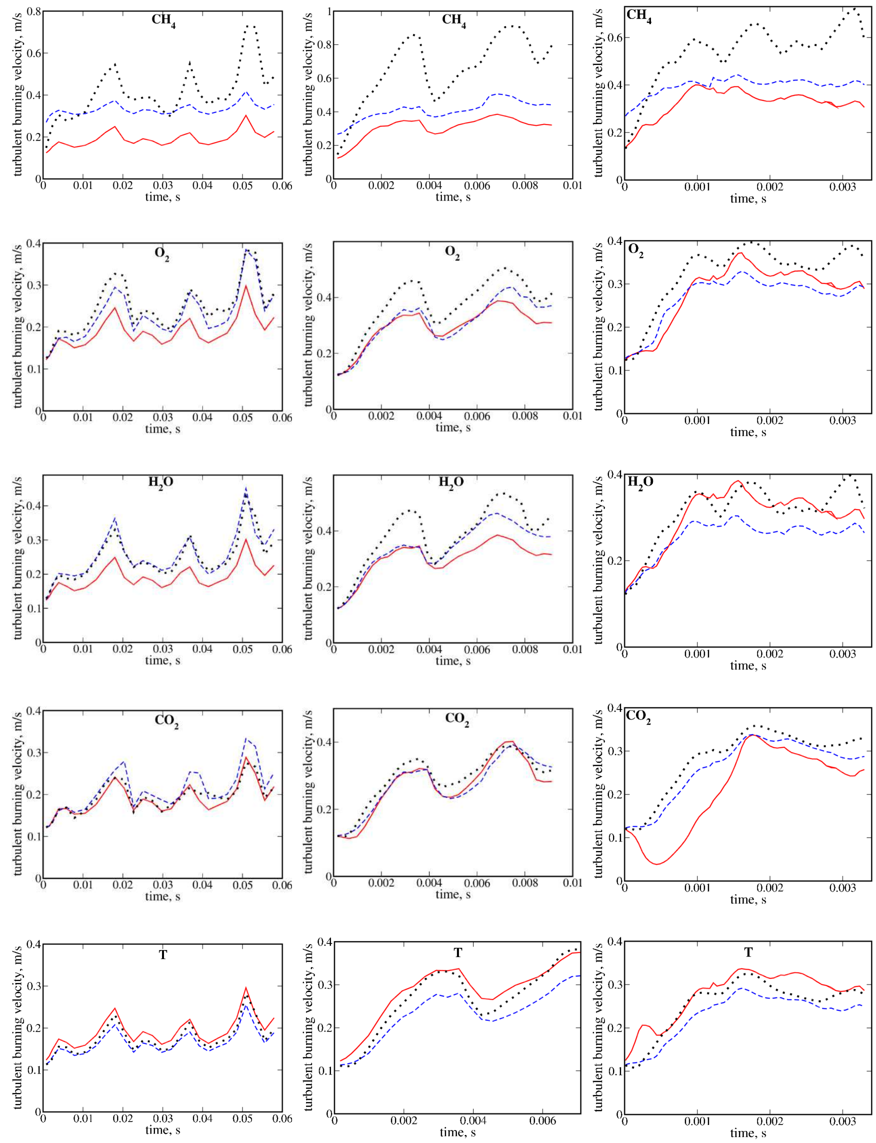

FIG. 15. Evolution of turbulent burning velocities evaluated using different combustion progress variables specified in the top of each subfigure. Solid lines show $U_{T,k}(t)$ calculated adopting $\overline{W}_k$ extracted from the DNS data. Dashed lines show $U_{T,k}(t)$ obtained using Eqs. (1), (7) or (8) and the PDF extracted from the DNS data. Dotted lines show $U_{T,k}(t)$ computed invoking the β-distribution PDF. Results obtained in cases A1, A2, and A3 are plotted in the left, middle, and right columns, respectively.

$$U_{T,6}(t) = \frac{1}{\rho_u(T_b - T_u)} \int_{-\infty}^{\infty} \langle\rho\rangle(x,t)\langle W\rangle_6[\langle c\rangle_6(x,t)]dx \tag{8}$$

for the temperature-based combustion progress variable c_6. For the fuel-based c_1, the actual $U_{T,1}(t)$, see solid lines in the top row, is substantially lower than $U_{T,1}(t)$ yielded by Eq. (1) with the actual PDF, see dashed lines, whereas the corresponding dependencies of $\overline{W}_{c,1}(\bar{c}_1)$ appear to be close to one another in the largest parts of the mean flame brushes, cf. solid and dashed lines in the top row in Fig. 13. This apparent inconsistency is associated with substantial contribution to the integral in Eq. (7) from thick zones characterized by large $\bar{c}_1$, where the two $\overline{W}_{c,1}(\bar{c}_1)$ differ from one another and the spatial gradient $d\bar{c}_1/dx$ is relatively low. Therefore, while results plotted in Figs. 13 and 14 highlight the fuel-based c_1, Fig. 15 does not do so.

On the contrary, Fig. 15 shows that, among the investigated c_k, the best agreement between the actual $U_{T,k}(t)$ and $U_{T,k}(t)$ yielded by Eq. (1) with the actual PDF has been obtained for the temperature-based c_6 and CO_2-based c_4 in case A1, the CO_2-based c_4 and O_2-based c_2 in case A2, and the O_2-based c_2, temperature-based c_5, and fuel-based c_1 in case A3. However, for instance, the dependencies of $\overline{W}_{c,4}(\bar{c}_4)$, plotted in solid and dashed lines in the left column in the fourth row in Fig. 13, are substantially different in case A1. Accordingly, comparison of Figs. 13 and 15 implies that the good results reported for the CO_2-based c_4 in case A1 in the latter figure stem, at least in part, from occasional mutual cancellation of errors in evaluation of $\overline{W}_{c,4}(\bar{c}_4)$ in different zones of the mean flame brush. This example demonstrates again the importance of using several different tests in a validation study.

If all three cases are considered together, Fig. 15 highlights the O_2-based c_2, the CO_2-based c_4, and, to a lesser extent, the temperature-based c_6. In particular, Eqs. (7) and (1) with the actual PDF perform excellent for the CO_2-based c_4 in cases A1 and A2 but fail in case A3. Moreover, the use of c_4 does not allow Eqs. (3) and (4) to predict the mean temperature and density, respectively, see the fourth rows in Figs. 1 and 2, respectively. Furthermore, Eq. (2) with c_4 performs substantially worse for CH_4, CO, see the fourth row in Fig. 4, and many intermediate species when compared to the same Eq. (2) with the temperature-based c_6. As far as the O_2-based c_2 is concerned, its use yields worse results for the mean density, see Fig. 1, as well as mass fractions of CO, see Fig. 4, CH_2O, see Fig. 5, CH_3, see Fig. 6, HCO and CH_3O, see Fig. 8.

IV. IMPLICATIONS FOR MODELING

The present DNS data show that Eq. (1), Eqs. (2)-(4), and Eq. (7) or (8) perform differently for differently defined combustion progress variables. In particular, Eqs. (2)-(4) perform best for the temperature-based c_6. However, application of Eq. (1) and Eq. (8) to c_6 yields underestimated $\overline{W}_{c,6}(\bar{c}_6)$ and $U_{T,6}(t)$. Equation (1) performs best for the fuel-based c_1 and, to a lesser extent, for the CO_2-based c_4, whereas Eq. (7) performs best for the O_2-based c_2 and for the CO_2-based c_4. However, as discussed earlier, Eqs. (2)-(4) perform substantially worse with c_1, c_2, c_4 or c_5 when compared to c_T. Thus, the present results considered all together imply that mean mass fractions of various species can be evaluated by adapting Eq. (2) independently of Eq. (1), for example, by invoking a model of the mean (or filtered) rate $\overline{W}_c$, which performs better than Eq. (1). The reader interested in such models is referred to review literature.[86,90-94]

If an appropriate model of the influence of turbulence on premixed combustion is invoked and the mean fields of $\bar{c}$ and $\overline{W}_c$ are obtained either directly within the RANS framework or by averaging the counterpart filtered fields within the LES framework, the mean mass fractions of various species can simply be calculated at a post-processing stage of the simulations using Eq. (2). To do so, not only a closure relation for the mean (or filtered) rate $\overline{W}_c$, but also a PDF $P(c,\mathbf{x},t)$ are required and modeling the PDF still challenges the combustion community. The issue could be addressed by developing the approach that deals with a transport equation for the PDF.[4,11-14] This research direction appears to be prioritized from the fundamental perspective and the present study provides additional motivation for developing it.

Nevertheless, from the application perspective, the presumed PDF approach may also deserve development, e.g. by taking the following opportunity. If Eq. (1) is not applied to close the mean rate $\overline{W}_c$, but another model of $\overline{W}_c$ is invoked, then the following equation

$$\overline{c^2}(\mathbf{x},t) = \int_0^1 c^2 P(c,\mathbf{x},t)dc, \tag{9}$$

which is commonly used to evaluate unknown parameters of a presumed PDF $P(c,\mathbf{x},t)$, could be substituted with a constraint of

$$\overline{W}_c(\mathbf{x},t) = \int_0^1 W_c(c) P(c,\mathbf{x},t)dc. \tag{10}$$

Therefore, the presumed PDF is calibrated by (i) invoking a closure relation for $\overline{W}_c(\mathbf{x},t)$ yielded by another model that is not based on a PDF $P(c,\mathbf{x},t)$ and (ii) adopting Eq. (10) instead of Eq. (9). The use of Eq. (10) for PDF calibration will, in particular, offer an opportunity to obtain a PDF that better predicts the probability of finding reaction zones. Indeed, the mean rate $\overline{W}_c(\mathbf{x},t)$ is directly linked with that probability, whereas such a link appears to be doubtful for the variance $\overline{c''^2}(\mathbf{x},t)$ or $\widetilde{c''^2}(\mathbf{x},t)$.[17,86] For instance, these variances are solely controlled by the probabilities of finding unburned (fresh) reactants and fully burned products in the BML limit.[69]

Encouraging results obtained in the present study by testing the flamelet Eqs. (2)-(4) suggest that the presumed PDF approach could substantially be advanced (i) adapting the classical flamelet PDF,[66] i.e. $1/(\delta_L|\nabla c|_L)$, but also (ii) invoking Eq. (10) to calibrate the PDF, as argued above. Recently, this proposal was developed[51,53] by analyzing DNS data obtained by Dave and Chaudhuri[54] and Im et al.[55-59] from a lean hydrogen-air flame characterized by two different equivalence ratios and four different Karlovitz numbers ranging from 0.75 to 126. Further development and assessment of such a presumed flamelet-based PDF will be a subject for future analysis of the present DNS data.

V. CONCLUDING REMARKS

A quantitative *a priori* assessment of the simplest version of flamelet approach to evaluating the mean density $\bar{\rho}$, the mean temperature $\overline{T}$, the mean mass fractions $\overline{Y}_n$ of various species, and the mean rates of the species production/consumption in a premixed turbulent flame has been performed by analysing complex-chemistry DNS data obtained earlier[45,60] from three lean methane-air flames characterized by three different Karlovitz numbers ranging from 6 to 540. The approach consists in (i) simulating the unperturbed laminar flame in order to obtain dependencies of the temperature, density, and mass fractions of various species on a single combustion progress variable c and (ii) averaging these dependencies by invoking a PDF for the same combustion progress variable, see Eqs. (2)-(4). When assessing the approach, six different choices of c have been probed and the PDF (i) either has been extracted directly from the DNS data or (ii) has been modelled invoking the well-known presumed β-function and using the first two moments of the c-field yielded by the DNS data. A similar method, see Eq. (1), has also been applied to assessing capabilities of the flamelet approach for predicting the mean source term $\overline{W}_c$ in the transport equation for the mean combustion progress variable.

The major results of this analysis are as follows.

- First, at all three Ka, substitution of (i) the actual PDF extracted from the DNS data and (ii) the simplest flamelet library $\rho_L(c)$, $T_L(c)$, and $Y_{n,L}(c)$, computed for a single unperturbed laminar premixed flame, into Eqs. (2)-(4) has allowed us to quantitatively predict the profiles of $\bar{\rho}(\bar{c})$, $\bar{T}(\bar{c})$, and $\bar{Y}_n(\bar{c})$ for CH_4, O_2, H_2O, CO_2, CO, CH_2O, CH_3, and HCO provided that the combustion progress variable is appropriately defined (it is based on the temperature for the studied lean methane-air flames). For the other seven species, with the exception of CH_3O at the highest Ka, the results are also encouraging.
- Second, the β-function PDF differs significantly from the actual PDF extracted from the DNS data and the use of the β-function PDF yields substantially worse results for intermediate species such as OH, O, H, CH_3, and HCO.
- Third, for all investigated combustion progress variables, the mean rates W_n of production/consumption of various species (e.g., the radicals O and OH) are poorly predicted by Eq. (1) even if the actual PDF is adopted. Moreover, if all three flames are considered together, Eq. (1) does not simultaneously predict (i) the profiles $\overline{W}_{c,k}(\bar{c}_k)$ of the mean rate of product creation and (ii) turbulent burning velocities $U_{t,k}$ obtained by integrating these profiles. For instance, $\overline{W}_{c,k}(\bar{c}_k)$ is reasonably well predicted adopting the fuel-based combustion progress variable but $U_{t,k}$ is reasonably well predicted using the oxygen-based combustion progress variable.

These three major findings are consistent with recent results[50,52] computed by analyzing other DNS data obtained from four lean hydrogen-air premixed turbulent flames characterized by two different equivalence ratios and Karlovitz numbers ranging from 0.75 to 126. However, the present study addresses a significantly higher $Ka = 540$ (case A3) and a more complicated chemical system (when compared to hydrogen, combustion of methane involves more reactions and more species). For instance, we are not aware of a study that shows capability of Eq. (2) for quantitatively predicting mean mass fractions of carbon-containing intermediate species (including CO) in premixed or stratified turbulent flames. Moreover, results obtained from flame A3 indicate, for the first time to the best of the present authors knowledge, that performance of Eq. (2) in highly turbulent flames can be improved by using a flamelet library obtained from equidiffusive unperturbed laminar flame.

Consistency of the present and recent[50,52] results implies that the three major findings highlighted above are sufficiently general, while other details (e.g. the best choice of a combustion progress variable) could be mixture sensitive. For instance, the fuel-based combustion progress variable performs better in the aforementioned hydrogen flames, while the temperature-based c performs sufficiently well also.

The highlighted findings imply that, in order to evaluate the mean temperature, density and species mass fractions, Eqs. (2)-(4) could be coupled with another model of premixed turbulent combustion whose predictive capabilities are better documented when compared to Eq. (1). In such a case, Eqs. (2)-(4) could be implemented as post-processing of a mean $\bar{c}$-field computed by numerically integrating a single transport equation for the mean combustion progress variable.

As already mentioned, the best predictions of the mean concentrations of various species in the studied lean methane-air flame were obtained using the temperature-based combustion progress variable, while this conclusion could be mixture sensitive. Selection of a progress variable c_k that yields the lowest maximum absolute value of the second derivative d^2Y_n/dc_k^2 in the laminar flame and, therefore, is associated with a less non-linear profile $Y_n(c_k)$ could be recommended for a study aimed at predicting the mean mass fraction $\bar{Y}_n$ using Eq. (2).

It is also worth noting that the use of the profiles $Y_{n,L,Le=1}(c)$ obtained from the equidiffusive laminar flame improves predictions of mean concentrations of certain (but not all) species at the highest Ka. This observation implies that (i) the boundary of validity of Eq. (2) with the canonical laminar-flame profiles $Y_{n,L}(c)$ is close to $Ka = O(540)$ for the studied lean methane-air mixture and (ii) the averaged influence of preferential diffusion phenomena on the local flame structure is reduced at higher Karlovitz numbers, in line with earlier studies.[80-84] If small-scale turbulent mixing changes the local flame structure, larger-scale eddies can still strain the flame. Accordingly, substitution into Eq. (2) of the profiles $Y_{n,L,Le=1}(c)$ obtained from equidiffusive strained laminar flames could be an interesting task for future research.

Similar to the vast majority of recent complex-chemistry DNS studies of highly turbulent premixed flames,[55-61,78-84] the present analysis is restricted to small-scale turbulence, because 3D complex-chemistry DNS of combustion in intense and large-scale turbulence is not yet computationally affordable. Accordingly, Damköhler numbers addressed in the present and other DNS works may appear to be too low when compared to conditions reached in contemporary engines. However, it is worth remembering that the explored flamelet approach is commonly considered to work better at higher Damköhker and lower Karlovitz numbers. Therefore, the conditions of the present study appear to be more challenging for its goals when compared to flames characterized by $Da > 1$. Accordingly, the major conclusions are expected to hold under higher Damköhler numbers.

All in all, the flamelet-based Eqs. (2)-(4) appear to be a useful CFD tool even at Karlovitz number as large as 540 provided that an appropriate definition of combustion progress variable is adopted, and the PDF is well modeled. Therefore, these results (i) indicate that the domain of the flamelet concept validity is substantially wider than it was earlier assumed, in line with recent studies,[48,49] and (ii) motivate modeling the PDF in Eqs. (2)-(4). Extension of the present work to filtered scalar fields and filtered density functions computed in a LES is another subject for future studies.

ACKNOWLEDGEMENTS

ANL gratefully acknowledges the financial support provided by CERC. TL, RY, and XSB gratefully acknowledge the financial support provided by the Swedish Research Council (VR). VAS gratefully acknowledges the financial support from ONERA and from the Grant of the Ministry of Education and Science of the Russian Federation (Contract No. 14.G39.31.0001 of February 13, 2017). Computations were performed on resources provided by the Swedish National Infrastructure for Computing (SNIC) at PDC and HPC2N.

DATA AVAILABILITY

The data that support the findings of this study are available from the corresponding author upon reasonable request.

REFERENCES

[1]E. E. O'Brien, "Turbulent mixing in systems with simple reactions," in *Turbulent Mixing in Nonreactive and Reactive Flows*, edited by S. N. B. Murthy (Springer-Verlag, Berlin, Germany, 1975), pp. 209–224.

[2]C. Dopazo and E. E. O'Brien, "Statistical treatment of non-isothermal chemical reactions in turbulence," Combust. Sci. Technol. **13**, 99 (1976).

[3]E. E. O'Brien, "Stochastic properties of scalar quantities advected by a non-buoyant plume," J. Fluid Mech. **89**, 209 (1978).

[4]E. E. O'Brien, "The probability density function (pdf) approach to reacting turbulent flows," in *Turbulent Reacting Flows*, edited by P. A. Libby and F. A. Williams (Springer-Verlag, Berlin, Germany, 1980), pp. 185–218.

[5]R. Meyers and E. E. O'Brien, "The joint pdf of a scalar and its gradient at a point in a turbulent fluid," Combust. Sci. Technol. **26**, 123 (1980).

[6]Y. Y. Kuo and E. E. O'Brien, "Two-point probability density function closure applied to a diffusive-reactive system," Phys. Fluids **24**, 194 (1981).

[7]F. Gao and E. E. O'Brien, "Joint probability density function of a scalar and its gradient in isotropic turbulence," Phys. Fluids A: Fluid Dyn. **3**, 1625 (1991)

[8]T. Jiang and E. E. O'Brien, "Schmidt, Damköhler and Reynolds number effects on second-order reactions in isotropic turbulence," Chem. Eng. Comm. **106**, 185 (1991)

[9]A. Sahay and E. E. O'Brien, "Uniform mean scalar gradient in grid turbulence: Conditioned dissipation and production," Phys. Fluids A: Fluid Dyn. **5**, 1076 (1993)

[10]F. Gao and E. E. O'Brien, "A large-eddy simulation scheme for turbulent reacting flows," Phys. Fluids A: Fluid Dyn. **5**, 1282 (1993)

[11]V. R. Kuznetsov and V. A. Sabelnikov, *Turbulence and Combustion* (Hemisphere Publishing Corporation, New York, 1990).

[12]C. Dopazo, "Recent developments in PDF methods," in Turbulent Reacting Flows, edited by P. A. Libby and F. A. Williams (Academic Press, London, 1994), pp. 375–474.

[12]D. C. Haworth, "Progress in probability density function methods for turbulent reacting flows," Prog. Energy Combust. Sci. **36**, 168 (2010).

[14]S. B. Pope, "Small scales, many species and the manifold challenges of turbulent combustion," Proc. Combust. Inst. **34**, 1 (2013).

[15]N. Peters, "Laminar flamelet concepts in turbulent combustion," Proc. Combust. Inst. **21**, 1231 (1986).

[16]L. Y. M. Gicquel, G. Staffelbach, and T. Poinsot, "Large Eddy Simulations of gaseous flames in gas turbine combustion chambers," Prog. Energy Combust. Sci. **38**, 782 (2012).

[17]A. N. Lipatnikov, "Stratified turbulent flames: Recent advances in understanding the influence of mixture inhomogeneities on premixed combustion and modeling challenges," Prog. Energy Combust. Sci. **62**, 87 (2017).

[18]O. Gicquel, N. Darabiha, and D. Thévenin, "Laminar premixed hydrogen/air counterflow flame simulations using flame prolongation of ILDM with differential diffusion," Proc. Combust. Inst. **28**, 1901 (2000).

[19]J. A. van Oijen and L. P. H. de Goey, "Modeling of premixed laminar flames using flamelet generated manifolds," Combust. Sci. Technol. **161**, 113 (2000).

[20]In applications, a flamelet library is sometimes stored adopting a set of independent variables $\boldsymbol{\xi}$, which may consist not only of a combustion progress variable c, but also of a mixture fraction in the case of stratified combustion, the mixture enthalpy in the case of non-adiabatic flame, pressure in the case of non-isobaric burning (e.g. in a piston engine), stretch rate in highly turbulent flames, etc. In the present paper, the generic case of a single independent scalar variable c is considered.

[21]B. Fiorina, O. Gicquel, L. Vervisch, S. Carpentier, and N. Darabiha, "Premixed turbulent combustion modeling using tabulated detailed chemistry and PDF," Proc. Combust. Inst. **30**, 867 (2005).

[22]P. Domingo, L. Vervisch, S. Payet, and R. Hauguel, "DNS of a premixed turbulent V flame and LES of a ducted flame using a FSD-PDF subgrid scale closure with FPI-tabulated chemistry," Combust. Flame **143**, 566 (2005).

[23]B. Jin, R. Grout, and W. K. Bushe, "Conditional source-term estimation as a method for chemical closure in premixed turbulent reacting flow," Flow Turbul. Combust. **81**, 563 (2008).

[24]J. Galpin, A. Naudin, L. Vervisch, C. Angelberger, O. Colin, and P. Domingo, "Large-eddy simulation of a fuel-lean premixed turbulent swirl-burner," Combust. Flame **155**, 247 (2008).

[25]A. W. Vreman, J. A. van Oijen, L. P. H. de Goey, and R. J. M. Bastiaans, "Subgrid scale modeling in large-eddy simulation of turbulent combustion using premixed flamelet chemistry," Flow Turbul. Combust. **82**, 511 (2009).
[26]M. M. Salehi and W. K. Bushe, "Presumed PDF modeling for RANS simulation of turbulent premixed flames," Combust. Theory Modelling **4**, 381 (2010).
[27]H. Kolla and N. Swaminathan, "Strained flamelets for turbulent premixed flames II: Laboratory flame results," Combust. Flame **157**, 1274 (2010).
[28]F. Hernández-Pérez, F. Yuen, C. Groth, and Ö. Gülder, "LES of a laboratory-scale turbulent premixed Bunsen flame using FSD, PCM-FPI and thickened flame models," Proc. Combust. Inst. **33**, 1365 (2011).
[29]G. Lecocq, S. Richard, O. Colin, and L. Vervisch, "Hybrid presumed pdf and flame surface density approaches for Large-Eddy Simulation of premixed turbulent combustion. Part 1: Formalism and simulation of a quasi-steady burner," Combust. Flame **158**, 1201 (2011).
[30]O. R. Darbyshire and N. Swaminathan, "A presumed joint PDF model for turbulent combustion with varying equivalence ratio," Combust. Sci. Technol. **184**, 2036 (2012).
[31]M. M. Salehi, W. K. Bushe, N. Shahbazian, and C. R. T. Groth, "Modified laminar flamelet presumed probability density function for LES of premixed turbulent combustion," Proc. Combust. Inst. **34**, 1203 (2013).
[32]E. V. Klapdor, F. di Mare, W. Kollmann, and J. Janicka, "A compressible pressure-based solution algorithm for gas turbine combustion chambers using the PDF/FGM model," Flow Turbul. Combust. **191**, 209 (2013).
[33]P. Trisjono, K. Kleinheinz, S. Kang, and H. Pitsch, "Large eddy simulation of stratified and sheared flames of a premixed turbulent stratified flame burner using a flamelet model with heat loss," Flow Turbul. Combust. **92**, 201 (2014).
[34]F. Hernández-Pérez, C. Groth, and Ö. Gülder, "Large-eddy simulation of lean hydrogen-methane turbulent premixed flames in the methane-dominated regime," Int. J. Hydrogen Energy 39, 7147 (2014).
[35]S. Nambully, P. Domingo, V. Moreau, and L. Vervisch, "A filtered-laminar-flame PDF sub-grid scale closure for LES of premixed turbulent flames: I. Formalism and application to a bluff-body burner with differential diffusion," Combust. Flame **161**, 1756 (2014).
[36]S. Nambully, P. Domingo, V. Moreau, and L. Vervisch, "A filtered-laminar-flame PDF sub-grid scale closure for LES of premixed turbulent flames: II. Application to a stratified bluff-body burner," Combust. Flame **161**, 1775 (2014).
[37]N. Shahbazian, M. M. Salehi, C. P. T. Groth, Ö. L. Gülder, and W. K. Bushe, "Performance of conditional source-term estimation model for LES of turbulent premixed flames in thin reaction zones regime," Proc. Combust. Inst. **35**, 1367 (2015).
[38]J. A. van Oijen, A. Donini, R. J. M. Bastiaans, J. H. M. ten Thije Boonkkamp, and L. P. H. de Goey, "State-of-the-art in premixed combustion modeling using flamelet generated manifolds," Prog. Energy Combust. Sci. **57**, 30 (2016).
[39]I. Langella, N. Swaminathan, "Unstrained and strained flamelets for LES of premixed combustion," Combust. Theory Modelling **20**, 410 (2016).
[40]G. M. Ottino, A. Fancello, M. Falcone, R. J. M. Bastiaans, and L. P. H. de Goey, "Combustion modeling including heat loss using Flamelet Generated Manifolds: A validation study in OpenFOAM," Flow Turbul. Combust. **96**, 773 (2016).
[41]I. Langella, N. Swaminathan, and R. W. Pitz, "Application of unstrained flamelet SGS closure for multiregime premixed combustion," Combust. Flame **173**, 161 (2016).
[42]S. Lapointe and G. Blanquart, "A priori filtered chemical source term modeling for LES of high Karlovitz number premixed flames," Combust. Flame **176**, 500 (2017).
[43]A. Donini, R. J. M. Bastiaans, J. A. van Oijen, and L. P. H. de Goey, "A 5-D implementation of FGM for the large eddy simulation of a stratified swirled flame with heat loss in a gas turbine combustor," Flow Turbul. Combust. **98**, 887 (2017).
[44]F. C. C. Galeazzo, B. Savard, H. Wang, E. R. Hawkes, J. H. Chen, and G. C. K. Filho, "Performance assessment of flamelet models in flame-resolved LES of a high Karlovitz methane/air stratified premixed jet flame," Proc. Combust. Inst. **37**, 2545 (2019).
[45]T. Nilsson, R. Yu, N. A. K. Doan, I. Langella, N. Swaminathan, and X. S. Bai, "Filtered reaction rate modelling in moderate and high Karlovitz number flames: an a priori analysis," Flow Turbul. Combust. **103**, 643 (2019).
[46]A. N. Lipatnikov and J. Chomiak, "Effects of premixed flames on turbulence and turbulent scalar transport," Prog. Energy Combust. Sci. **36**, 1 (2010).
[47]V. A. Sabelnikov and A. N. Lipatnikov, "Recent advances in understanding of thermal expansion effects in premixed turbulent flames," Annu. Rev. Fluid Mech. **49**, 91 (2017).
[48]J. F. Driscoll, J. H. Chen, A. W. Skiba, C. D. Carter, E. R. Hawkes, and H. Wang, "Premixed flames subjected to extreme turbulence: Some questions and recent answers," Prog. Energy Combust. Sci. **76**, 100802 (2020).
[49]A. W. Skiba, C. D. Carter, S. D. Hammack, and J. F. Driscoll, "Experimental assessment of the progress variable space structure of premixed flames subjected to extreme turbulence," Proc. Combust. Inst. **38**, https://doi.org/10.1016/j.proci.2020.06.129
[50]A. N. Lipatnikov and V. A: Sabelnikov, "Evaluation of mean species mass fractions in premixed turbulent flames: A DNS study," Proc. Combust. Inst. **38**, https://doi.org/10.1016/j.proci.2020.05.006
[51]A. N. Lipatnikov and V. A. Sabelnikov, "An extended flamelet-based presumed probability density function for predicting mean concentrations of various species in premixed turbulent flames," Int. J. Hydrogen Energy **45**, 31162 (2020).
[52]A. N. Lipatnikov, V. A. Sabelnikov, F. E. Hernández-Pérez, W. Song, and H. G. Im, "A priori DNS study of applicability of flamelet concept to predicting mean concentrations of species in turbulent premixed flames at various Karlovitz numbers," Combust. Flame **222**, 370 (2020).
[53]A. N. Lipatnikov, V. A. Sabelnikov, F. E. Hernández-Pérez, W. Song, and H. G. Im, "Prediction of mean radical concentrations in lean hydrogen-air turbulent flames at different Karlovitz numbers adopting a newly extended flamelet-based presumed PDF," Combust. Flame **226**, 248 (2021).
[54]H. Dave and S. Chaudhuri, "Evolution of local flame displacement speeds in turbulence," J. Fluid Mech. **884**, A46 (2020).
[55]H. A. Uranakara, S. Chaudhuri, H. L. Dave, P. G. Arias, and H. G. Im, "A flame particle tracking analysis of turbulence-chemistry interaction in hydrogen-air premixed flames," Combust. Flame 163, **220** (2016).

[56]H. G. Im, P. G. Arias, S. Chaudhuri, H. A. Uranakara, "Direct numerical simulations of statistically stationary turbulent premixed flames," Combust. Sci. Technol. **188**, 1182 (2016).
[57]D. H. Wacks, N. Chakraborty, M. Klein, P. G. Arias, and H. G. Im, "Flow topologies in different regimes of premixed turbulent combustion: A direct numerical simulation analysis," Phys. Rev. Fluids **1**, 083401 (2016).
[58]D. M. Manias, E. Al. Tingas, F. E. Hernández Pérez, R. M. Galassi, P. P. Ciottoli, M. Valorani, and H. G. Im, "Investigation of the turbulent flame structure and topology at different Karlovitz numbers using the tangential stretching rate index," Combust. Flame **200**, 155 (2019).
[59]M. Klein, A. Herbert, H. Kosaka, B. Böhm, A. Dreizler, N. Chakraborty, V. Papapostolou, H. G. Im, and J. Hasslberger, "Evaluation of flame area based on detailed chemistry DNS of premixed turbulent hydrogen-air flames in different regimes of combustion," Flow Turbul. Combust. **104**, 403 (2020).
[60]T. Nilsson, H. Carlsson, R. Yu, and X. S. Bai, "Structures of turbulent flames in the high Karlovitz number regime – DNS analysis," Fuel **216**, 627 (2018).
[61]R. Yu, T. Nilsson, X. S. Bai, and A. N. Lipatnikov, "Evolution of averaged local premixed flame thickness in a turbulent flow," Combust. Flame **207**, 232 (2019).
[62]N. Peters, "The premixed turbulent flame in the limit of a large activation energy," J. Non-Equil. Thermodyn. **7**, 25 (1982).
[63]D. Bradley, P. H. Gaskell, and A. K. C. Lau, "A mixedness-reactedness flamelet model for turbulent diffusion flames," Proc. Combust. Inst. **23**, 685 (1990).
[64]D. Bradley, P. H. Gaskell, and X. J. Gu, "The mathematical modeling of liftoff and blowoff of turbulent non-premixed methane jet flames at high strain rates," Proc. Combust. Inst. **27**, 1199 (1998).
[65]P. A. Libby and F. A. Williams, "Presumed PDF analysis of partially premixed turbulent combustion," Combust. Sci. Technol. **161**, 359 (2000).
[66]K. N. C. Bray, M. Champion, P. A. Libby, and N. Swaminathan, "Finite rate chemistry and presumed PDF models for premixed turbulent combustion," Combust. Flame **146**, 665 (2006).
[67]M. Pfitzner, "A new analytic pdf for simulations of premixed turbulent combustion," Flow Turbul. Combust. https://doi.org/10.1007/s10494-020-00137-x
[68]M. Pfitzner and M. Klein, "A near-exact analytic solution of progress variable and pdf for single-step Arrhenius chemistry," Combust. Flame **226**, 380 (2021).
[69]K. N. C. Bray, P. A. Libby, and J. B. Moss, "Unified modeling approach for premixed turbulent combustion - Part I: General formulation," Combust. Flame 61, **87** (1985).
[70]S. Ghosal, T. S. Lund, P. Moin, and K. Akselvoll, "A dynamic localization model for large-eddy simulation of turbulent flows," J. Fluid Mech. **286**, 229 (1995).
[71]R. Yu and A. N. Lipatnikov, "DNS study of dependence of bulk consumption velocity in a constant-density reacting flow on turbulence and mixture characteristics," Phys. Fluids **29**, 065116 (2017).
[72]M. D. Smooke and V. Giovangigli, *Reduced Kinetic Mechanisms and Asymptotic Approximation for Methane-air Flames* (Springer, Berlin, Germany, 1991).
[73]R. Yu, J. Yu, and X. S. Bai, "An improved high-order scheme for DNS of low Mach number turbulent reacting flows based on stiff chemistry solver," J. Comp. Phys. **231**, 5504 (2012).
[74]G. Strang, "On the construction and comparison of difference schemes," Siam J. Num. Anal. **5**, 506 (1968).
[75]P. N. Brown, G. D. Bryne, and A. C. Hindmarsch, "VODE, a variable-coefficient ODE solver," SIAM J. Sci. Stat. Comp. **10**, 1038 (1989).
[76]R. Yu and X. S. Bai, "A semi-implicit scheme for large eddy simulation of piston engine flow and combustion," Int. J. Numer. Methods Fluids 71, **13** (2013).
[77]H. Carlsson, R. Yu, and X. S. Bai, "Direct numerical simulation of lean premixed CH_4/air and H_2/air flames at high Karlovitz numbers," Int. J. Hydrogen Energy **39**, 20216 (2014).
[78]A. J. Aspden, M. S., Day, and J. B. Bell, "Turbulence-chemistry interaction in lean premixed hydrogen combustion," Proc. Combust. Inst. **35**, 1321 (2015).
[79]D. Dasgupta, W. Sun, M. Day, and T. Lieuwen, "Effect of turbulence-chemistry interactions on chemical pathways for turbulent hydrogen-air premixed flames," Combust. Flame **176**, 191 (2017).
[80]A. J. Aspden, M. S. Day, and J. B. Bell, "Turbulence-flame interactions in lean premixed hydrogen: transition to the distributed burning regime," J. Fluid Mech. **680**, 287 (2011).
[81]B. Savard, G. Blanquart, "An a priori model for the effective species Lewis numbers in premixed turbulent flames," Combust. Flame **161**, 1547 (2014).
[82]S. Lapointe, B., Savard, and G. Blanquart, "Differential diffusion effects, distributed burning, and local extinction in high Karlovitz premixed flames," Combust. Flame **162**, 3341 (2015).
[83]A. J. Aspden, M. S. Day, and J. B. Bell, "Three-dimensional direct numerical simulation of turbulent lean premixed methane combustion with detailed kinetics," Combust. Flame **166**, 266 (2016).
[84]A. J. Aspden, M. S. Day, and J. B. Bell, "Towards the distributed burning regime in turbulent premixed flames," J. Fluid Mech. **871**, 1 (2019).
[85]A. N. Lipatnikov and J. Chomiak, "Molecular transport effects on turbulent flame propagation and structure," Prog. Energy Combust. Sci. **31**, 1 (2005).
[86]A. N. Lipatnikov, *Fundamentals of Premixed Turbulent Combustion* (CRC Press, Boca Raton, Florida, 2012).
[87]P. Venkateswaran, A. Marshall, D.H. Shin, D. Noble, J. Seitzman, and T. Lieuwen, "Measurements and analysis of turbulent consumption speeds of H_2/CO mixtures," Combust. Flame **158**, 1602 (2011).
[88]P. Venkateswaran, A. Marshall, J. Seitzman, and T. Lieuwen, "Pressure and fuel effects on turbulent consumption speeds of H_2/CO blends," Proc. Combust. Inst. **34**, 1527 (2013).
[89]S. Yang, A. Saha, W. Liang, F. Wu, and C.K. Law, "Extreme role of preferential diffusion in turbulent flame propagation," Combust. Flame **188**, 498 (2018).

[90]A. N. Lipatnikov and J. Chomiak, "Turbulent flame speed and thickness: Phenomenology, evaluation, and application in multi-dimensional simulations," Prog. Energy Combust. Sci. **28**, 1 (2002).
[91]T. Poinsot and D. Veynante, *Theoretical and Numerical Combustion*, 2nd ed. (Edwards, Philadelphia, 2005).
[92]R. W. Bilger, S. B. Pope, K. N. C. Bray, and J. F. Driscoll, "Paradigms in turbulent combustion research," Proc. Combust. Inst. **30**, 21 (2005).
[93]T. Echekki and E. Mastorakos (Eds.), *Turbulent Combustion Modeling* (Springer, Berlin, 2011).
[94]N. Swaminathan, K.N.C. Bray (Eds.), *Turbulent Premixed Flames* (Cambridge University Press, Cambridge, U.K., 2011).

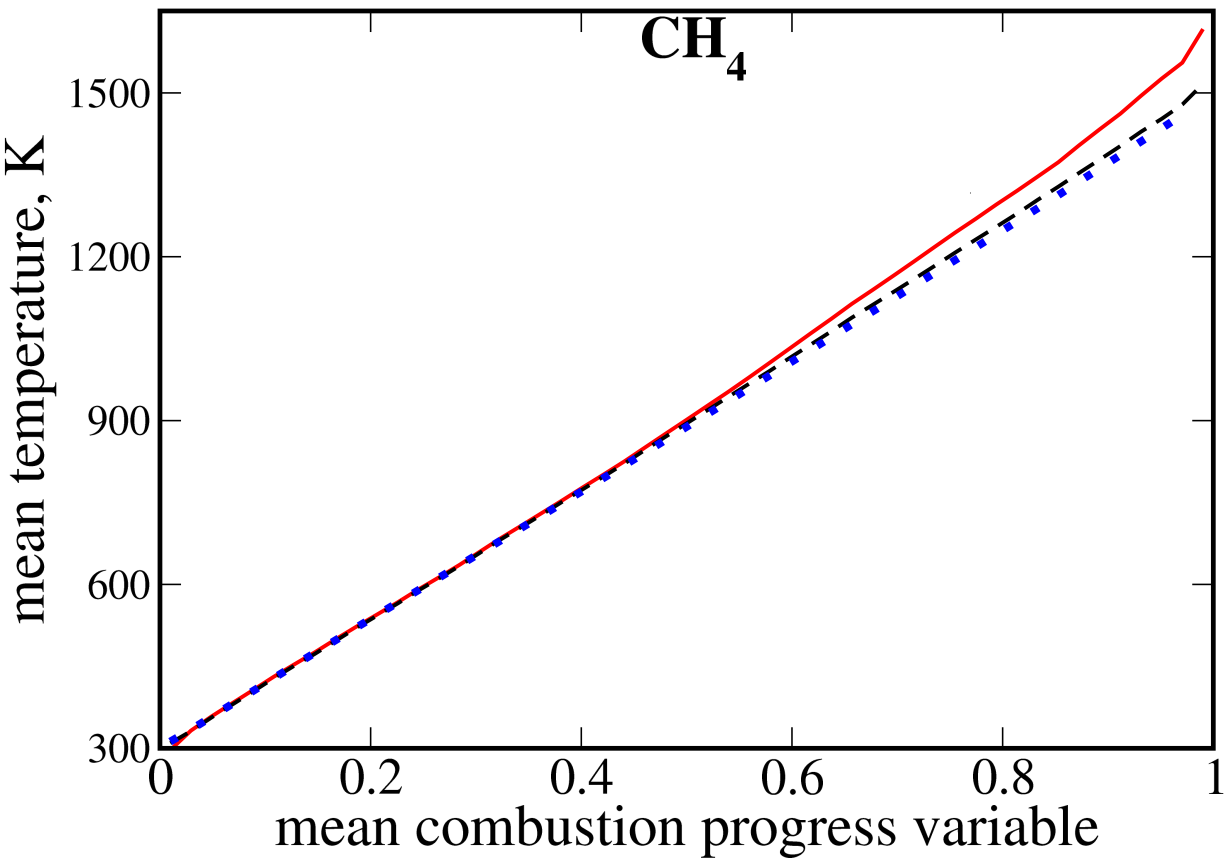
CH4
1500
1200
900
600
300
0
0.2
0.4
0.6
0.8
1
mean temperature, K
mean combustion progress variable

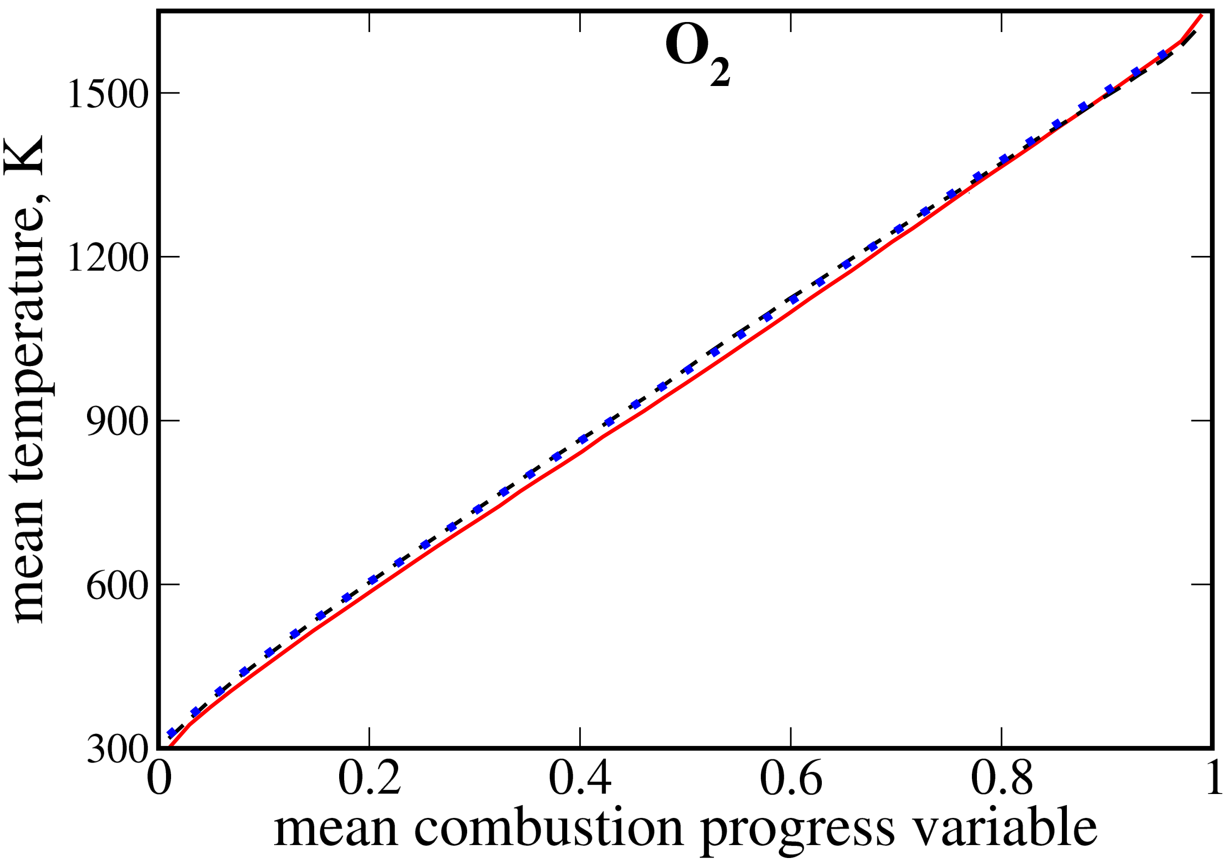
O_2
mean temperature, K
300
600
900
1200
1500
0
0.2
0.4
0.6
0.8
1
mean combustion progress variable

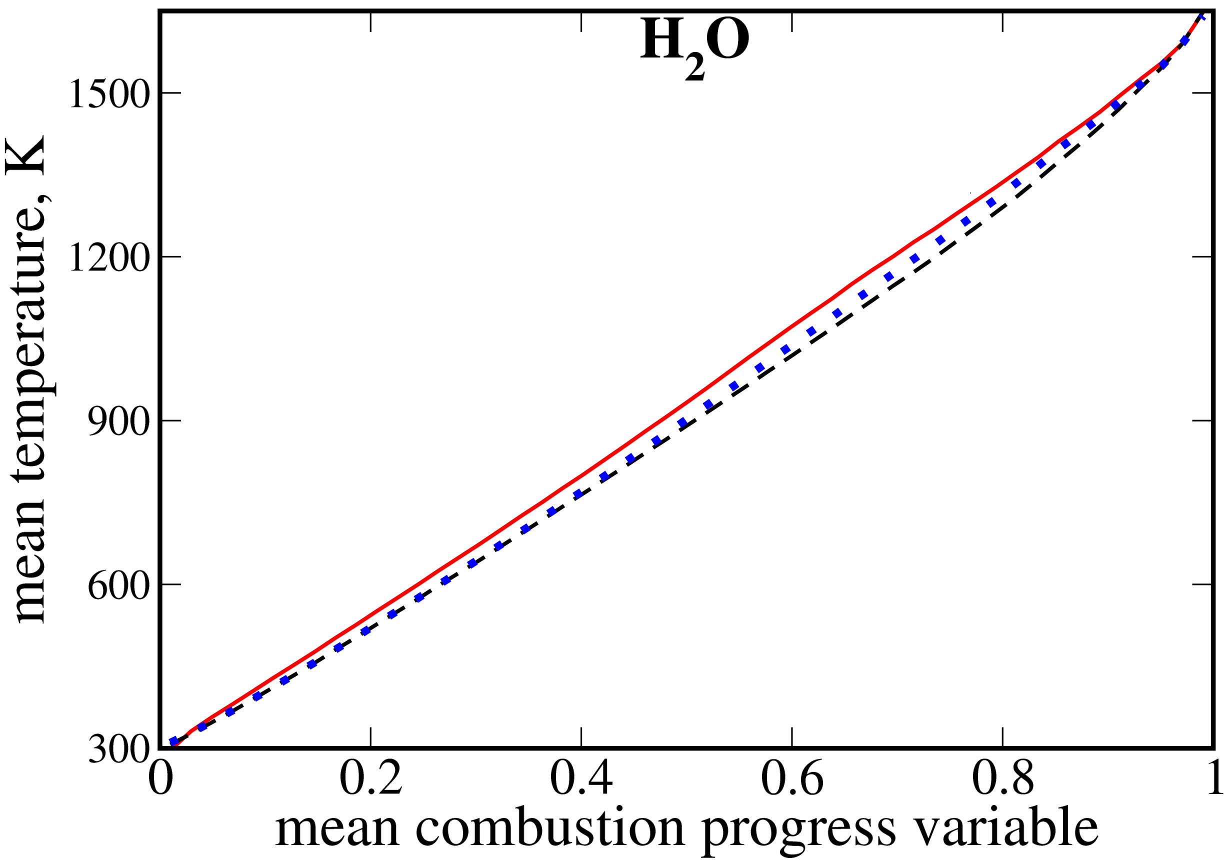
H_2O
mean temperature, K
300
600
900
1200
1500
0
0.2
0.4
0.6
0.8
1
mean combustion progress variable

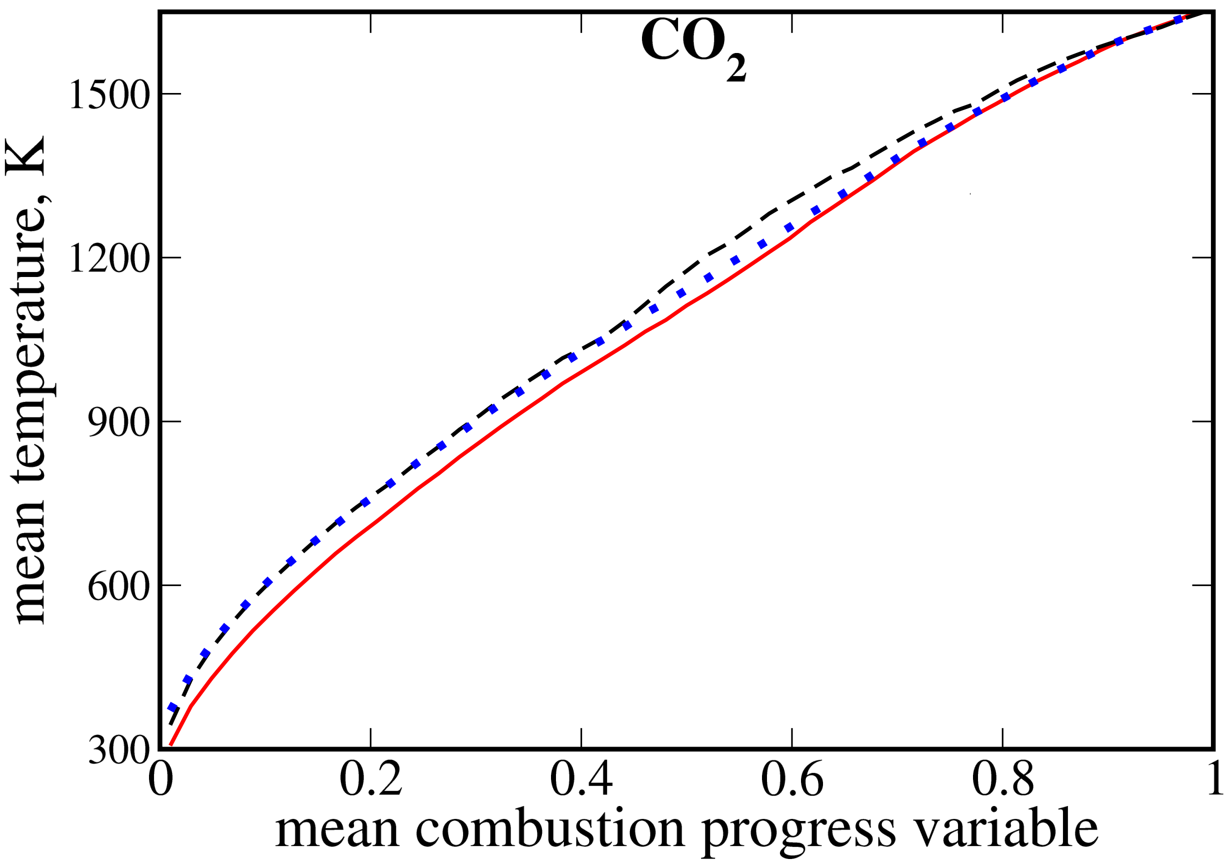
CO_2
mean temperature, K
300
600
900
1200
1500
0
0.2
0.4
0.6
0.8
1
mean combustion progress variable

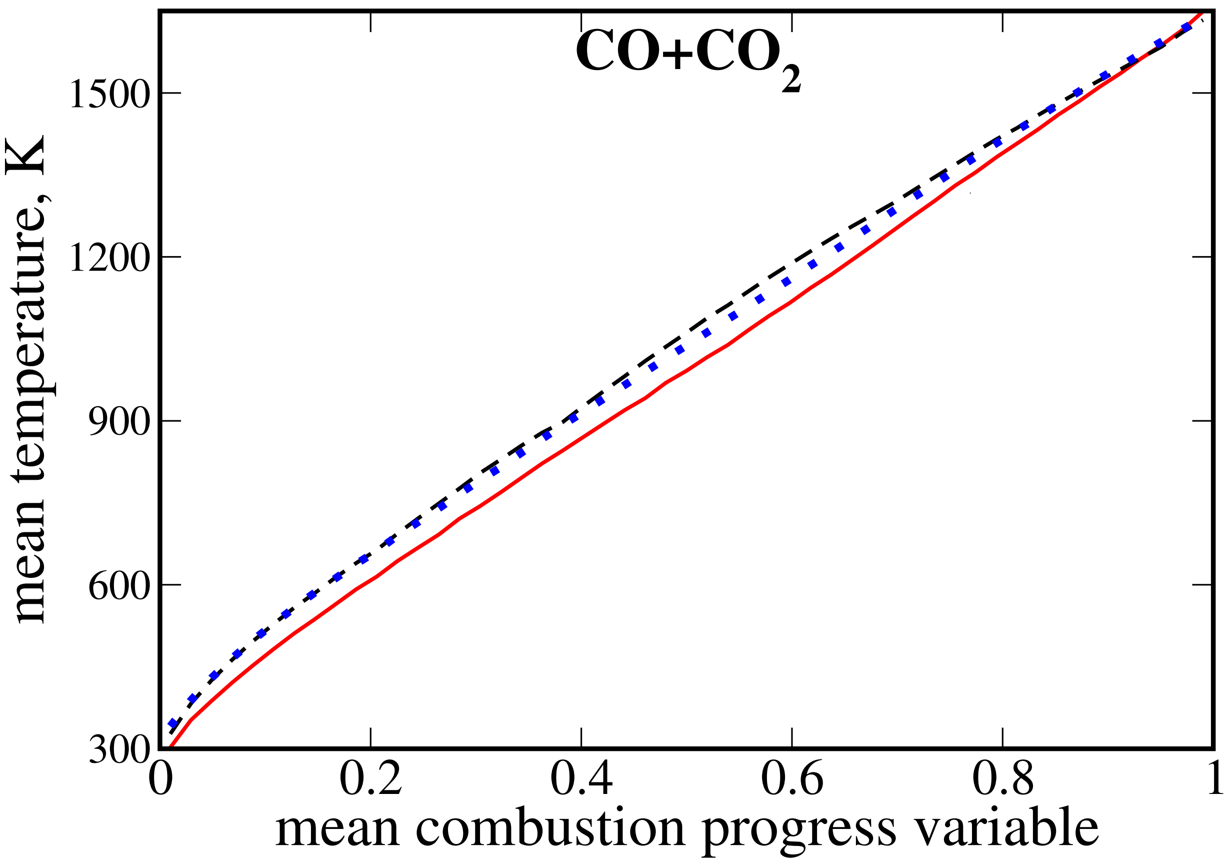
CO+CO$_2$
mean temperature, K
300
600
900
1200
1500
0
0.2
0.4
0.6
0.8
1
mean combustion progress variable

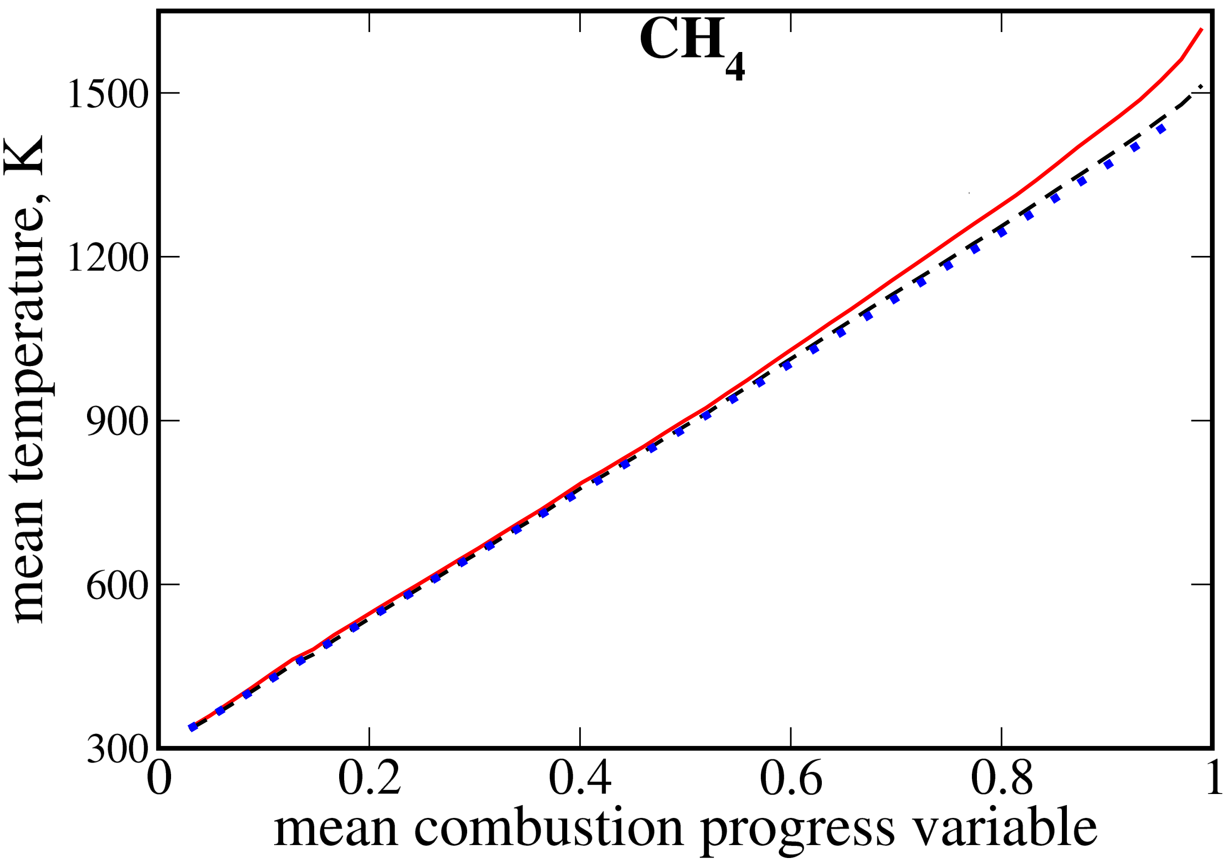
CH4
1500
1200
900
600
300
0
0.2
0.4
0.6
0.8
1
mean temperature, K
mean combustion progress variable

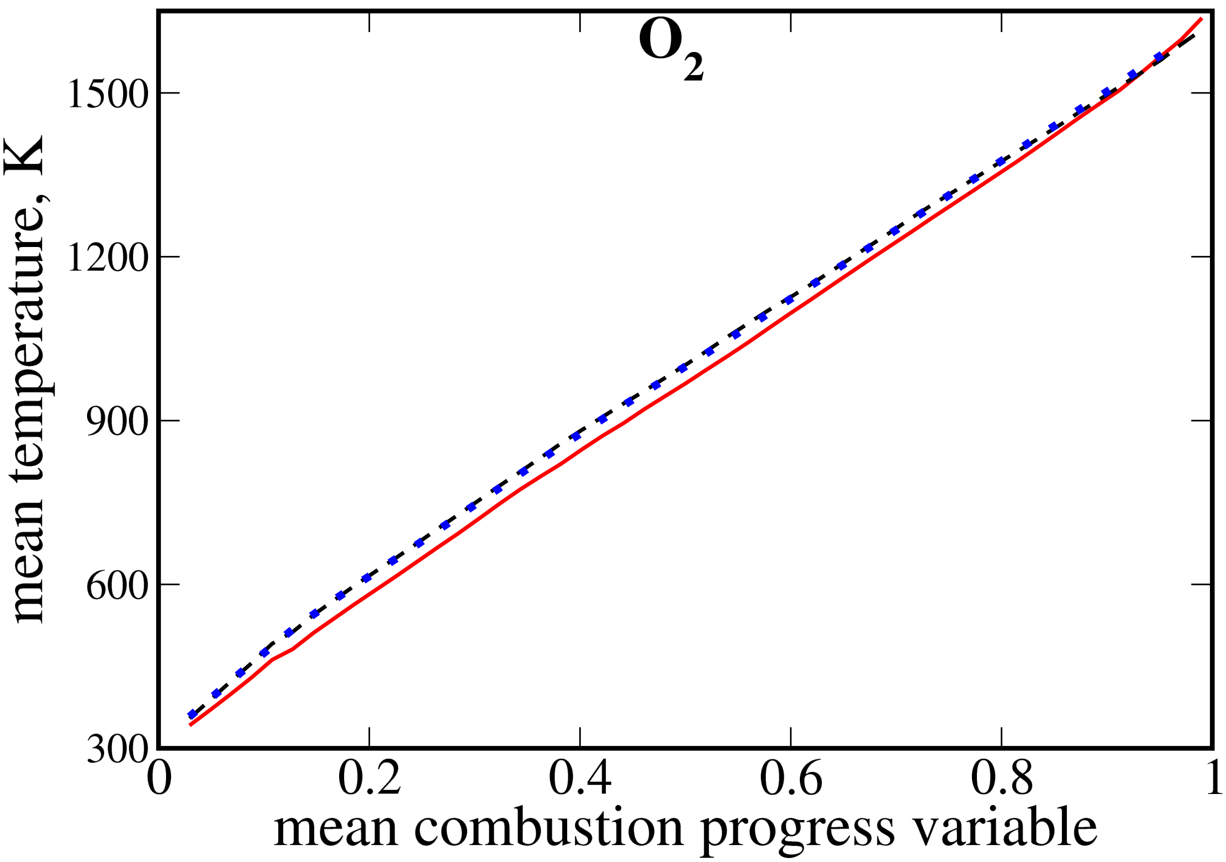
O_2
mean temperature, K
300
600
900
1200
1500
0
0.2
0.4
0.6
0.8
1
mean combustion progress variable

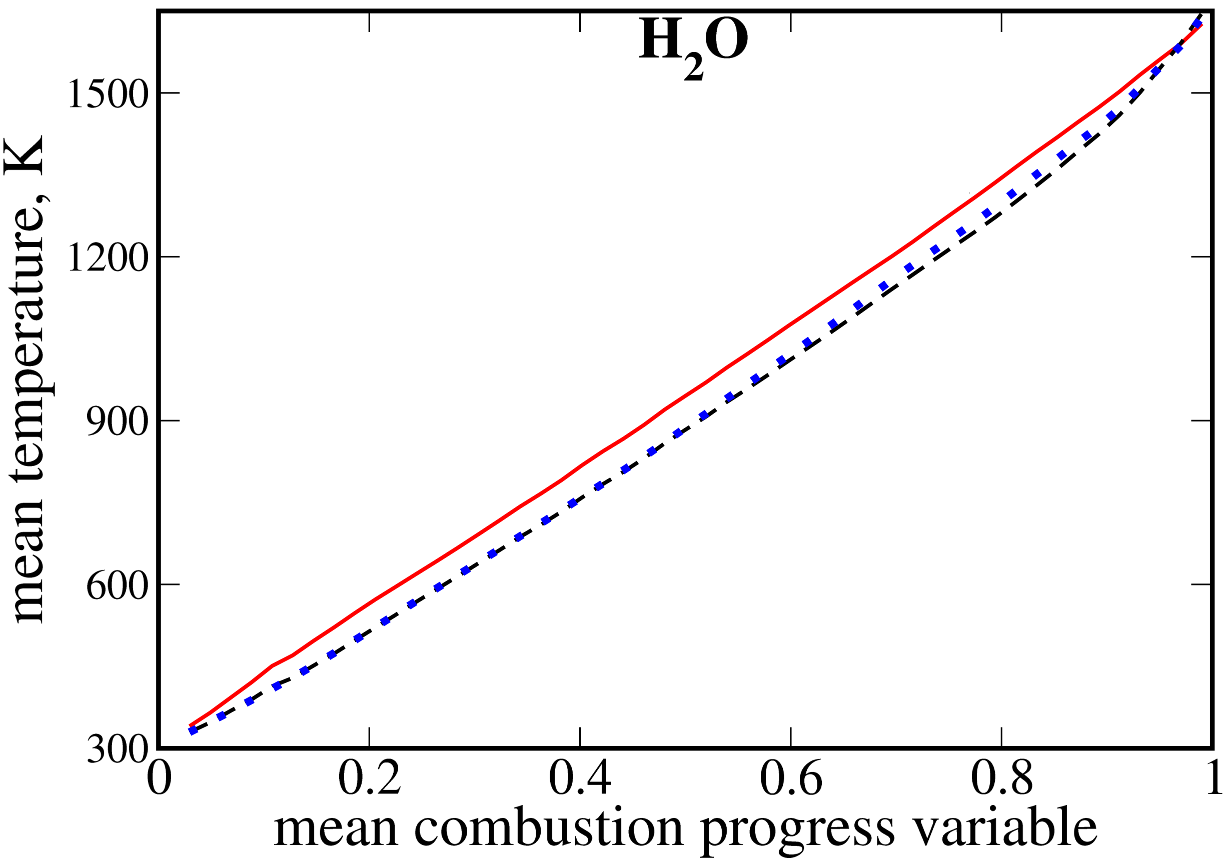
H2O
mean temperature, K
300
600
900
1200
1500
0
0.2
0.4
0.6
0.8
1
mean combustion progress variable

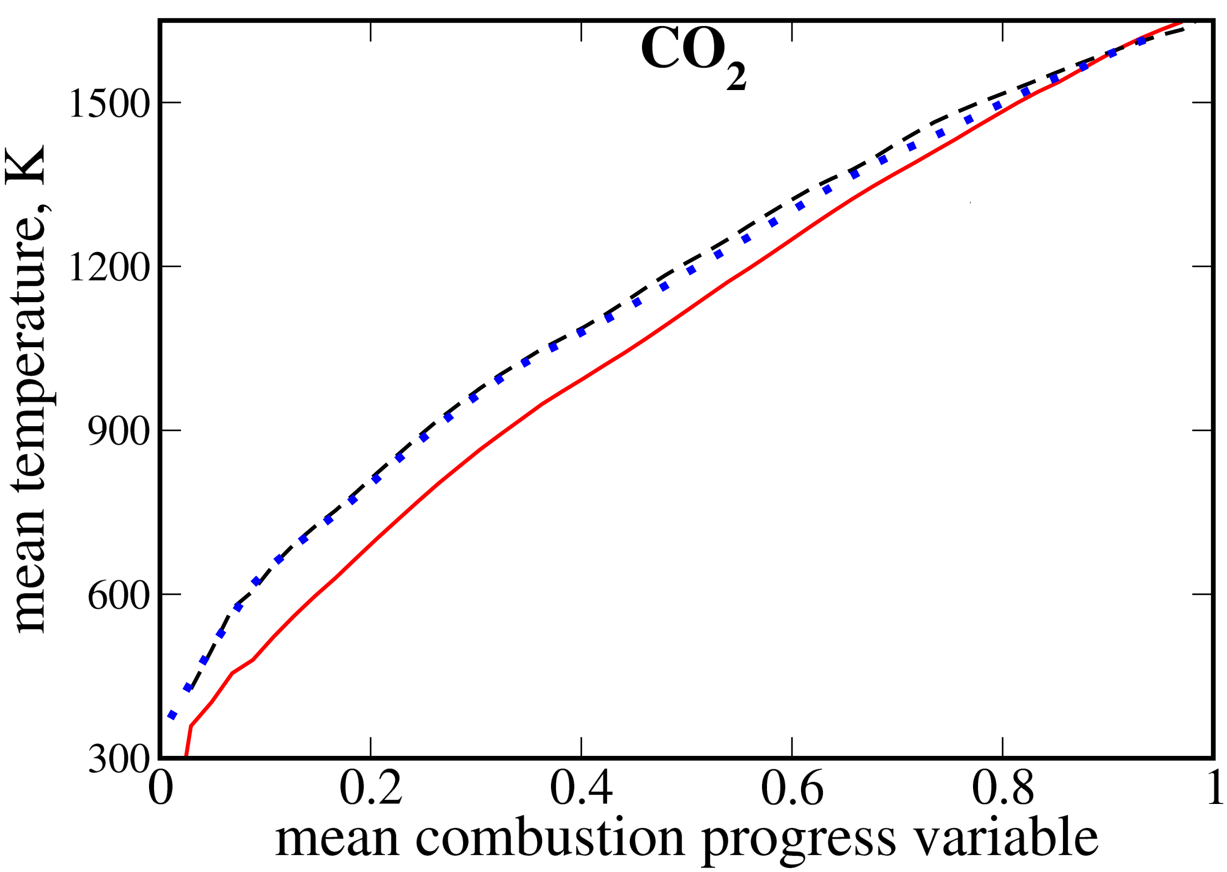
CO2
mean temperature, K
300
600
900
1200
1500
0
0.2
0.4
0.6
0.8
1
mean combustion progress variable

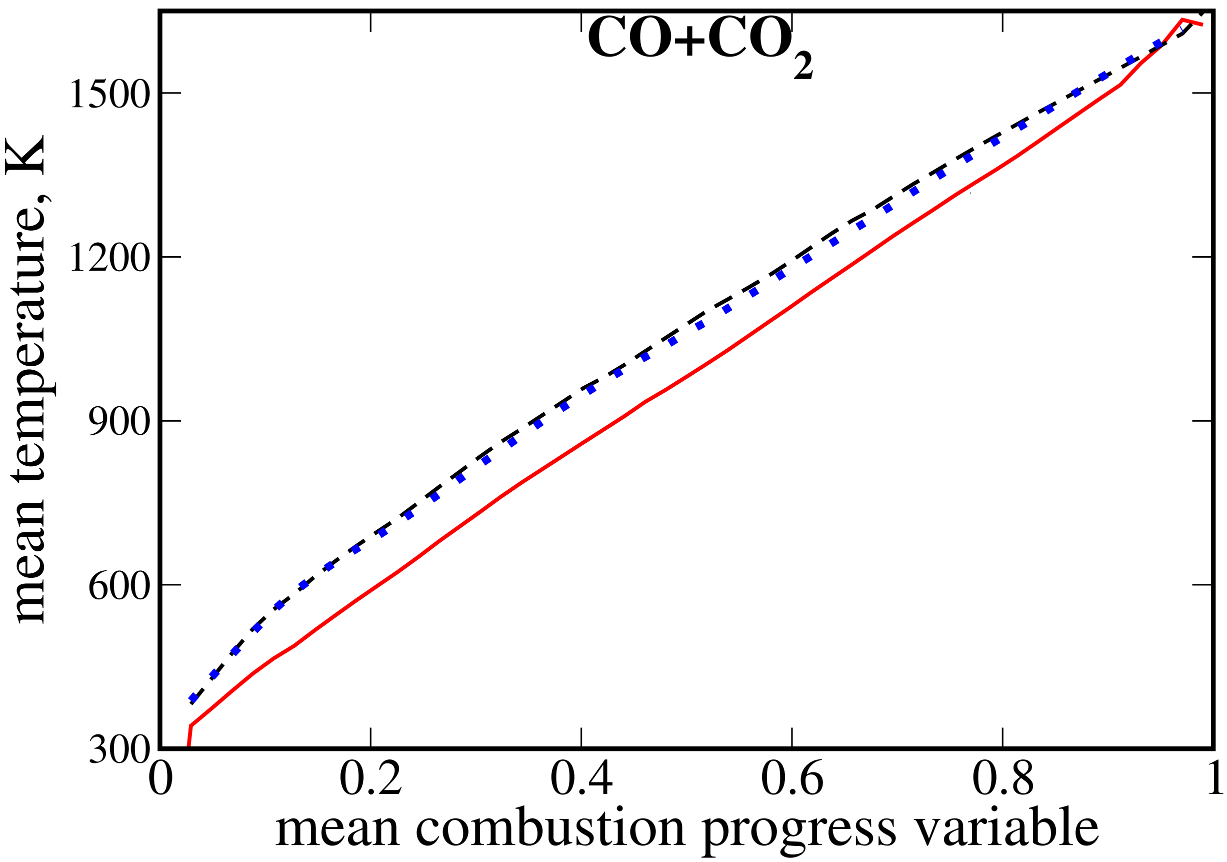
CO+CO2
mean temperature, K
300
600
900
1200
1500
0
0.2
0.4
0.6
0.8
1
mean combustion progress variable

PLEASE CITE THIS ARTICLE AS DOI: 10.1063/5.0047500

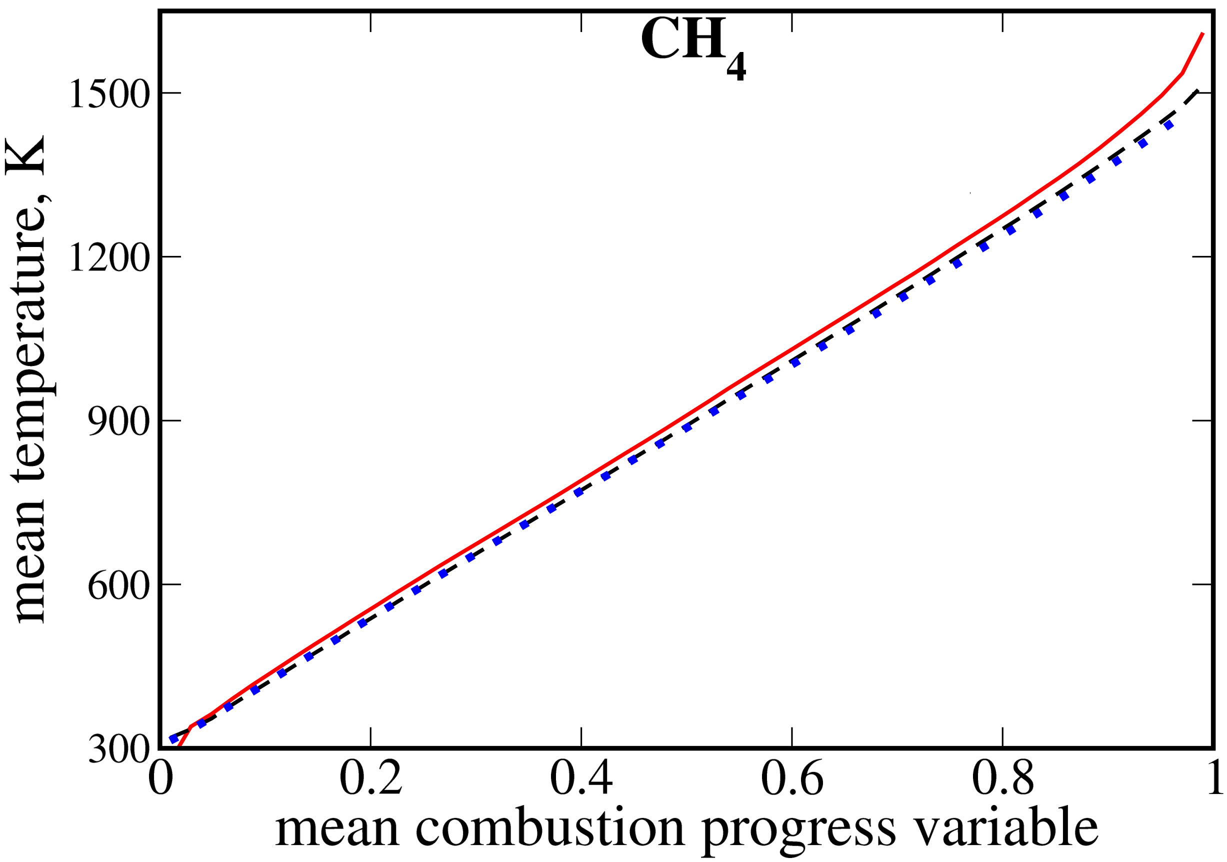

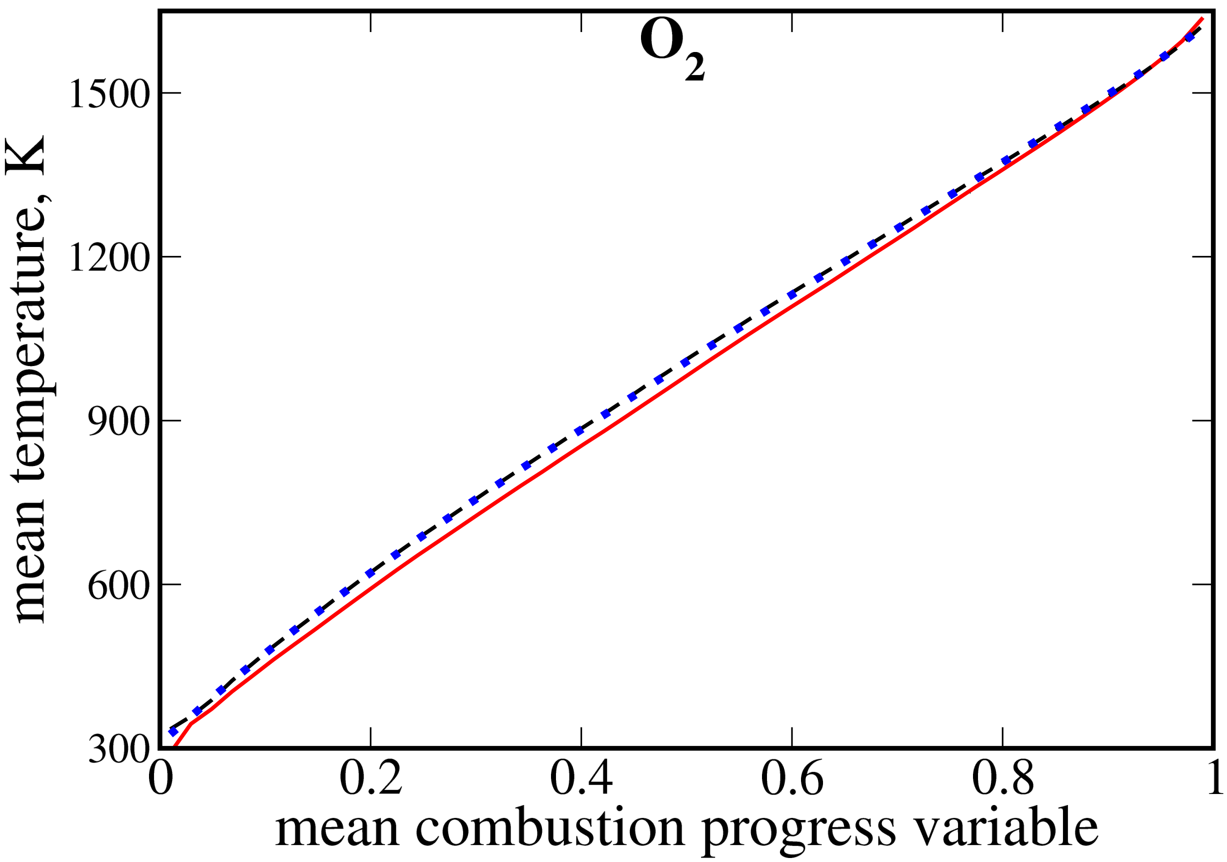
O$_2$
mean temperature, K
mean combustion progress variable
300
600
900
1200
1500
0
0.2
0.4
0.6
0.8
1

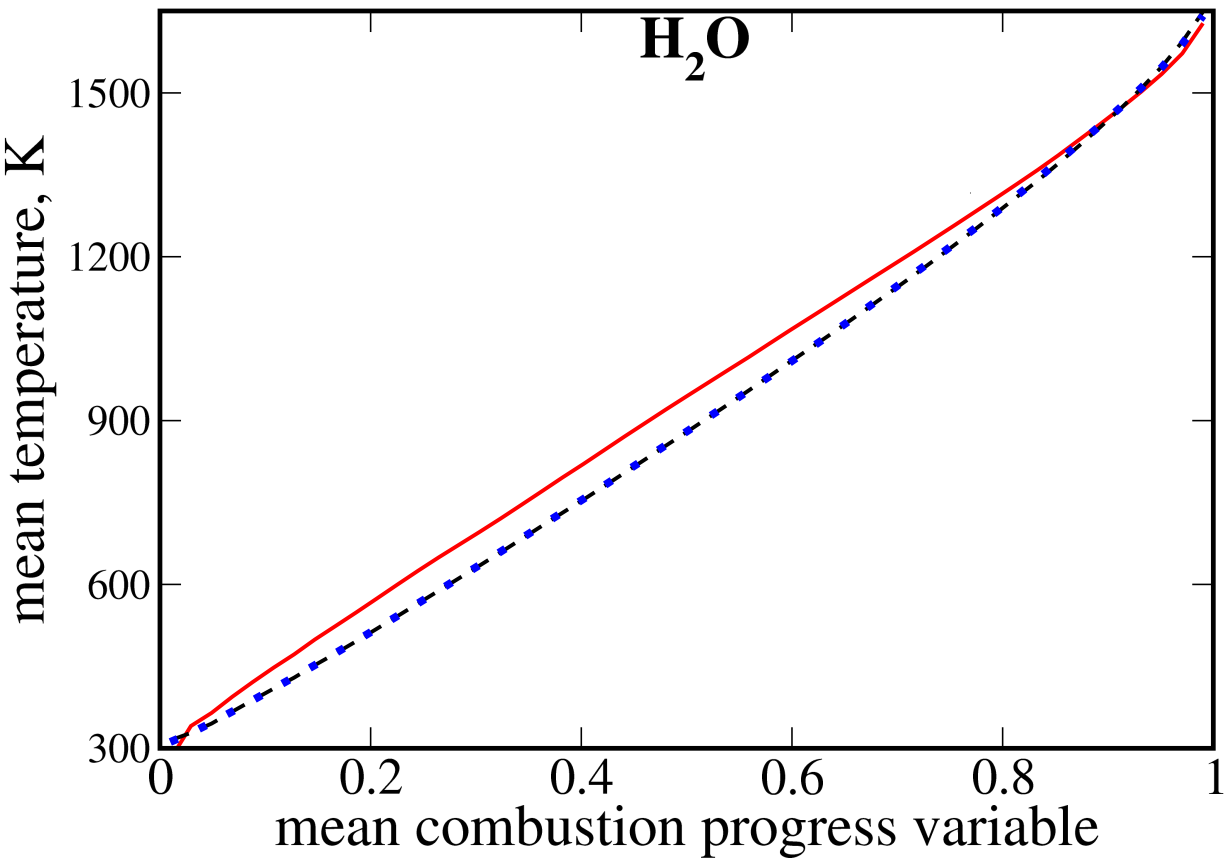
H2O
mean temperature, K
300
600
900
1200
1500
0
0.2
0.4
0.6
0.8
1
mean combustion progress variable

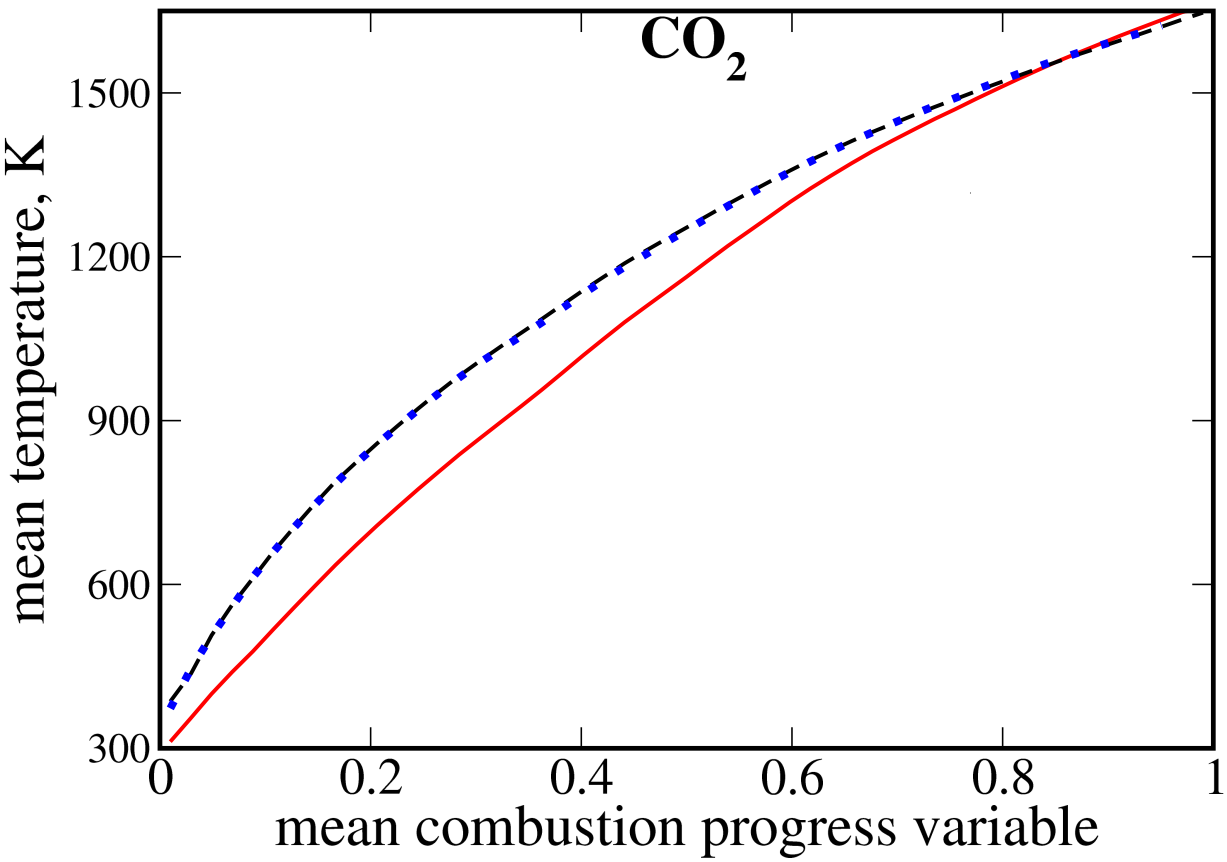
CO_2
mean temperature, K
1500
1200
900
600
300
0
0.2
0.4
0.6
0.8
1
mean combustion progress variable

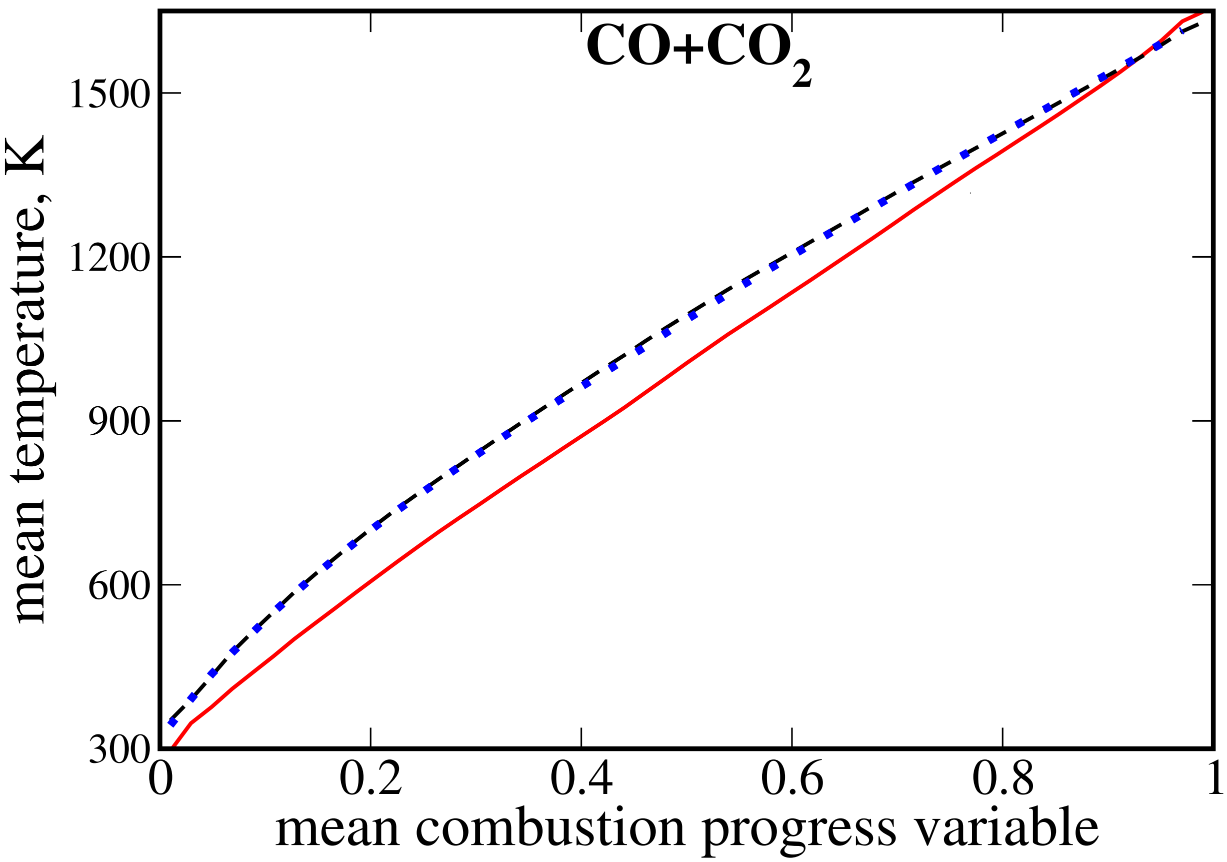
CO+CO$_2$
1500
1200
900
600
300
mean temperature, K
0
0.2
0.4
0.6
0.8
1
mean combustion progress variable

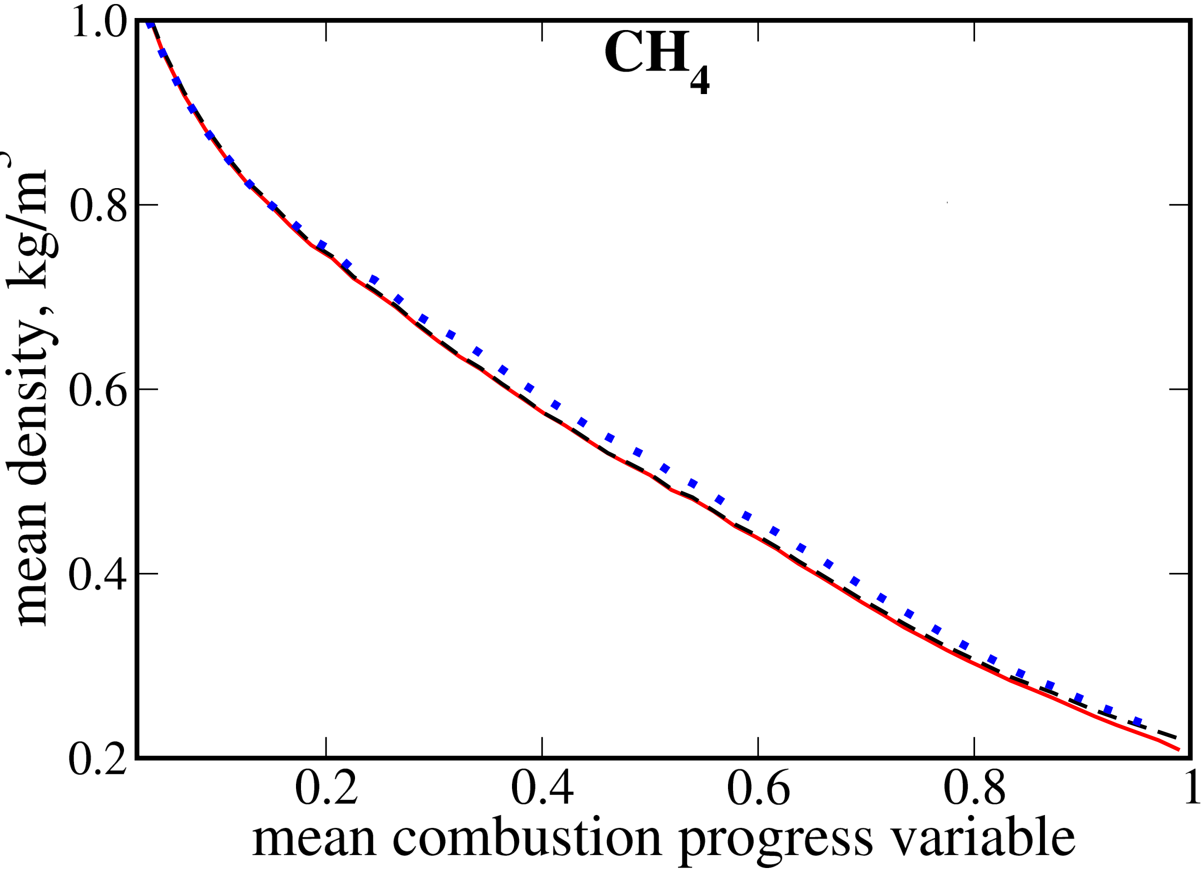
CH4
mean density, kg/m3
mean combustion progress variable
1.0
0.8
0.6
0.4
0.2
0.2
0.4
0.6
0.8
1

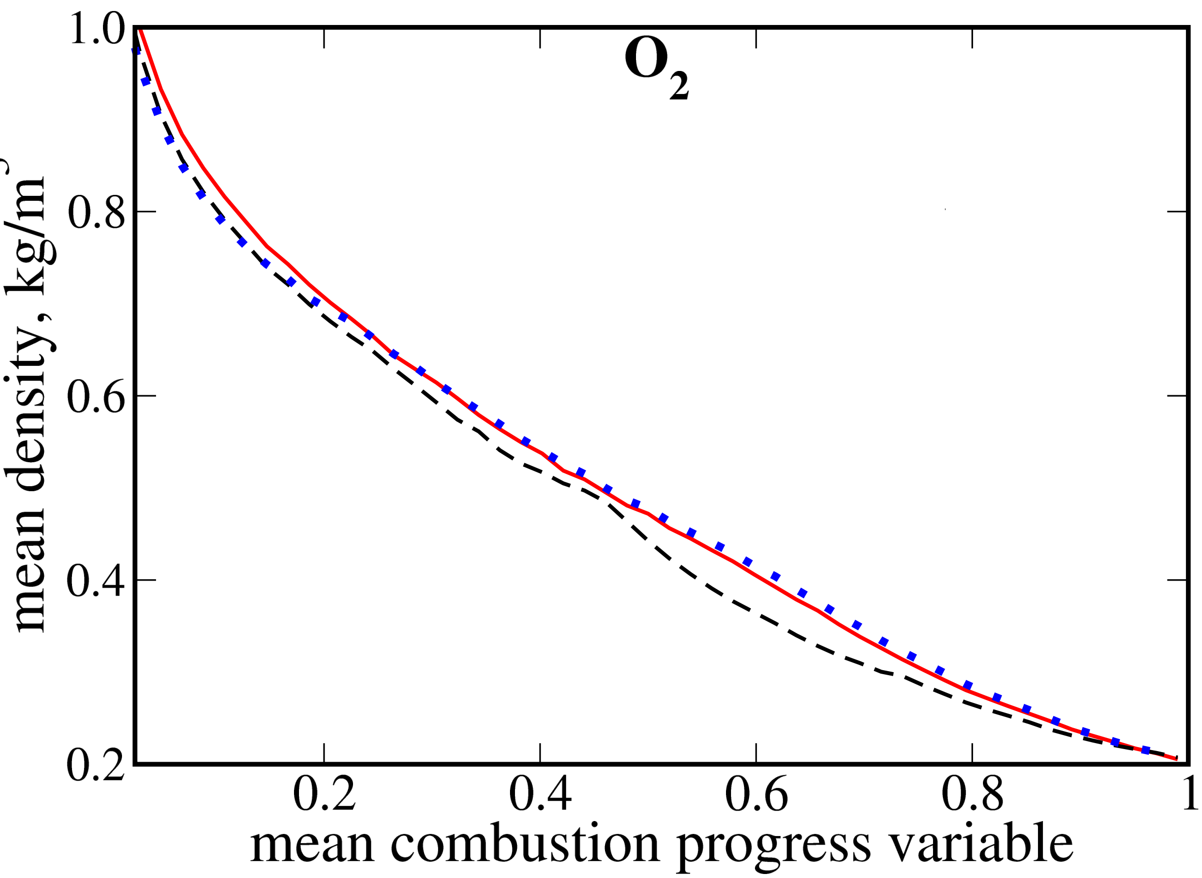
O2
mean density, kg/m3
mean combustion progress variable
1.0
0.8
0.6
0.4
0.2
0.2
0.4
0.6
0.8
1

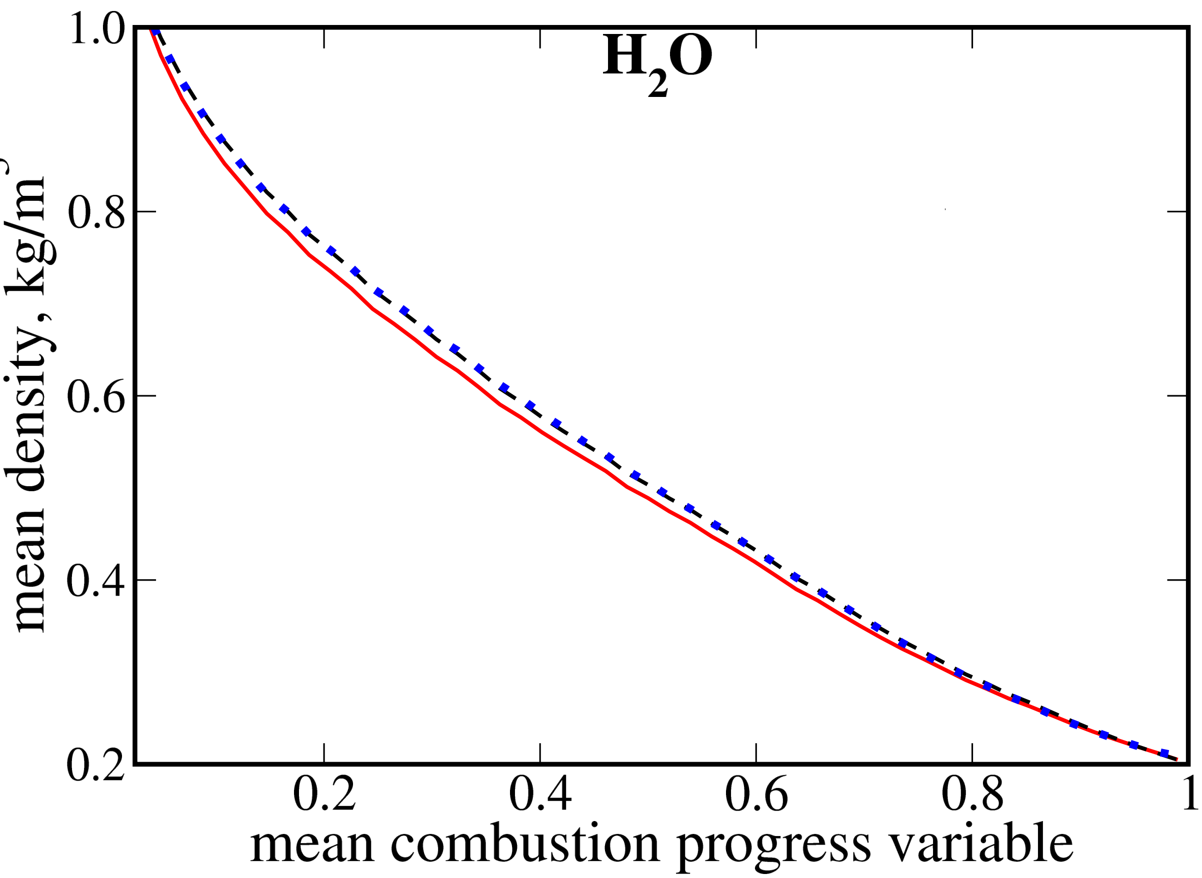
H_2O
mean density, kg/m^3
1.0
0.8
0.6
0.4
0.2
0.2
0.4
0.6
0.8
1
mean combustion progress variable

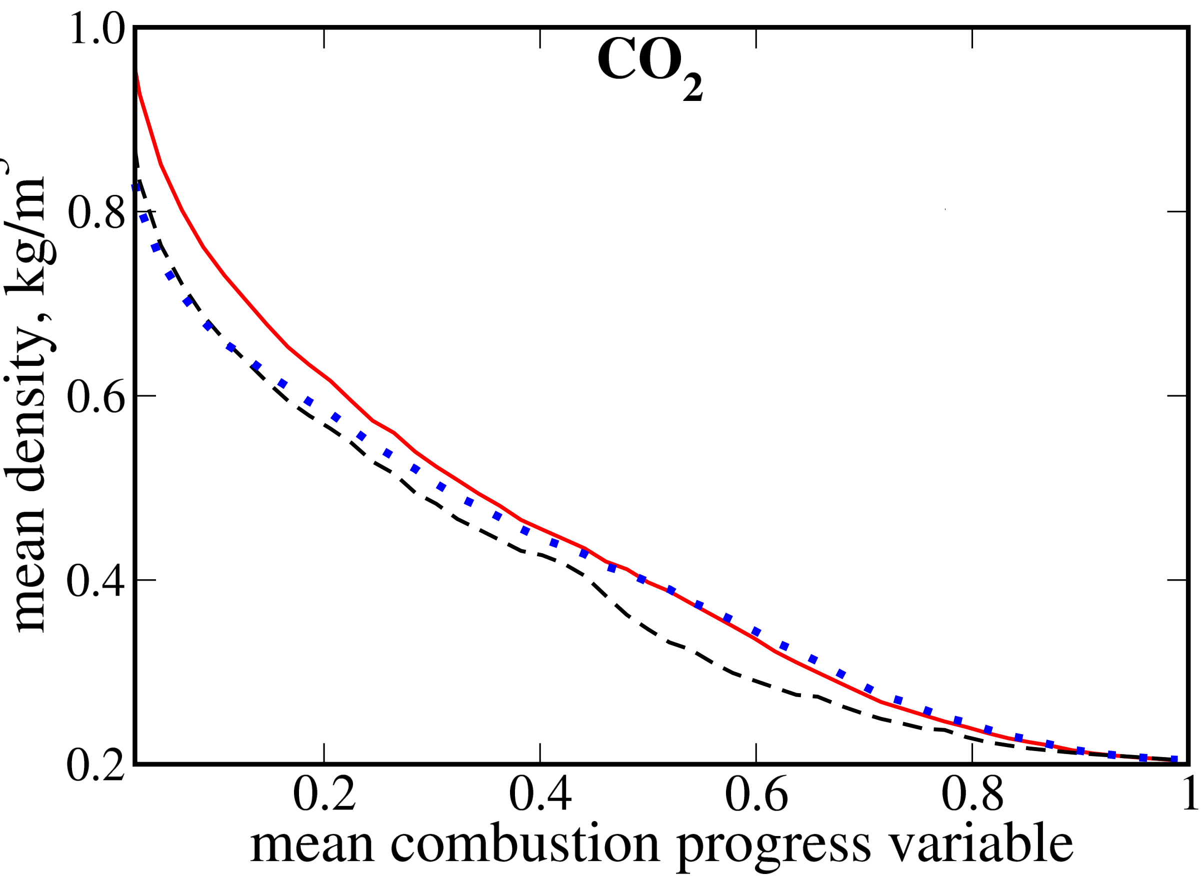
CO2
mean density, kg/m3
mean combustion progress variable
1.0
0.8
0.6
0.4
0.2
0.2
0.4
0.6
0.8
1

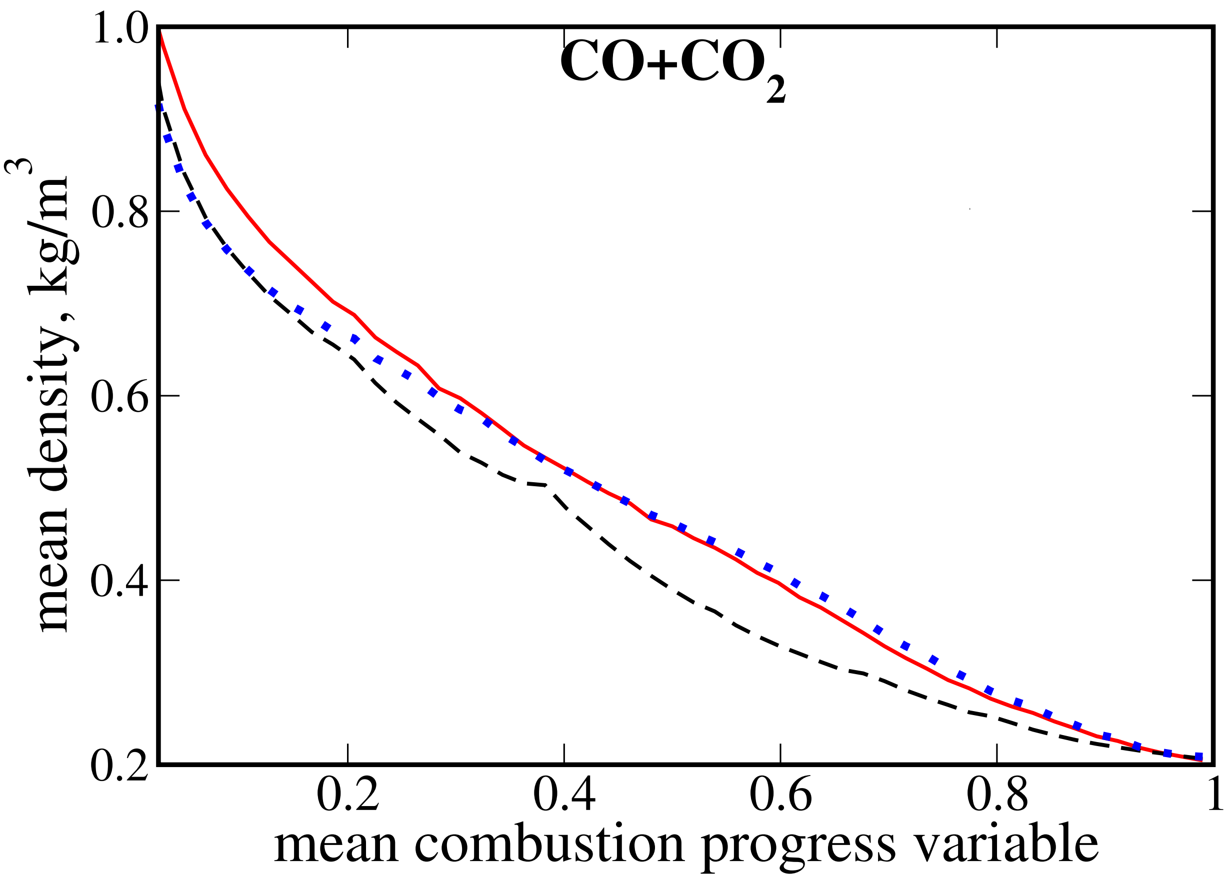
CO+CO2
mean density, kg/m3
mean combustion progress variable
1.0
0.8
0.6
0.4
0.2
0.2
0.4
0.6
0.8
1

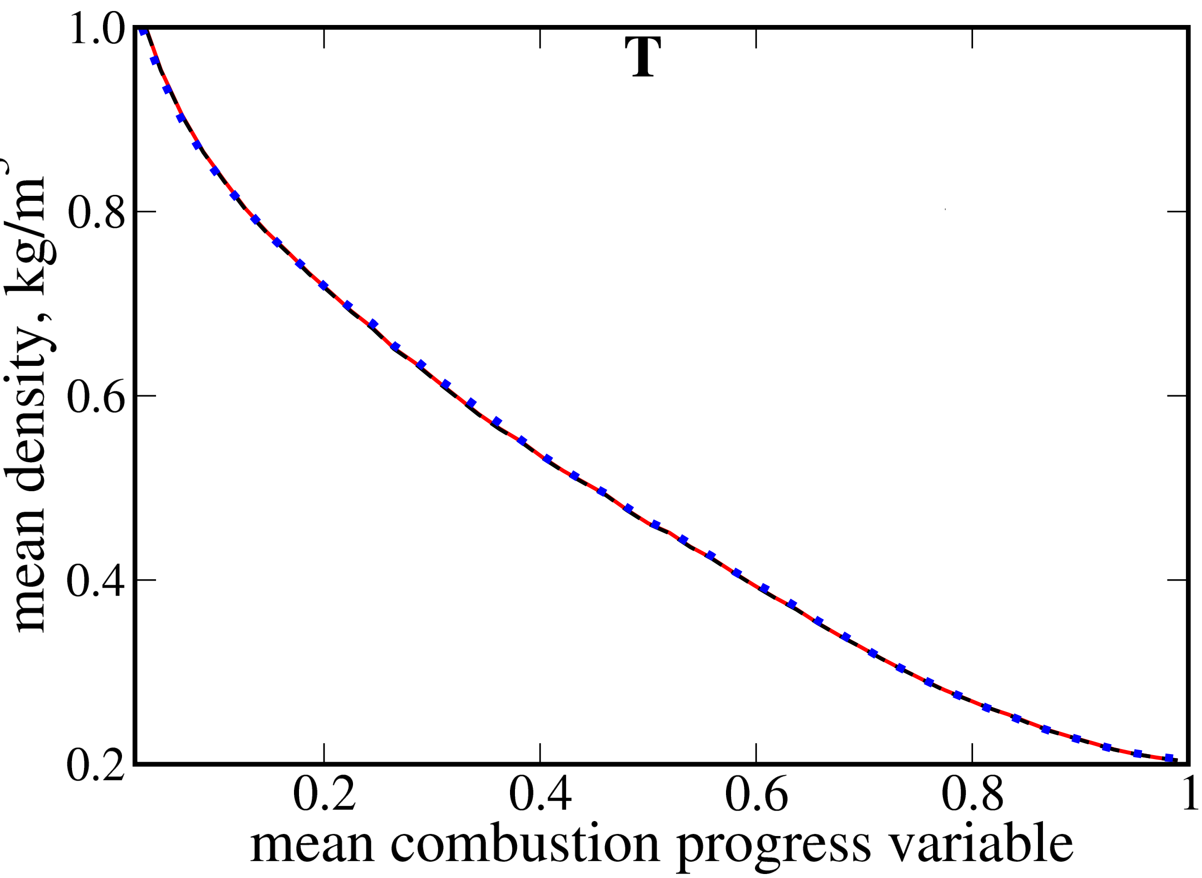
T
mean density, kg/m³
1.0
0.8
0.6
0.4
0.2
0.2
0.4
0.6
0.8
1
mean combustion progress variable

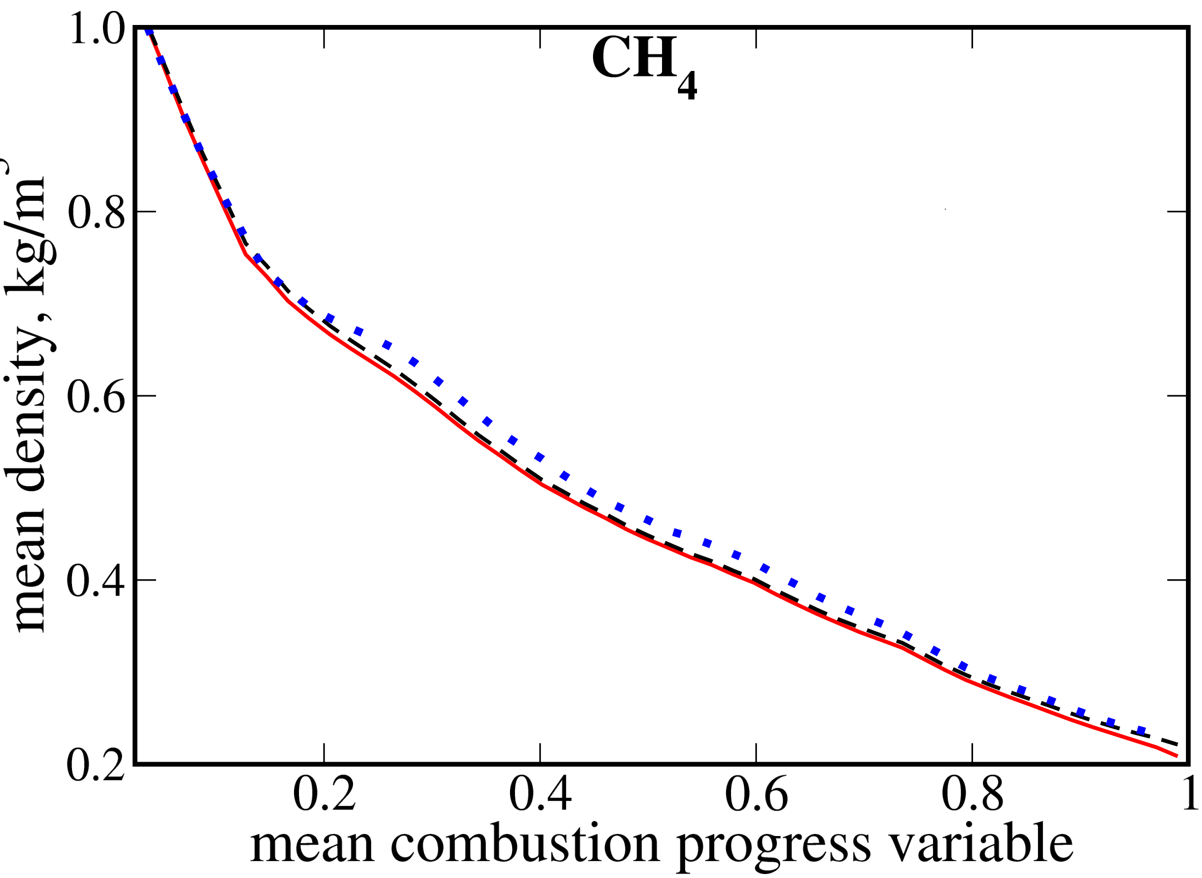
CH4
mean density, kg/m3
mean combustion progress variable
1.0
0.8
0.6
0.4
0.2
0.2
0.4
0.6
0.8
1

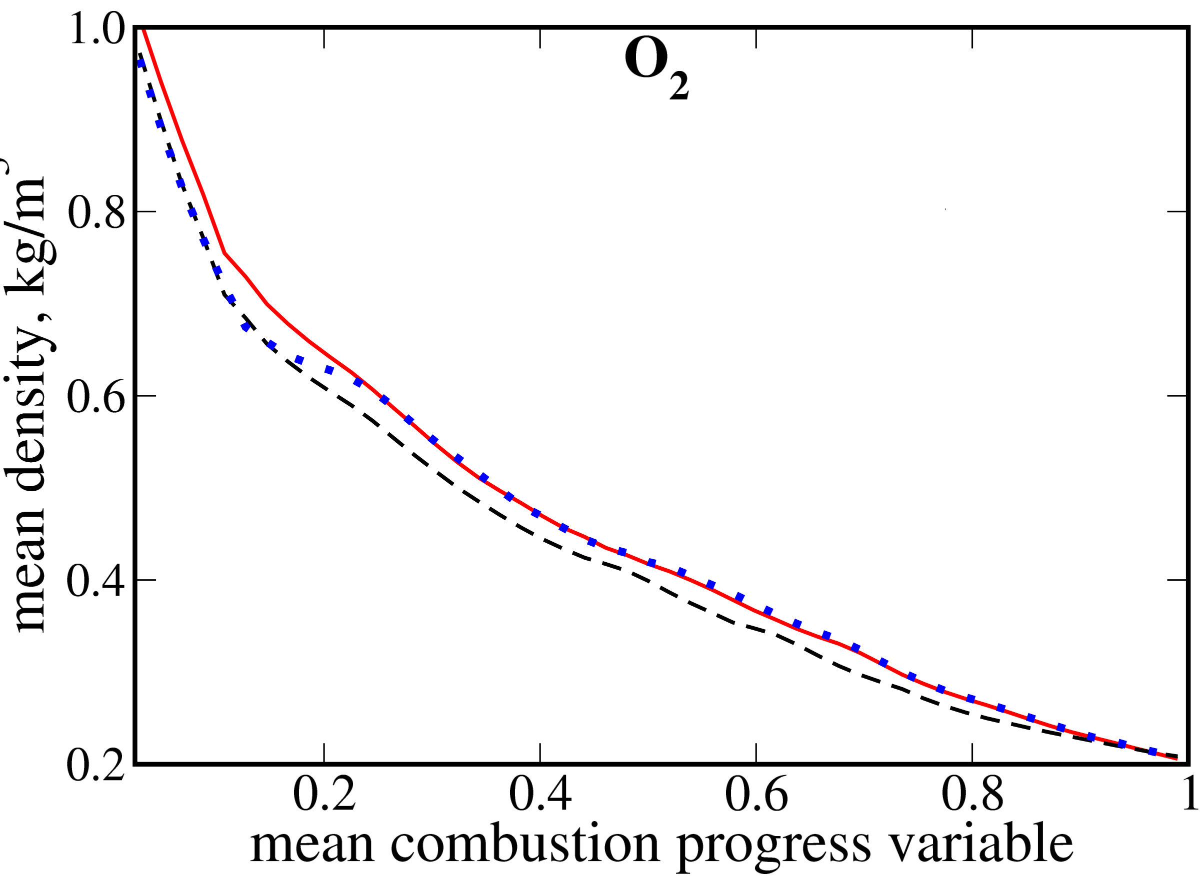
O2
mean density, kg/m3
1.0
0.8
0.6
0.4
0.2
0.2
0.4
0.6
0.8
1
mean combustion progress variable

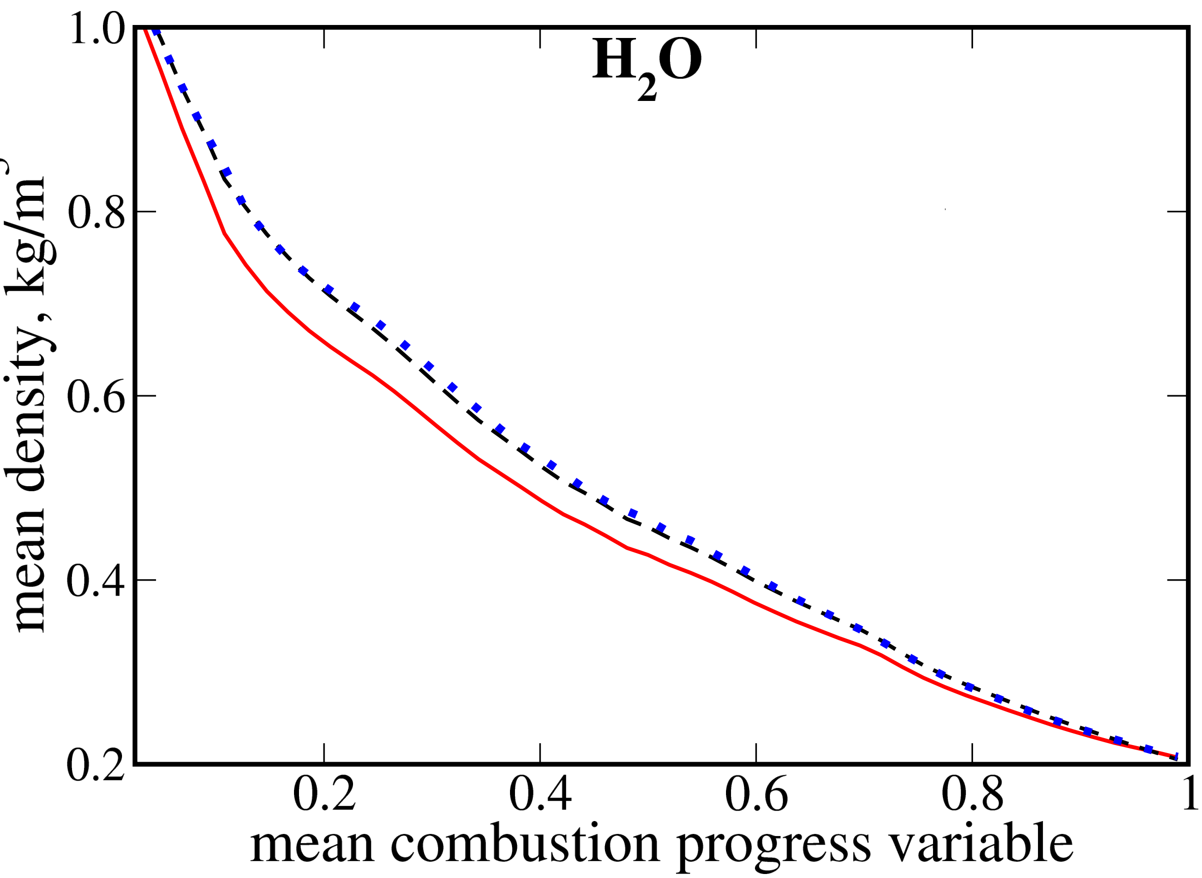
H2O
mean density, kg/m3
mean combustion progress variable
1.0
0.8
0.6
0.4
0.2
0.2
0.4
0.6
0.8
1

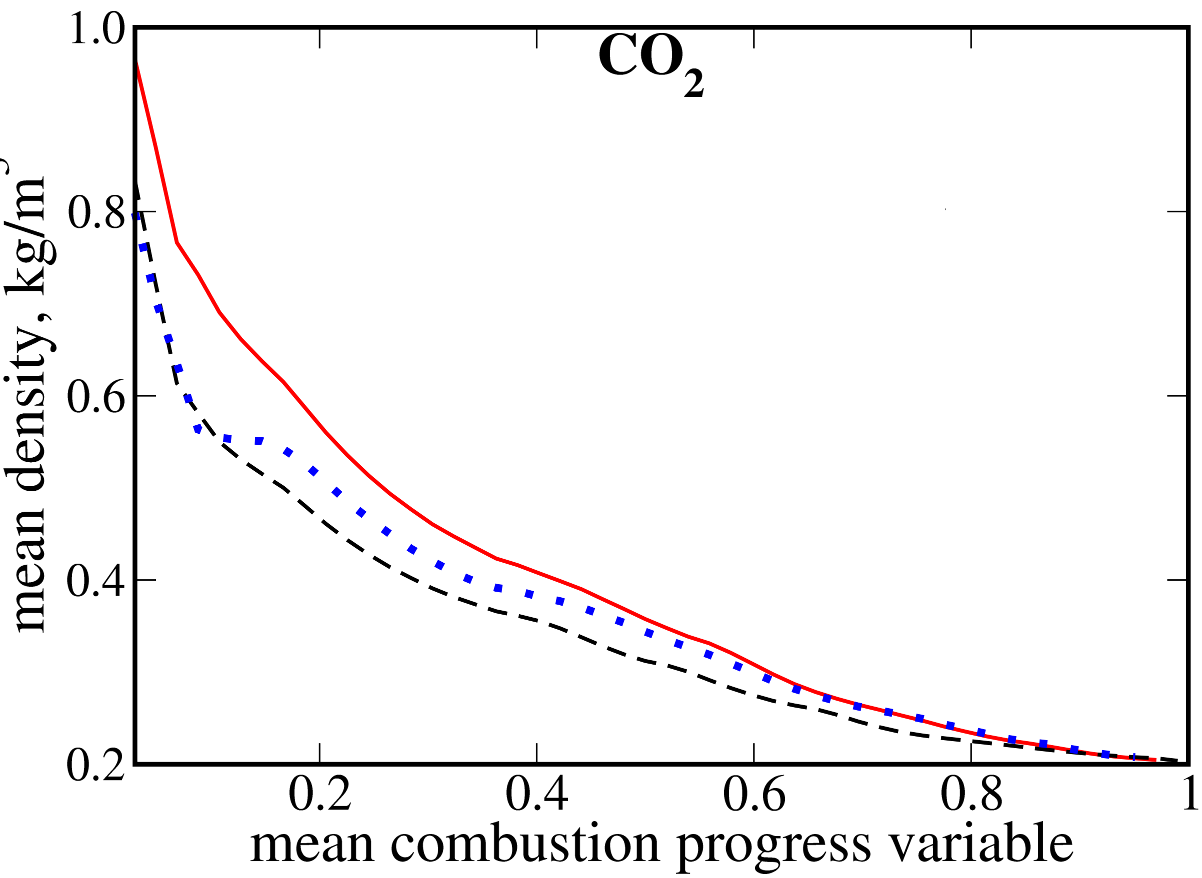
CO_2
mean density, kg/m^3
mean combustion progress variable
1.0
0.8
0.6
0.4
0.2
0.2
0.4
0.6
0.8
1

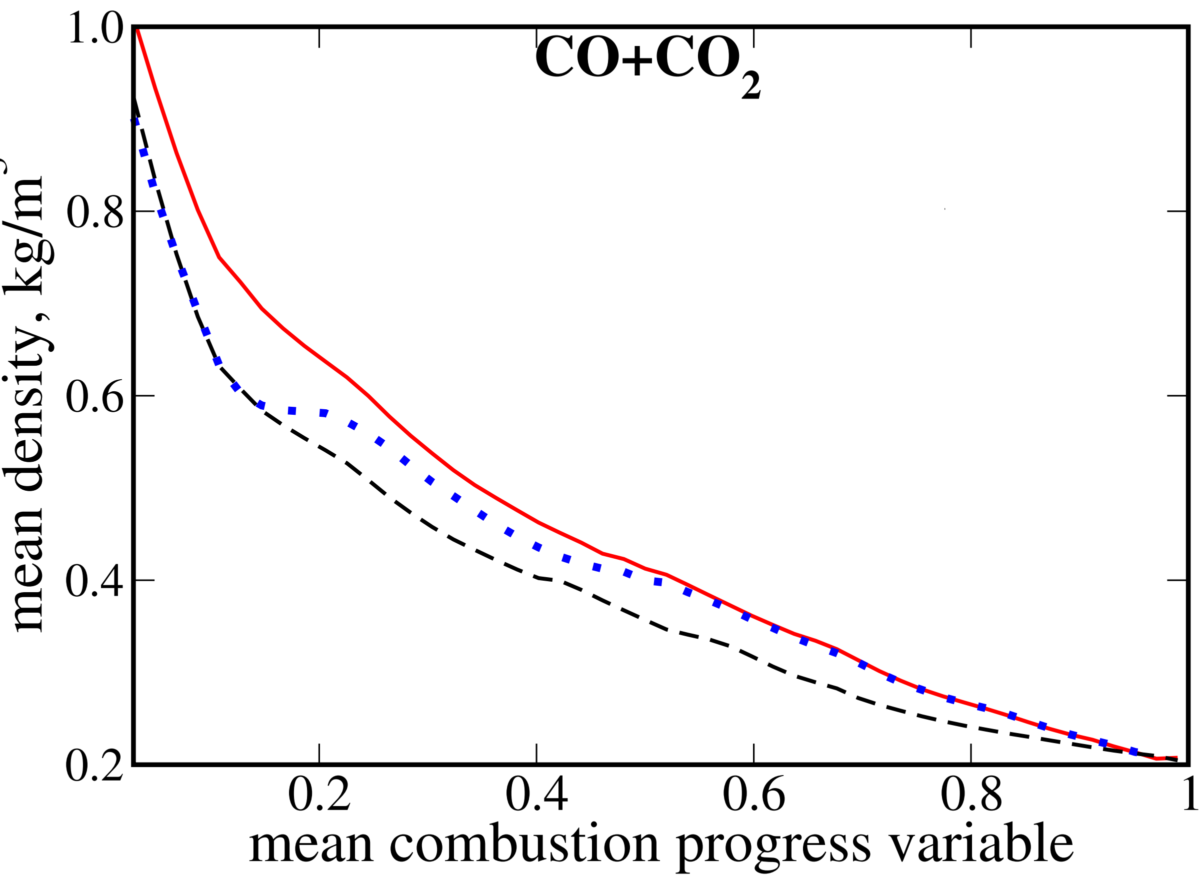
CO+CO2
mean density, kg/m3
mean combustion progress variable
1.0
0.8
0.6
0.4
0.2
0.2
0.4
0.6
0.8
1

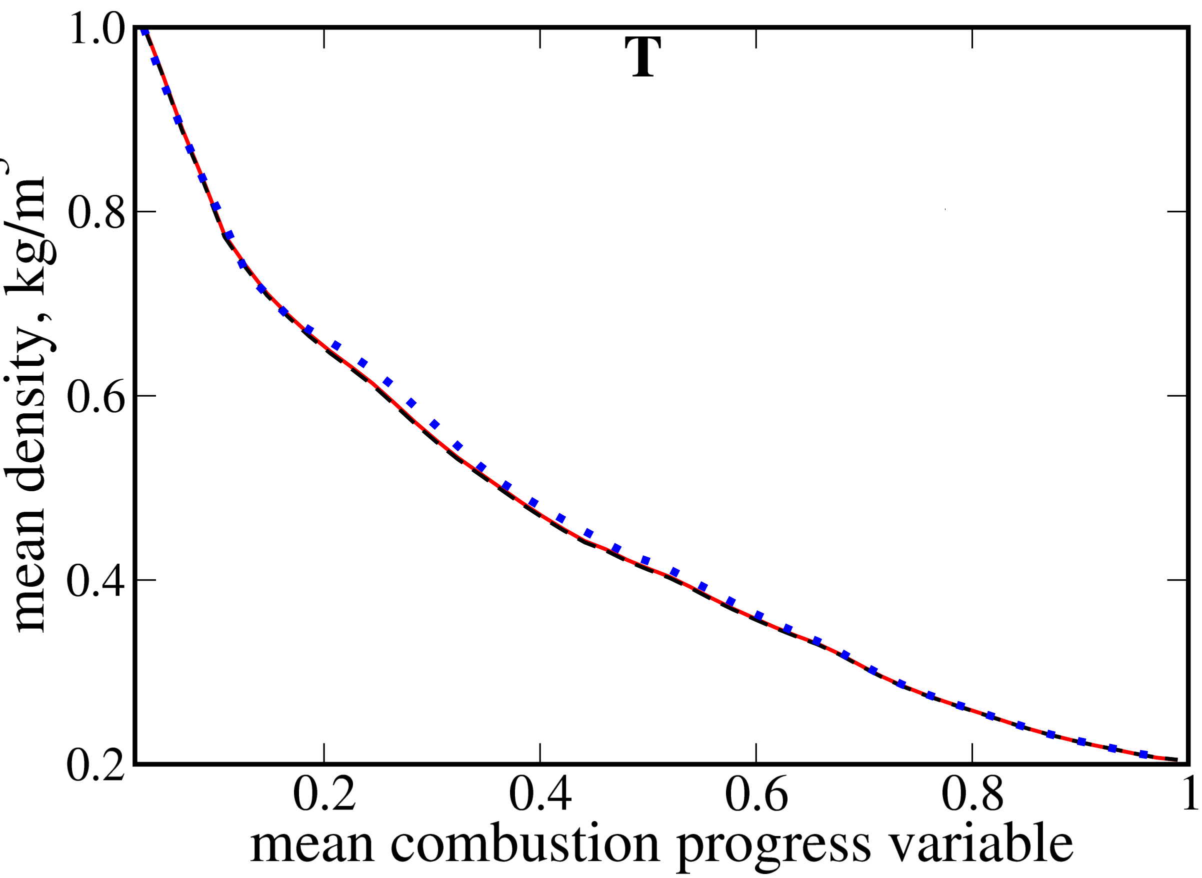
T
mean density, kg/m^3
1.0
0.8
0.6
0.4
0.2
0.2
0.4
0.6
0.8
1
mean combustion progress variable

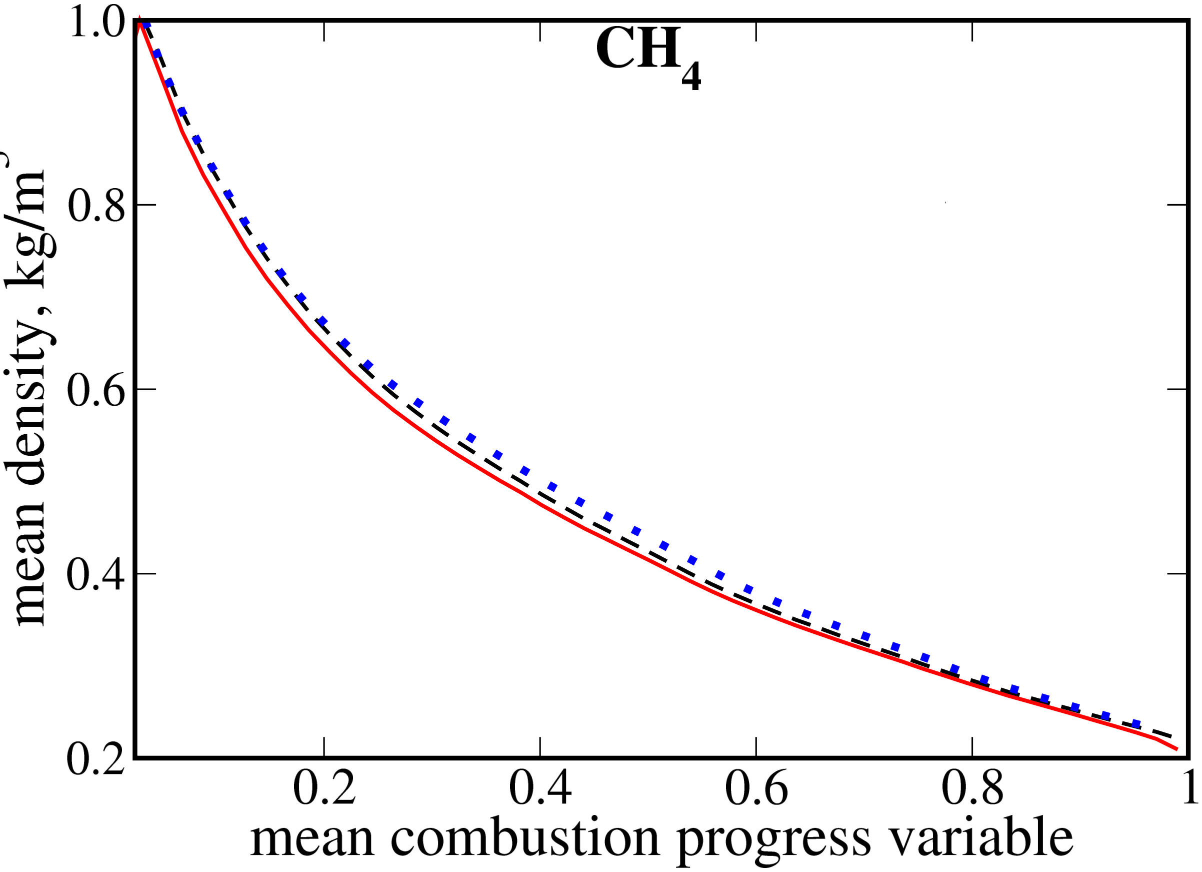
CH4
mean density, kg/m3
1.0
0.8
0.6
0.4
0.2
0.2
0.4
0.6
0.8
1
mean combustion progress variable

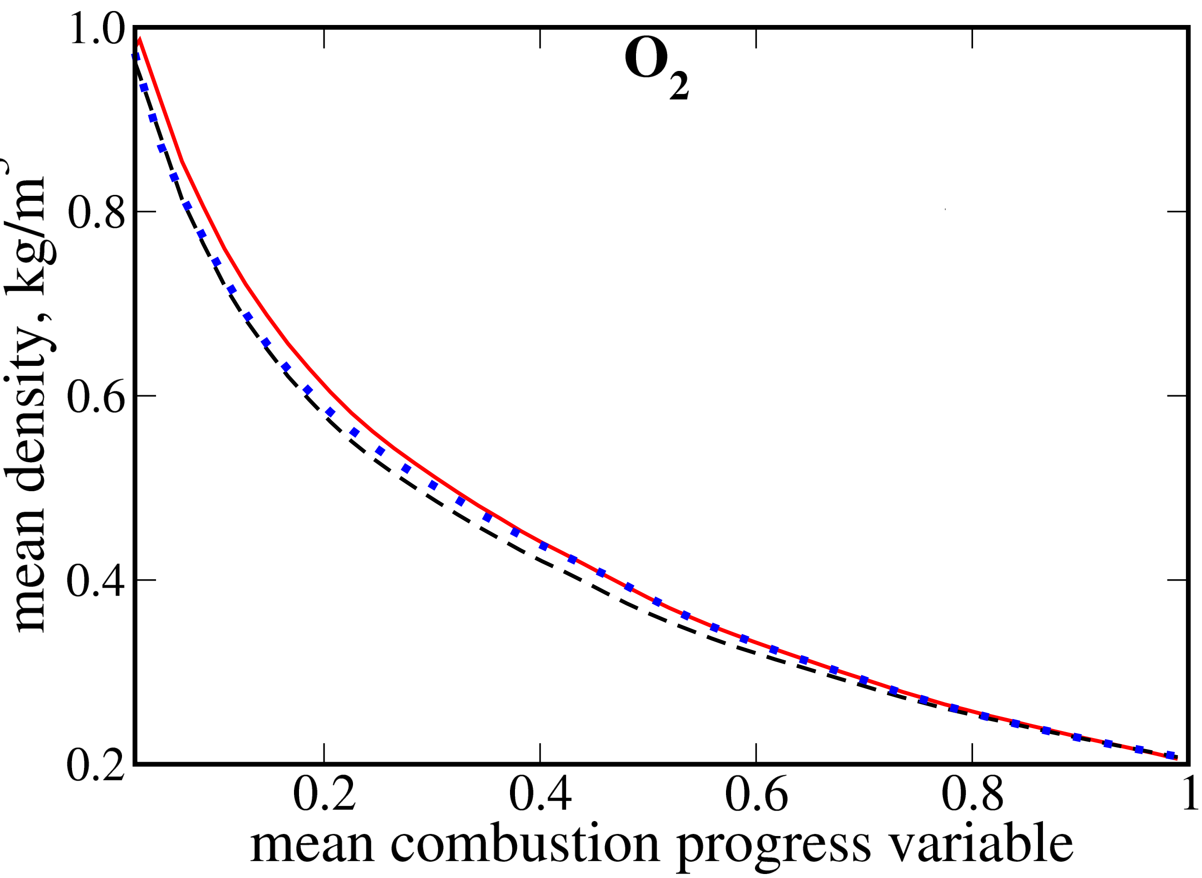
O2
mean density, kg/m3
mean combustion progress variable
1.0
0.8
0.6
0.4
0.2
0.2
0.4
0.6
0.8
1

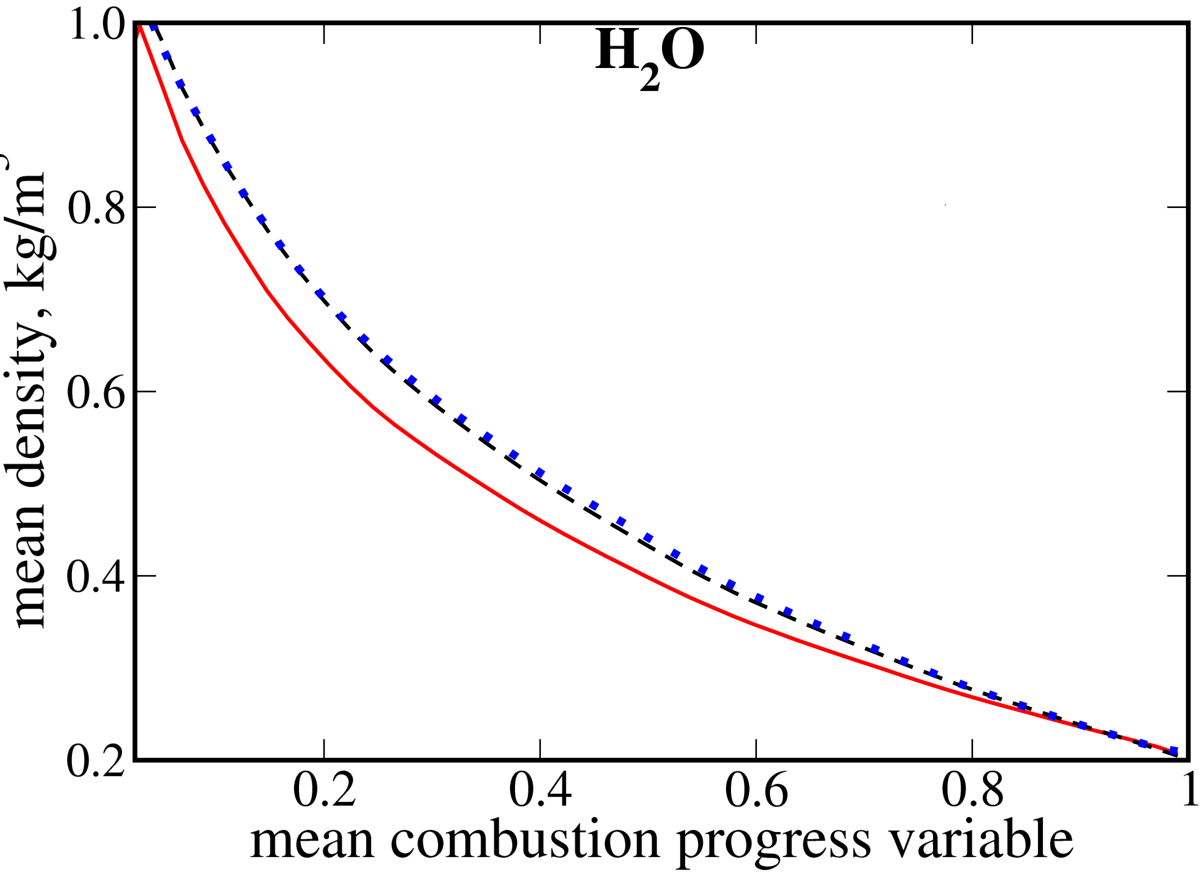
H_2O
mean density, kg/m^3
1.0
0.8
0.6
0.4
0.2
0.2
0.4
0.6
0.8
1
mean combustion progress variable

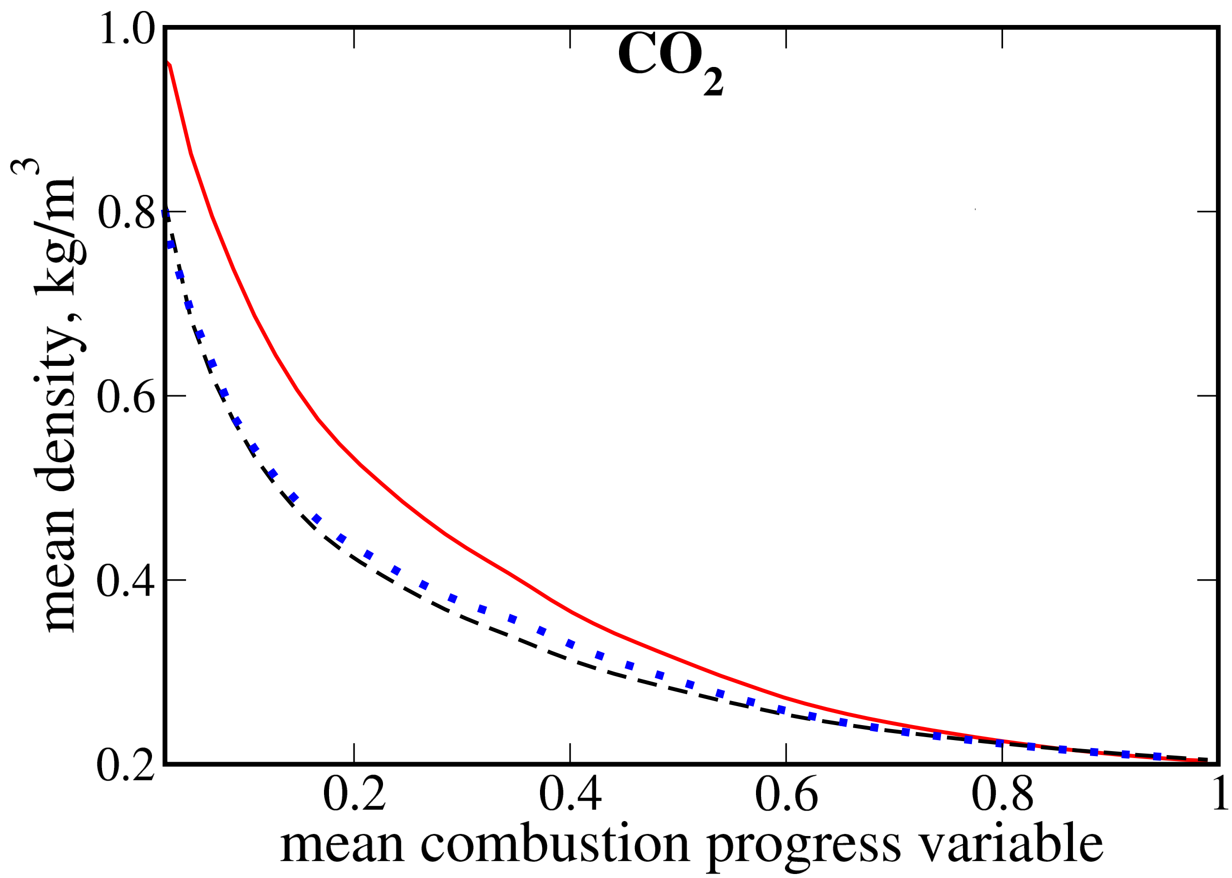
CO2
mean density, kg/m3
mean combustion progress variable
1.0
0.8
0.6
0.4
0.2
0.2
0.4
0.6
0.8
1

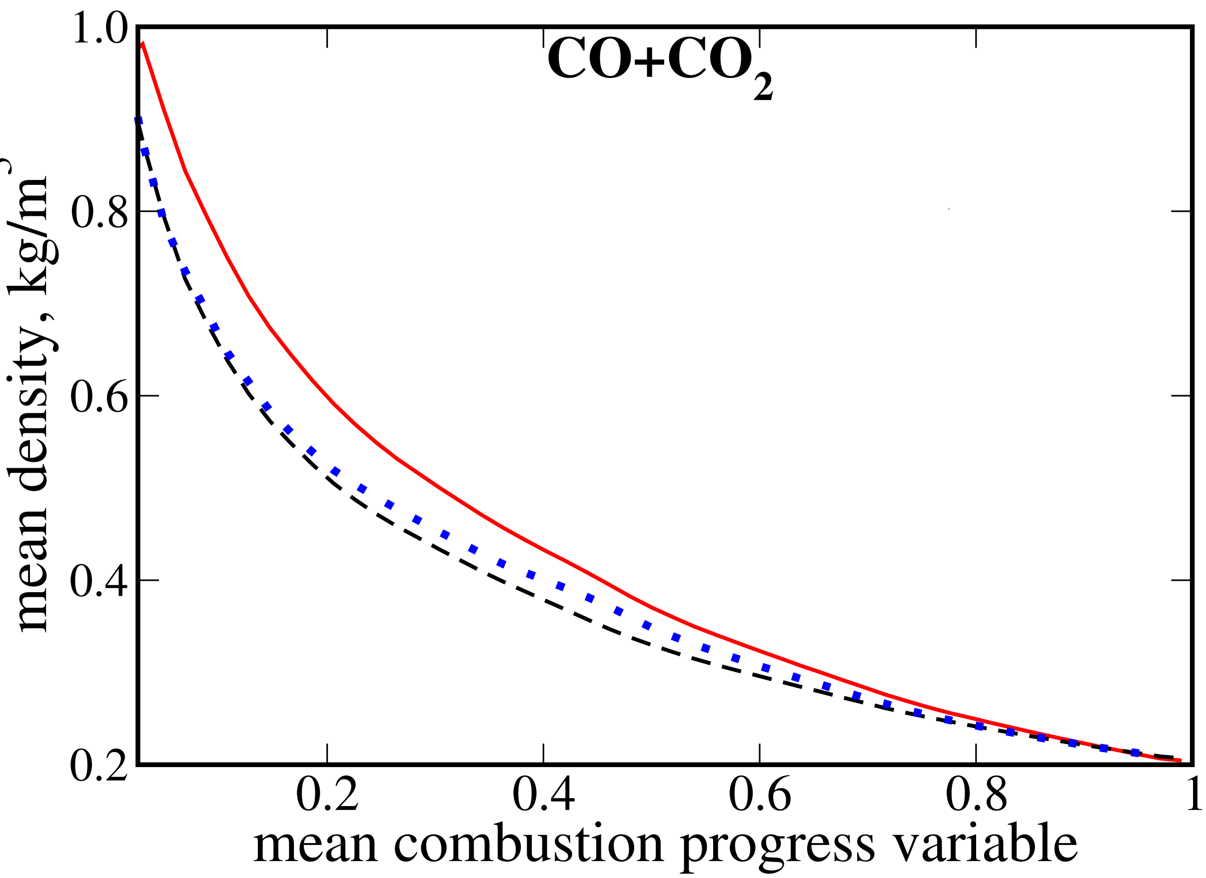
CO+CO2
mean density, kg/m3
mean combustion progress variable
1.0
0.8
0.6
0.4
0.2
0.2
0.4
0.6
0.8
1

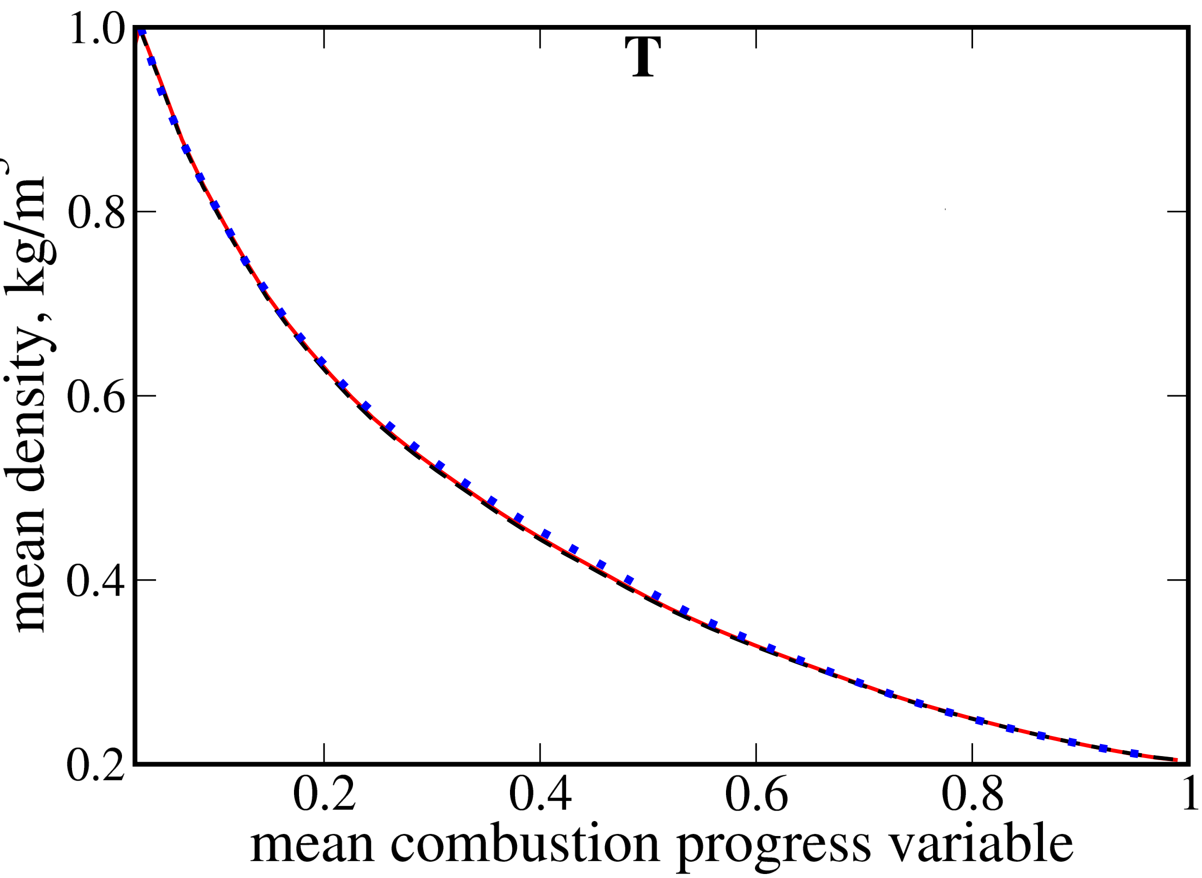
T
mean density, kg/m^3
mean combustion progress variable
1.0
0.8
0.6
0.4
0.2
0.2
0.4
0.6
0.8
1

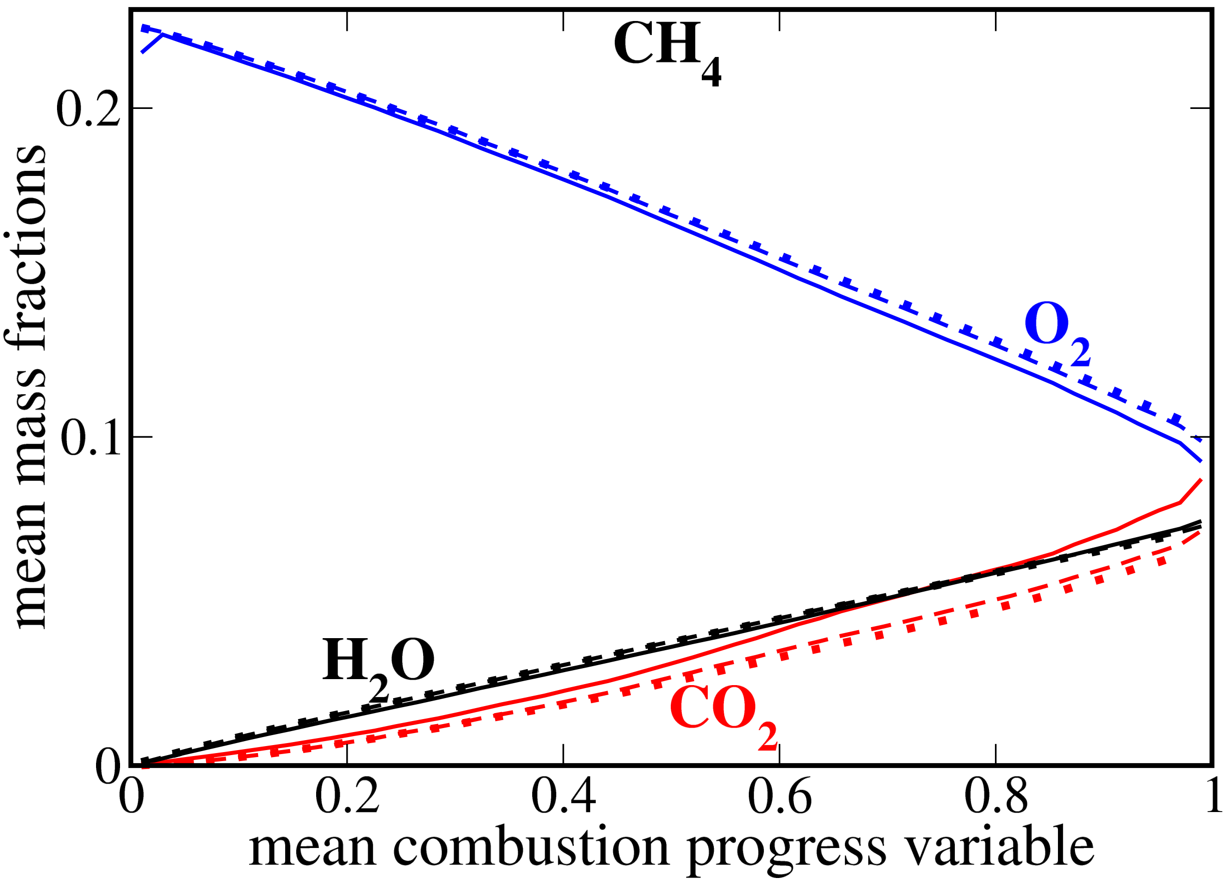
CH4
O2
H2O
CO2
0.2
0.1
0
0
0.2
0.4
0.6
0.8
1
mean mass fractions
mean combustion progress variable

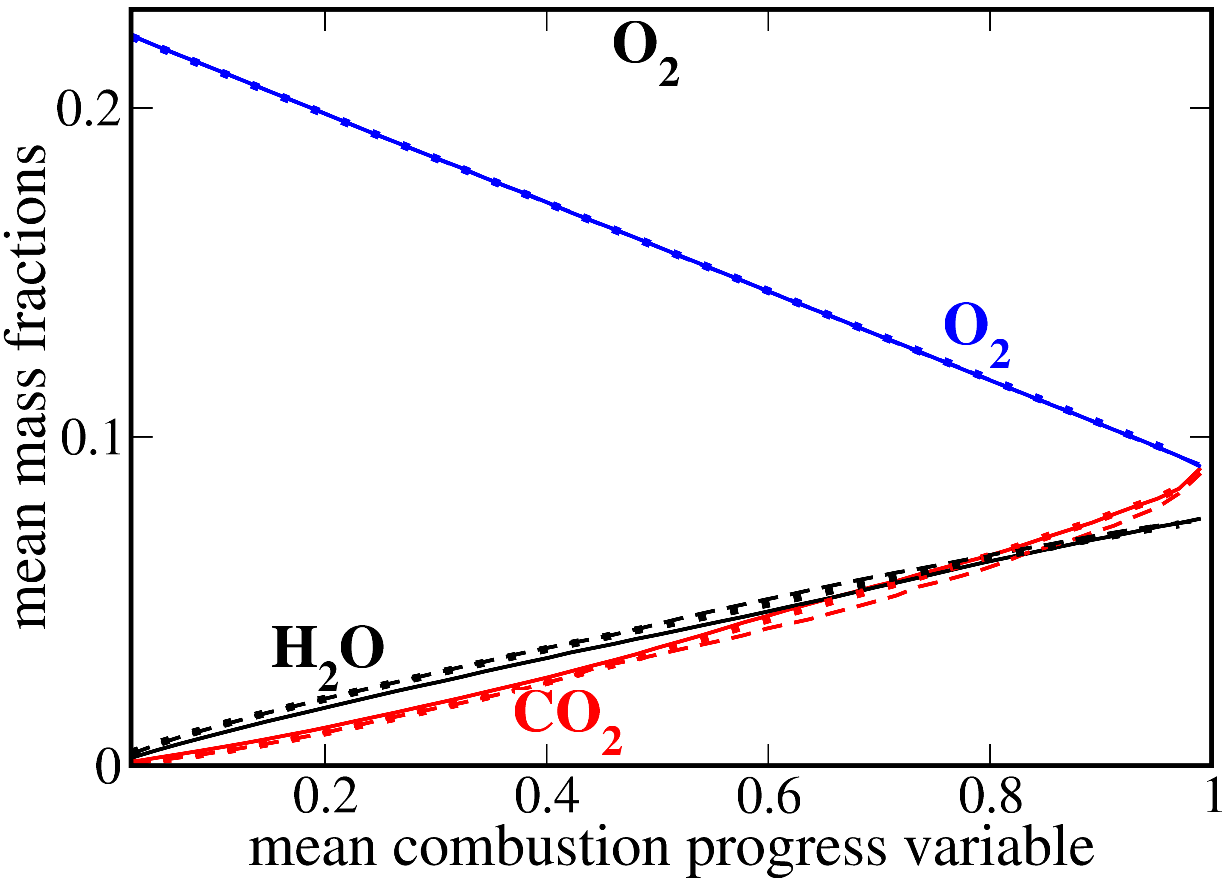
O_2
O_2
H_2O
CO_2
0.2
0.1
0
0.2
0.4
0.6
0.8
1
mean mass fractions
mean combustion progress variable

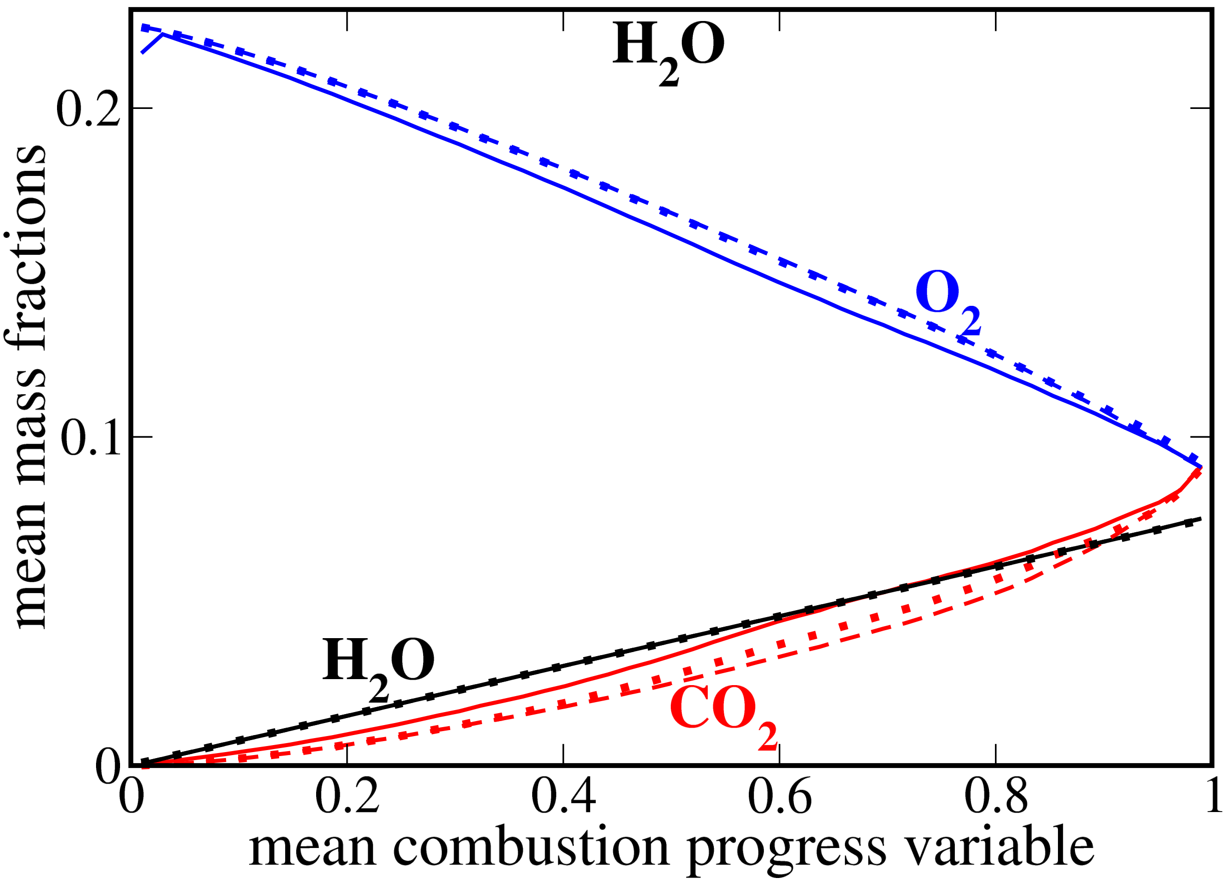
H_2O
O_2
H_2O
CO_2
0
0.1
0.2
0
0.2
0.4
0.6
0.8
1
mean mass fractions
mean combustion progress variable

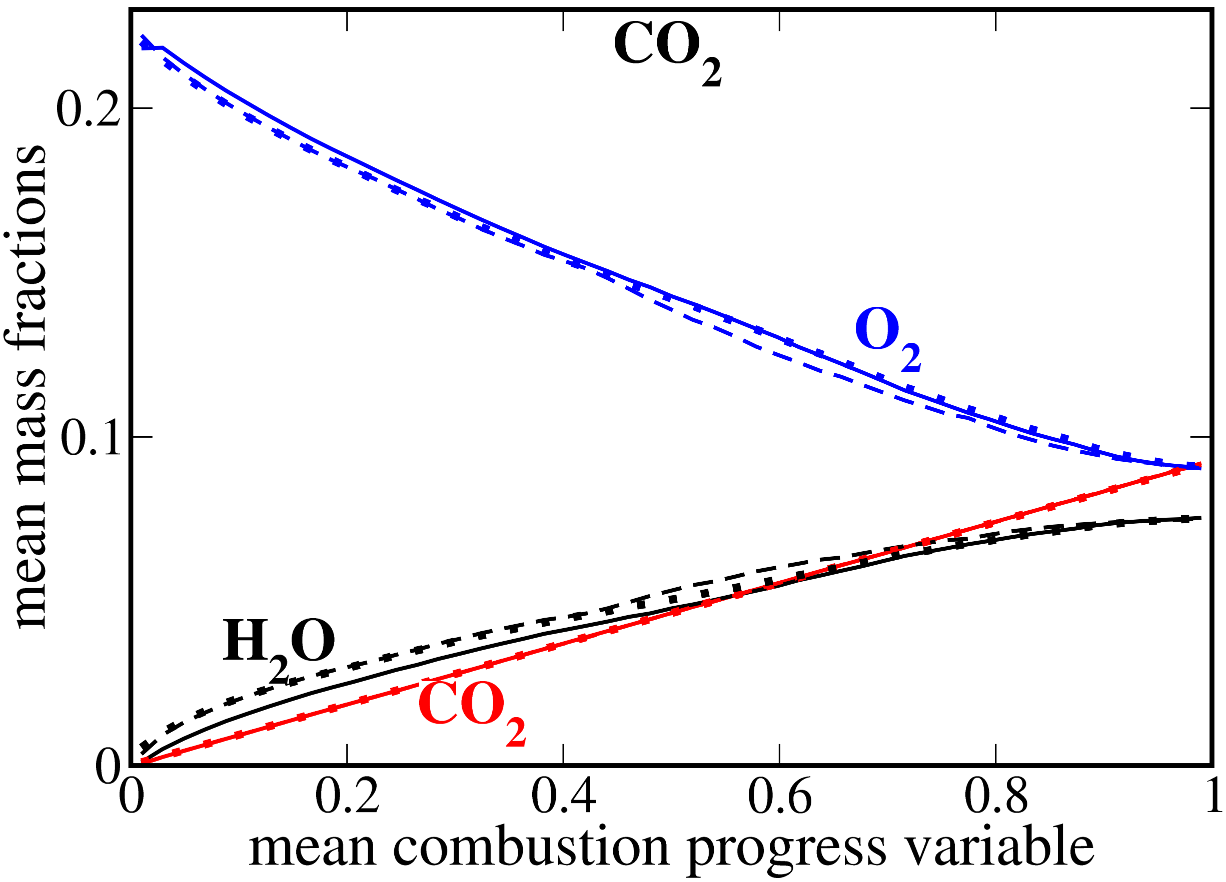
CO_2
O_2
H_2O
CO_2
mean mass fractions
mean combustion progress variable
0
0.1
0.2
0
0.2
0.4
0.6
0.8
1

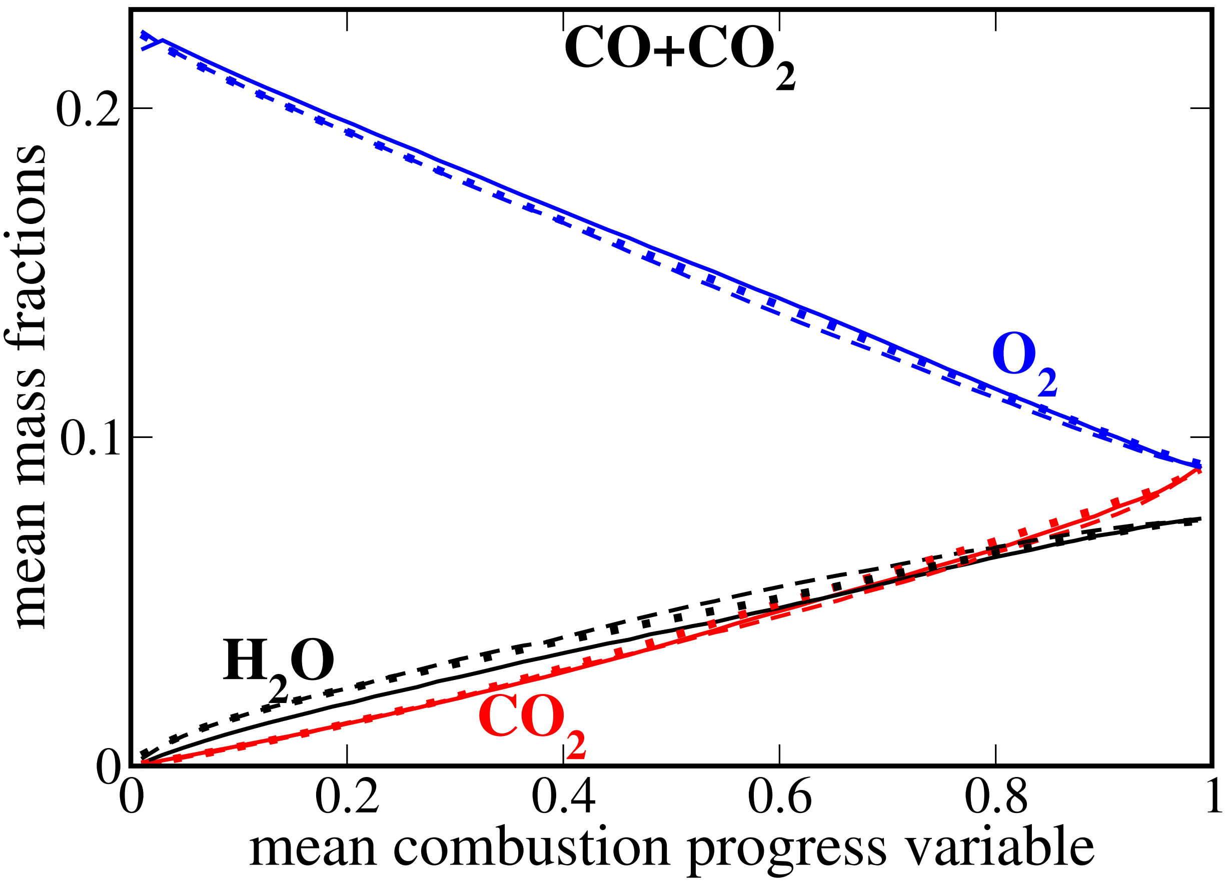
CO+CO$_2$
O$_2$
H$_2$O
CO$_2$
mean mass fractions
mean combustion progress variable
0
0.1
0.2
0
0.2
0.4
0.6
0.8
1

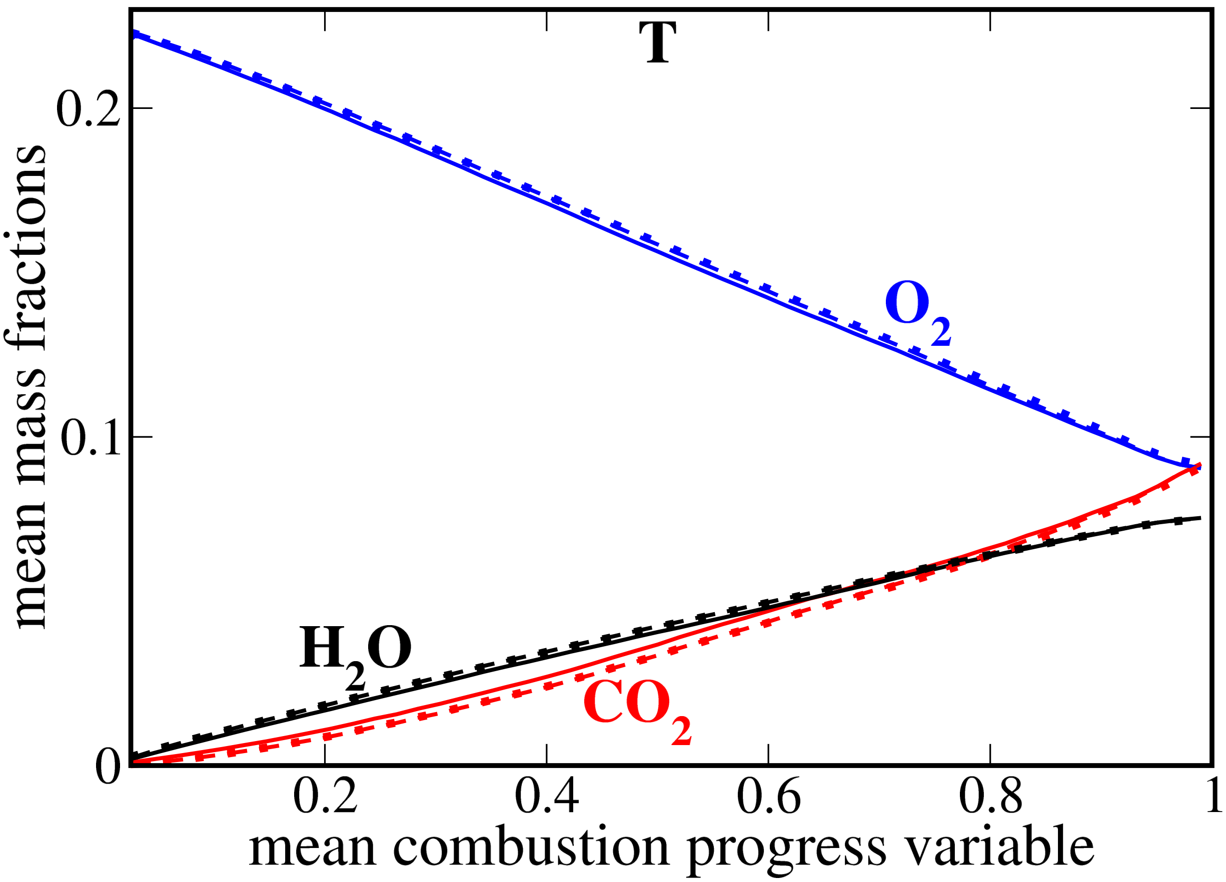
T
O_2
H_2O
CO_2
0
0.1
0.2
0.2
0.4
0.6
0.8
1
mean mass fractions
mean combustion progress variable

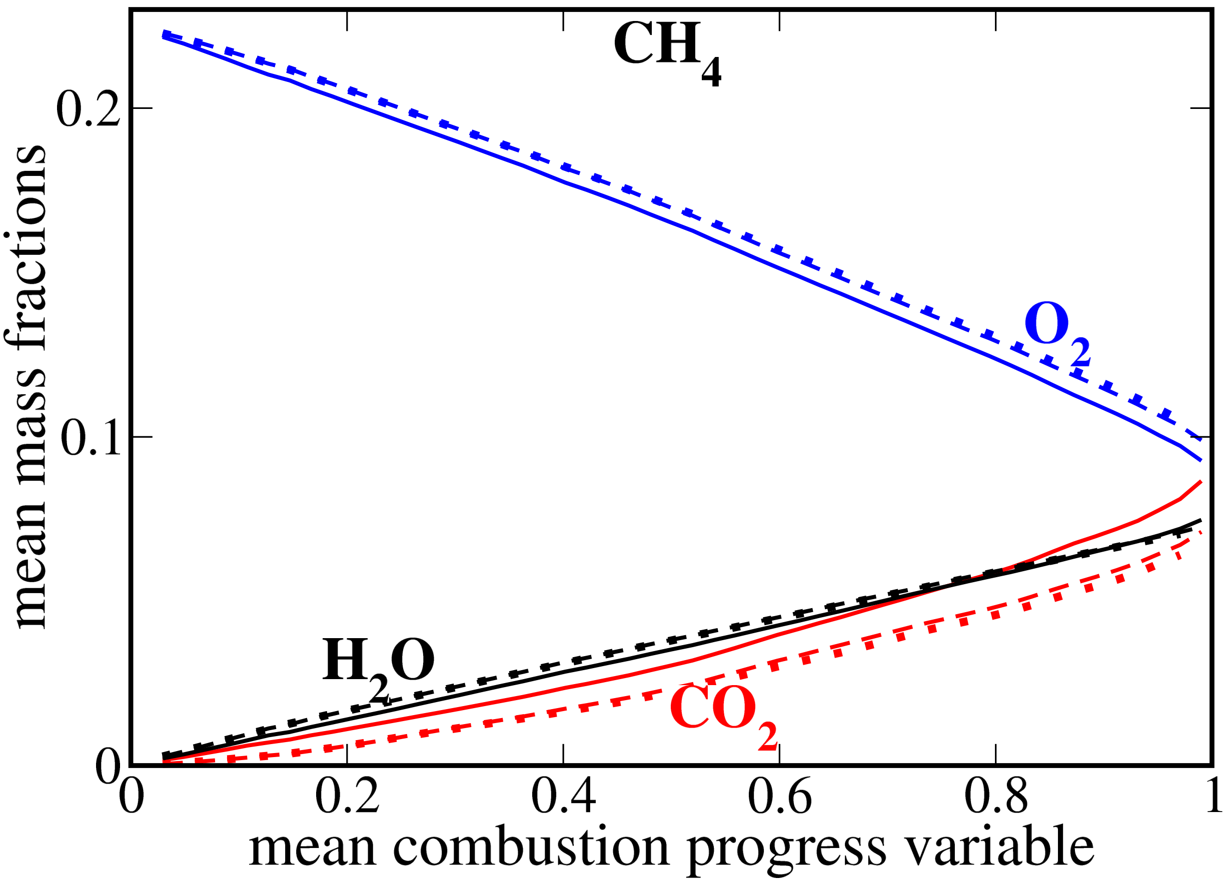
CH_4
O_2
H_2O
CO_2
0
0.1
0.2
0
0.2
0.4
0.6
0.8
1
mean mass fractions
mean combustion progress variable

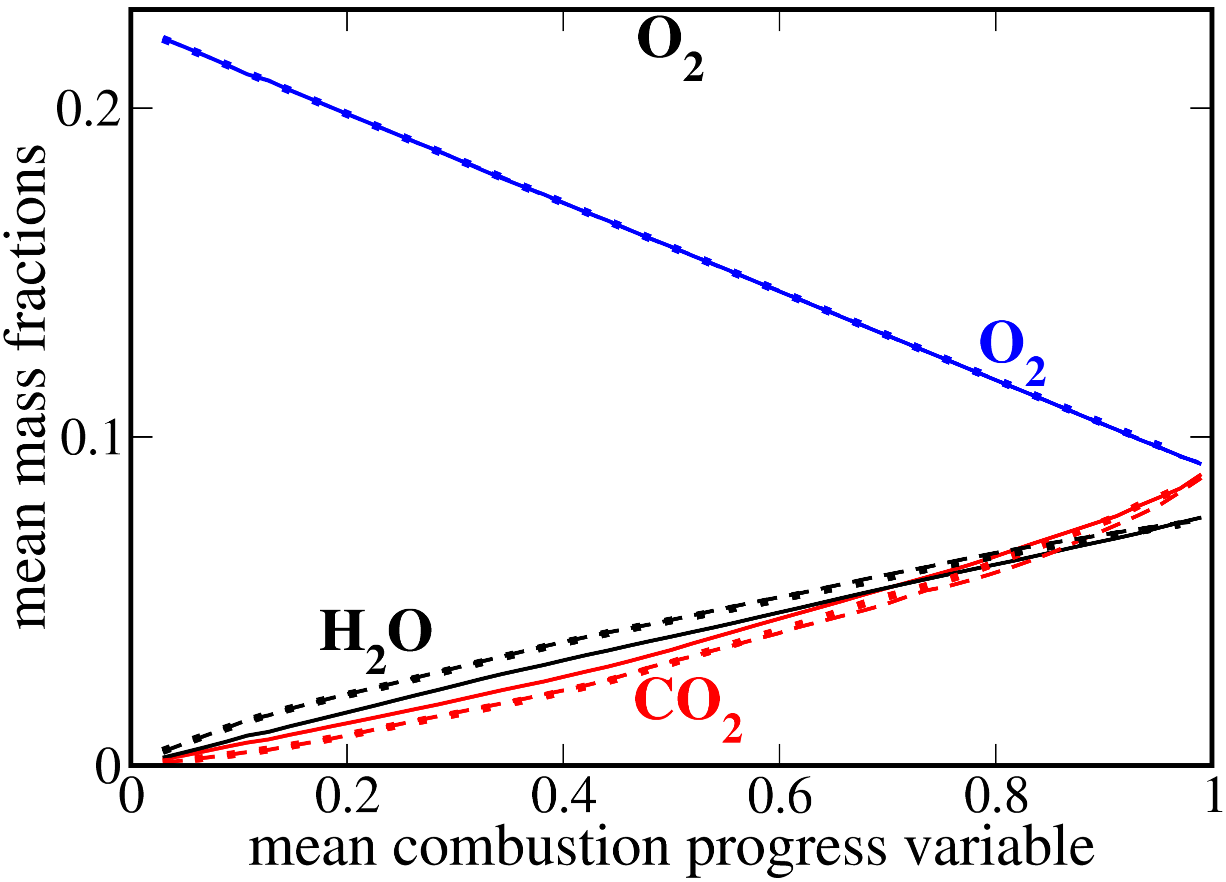
O_2
O_2
H_2O
CO_2
0
0.1
0.2
0
0.2
0.4
0.6
0.8
1
mean mass fractions
mean combustion progress variable

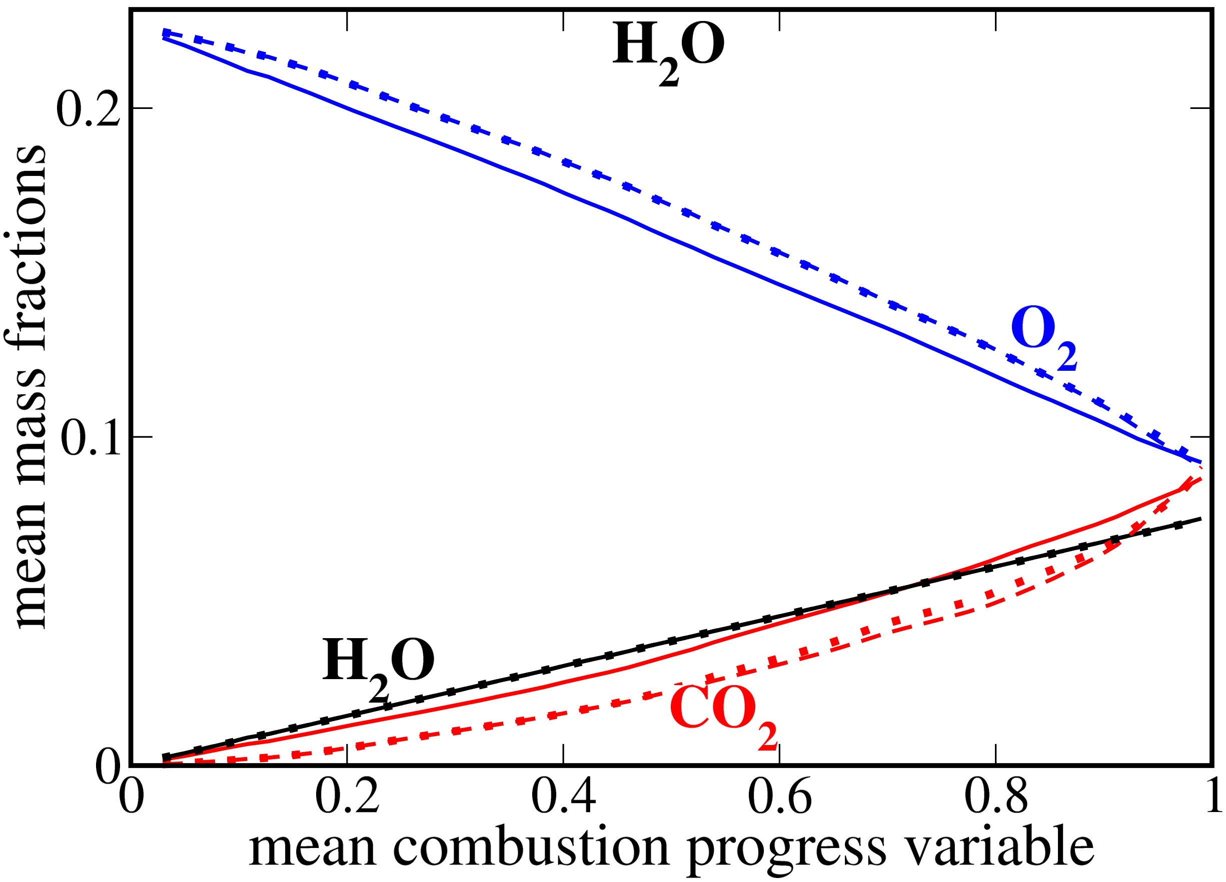
H_2O
O_2
H_2O
CO_2
0.2
0.1
0
0
0.2
0.4
0.6
0.8
1
mean mass fractions
mean combustion progress variable

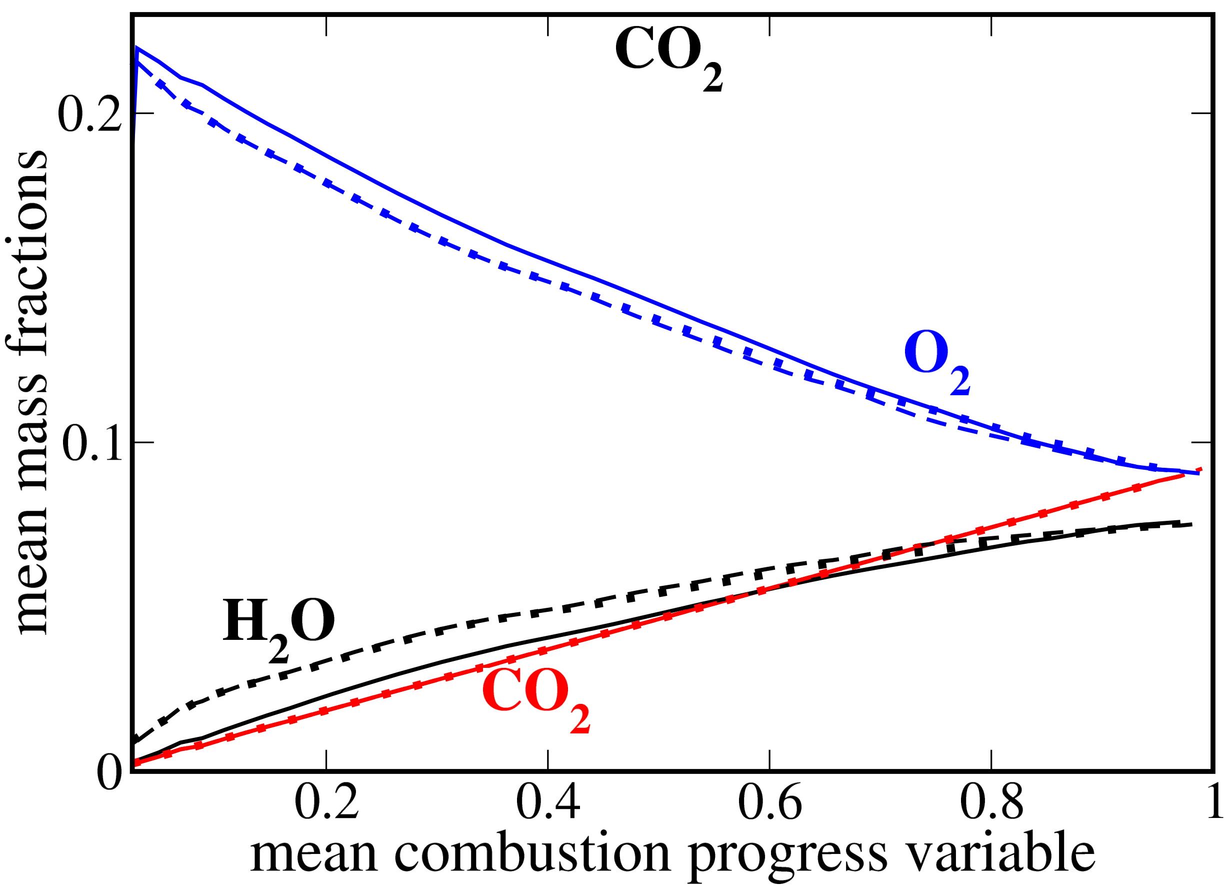
CO_2
0.2
0.1
0
mean mass fractions
O_2
H_2O
CO_2
0.2
0.4
0.6
0.8
1
mean combustion progress variable

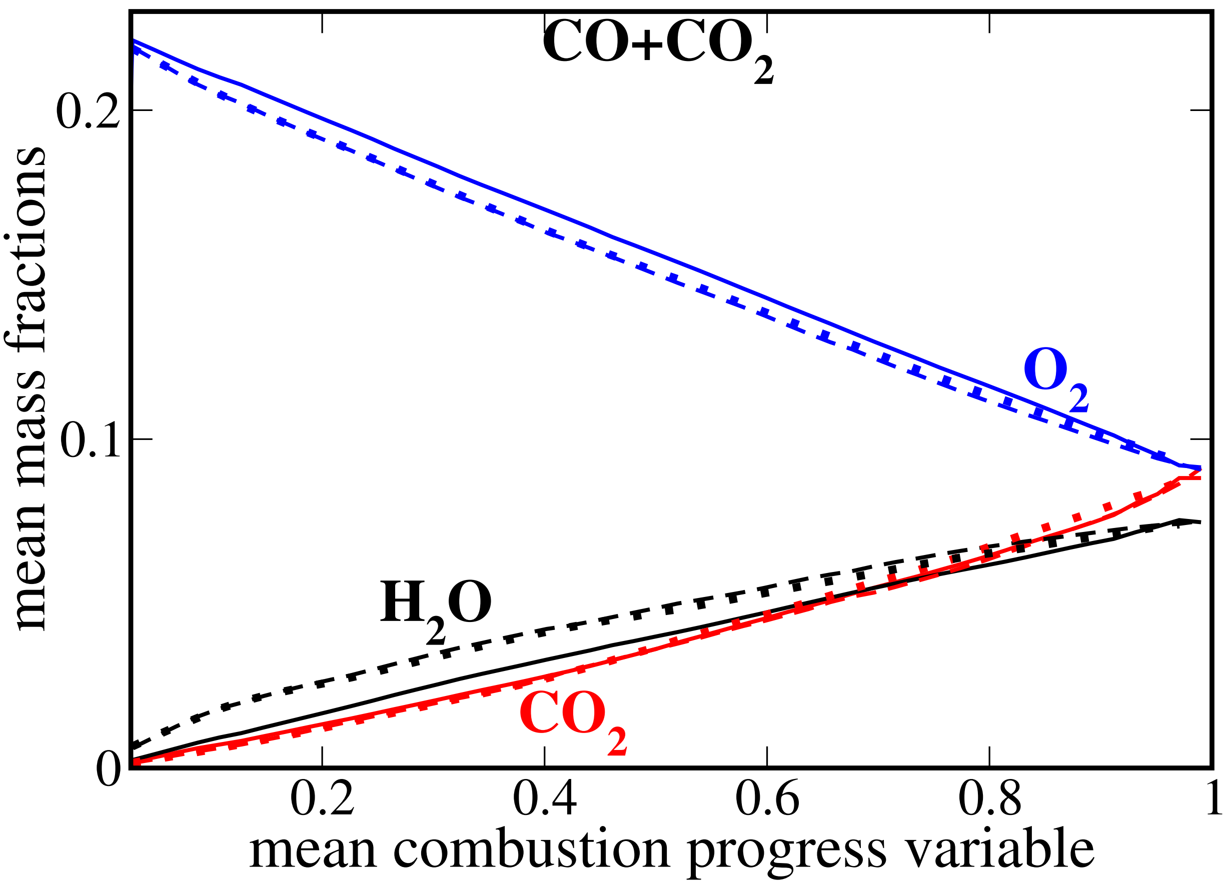
CO+CO2
O2
H2O
CO2
0
0.1
0.2
0.2
0.4
0.6
0.8
1
mean mass fractions
mean combustion progress variable

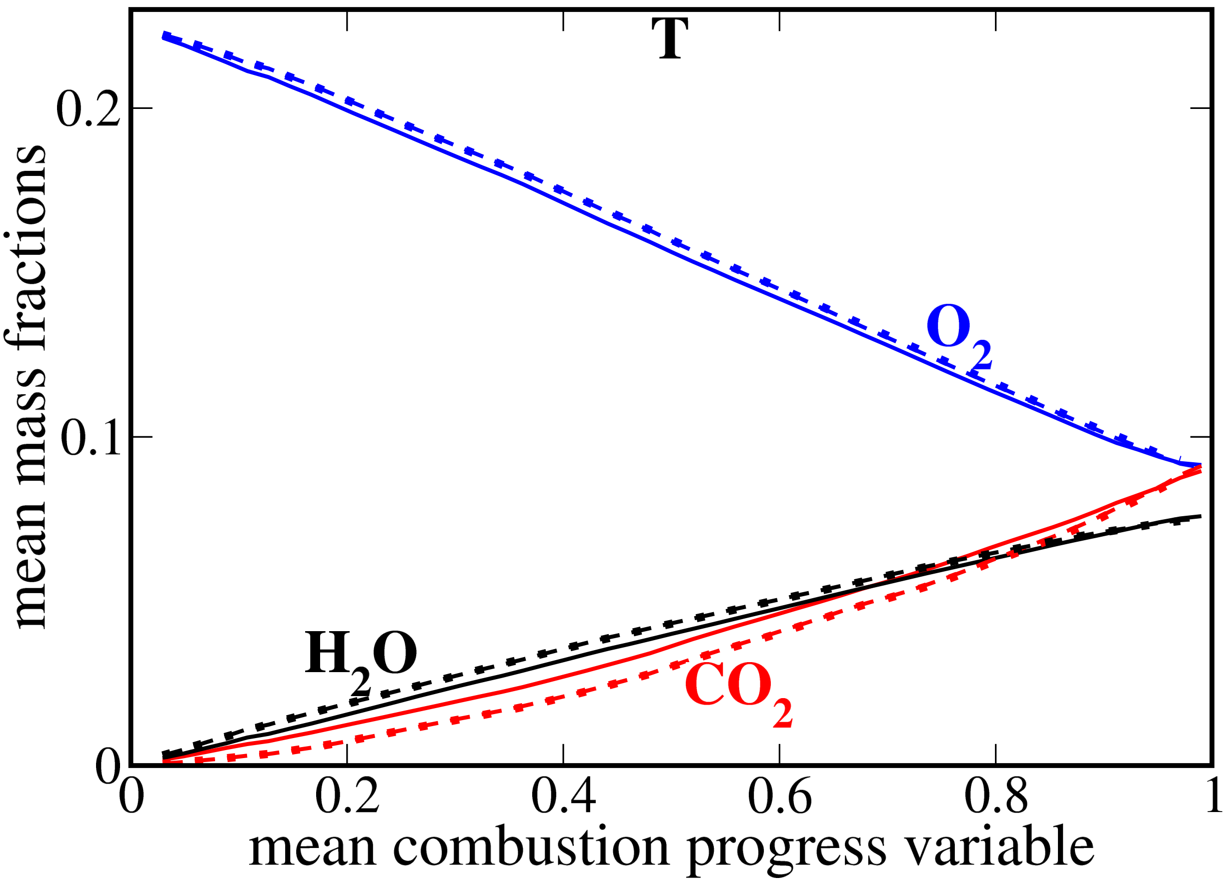
T
O_2
H_2O
CO_2
mean mass fractions
mean combustion progress variable
0
0.1
0.2
0
0.2
0.4
0.6
0.8
1

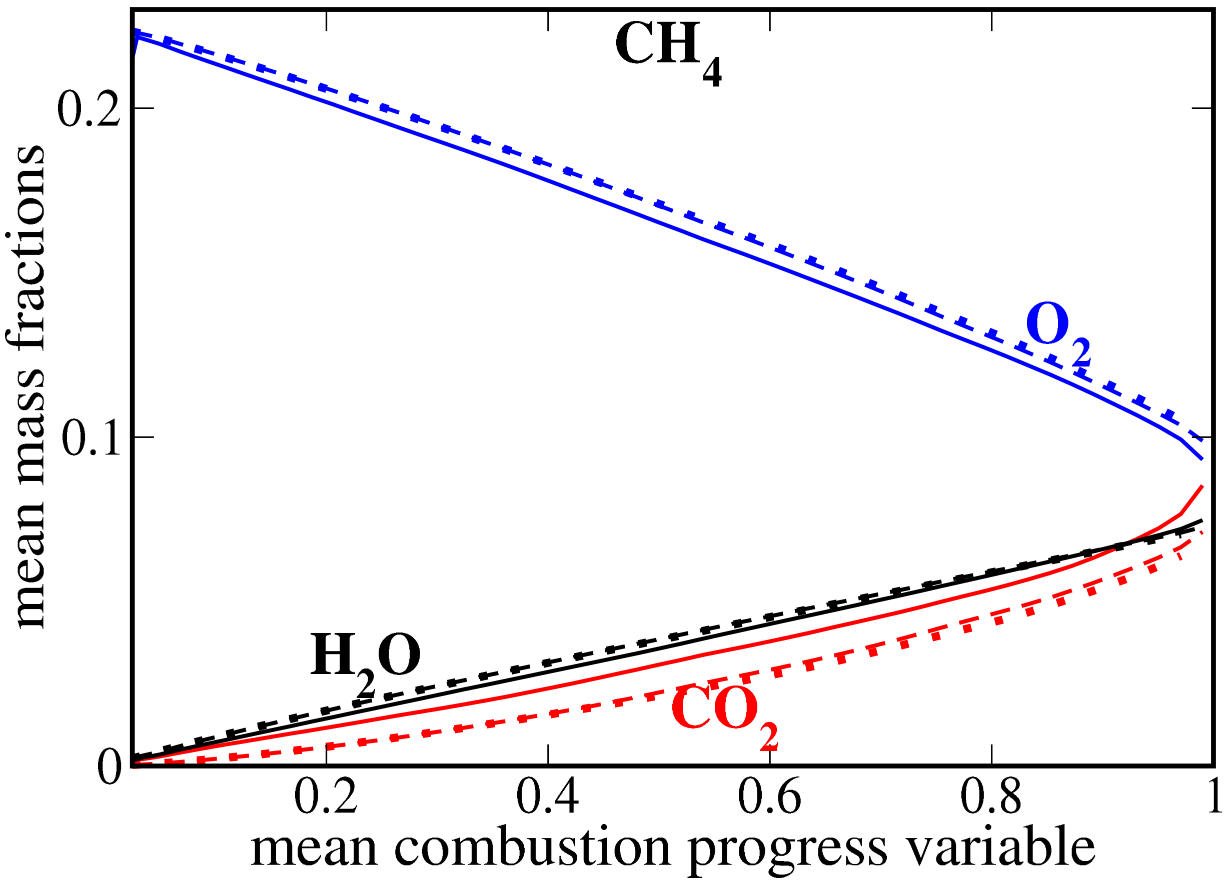
mean mass fractions
0.2
0.1
0
mean combustion progress variable
0.2
0.4
0.6
0.8
1
CH4
O2
H2O
CO2

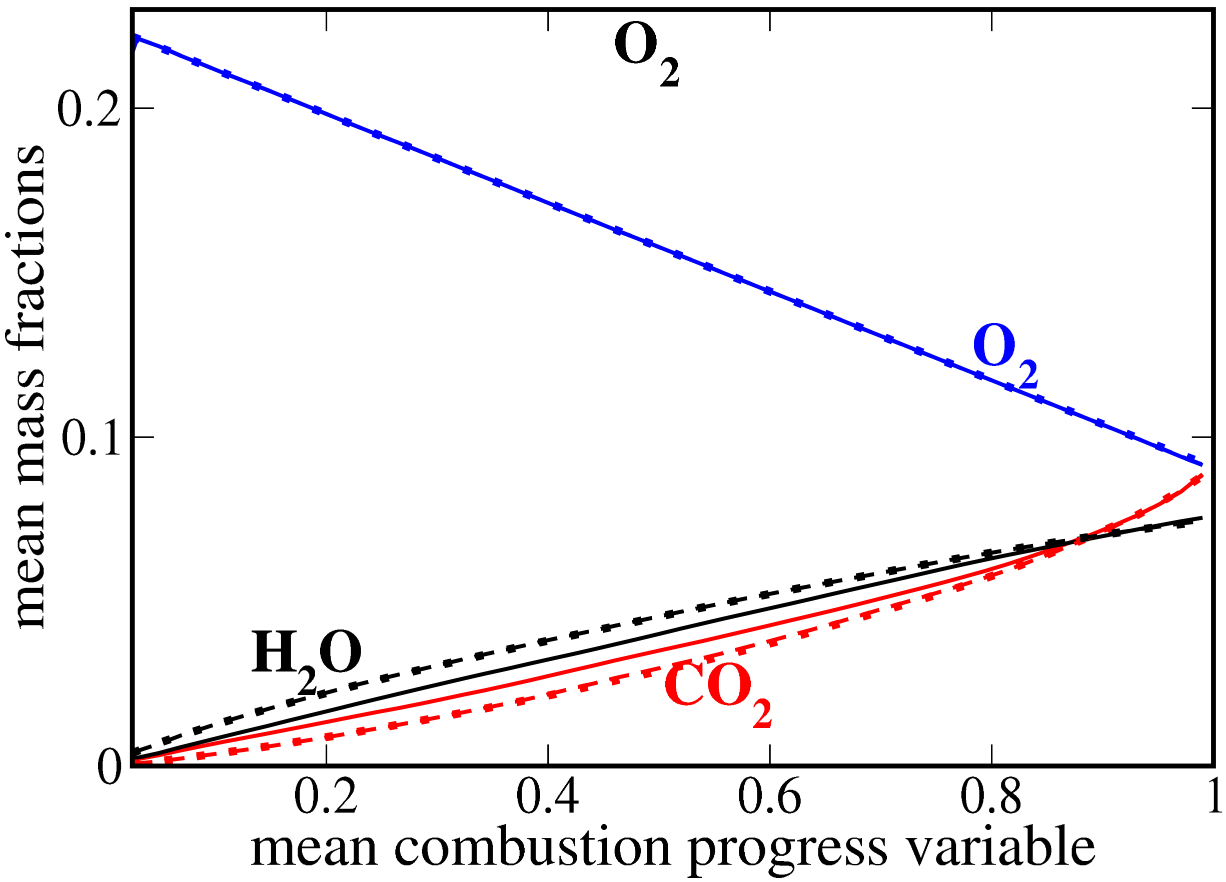

O_2
0.2
0.1
0
O_2
H_2O
CO_2
mean mass fractions
0.2
0.4
0.6
0.8
1
mean combustion progress variable

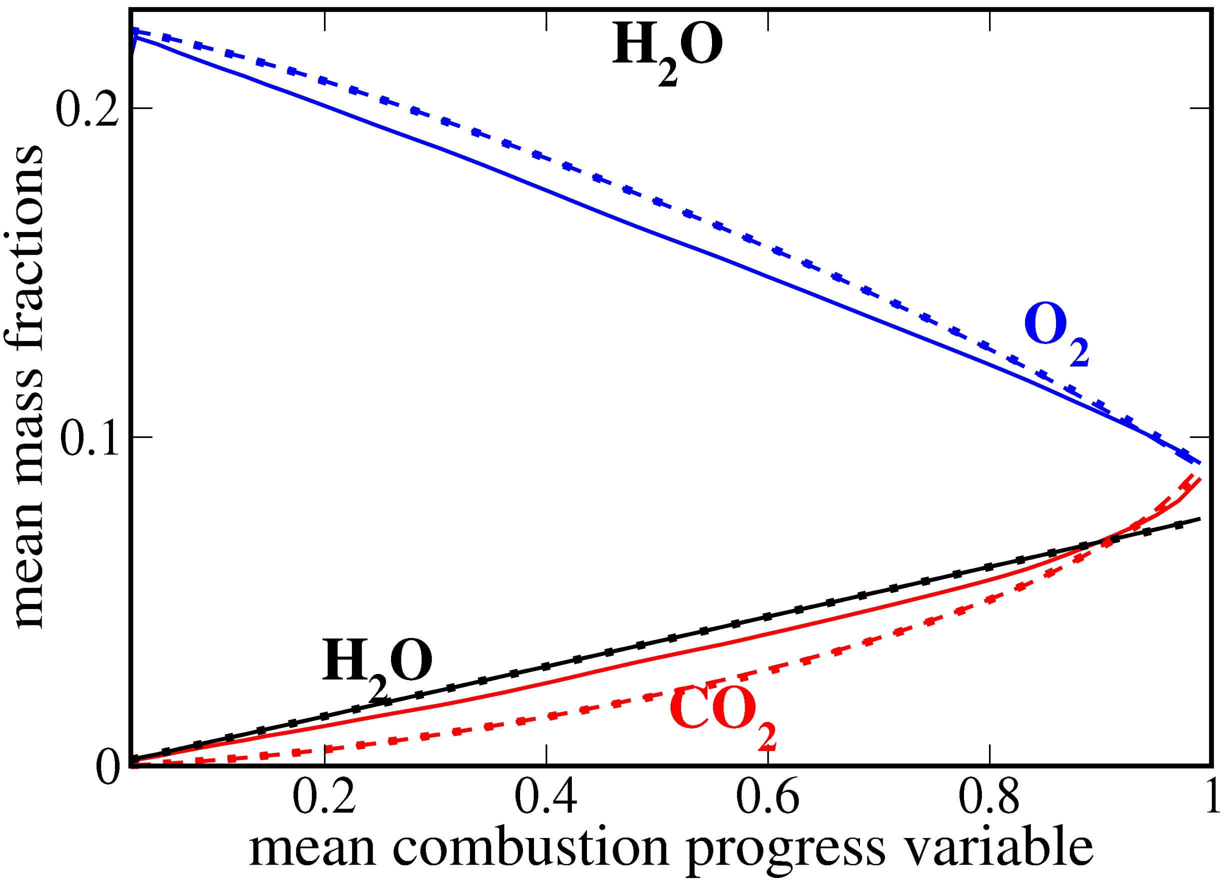
H2O
O2
H2O
CO2
0
0.1
0.2
0.2
0.4
0.6
0.8
1
mean mass fractions
mean combustion progress variable

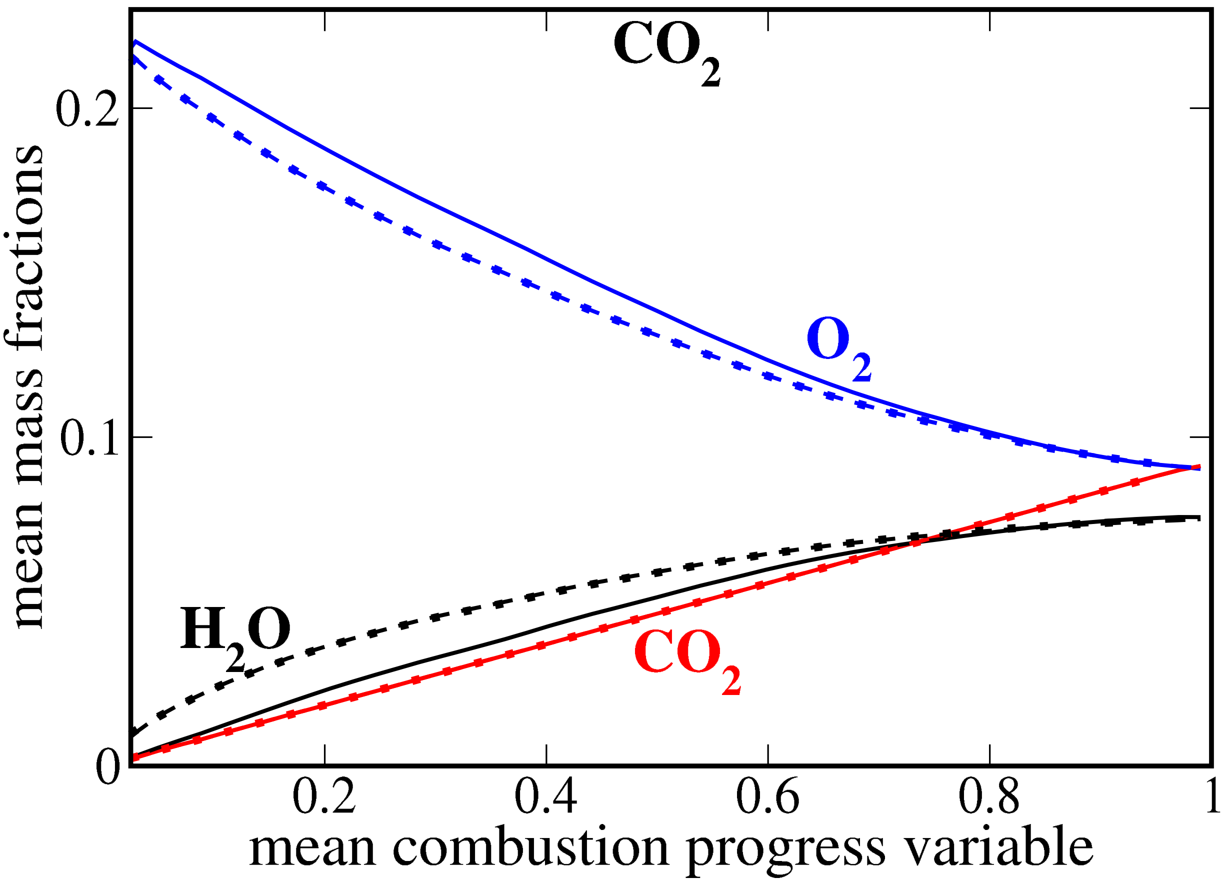
CO2
O2
H2O
CO2
0
0.1
0.2
0.2
0.4
0.6
0.8
1
mean mass fractions
mean combustion progress variable

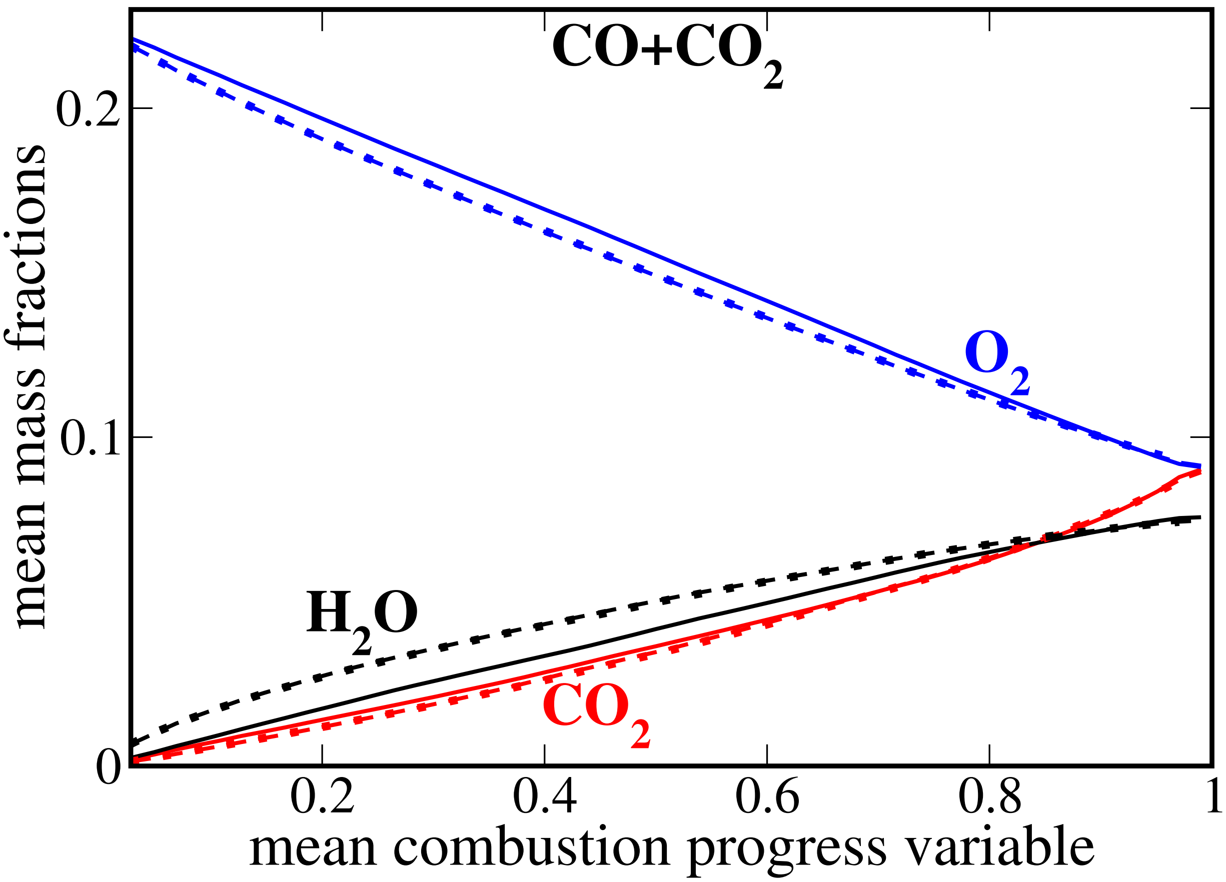
CO+CO2
O2
H2O
CO2
0.2
0.1
0
0.2
0.4
0.6
0.8
1
mean mass fractions
mean combustion progress variable

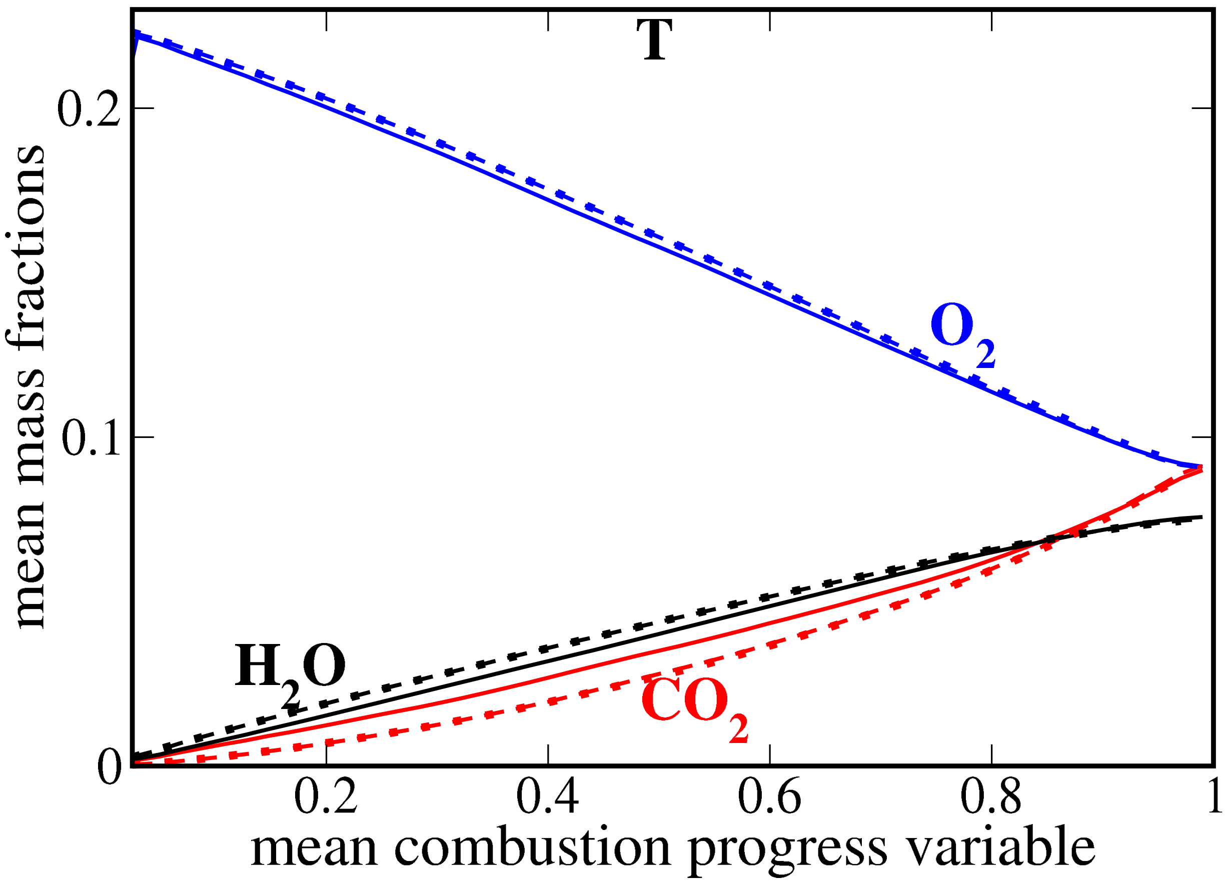
T
O_2
H_2O
CO_2
0.2
0.1
0
0.2
0.4
0.6
0.8
1
mean mass fractions
mean combustion progress variable

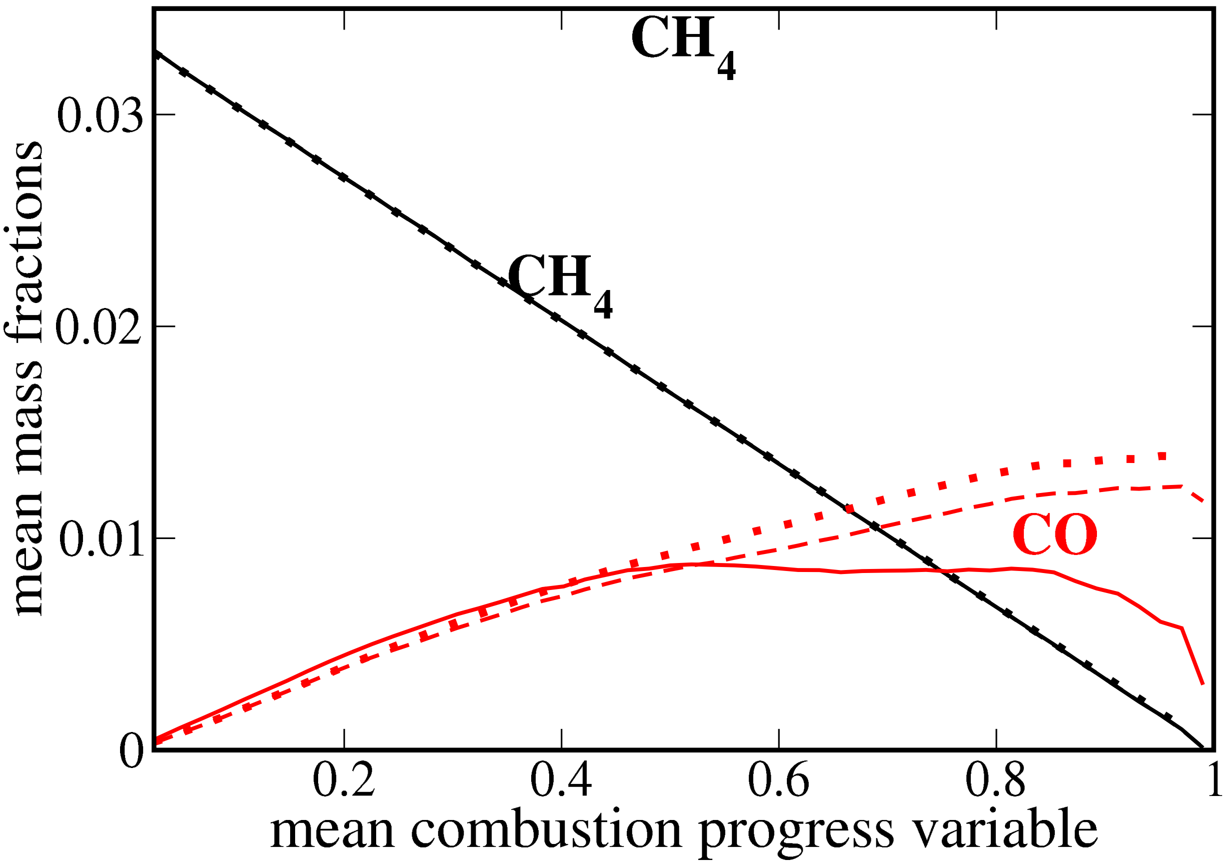
CH4
CH4
CO
0.03
0.02
0.01
0
0.2
0.4
0.6
0.8
1
mean mass fractions
mean combustion progress variable

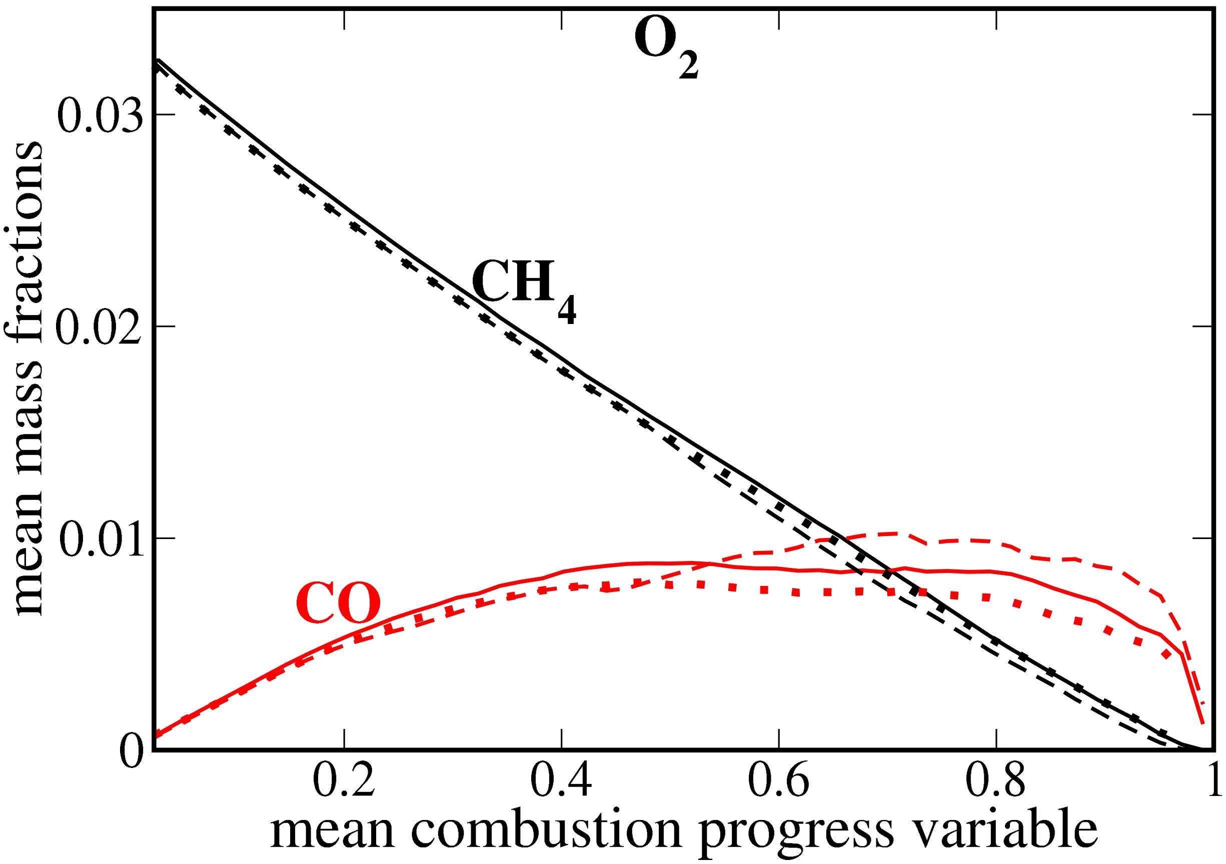
O_2
CH_4
CO
mean mass fractions
mean combustion progress variable
0
0.01
0.02
0.03
0.2
0.4
0.6
0.8
1

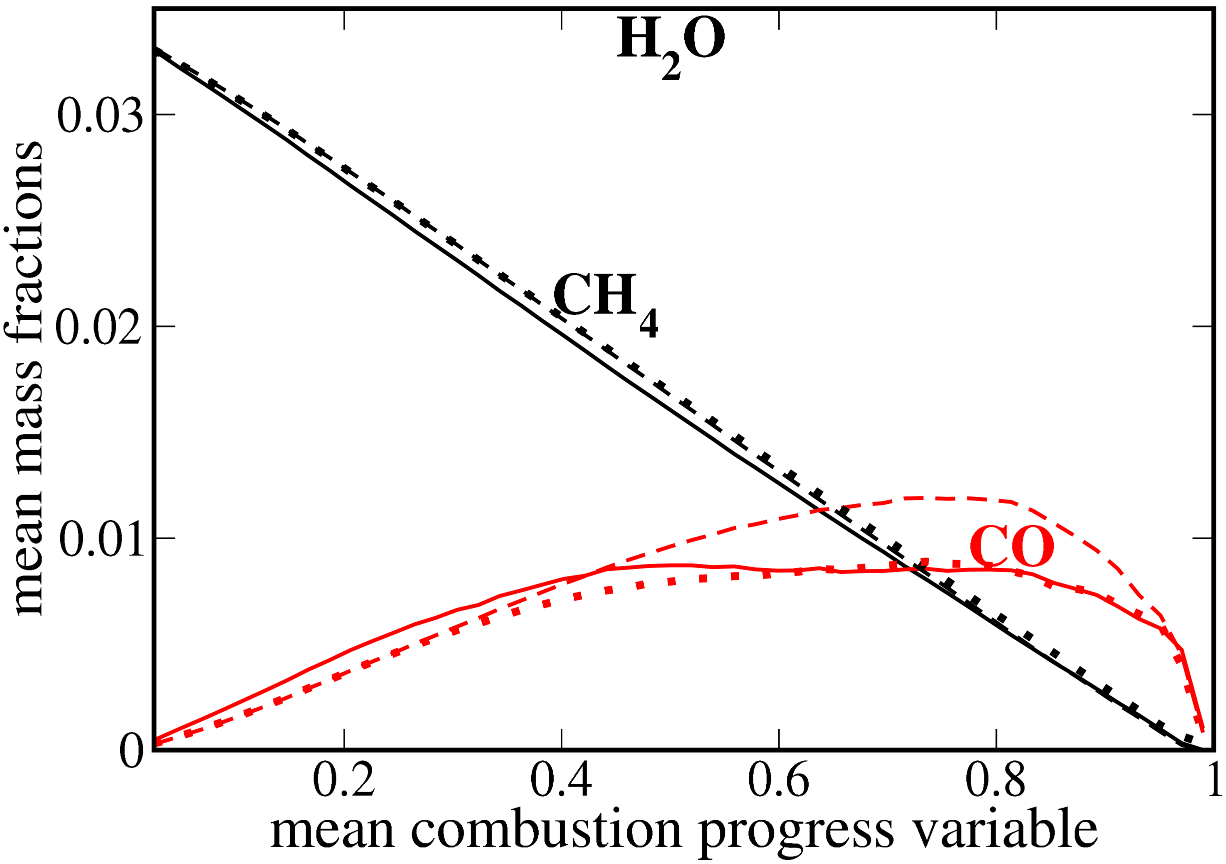
H2O
CH4
CO
0.03
0.02
0.01
0
0.2
0.4
0.6
0.8
1
mean mass fractions
mean combustion progress variable

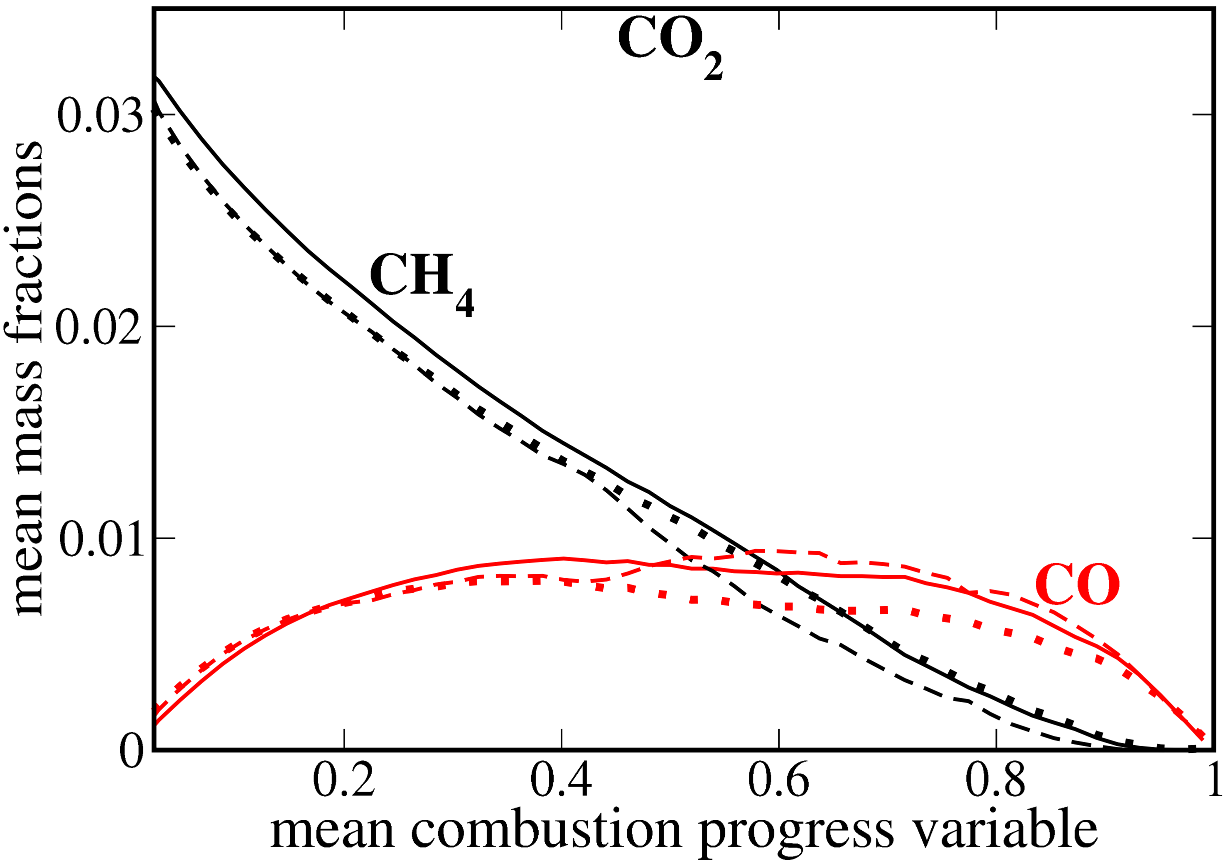
CO2
CH4
CO
mean mass fractions
0
0.01
0.02
0.03
0.2
0.4
0.6
0.8
1
mean combustion progress variable

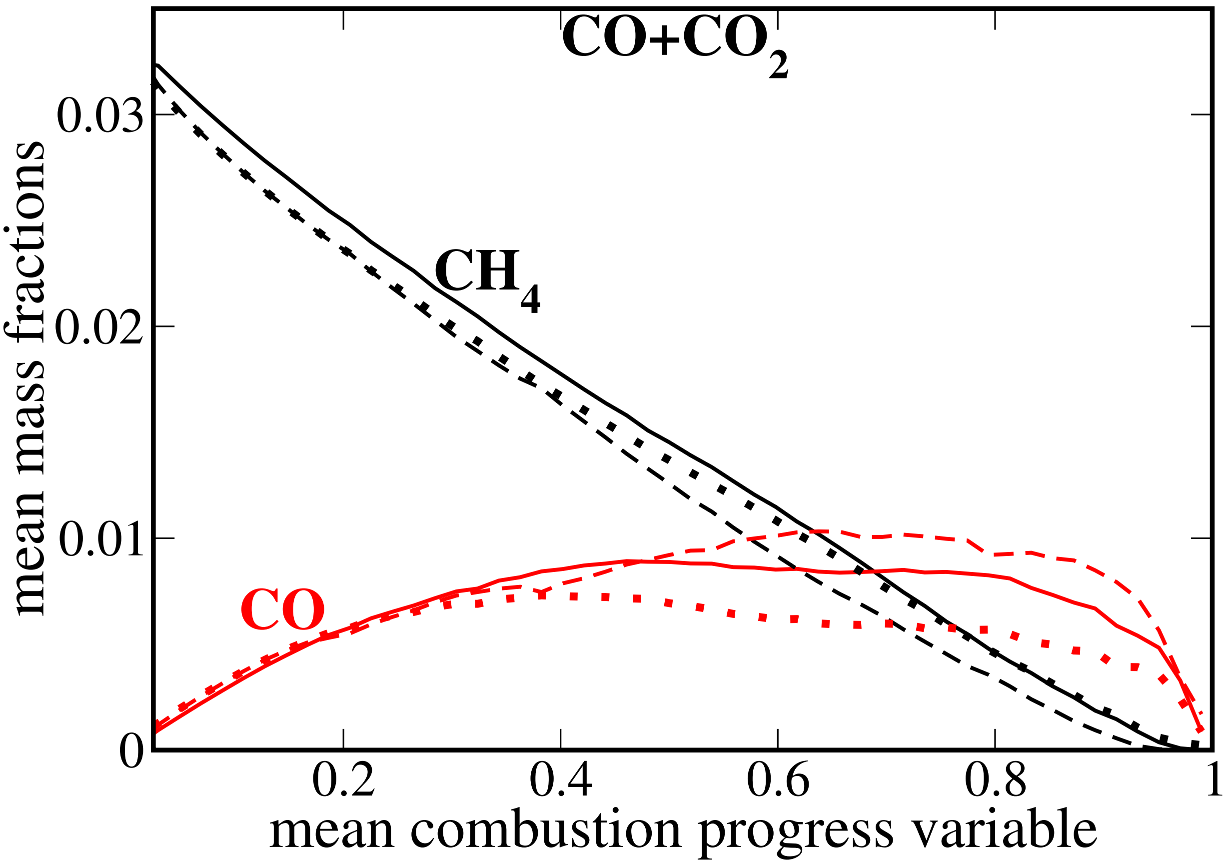
CO+CO2
CH4
CO
0.03
0.02
0.01
0
0.2
0.4
0.6
0.8
1
mean mass fractions
mean combustion progress variable

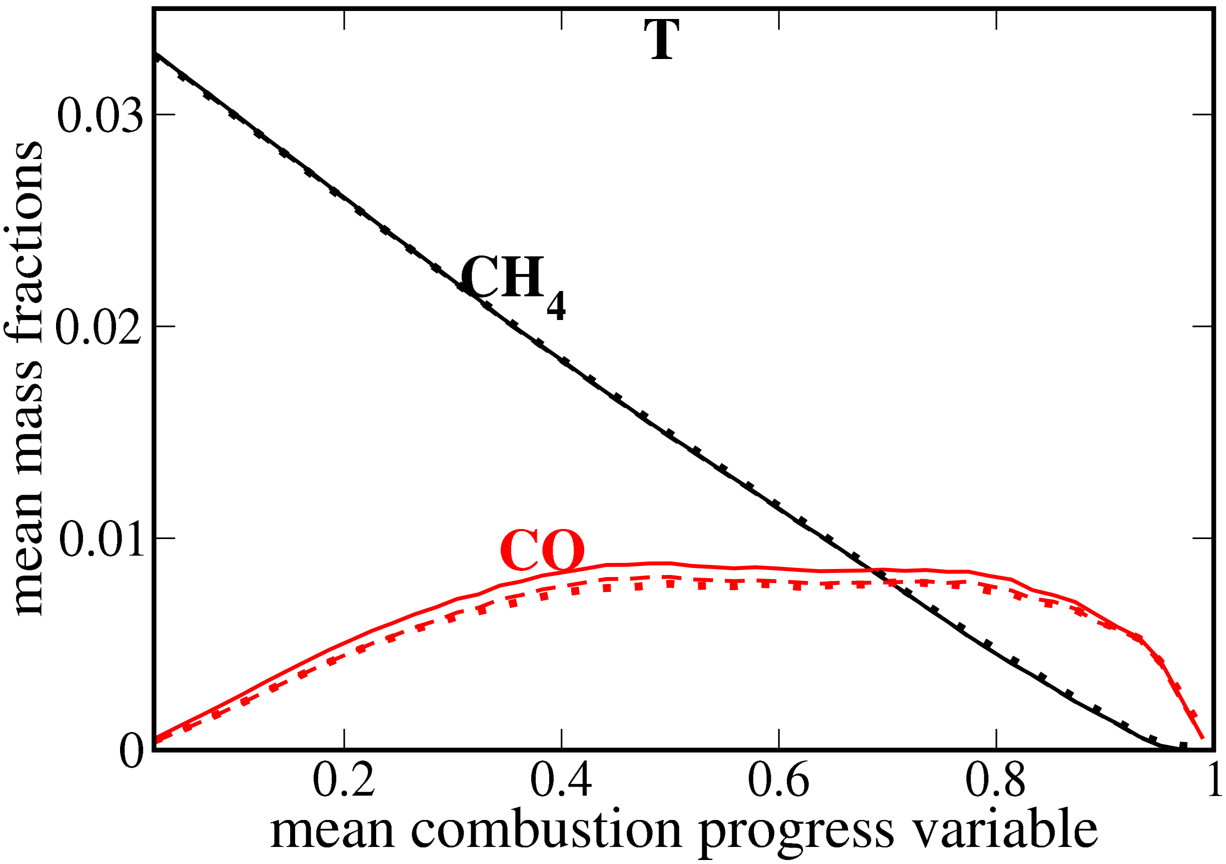
T
CH_4
CO
0.03
0.02
0.01
0
0.2
0.4
0.6
0.8
1
mean mass fractions
mean combustion progress variable

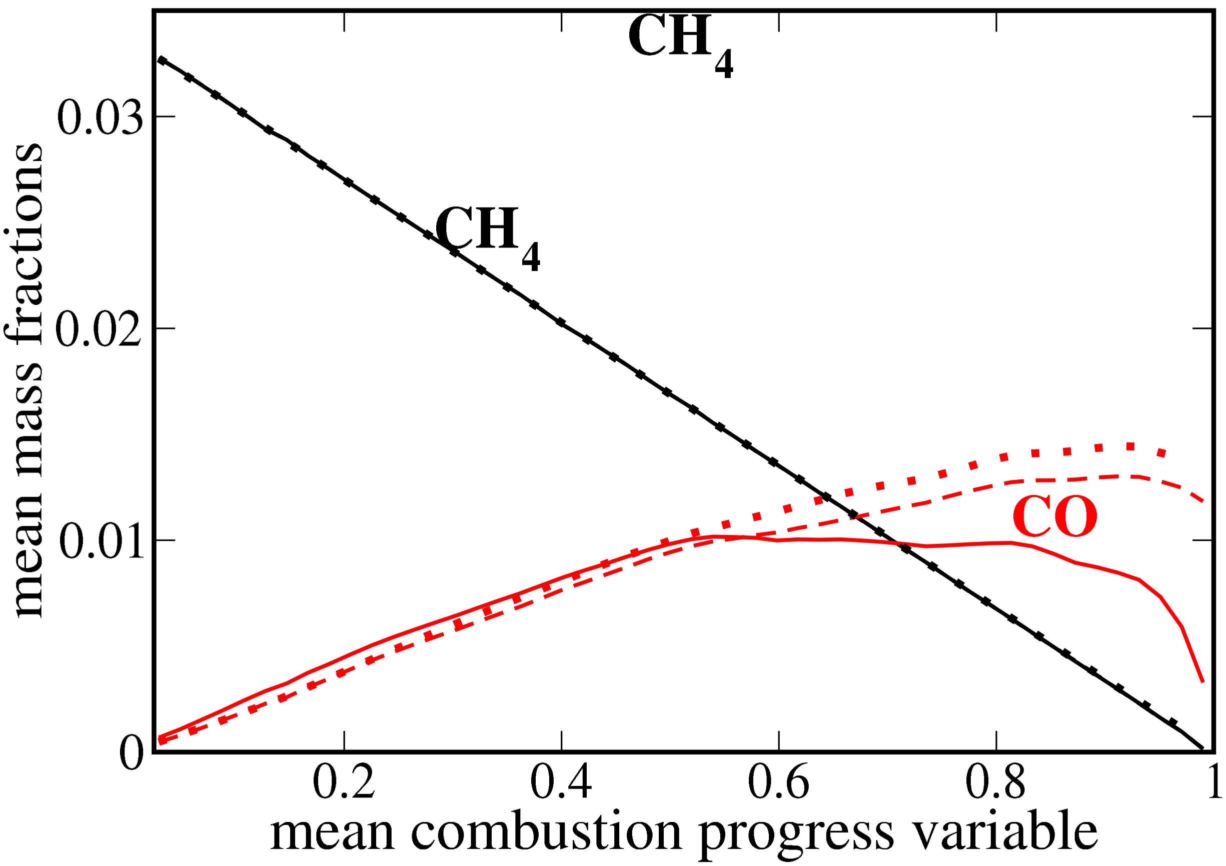
CH4
CH4
CO
0.03
0.02
0.01
0
0.2
0.4
0.6
0.8
1
mean mass fractions
mean combustion progress variable

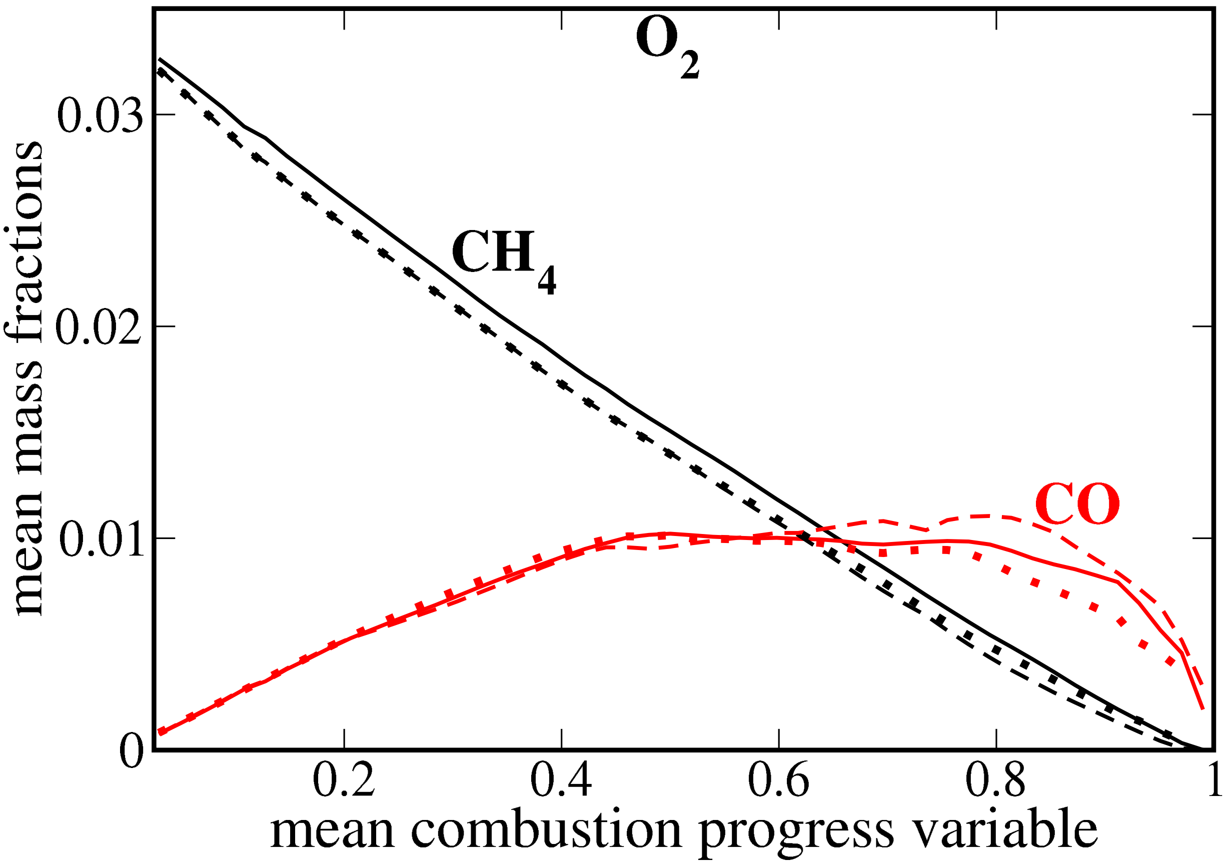
O2
CH4
CO
mean mass fractions
0.03
0.02
0.01
0
0.2
0.4
0.6
0.8
1
mean combustion progress variable

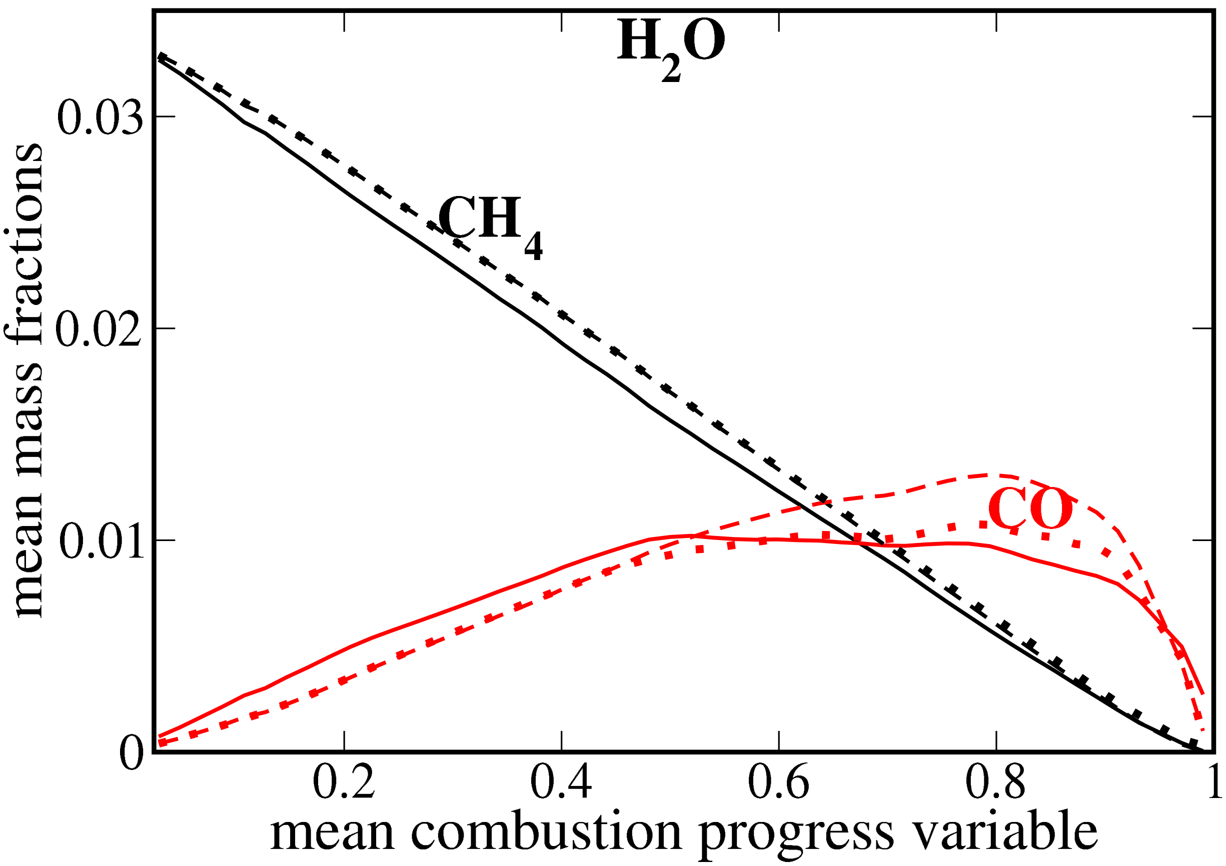
H_2O
CH_4
CO
0.03
0.02
0.01
0
0.2
0.4
0.6
0.8
1
mean mass fractions
mean combustion progress variable

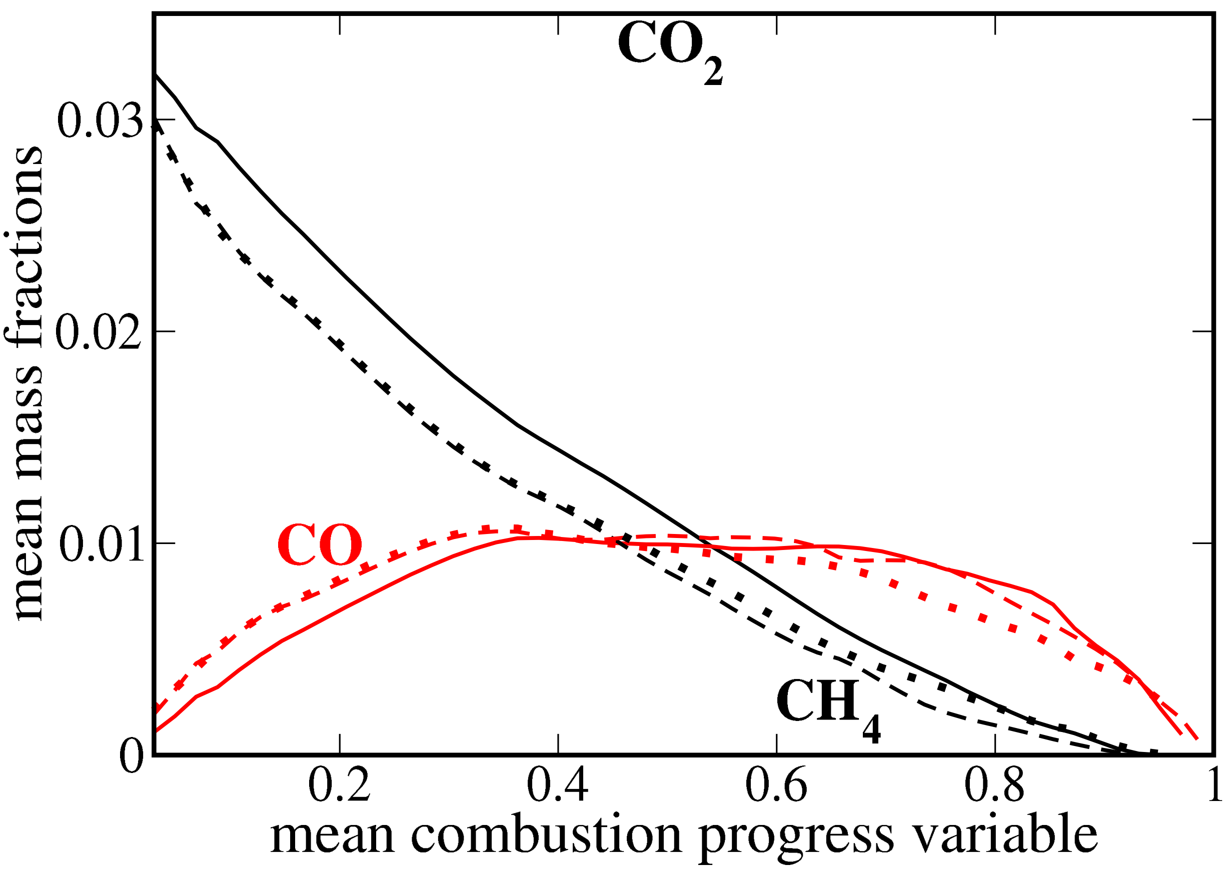
CO2
CO
CH4
0.03
0.02
0.01
0
0.2
0.4
0.6
0.8
1
mean mass fractions
mean combustion progress variable

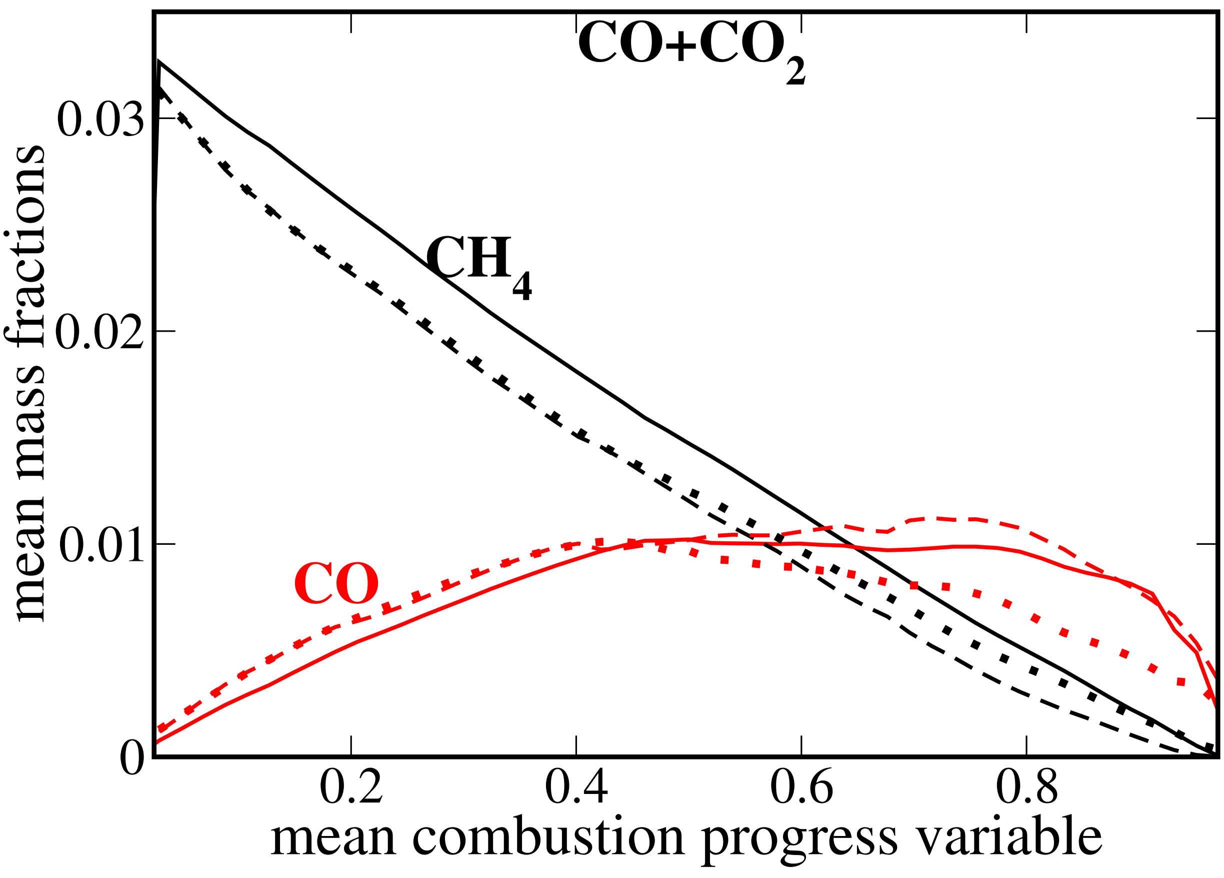
CO+CO$_2$
CH$_4$
CO
0.03
0.02
0.01
0
0.2
0.4
0.6
0.8
mean mass fractions
mean combustion progress variable

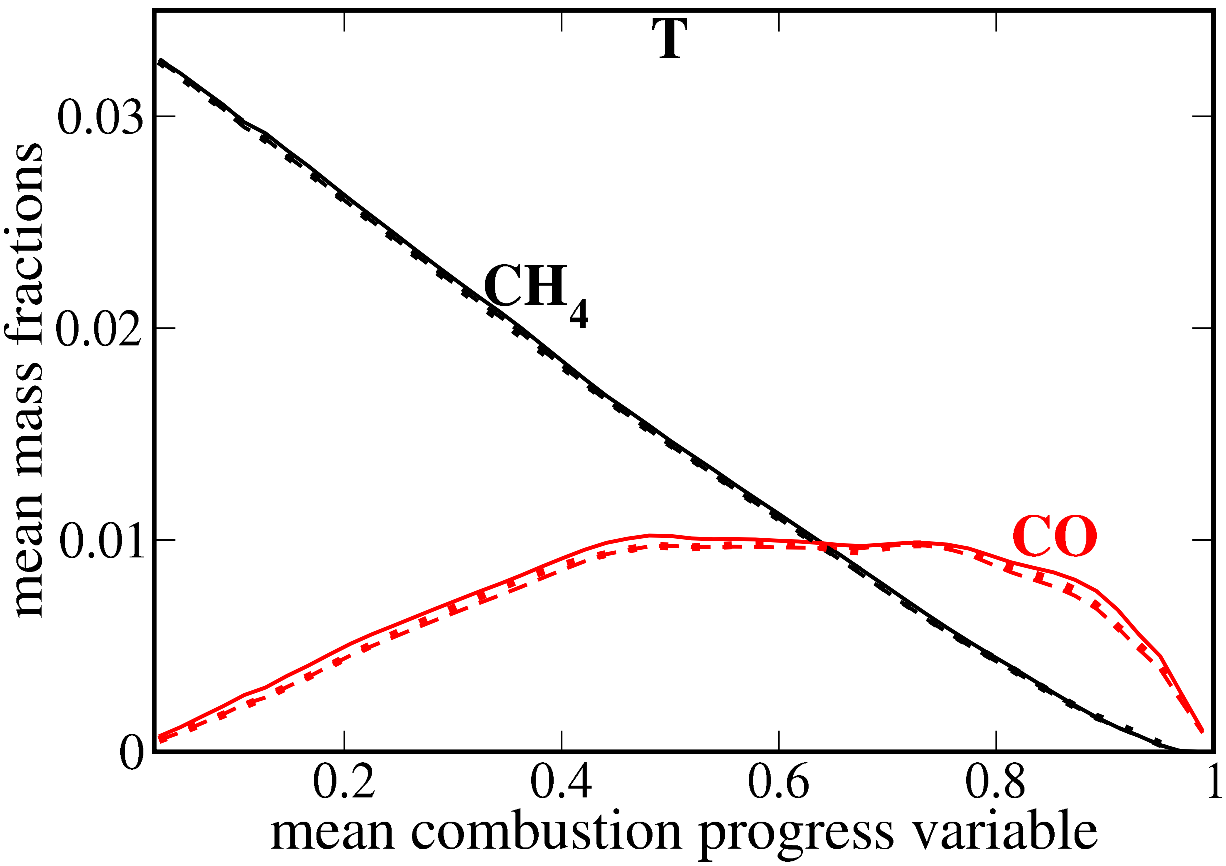
T
CH4
CO
0.03
0.02
0.01
0
0.2
0.4
0.6
0.8
1
mean mass fractions
mean combustion progress variable

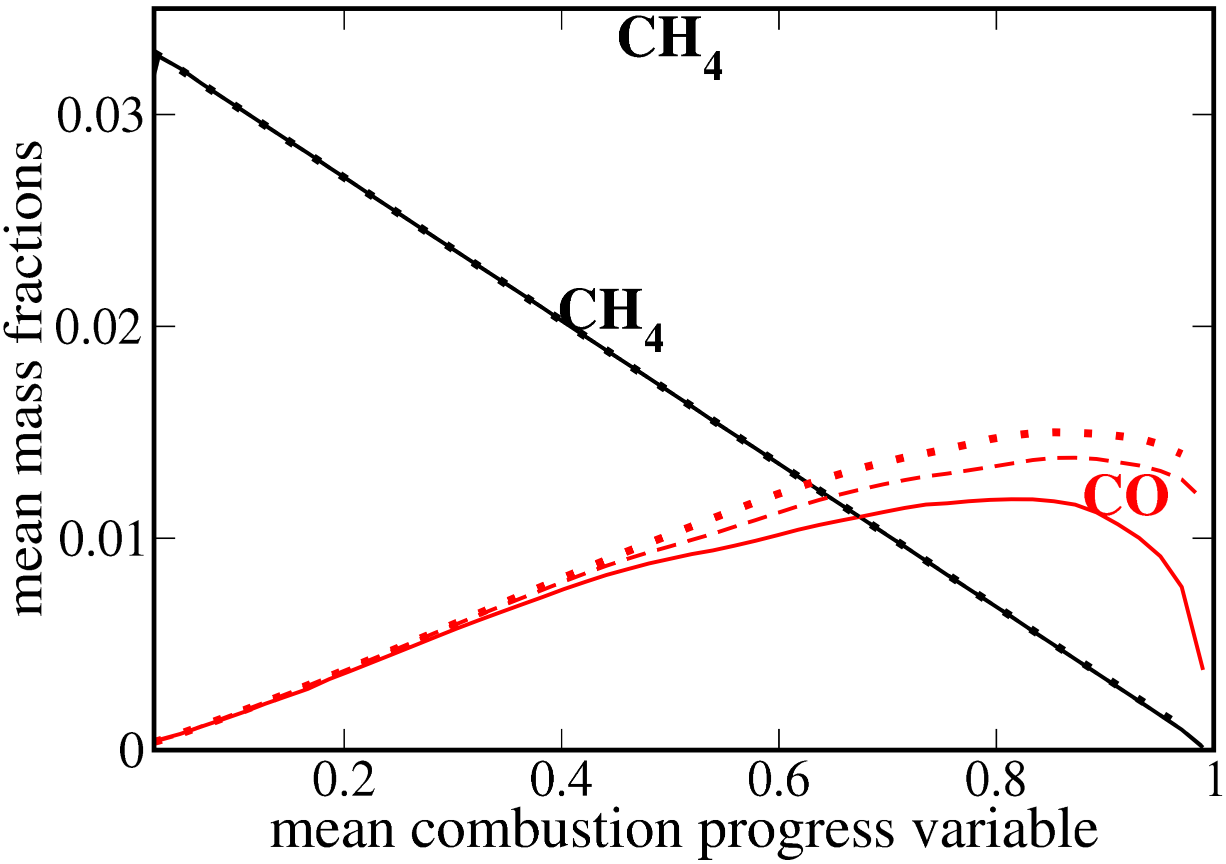
CH4
CH4
CO
0.03
0.02
0.01
0
0.2
0.4
0.6
0.8
1
mean mass fractions
mean combustion progress variable

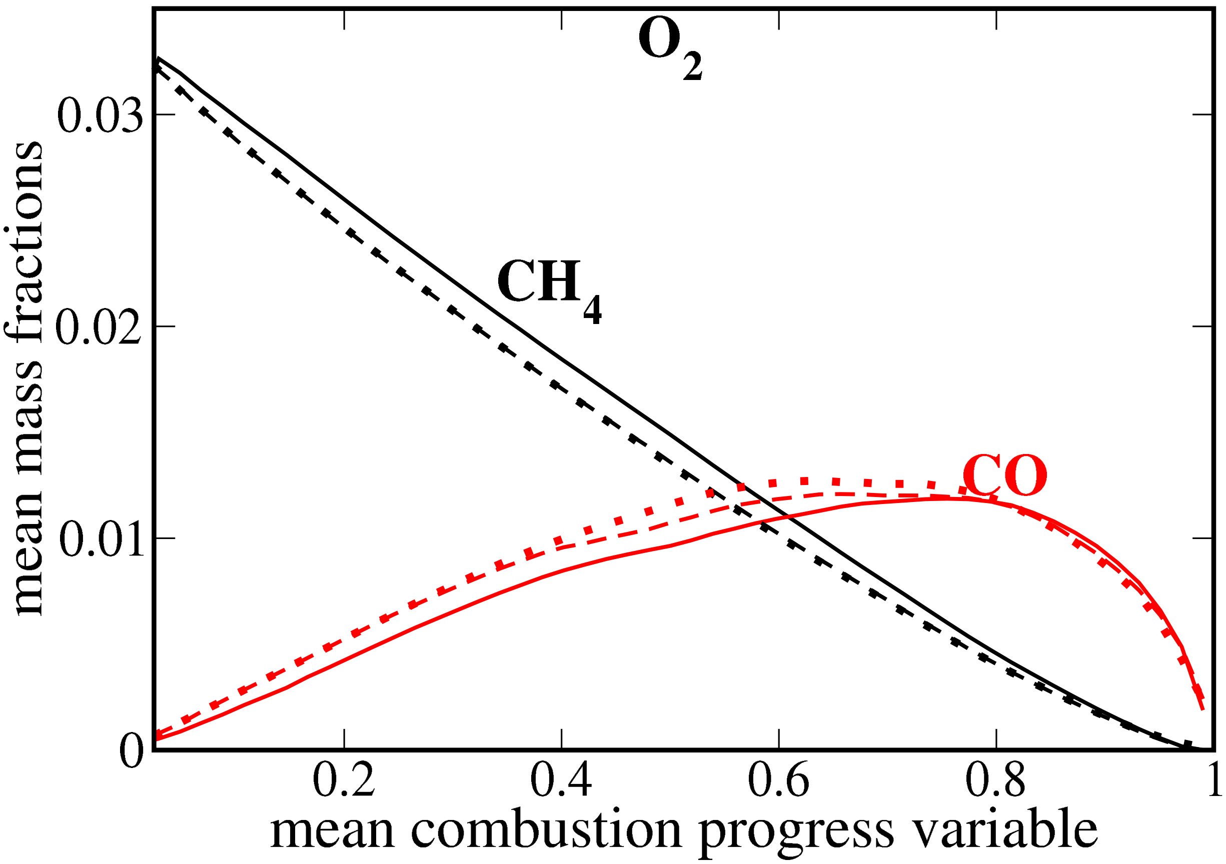
O_2
CH_4
CO
mean mass fractions
0
0.01
0.02
0.03
0.2
0.4
0.6
0.8
1
mean combustion progress variable

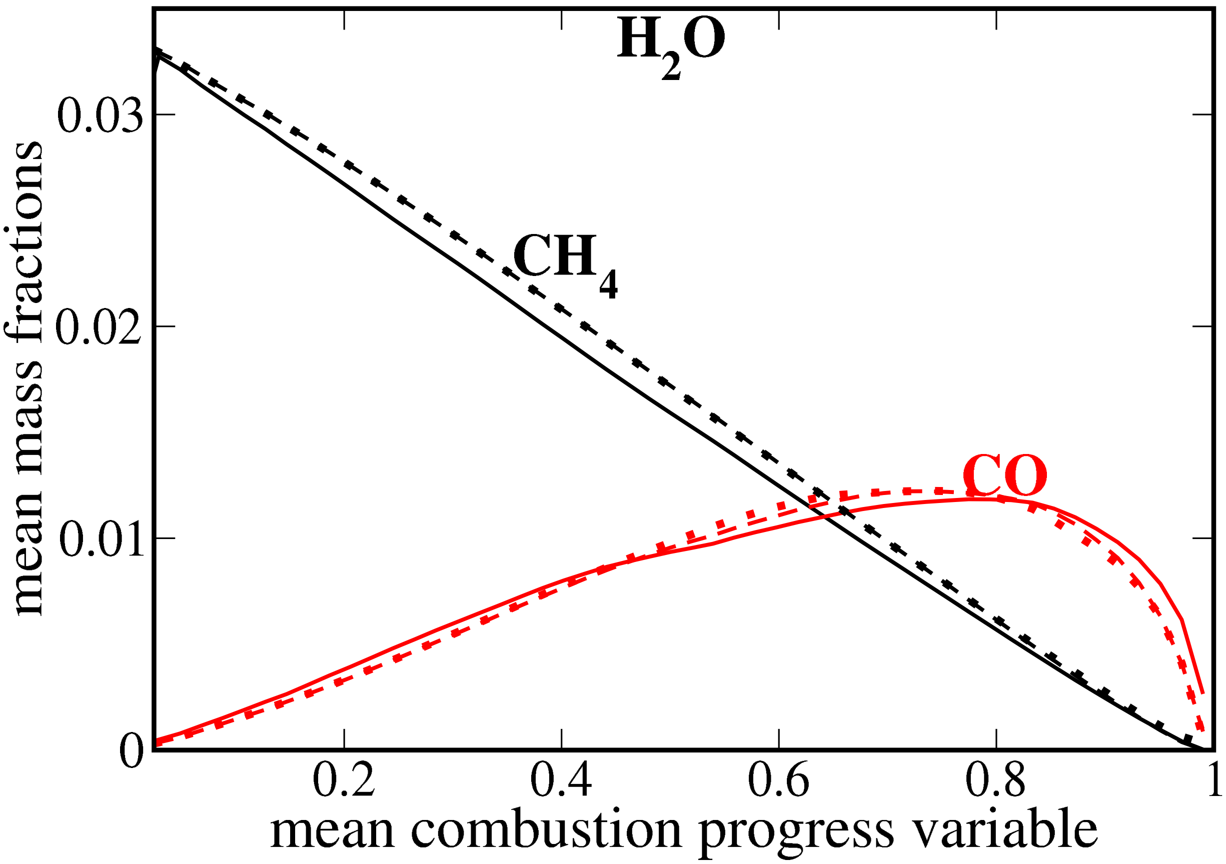
H2O
CH4
CO
0.03
0.02
0.01
0
0.2
0.4
0.6
0.8
1
mean mass fractions
mean combustion progress variable

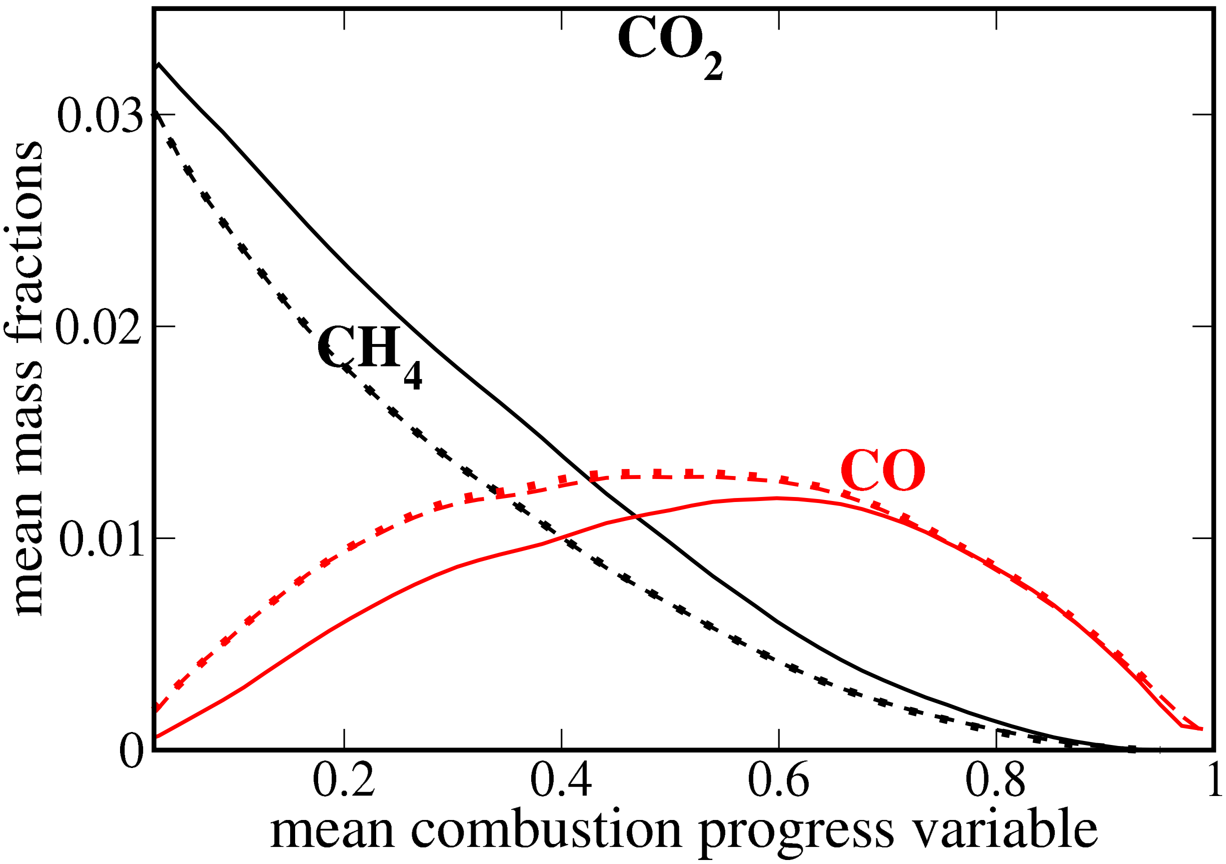
CO_2
CH_4
CO
mean mass fractions
mean combustion progress variable
0
0.01
0.02
0.03
0.2
0.4
0.6
0.8
1

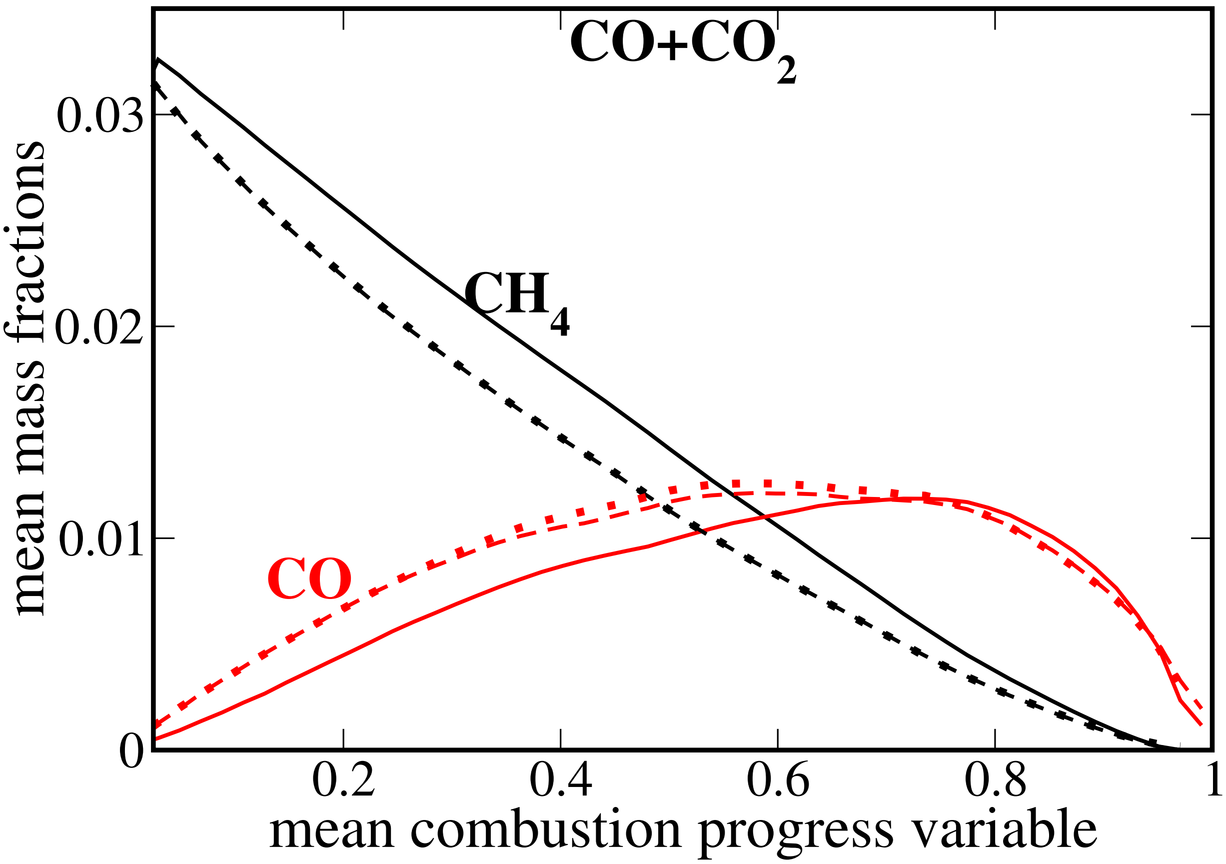
CO+CO$_2$
CH$_4$
CO
mean mass fractions
0
0.01
0.02
0.03
0.2
0.4
0.6
0.8
1
mean combustion progress variable

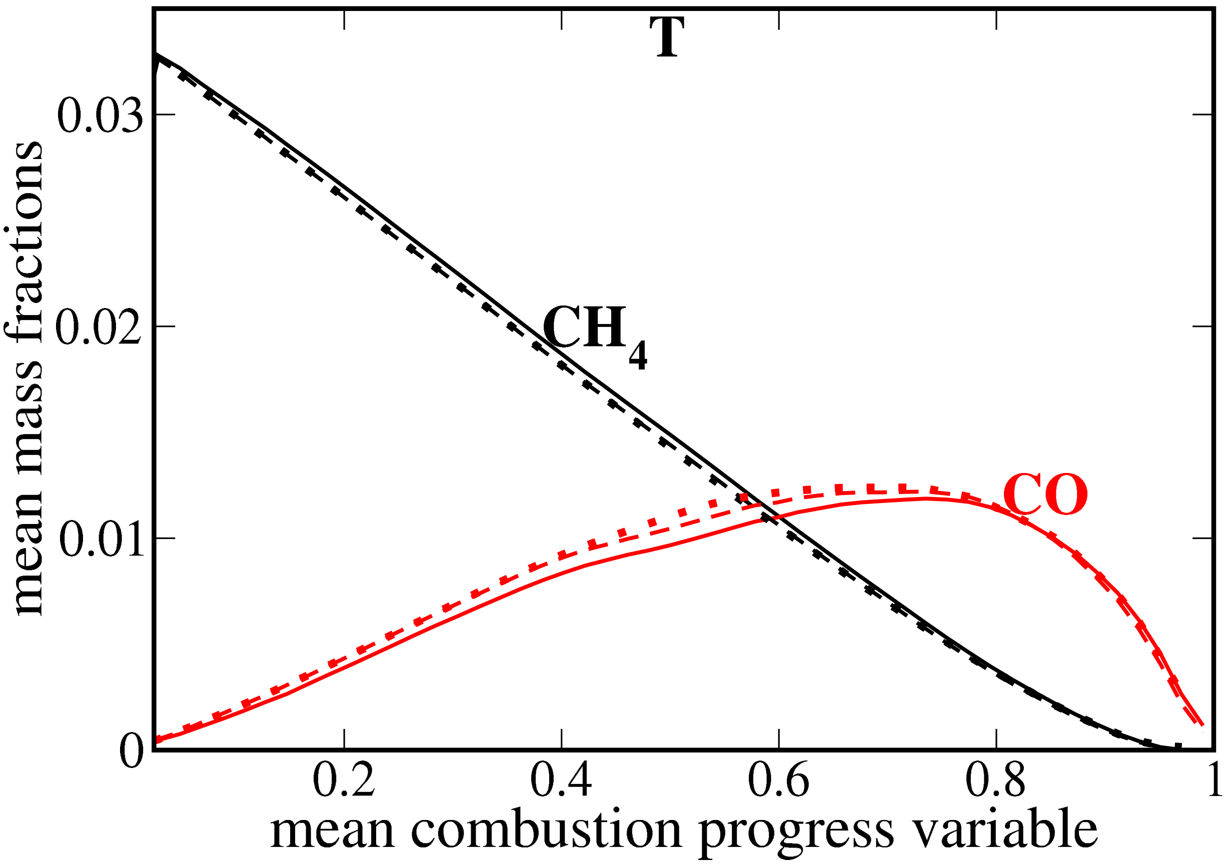
T
CH4
CO
0.03
0.02
0.01
0
0.2
0.4
0.6
0.8
1
mean mass fractions
mean combustion progress variable

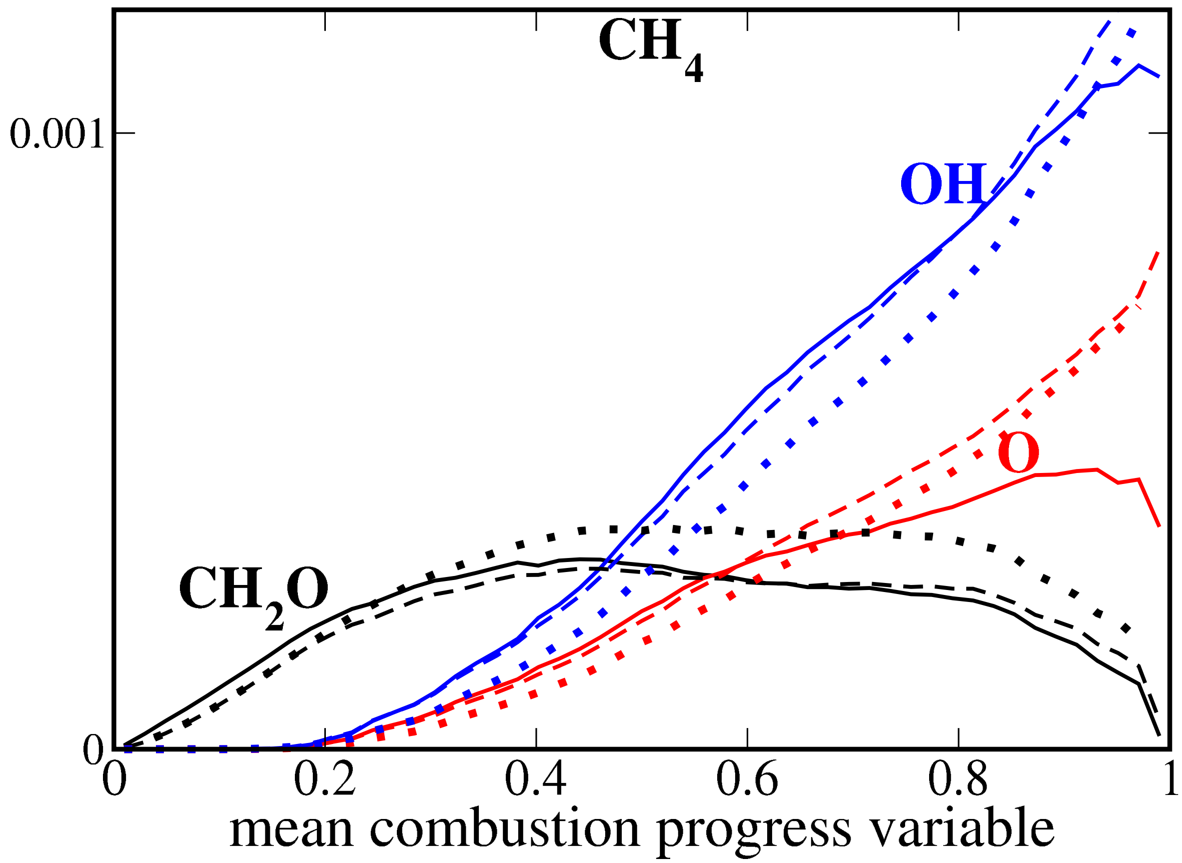
CH_4
0.001
0
OH
O
CH_2O
mean mass fractions
0
0.2
0.4
0.6
0.8
1
mean combustion progress variable

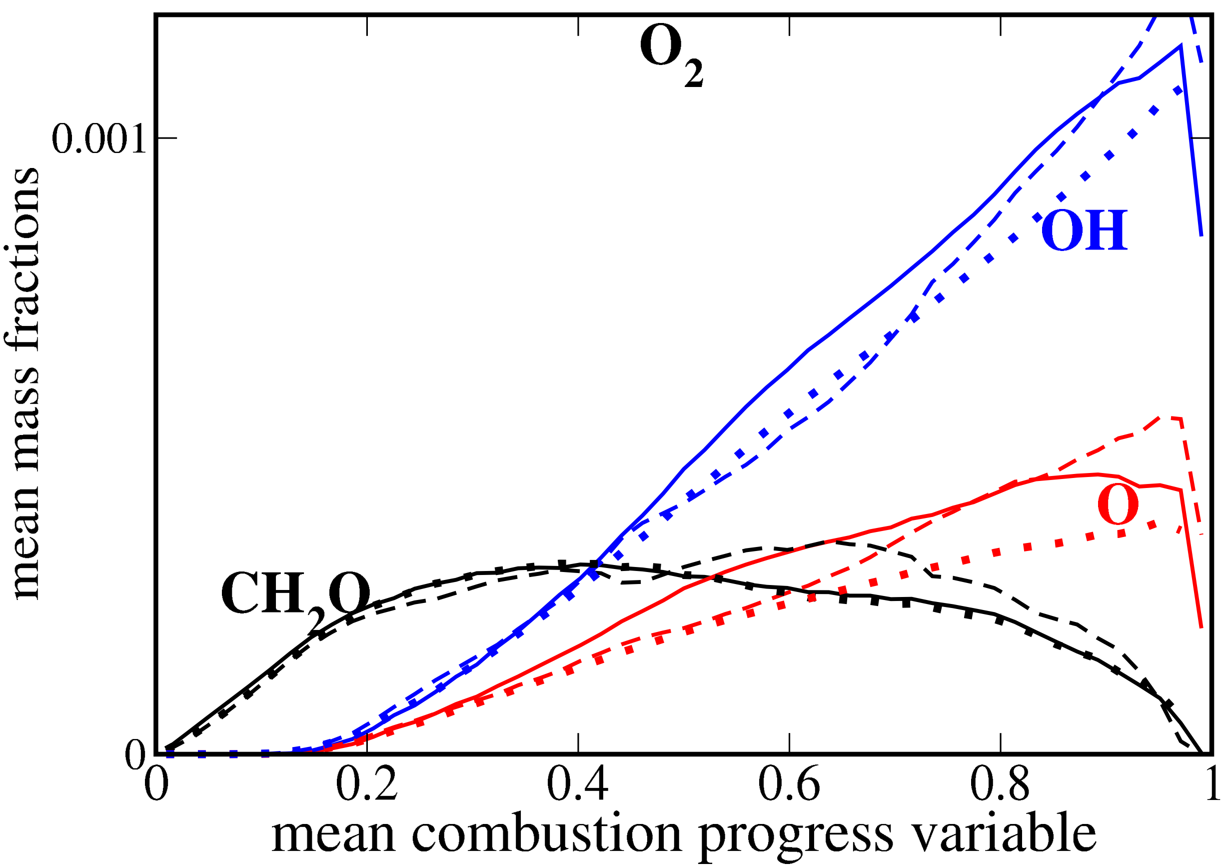
O2
0.001
OH
O
CH2O
0
mean mass fractions
0
0.2
0.4
0.6
0.8
1
mean combustion progress variable

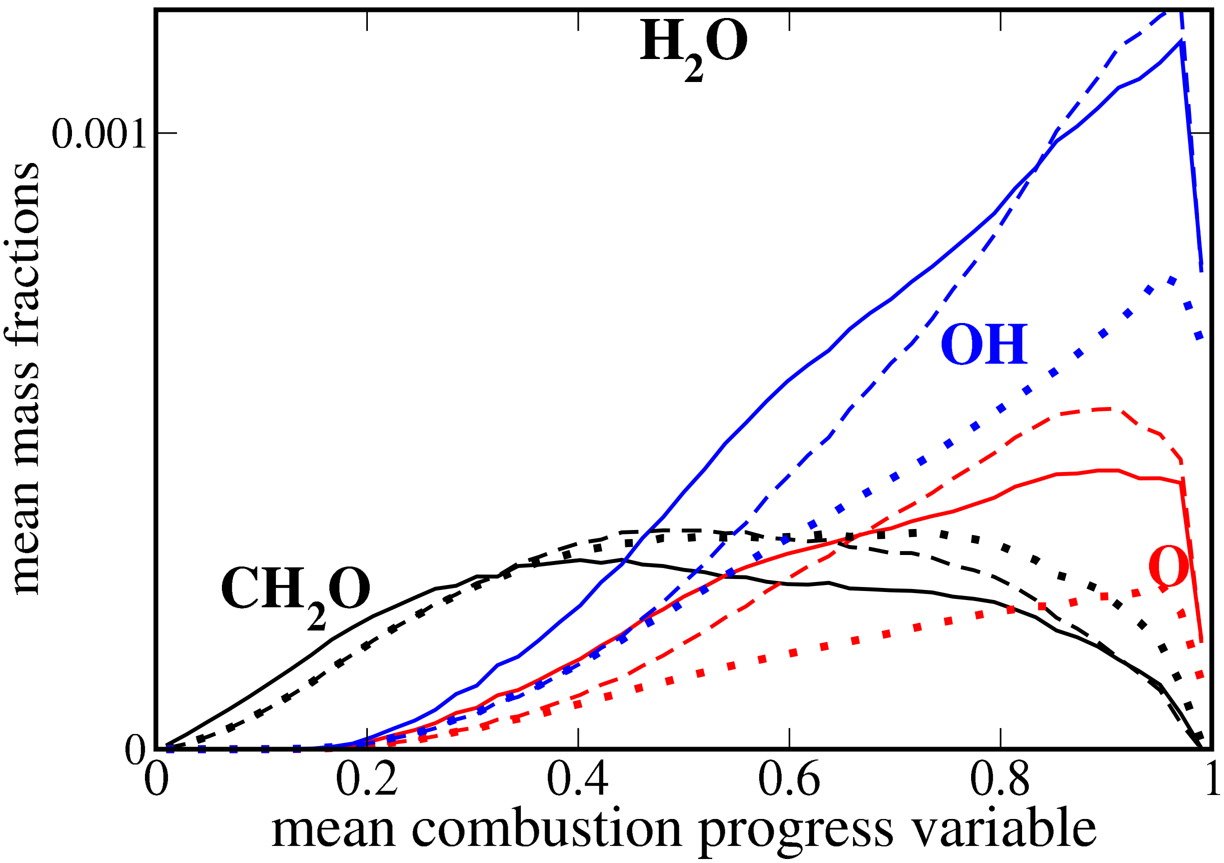
H2O
OH
O
CH2O
0.001
0
0
0.2
0.4
0.6
0.8
1
mean mass fractions
mean combustion progress variable

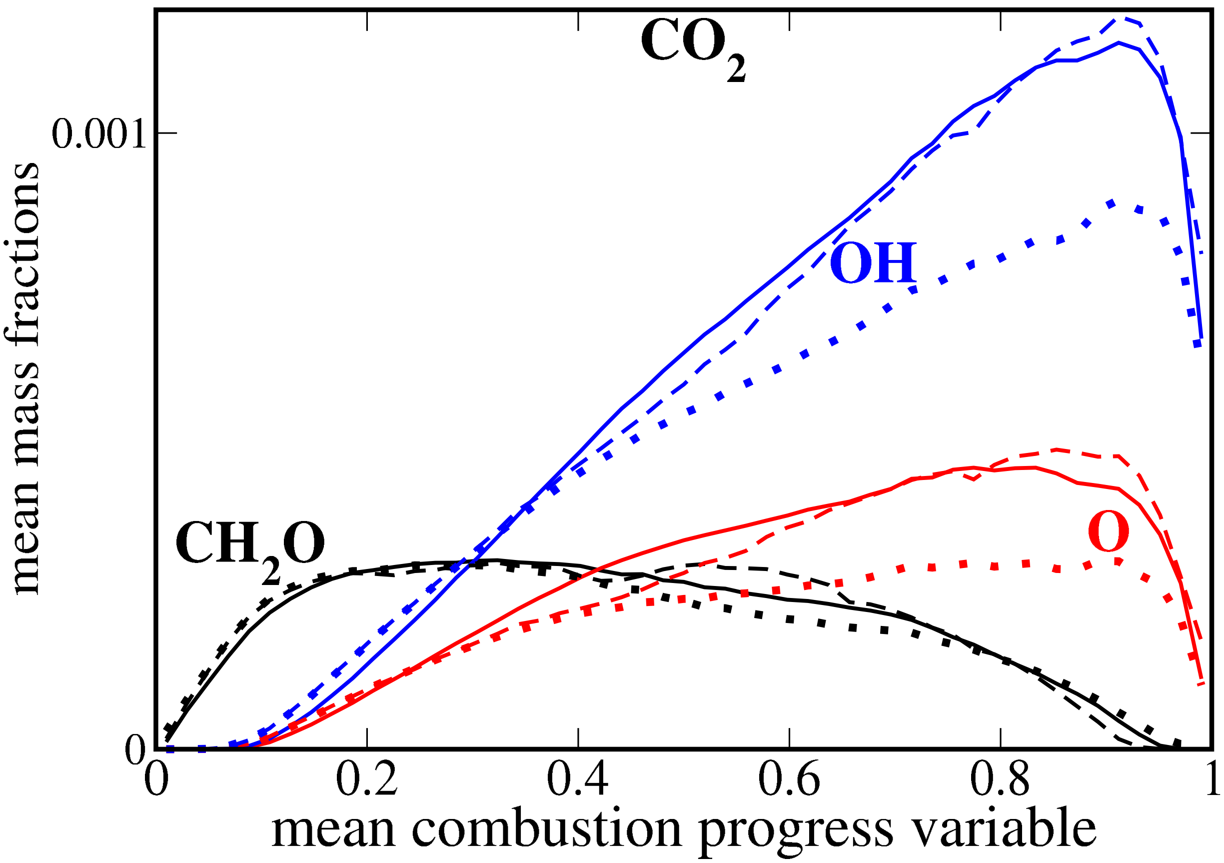
CO_2
OH
O
CH_2O
0.001
0
0
0.2
0.4
0.6
0.8
1
mean mass fractions
mean combustion progress variable

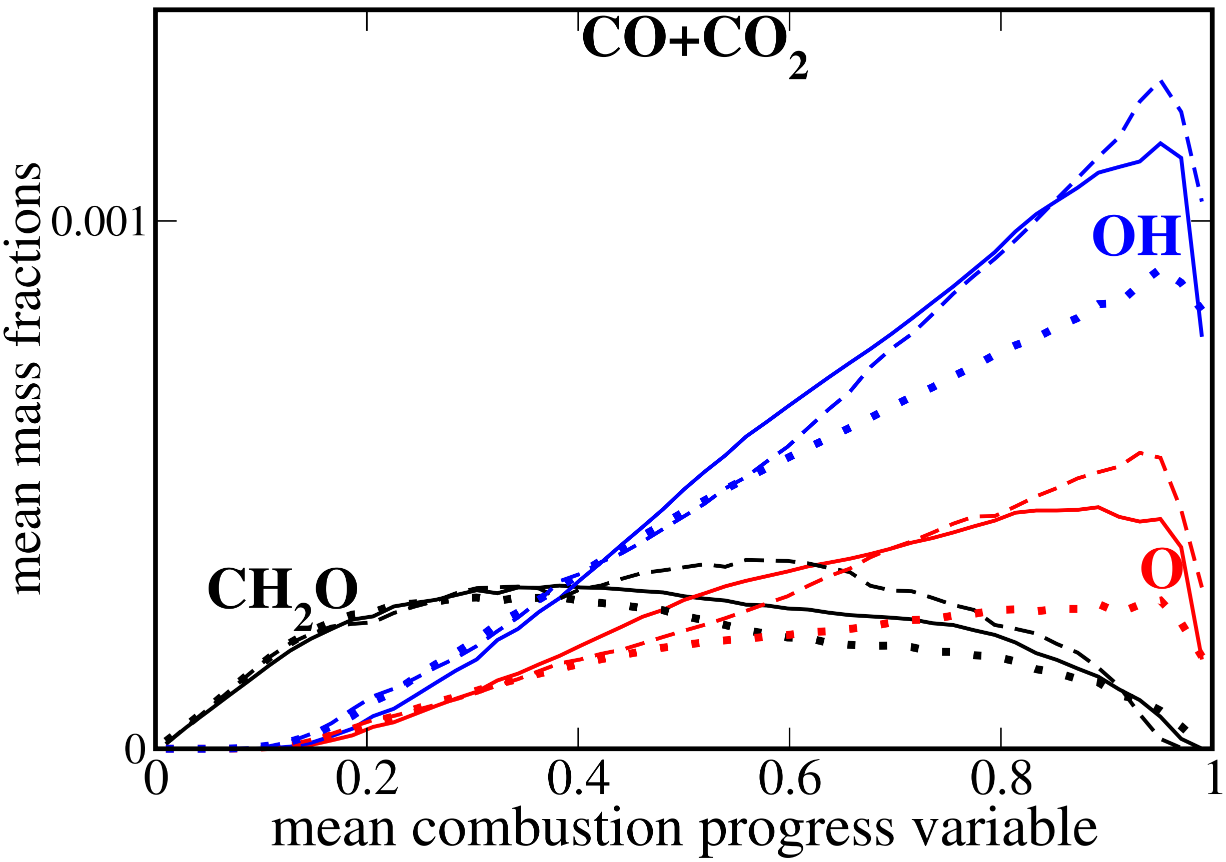
CO+CO$_2$
OH
O
CH$_2$O
mean mass fractions
0.001
0
0
0.2
0.4
0.6
0.8
1
mean combustion progress variable

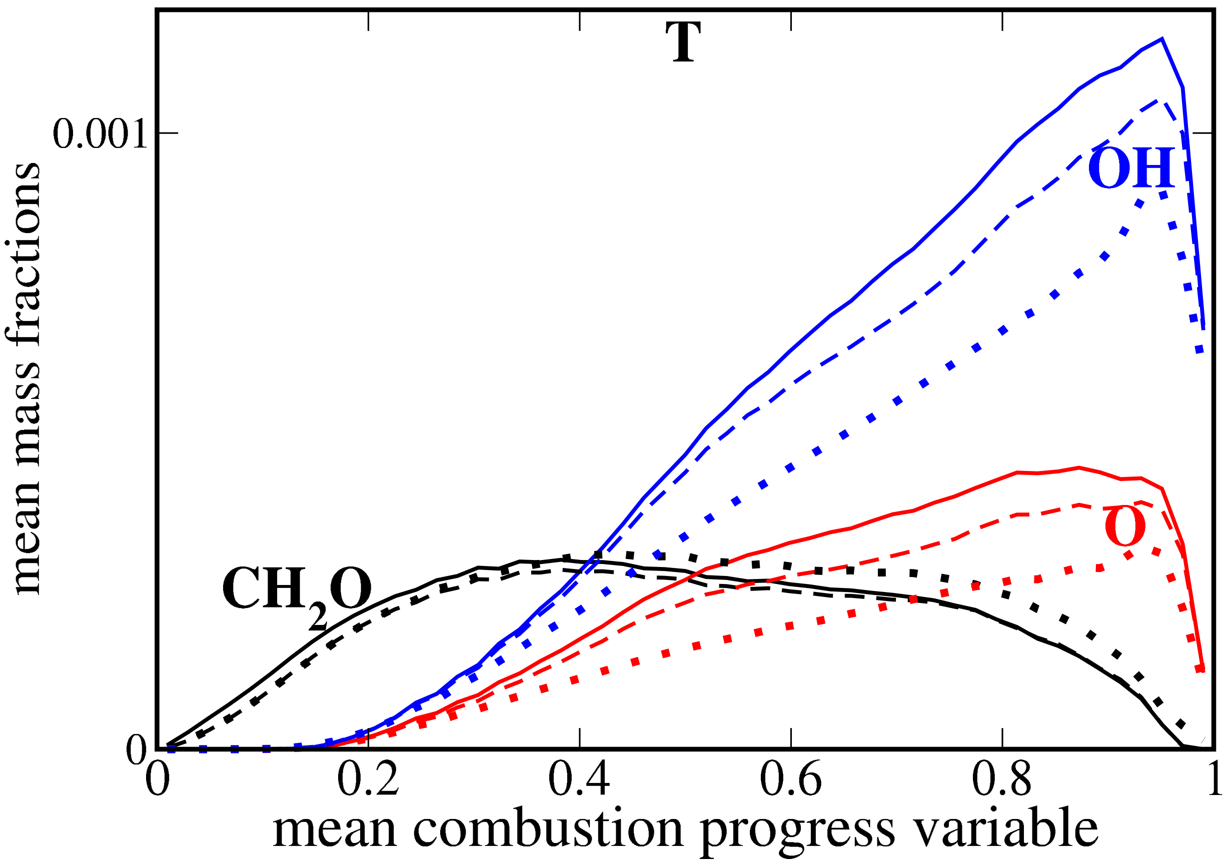
T
0.001
0
OH
O
CH2O
mean mass fractions
0
0.2
0.4
0.6
0.8
1
mean combustion progress variable

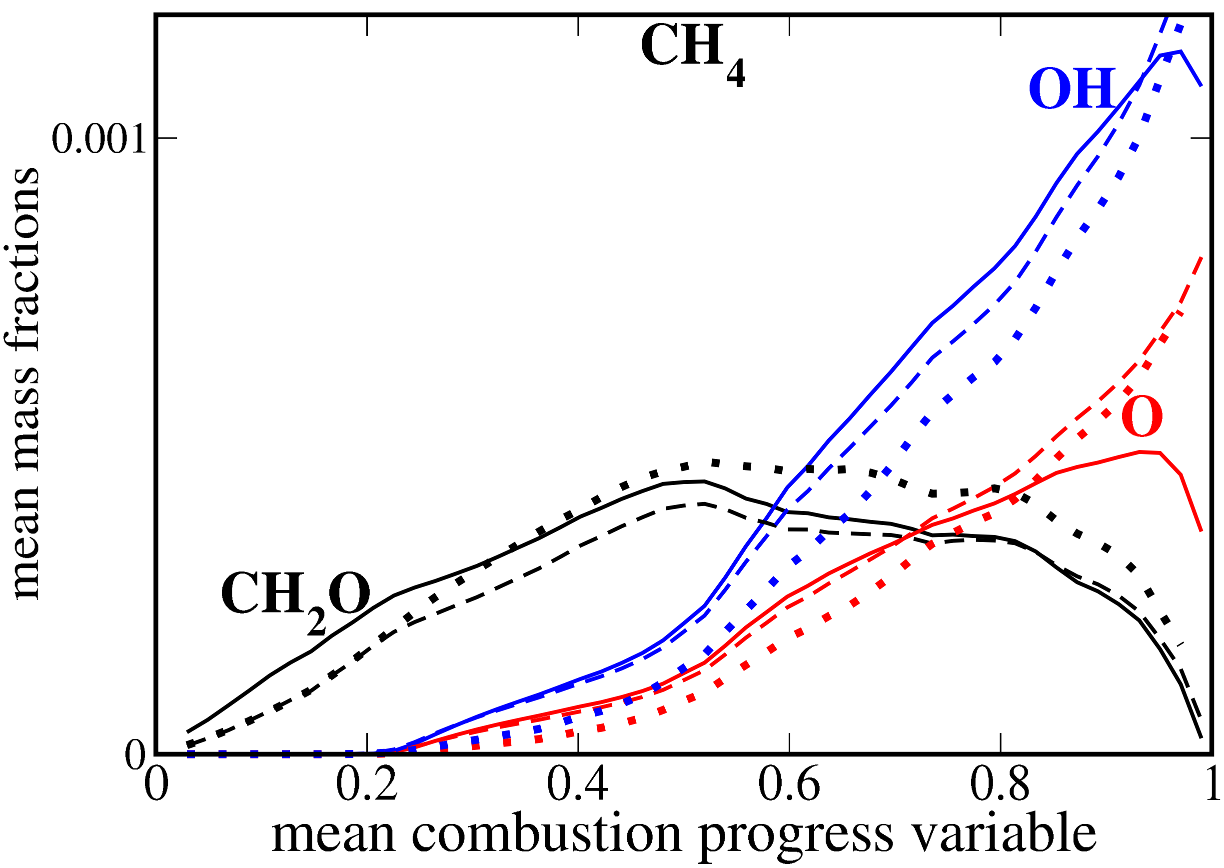
CH4
OH
O
CH2O
0.001
0
mean mass fractions
0
0.2
0.4
0.6
0.8
1
mean combustion progress variable

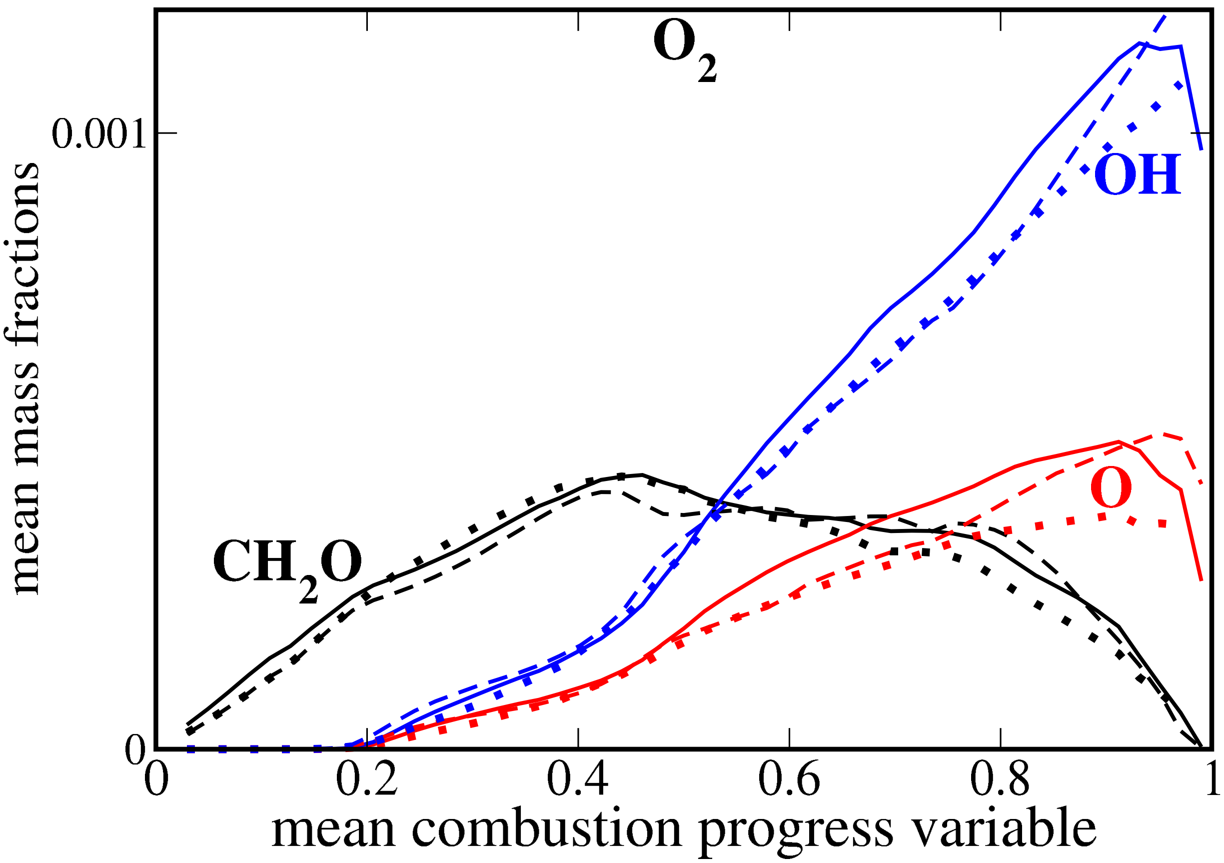
O2
0.001
OH
O
CH2O
0
0
0.2
0.4
0.6
0.8
1
mean mass fractions
mean combustion progress variable

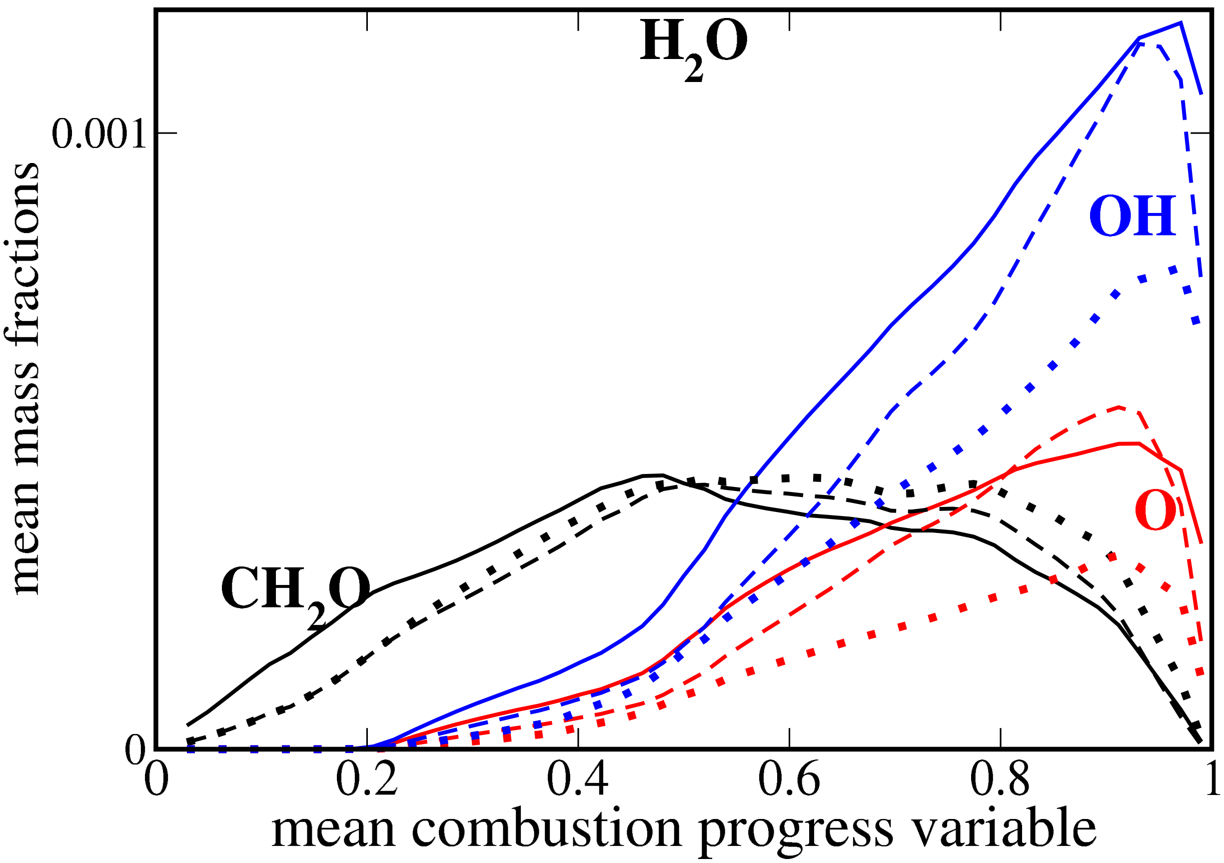
H2O
OH
O
CH2O
0.001
0
0
0.2
0.4
0.6
0.8
1
mean mass fractions
mean combustion progress variable

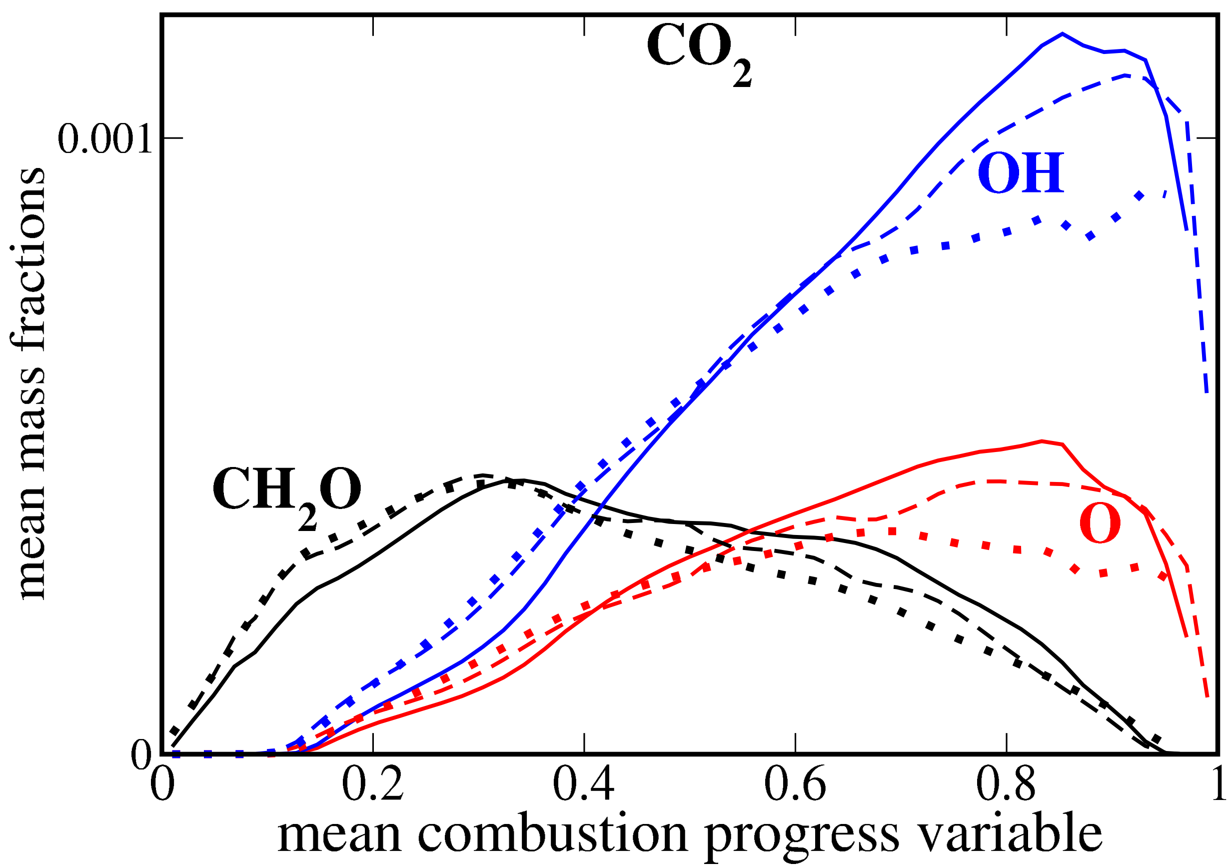
CO_2
OH
CH_2O
O
0.001
0
0
0.2
0.4
0.6
0.8
1
mean mass fractions
mean combustion progress variable

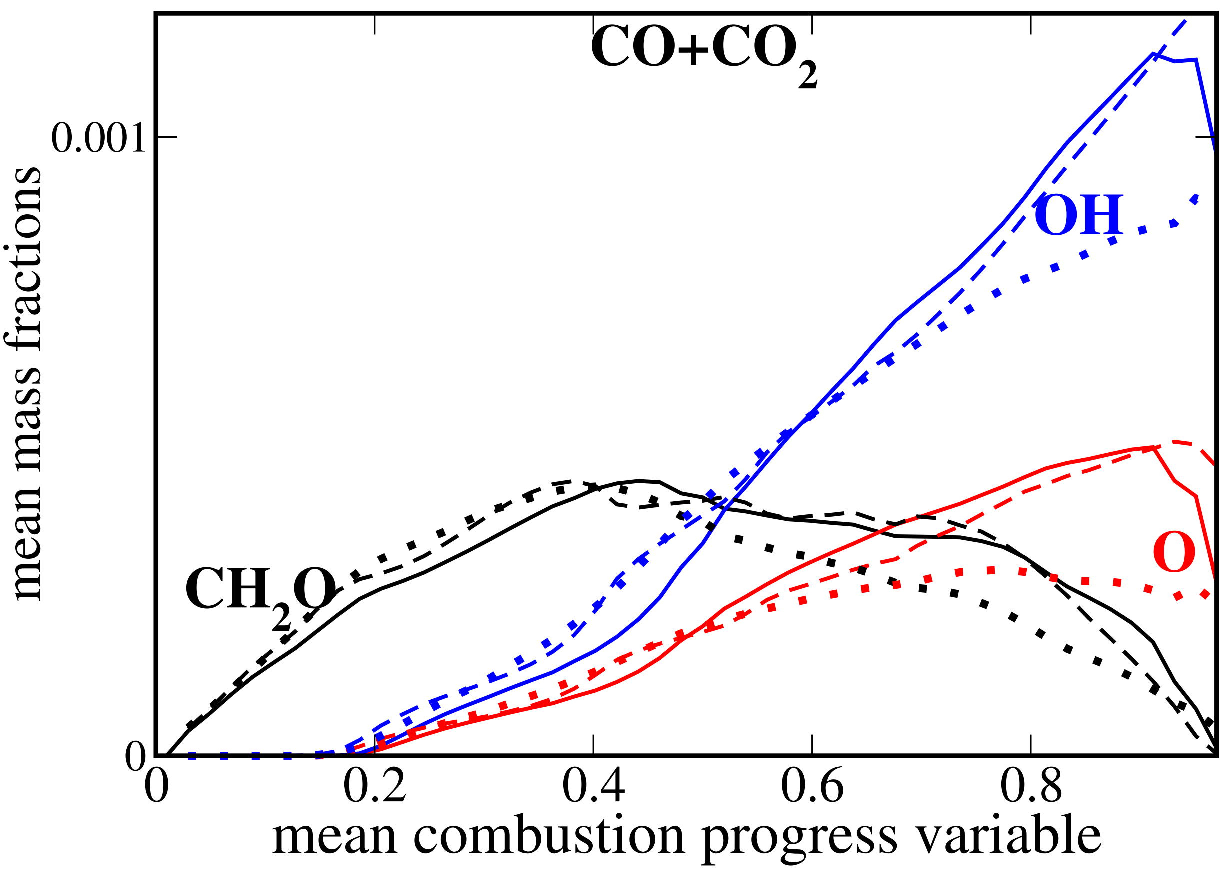
CO+CO2
OH
O
CH2O
0.001
0
mean mass fractions
0
0.2
0.4
0.6
0.8
mean combustion progress variable

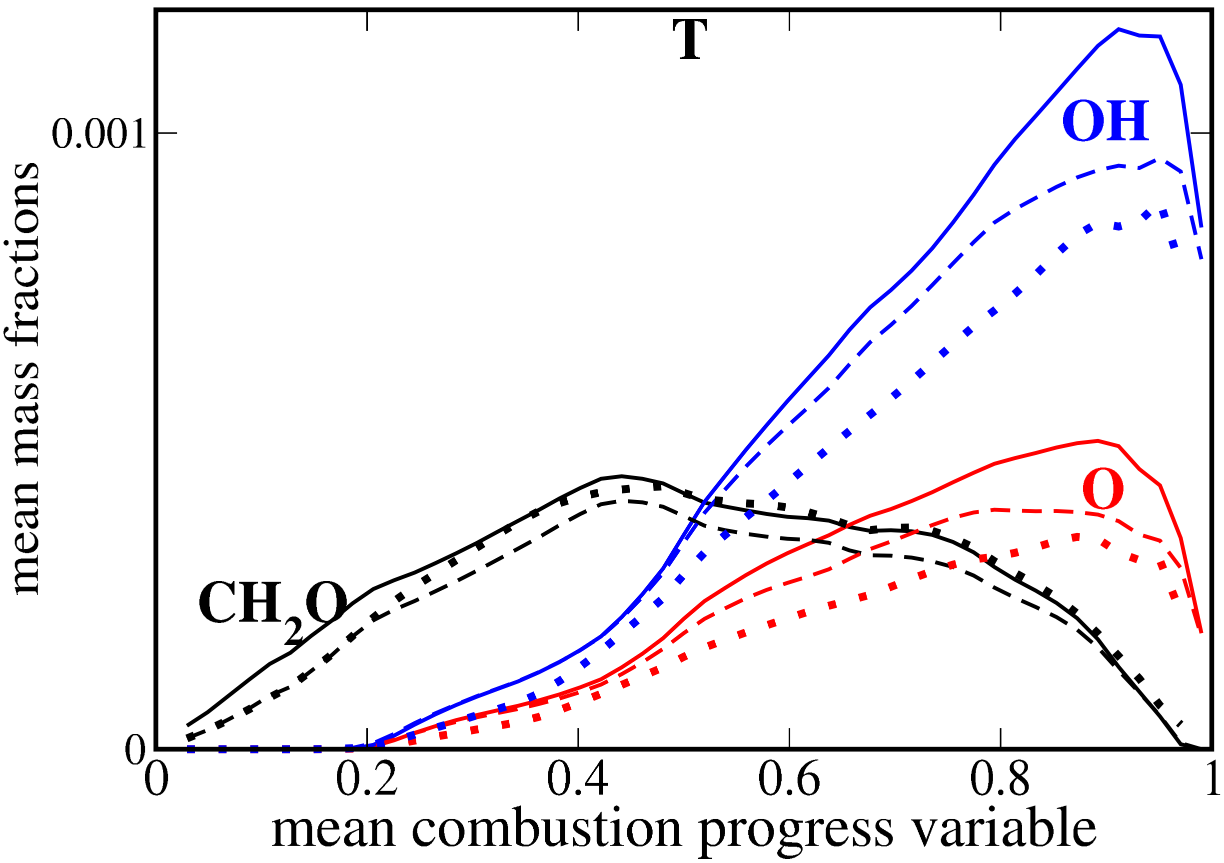
T
OH
O
CH_2O
0.001
0
0
0.2
0.4
0.6
0.8
1
mean mass fractions
mean combustion progress variable

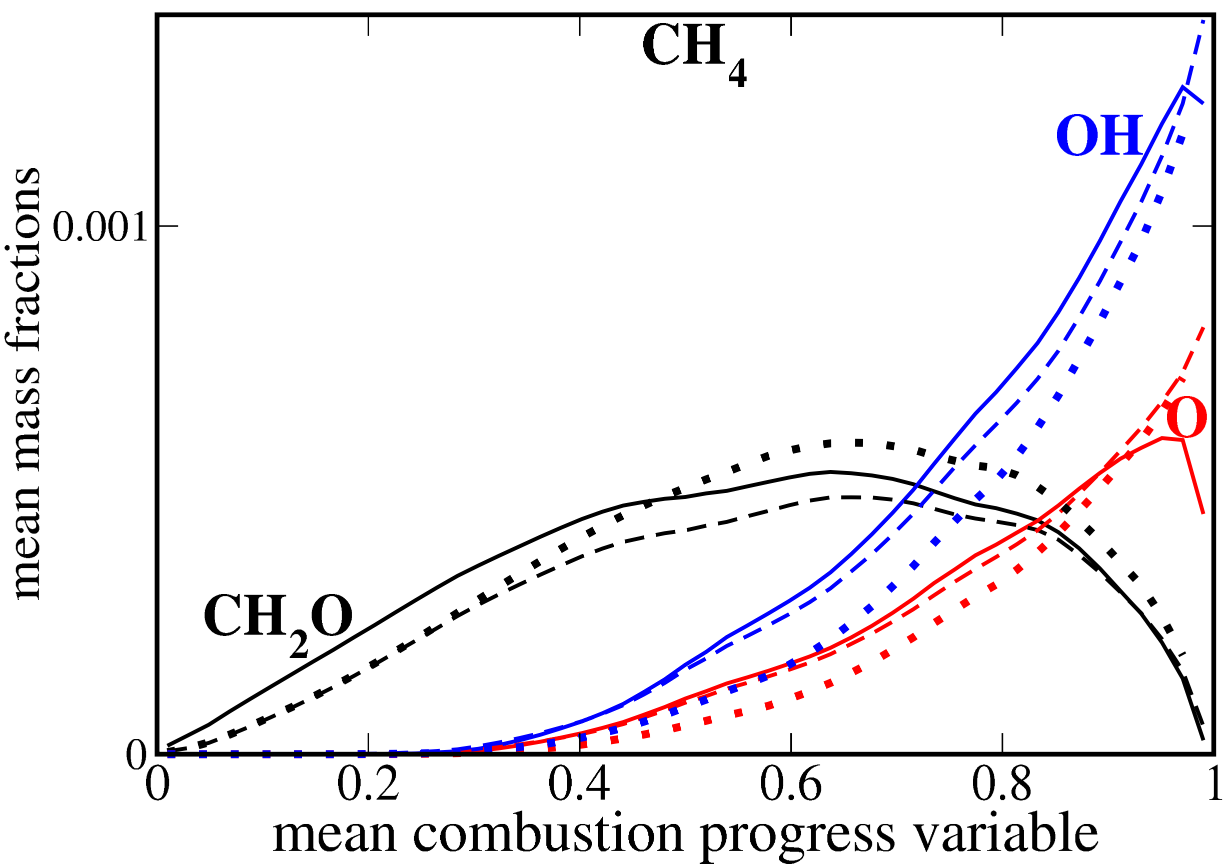
CH$_4$
OH
O
CH$_2$O
0.001
0
0
0.2
0.4
0.6
0.8
1
mean mass fractions
mean combustion progress variable

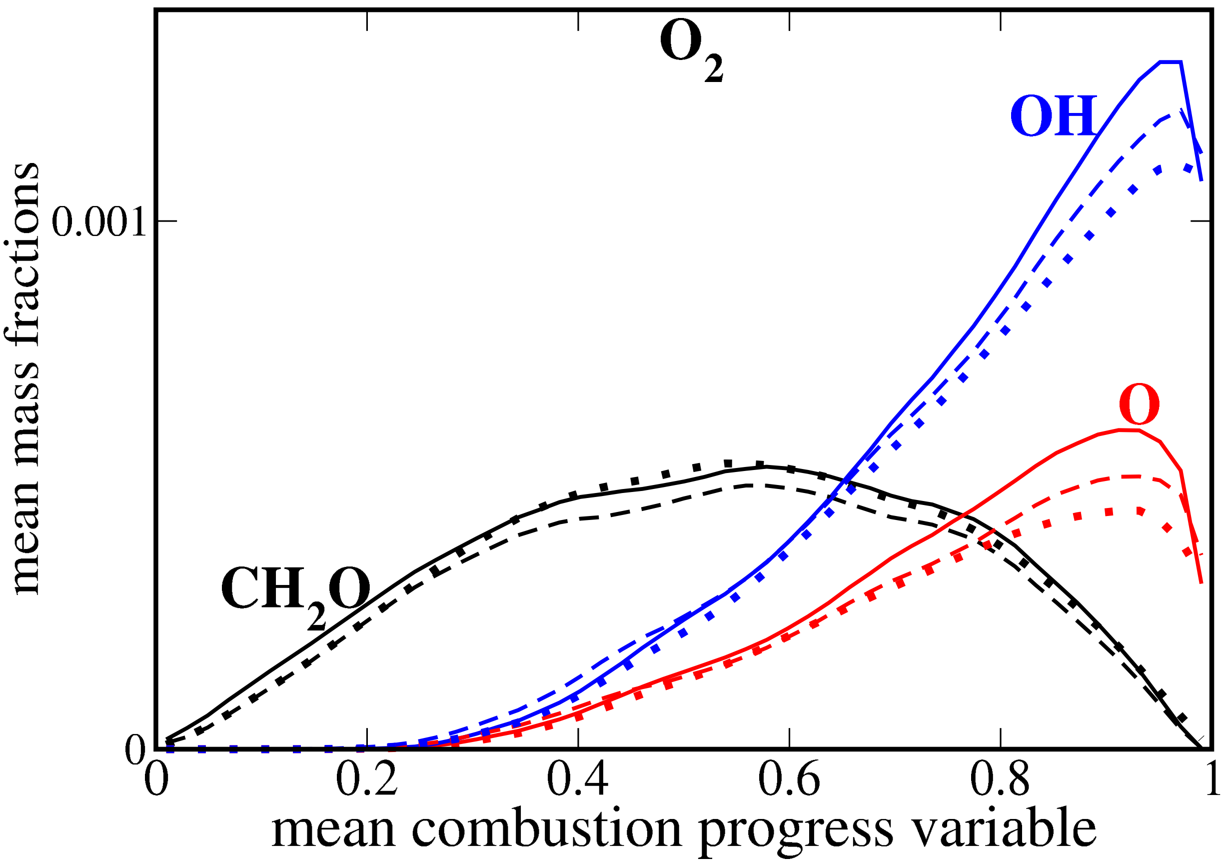
O2
OH
O
CH2O
0.001
0
0
0.2
0.4
0.6
0.8
1
mean mass fractions
mean combustion progress variable

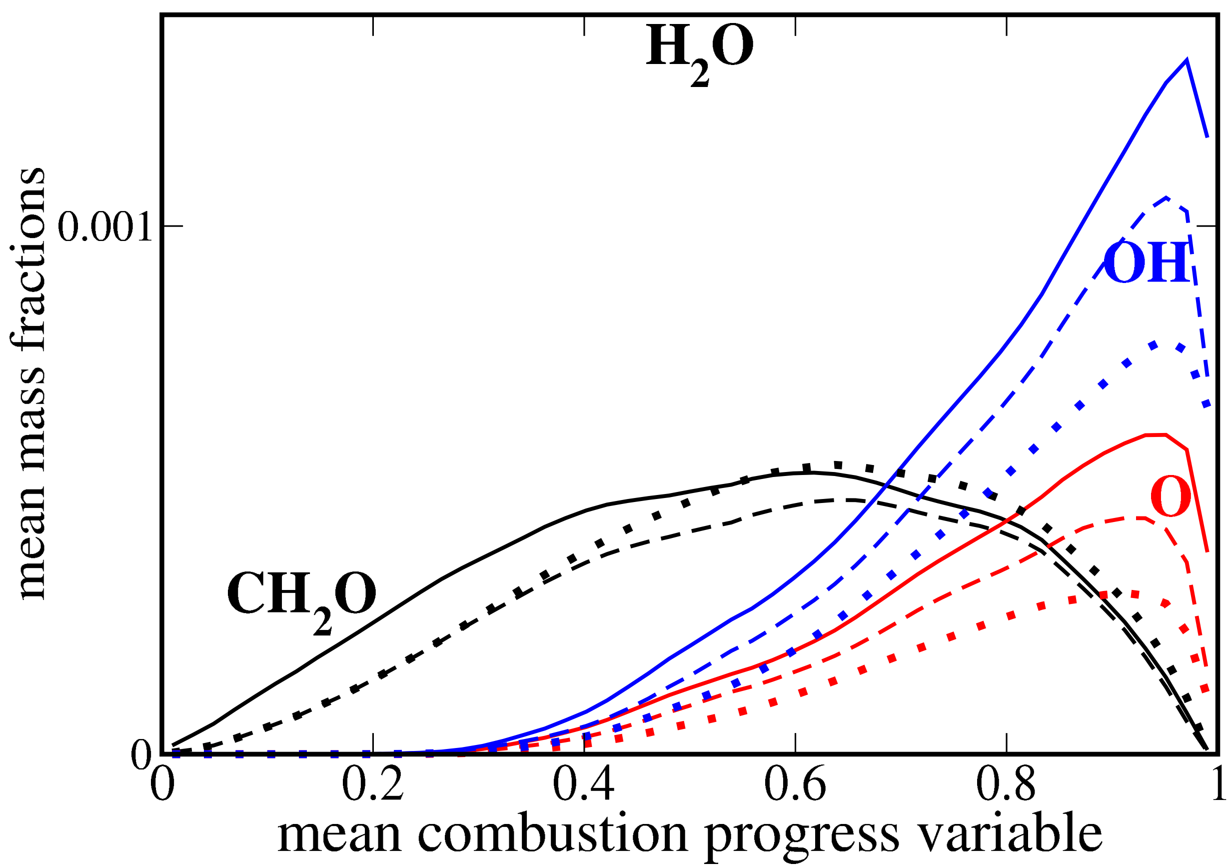
H$_2$O
OH
O
CH$_2$O
0.001
0
0
0.2
0.4
0.6
0.8
1
mean mass fractions
mean combustion progress variable

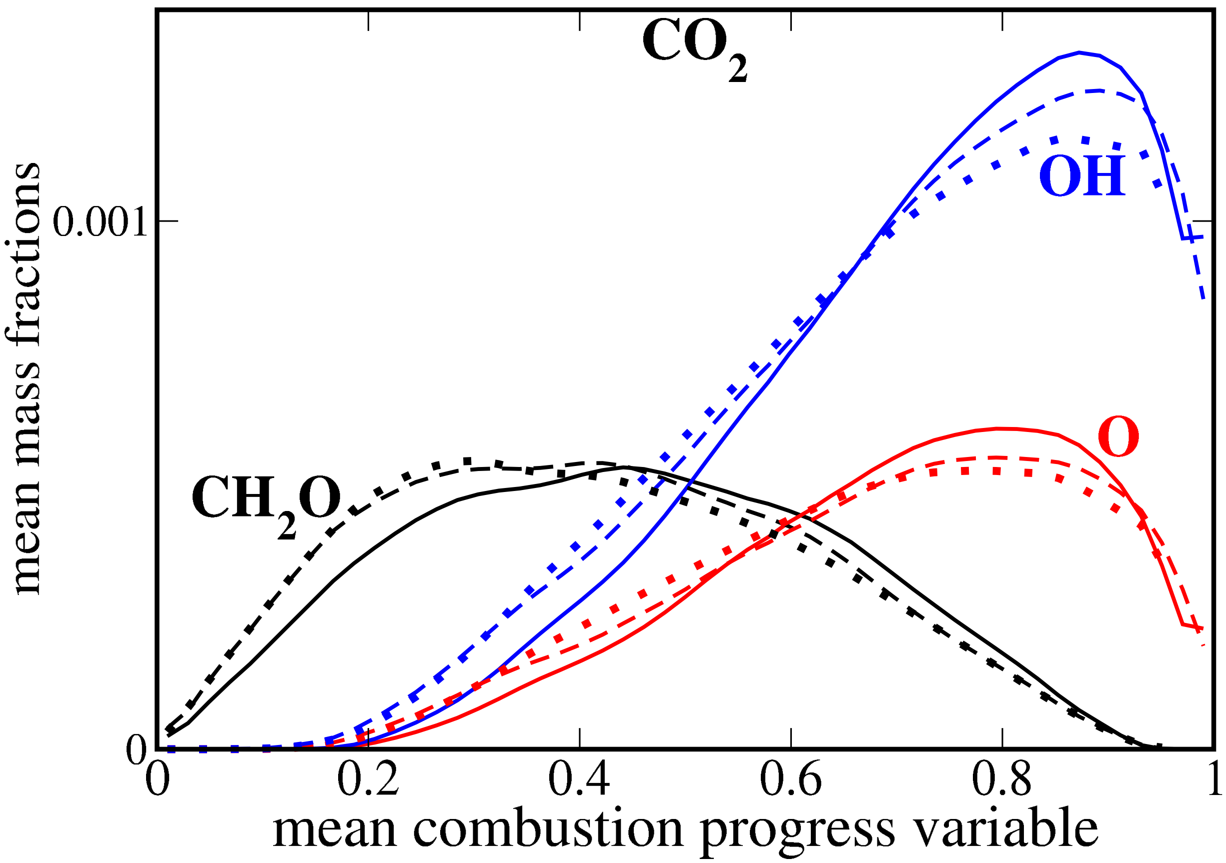
CO_2
OH
O
CH_2O
0.001
0
0
0.2
0.4
0.6
0.8
1
mean mass fractions
mean combustion progress variable

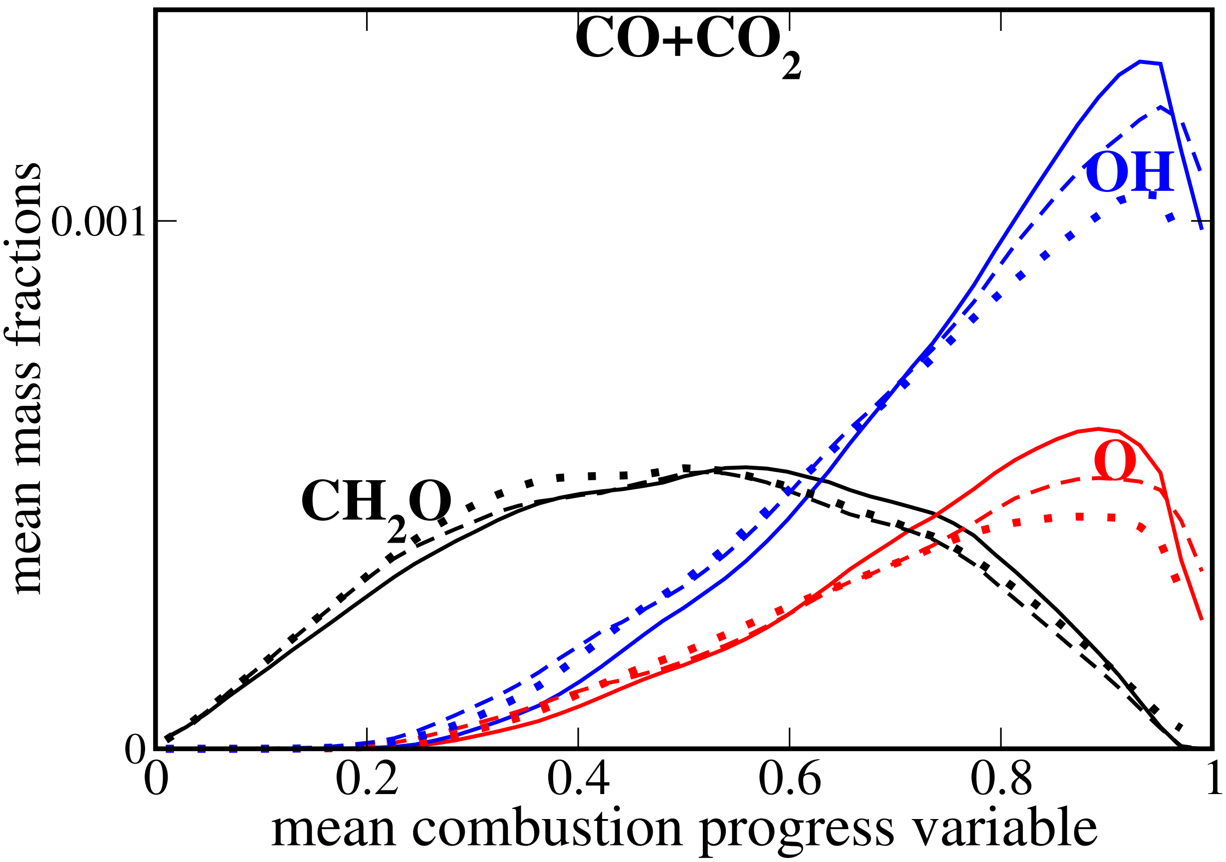
CO+CO2
OH
O
CH2O
0.001
0
0
0.2
0.4
0.6
0.8
1
mean mass fractions
mean combustion progress variable

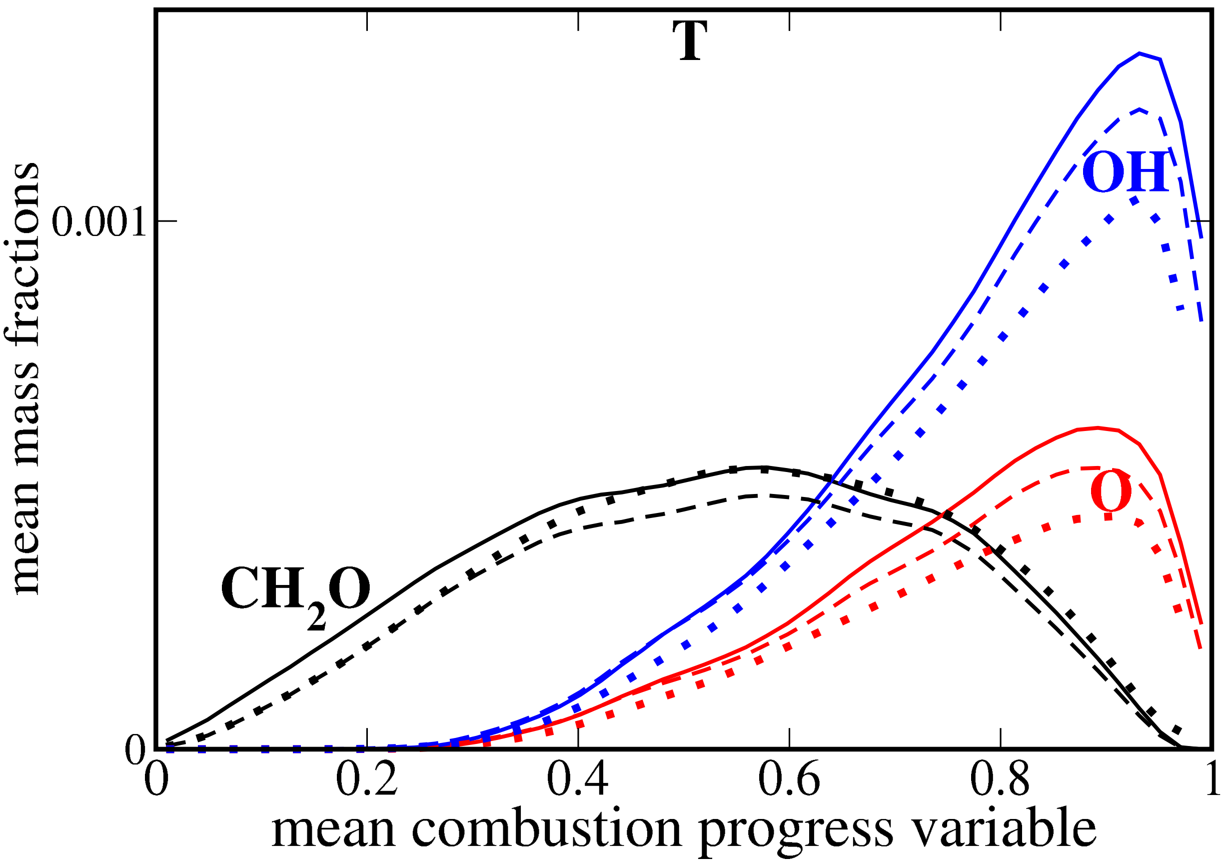
T
OH
O
CH_2O
0.001
0
0
0.2
0.4
0.6
0.8
1
mean mass fractions
mean combustion progress variable

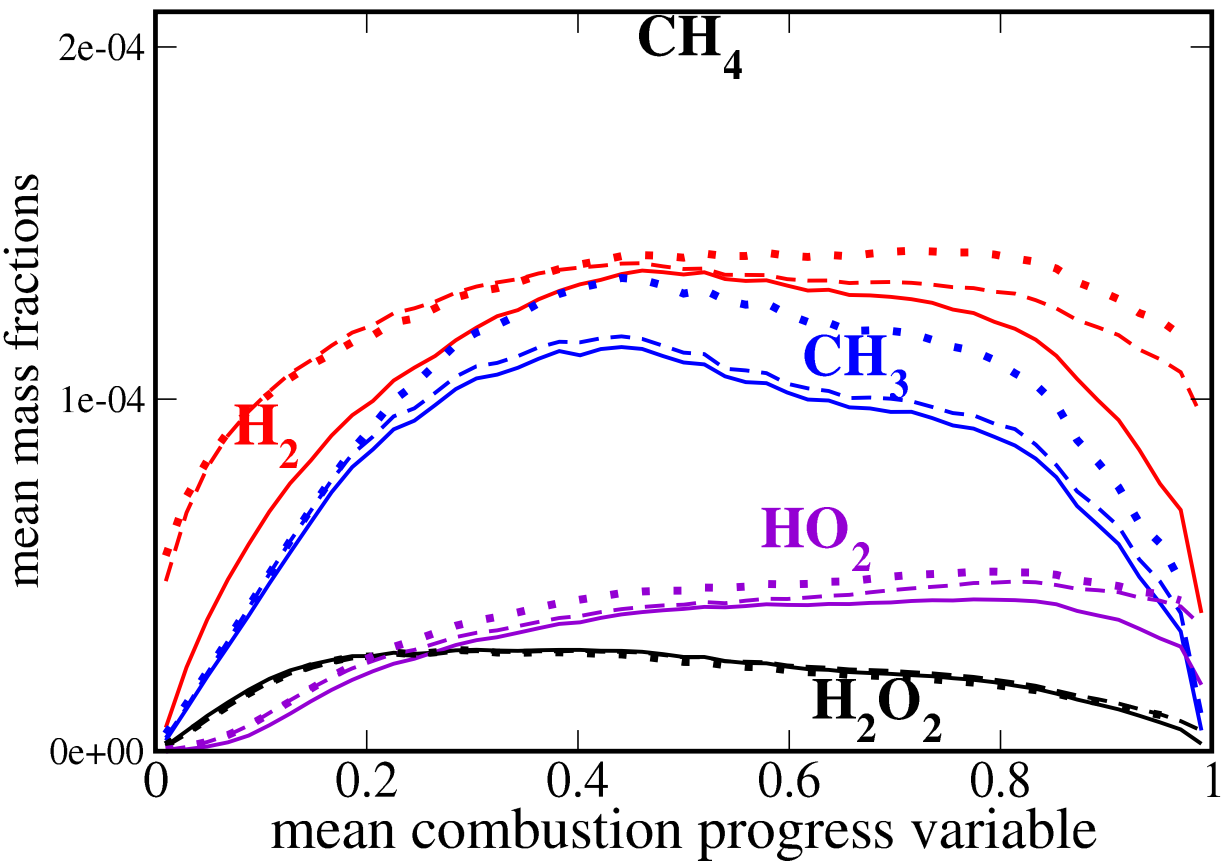
CH4
H2
CH3
HO2
H2O2
2e-04
1e-04
0e+00
0
0.2
0.4
0.6
0.8
1
mean mass fractions
mean combustion progress variable

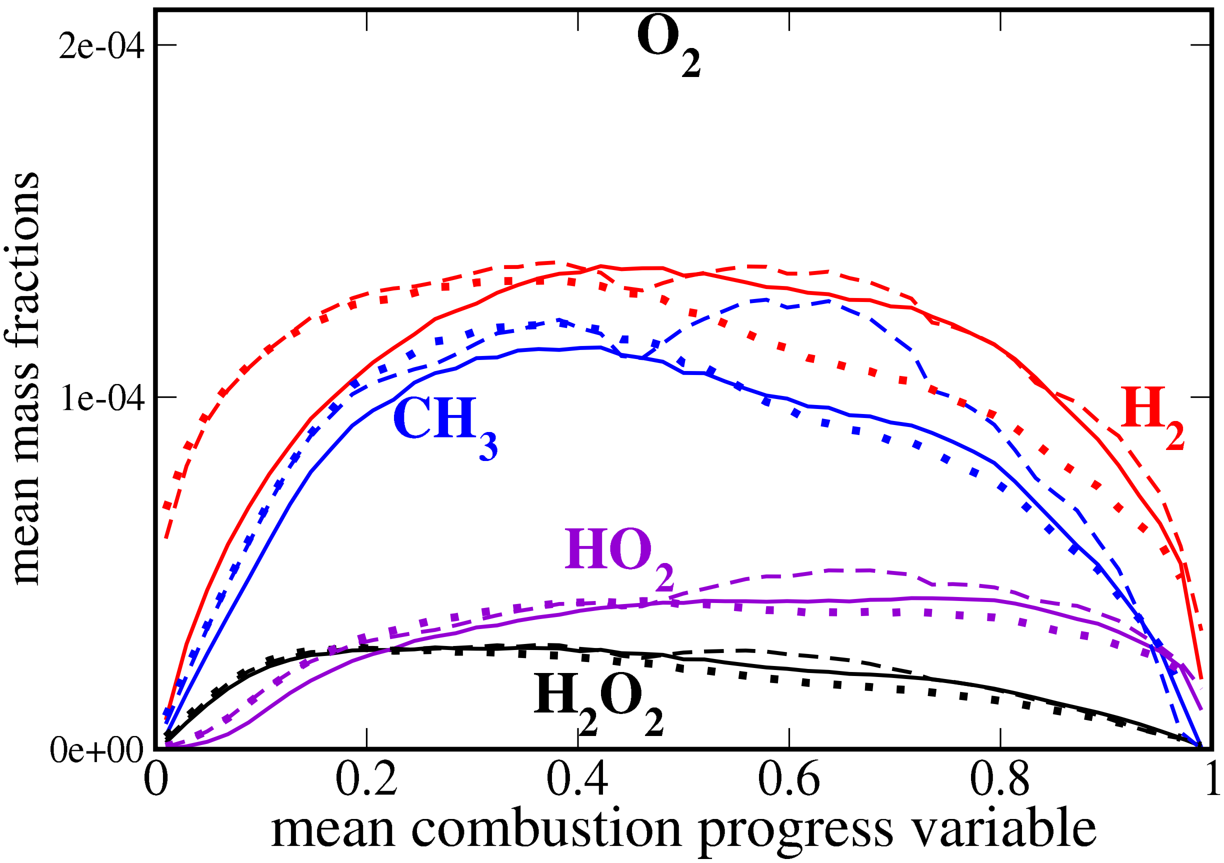
O_2
CH_3
H_2
HO_2
H_2O_2
2e-04
1e-04
0e+00
0
0.2
0.4
0.6
0.8
1
mean mass fractions
mean combustion progress variable

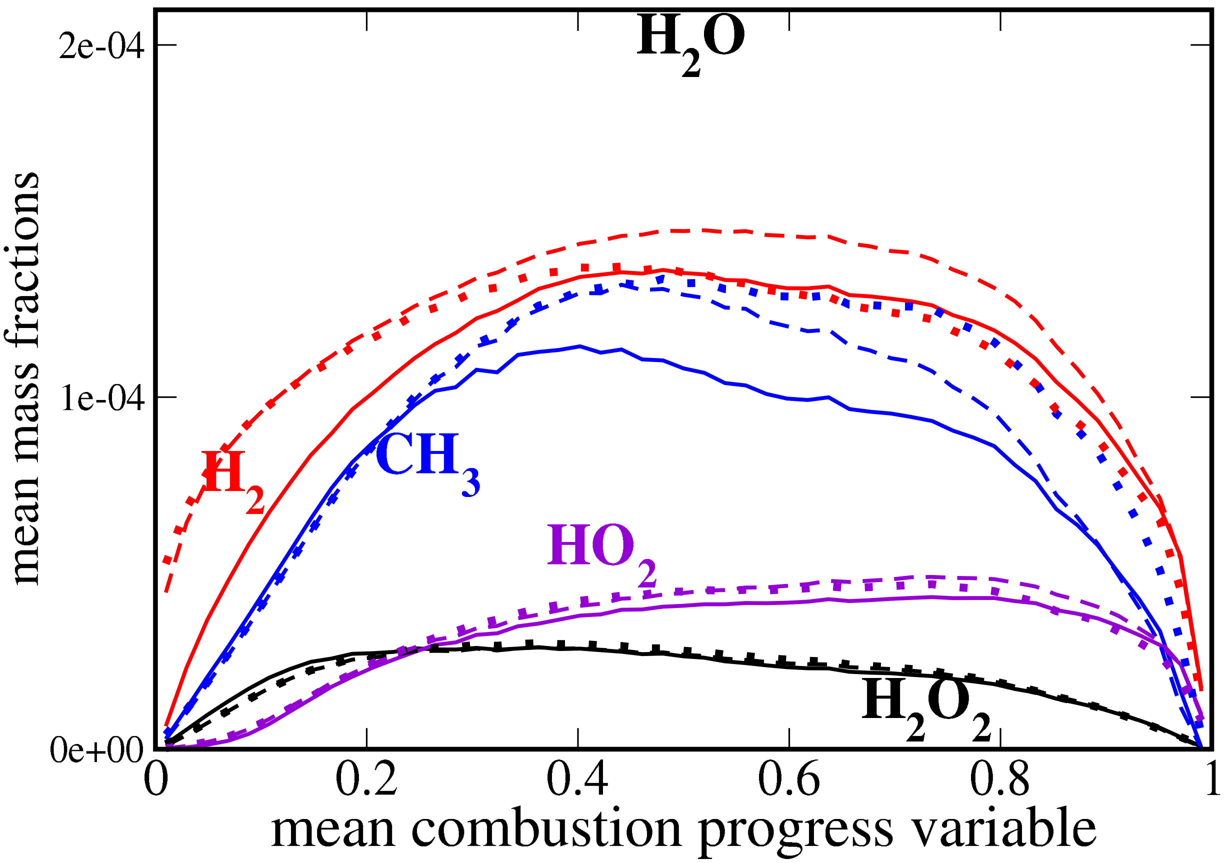
H2O
H2
CH3
HO2
H2O2
mean mass fractions
2e-04
1e-04
0e+00
0
0.2
0.4
0.6
0.8
1
mean combustion progress variable

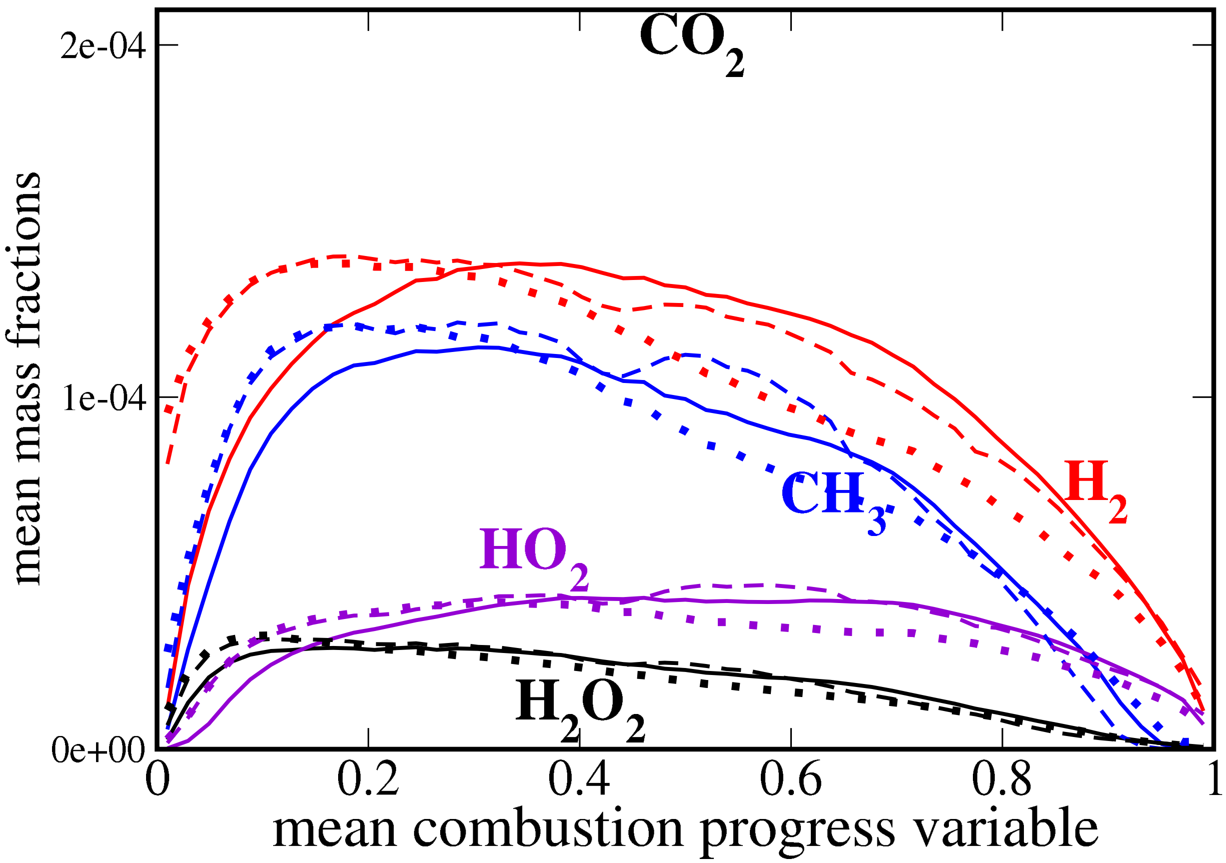
CO_2
H_2
CH_3
HO_2
H_2O_2
mean mass fractions
mean combustion progress variable
2e-04
1e-04
0e+00
0
0.2
0.4
0.6
0.8
1

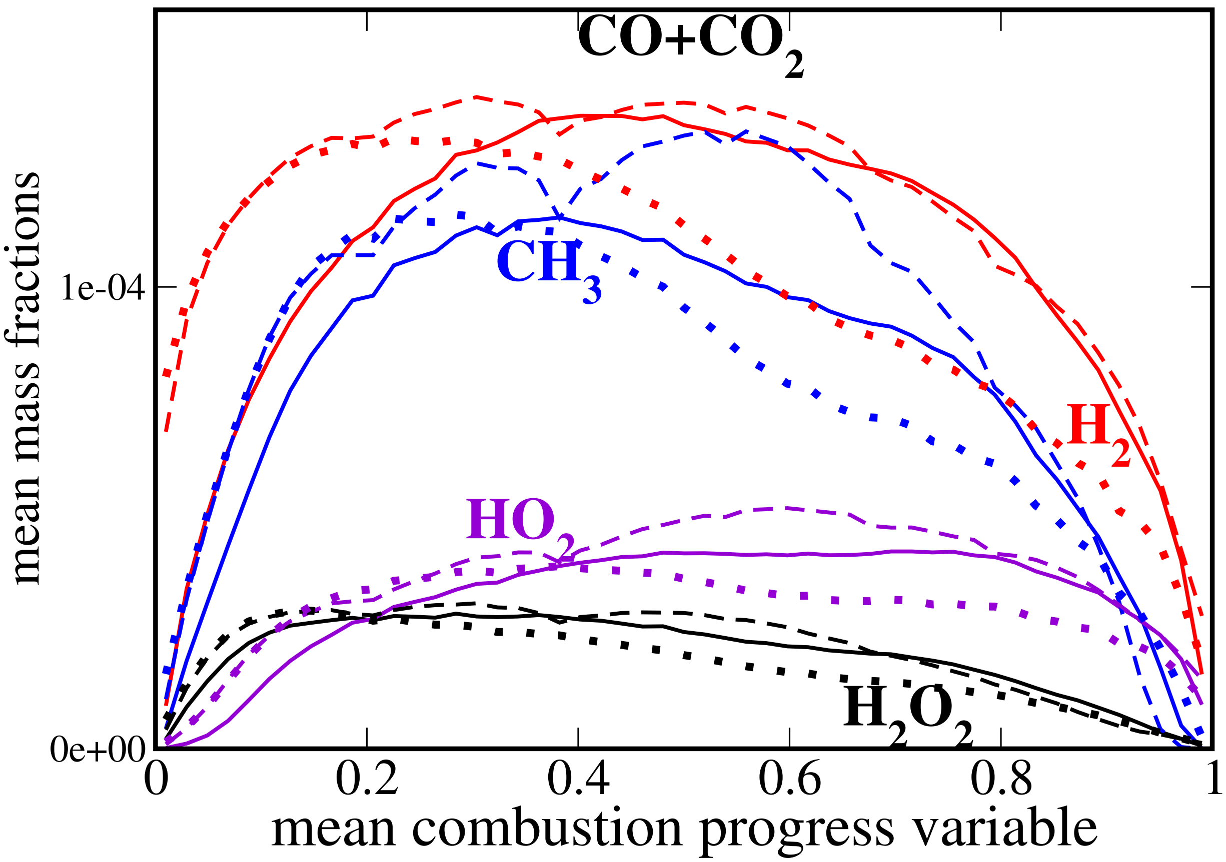
CO+CO$_2$
CH$_3$
H$_2$
HO$_2$
H$_2$O$_2$
1e-04
0e+00
0
0.2
0.4
0.6
0.8
1
mean mass fractions
mean combustion progress variable

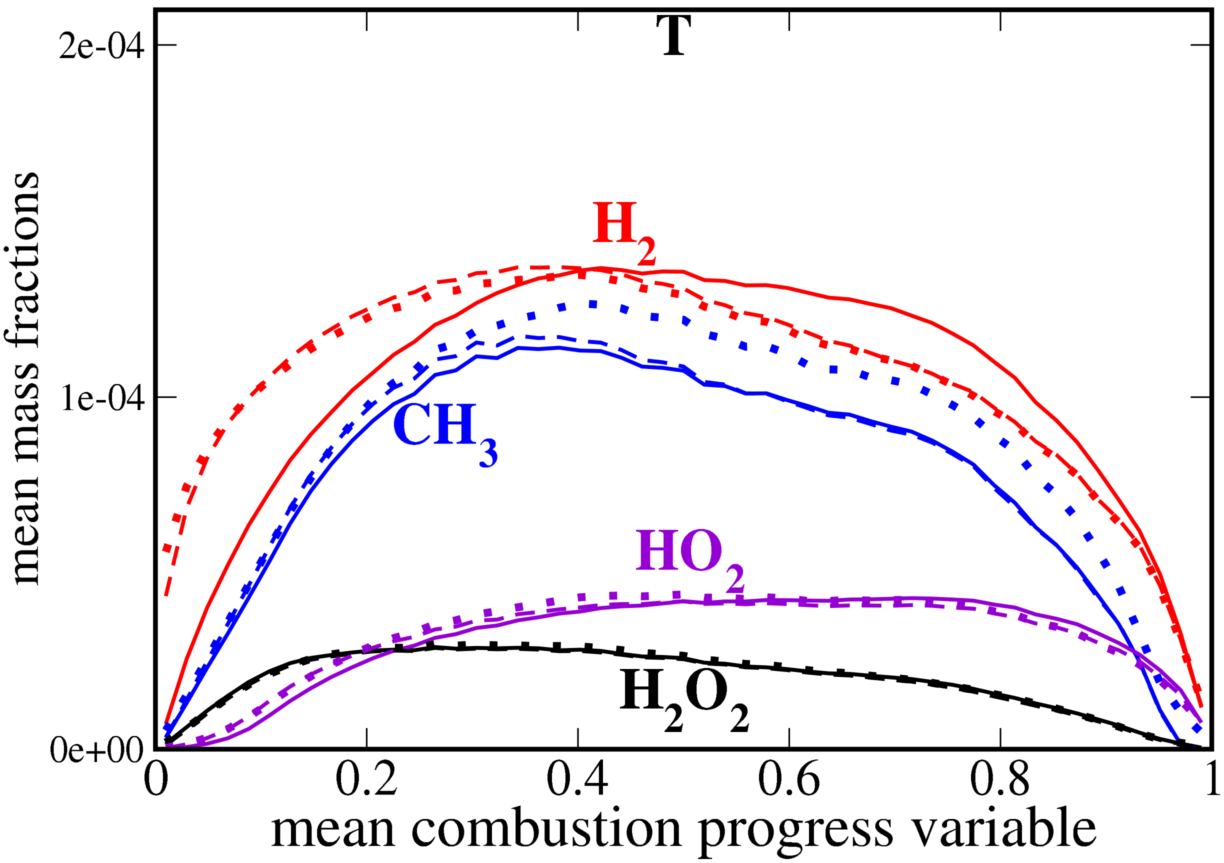
T
H2
CH3
HO2
H2O2
2e-04
1e-04
0e+00
0
0.2
0.4
0.6
0.8
1
mean mass fractions
mean combustion progress variable

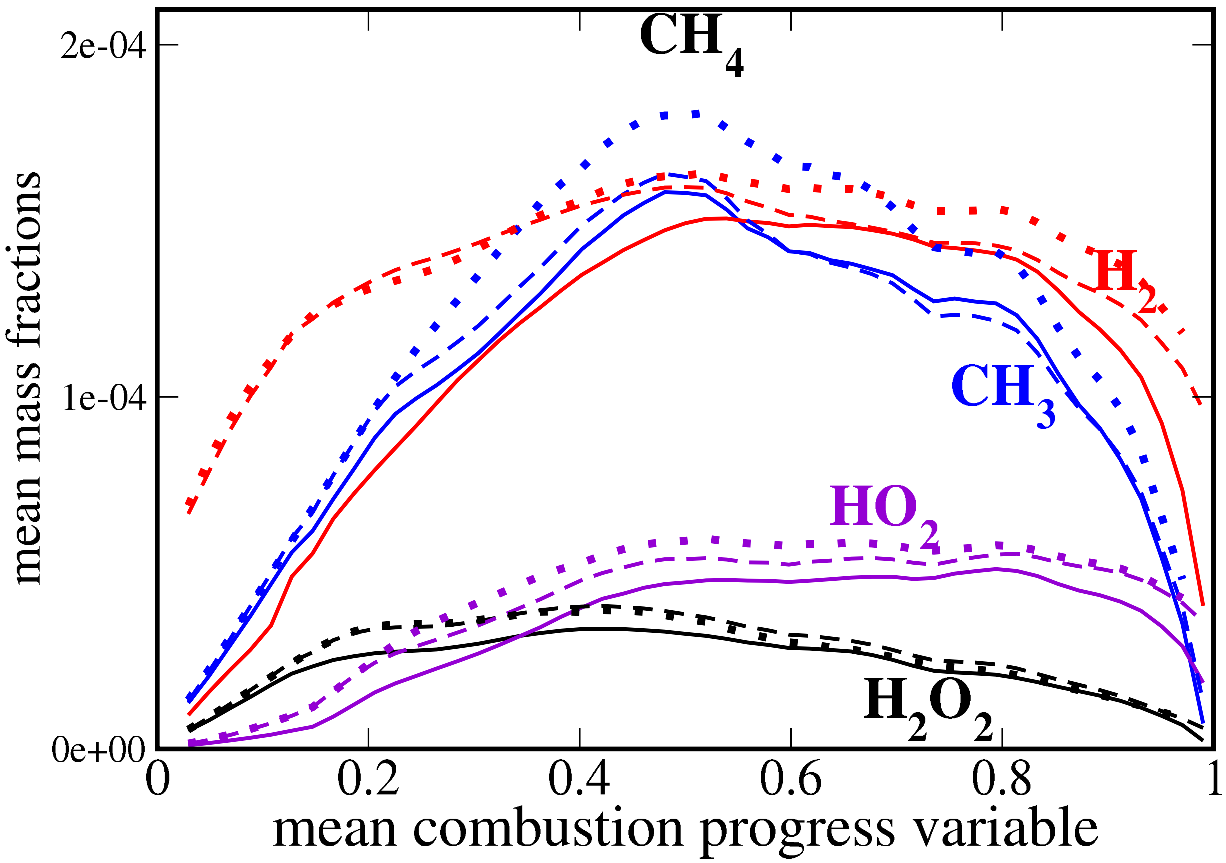
CH4
H2
CH3
HO2
H2O2
2e-04
1e-04
0e+00
0
0.2
0.4
0.6
0.8
1
mean mass fractions
mean combustion progress variable

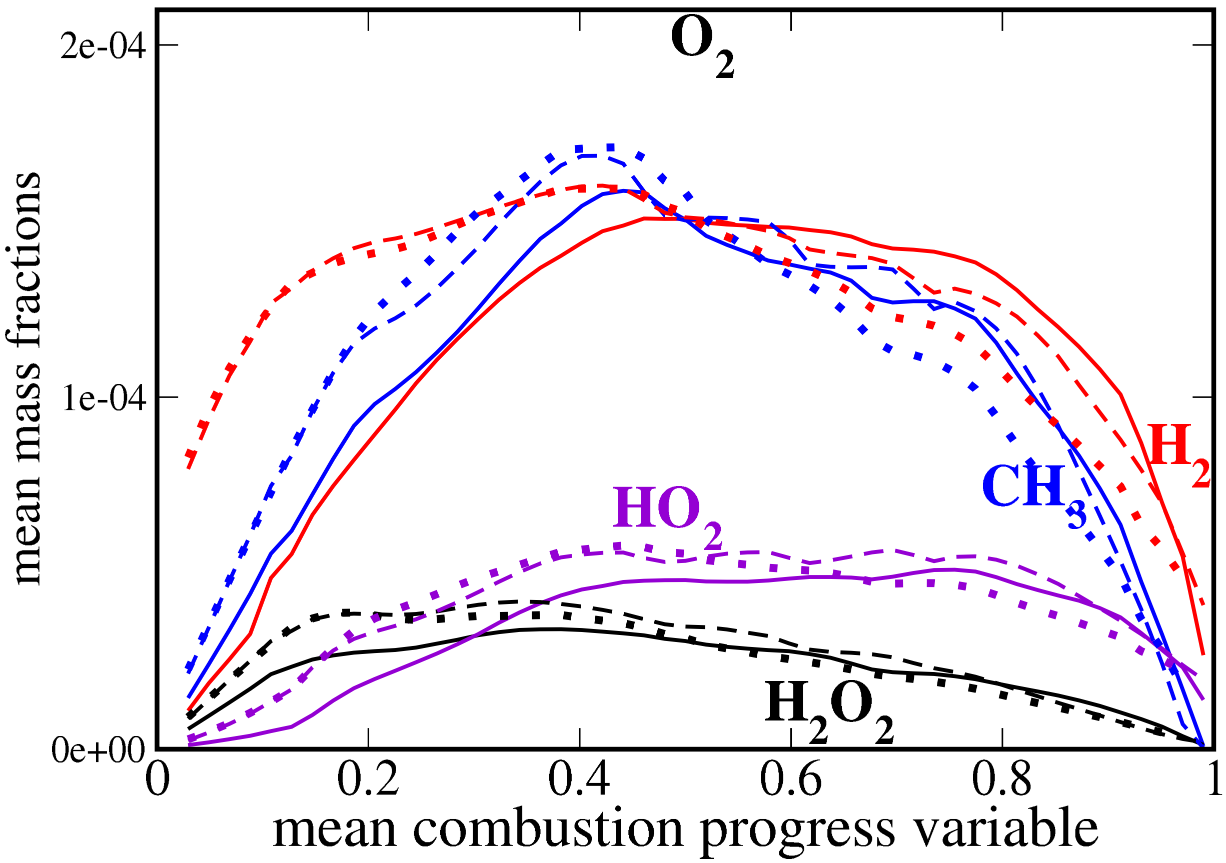
O2
H2
CH3
HO2
H2O2
2e-04
1e-04
0e+00
0
0.2
0.4
0.6
0.8
1
mean mass fractions
mean combustion progress variable

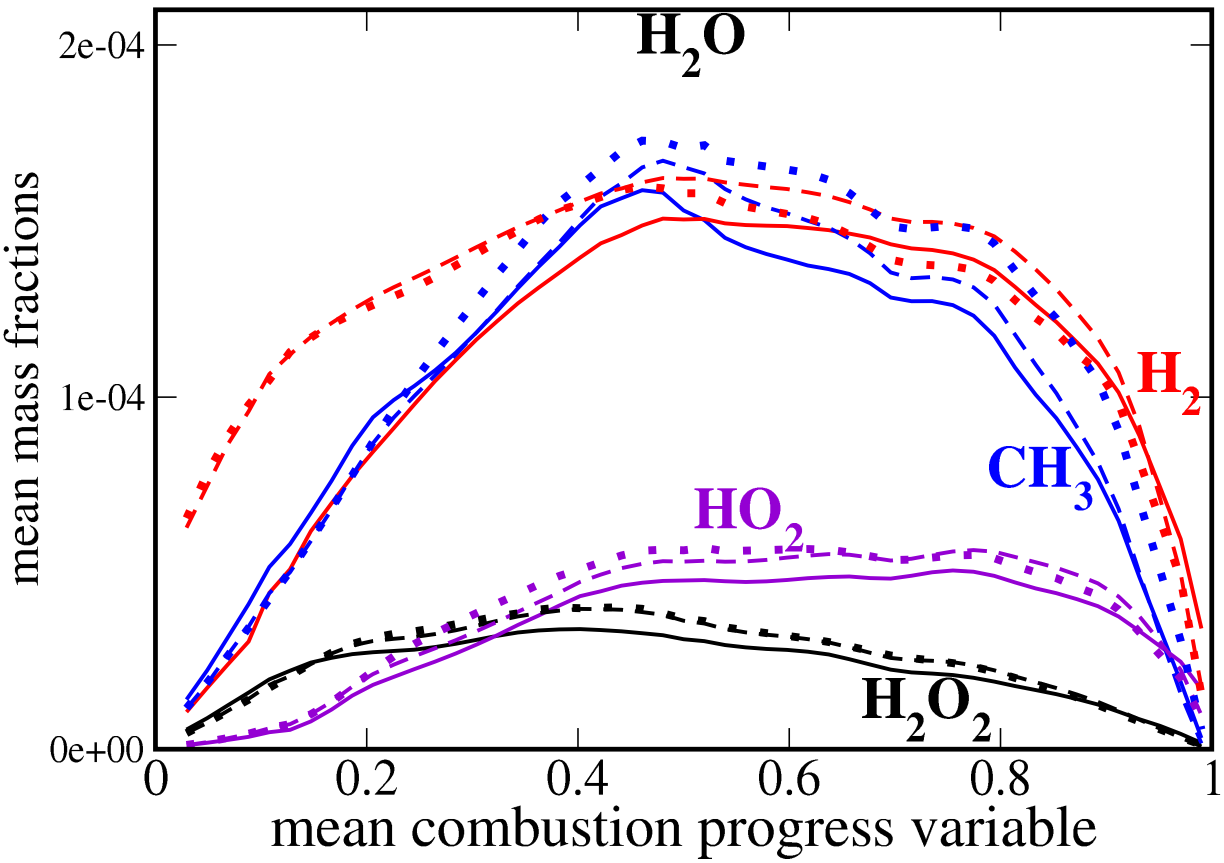
H2O
H2
CH3
HO2
H2O2
2e-04
1e-04
0e+00
0
0.2
0.4
0.6
0.8
1
mean mass fractions
mean combustion progress variable

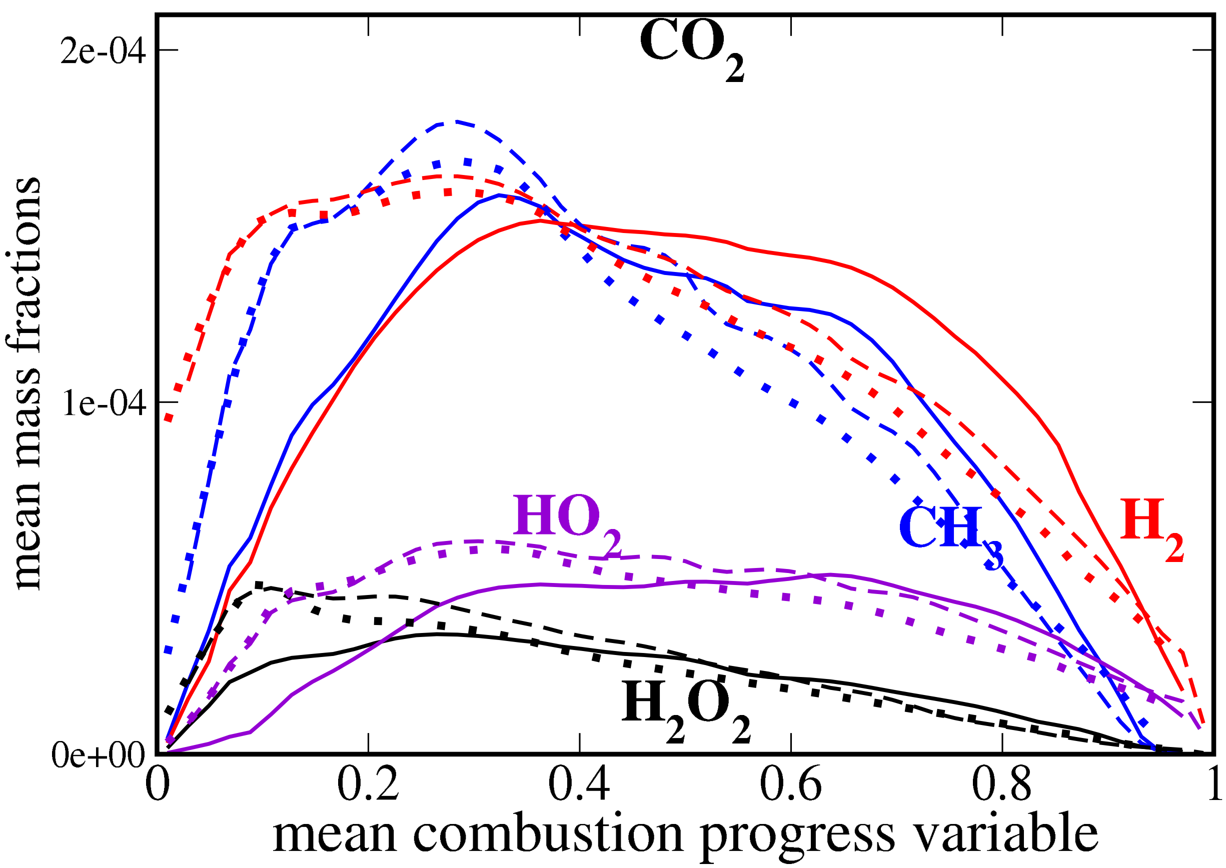
CO_2
HO_2
CH_3
H_2
H_2O_2
2e-04
1e-04
0e+00
0
0.2
0.4
0.6
0.8
1
mean mass fractions
mean combustion progress variable

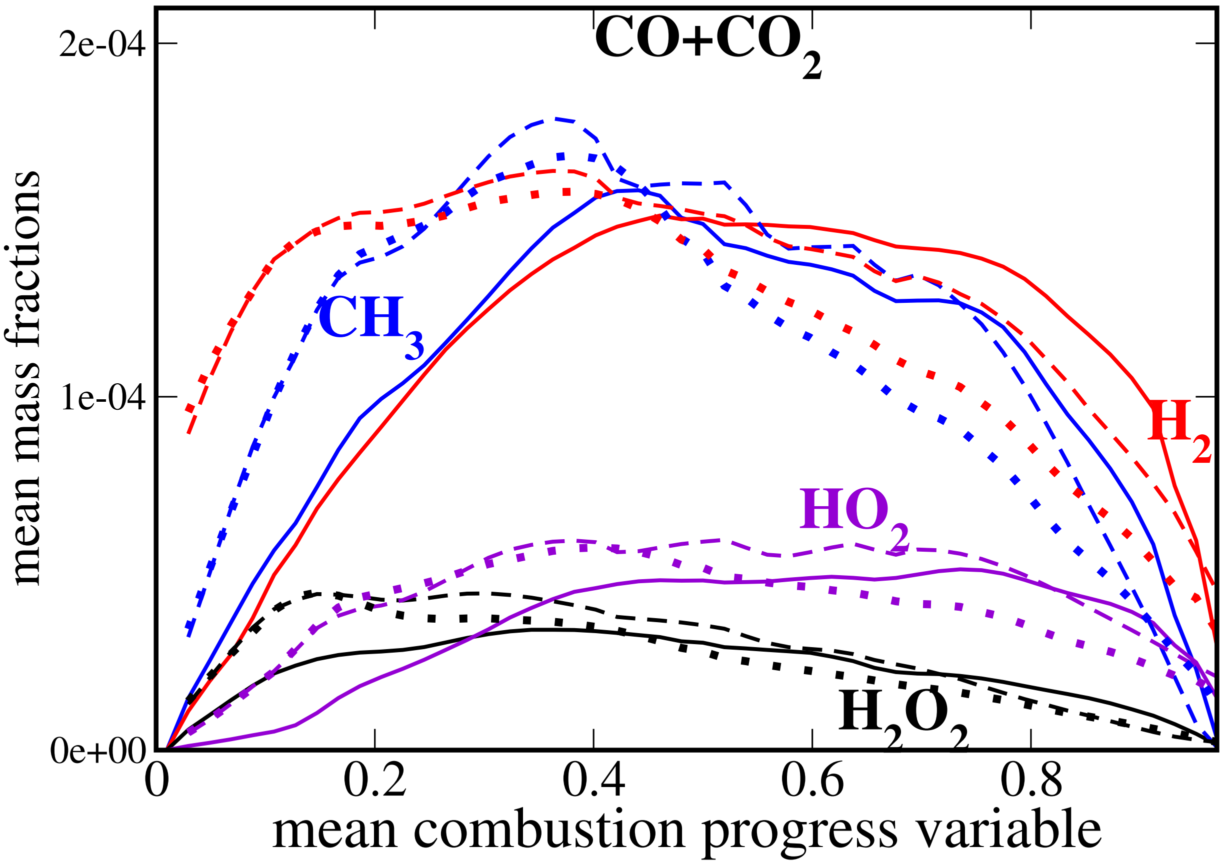
CO+CO2
CH3
H2
HO2
H2O2
2e-04
1e-04
0e+00
0
0.2
0.4
0.6
0.8
mean mass fractions
mean combustion progress variable

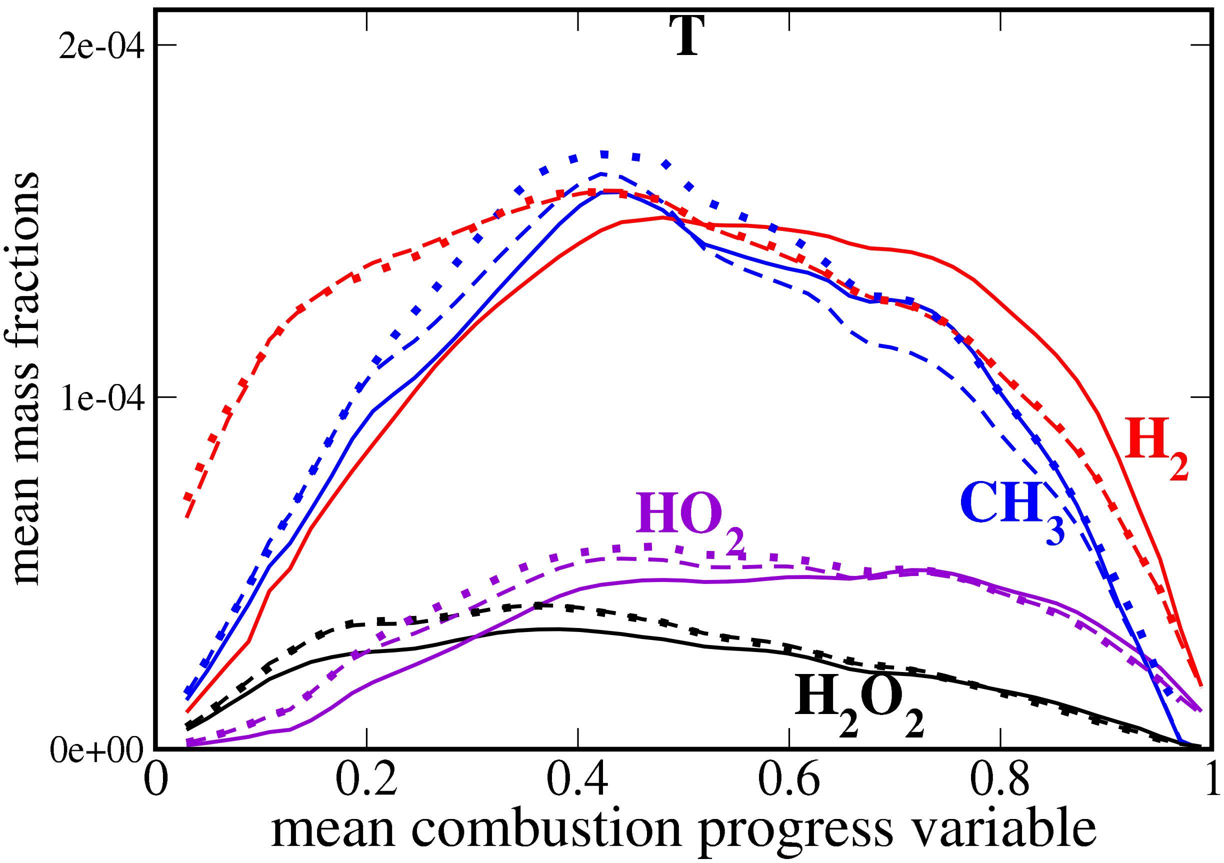
T
2e-04
1e-04
0e+00
mean mass fractions
H2
CH3
HO2
H2O2
0
0.2
0.4
0.6
0.8
1
mean combustion progress variable

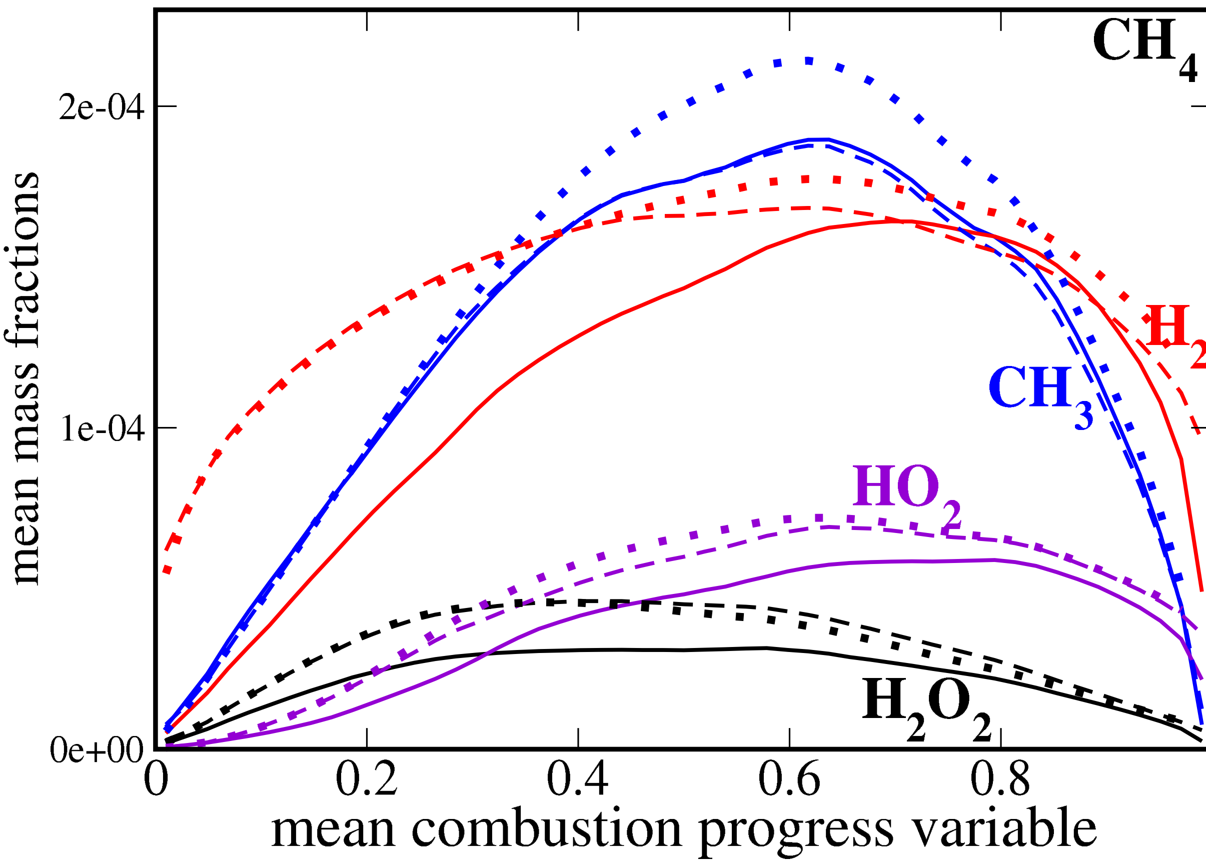
CH4
H2
CH3
HO2
H2O2
mean mass fractions
mean combustion progress variable
0e+00
1e-04
2e-04
0
0.2
0.4
0.6
0.8
1

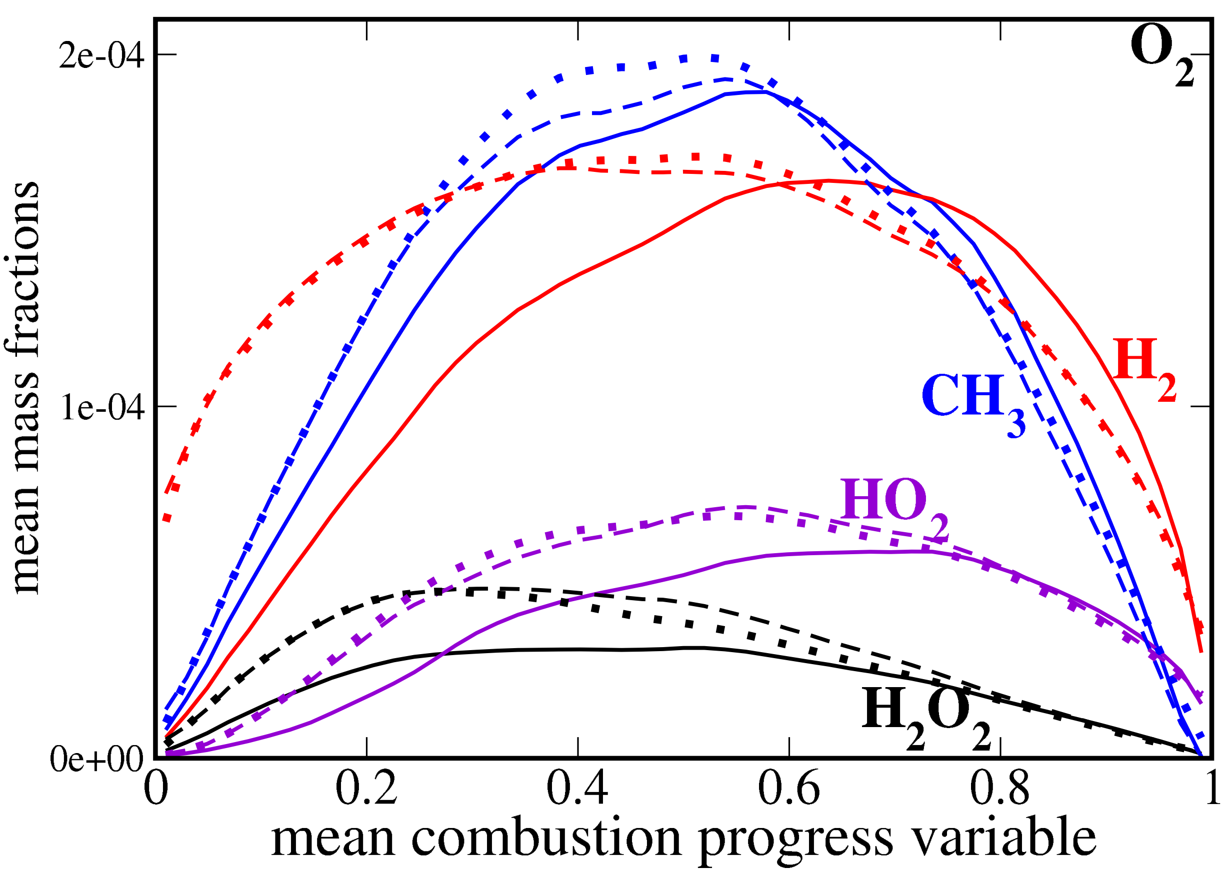
2e-04
1e-04
0e+00
0
0.2
0.4
0.6
0.8
1
mean mass fractions
mean combustion progress variable
O2
H2
CH3
HO2
H2O2

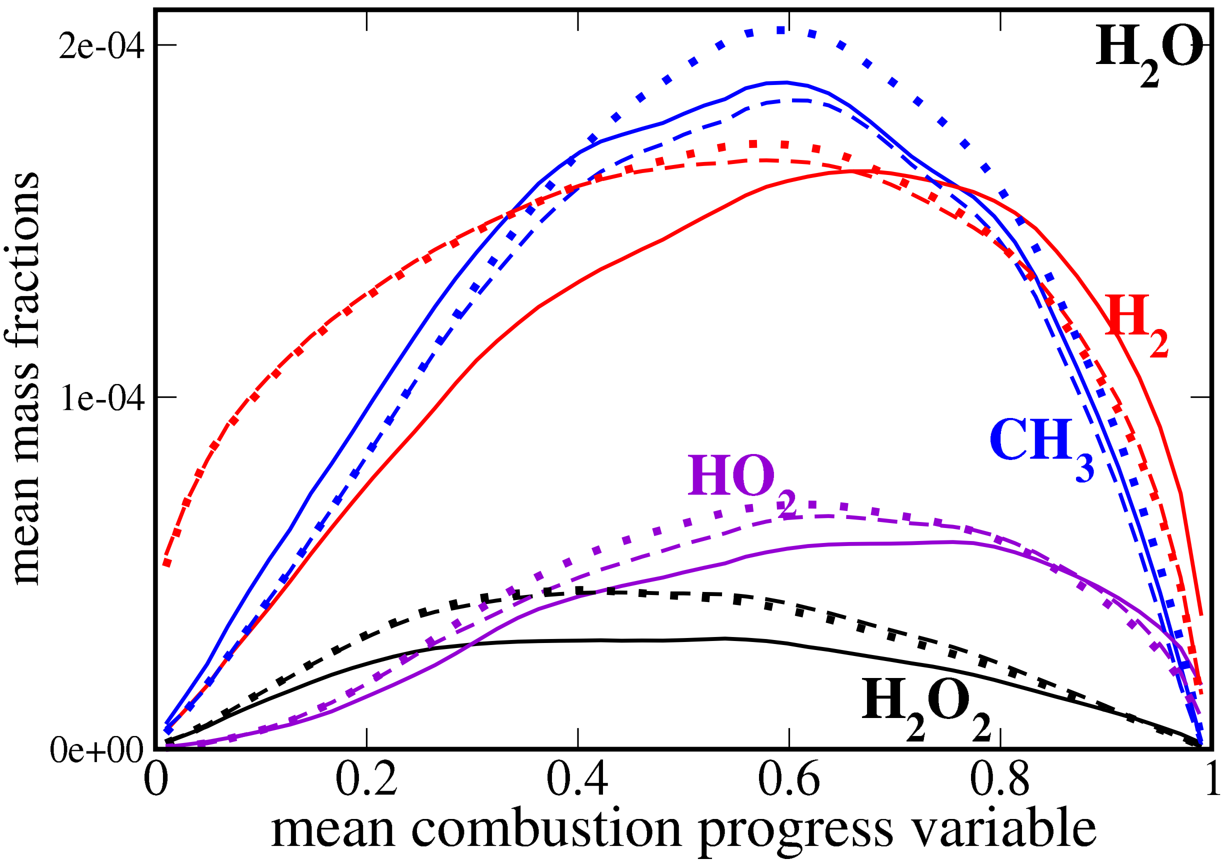
H2O
H2
CH3
HO2
H2O2
2e-04
1e-04
0e+00
0
0.2
0.4
0.6
0.8
1
mean mass fractions
mean combustion progress variable

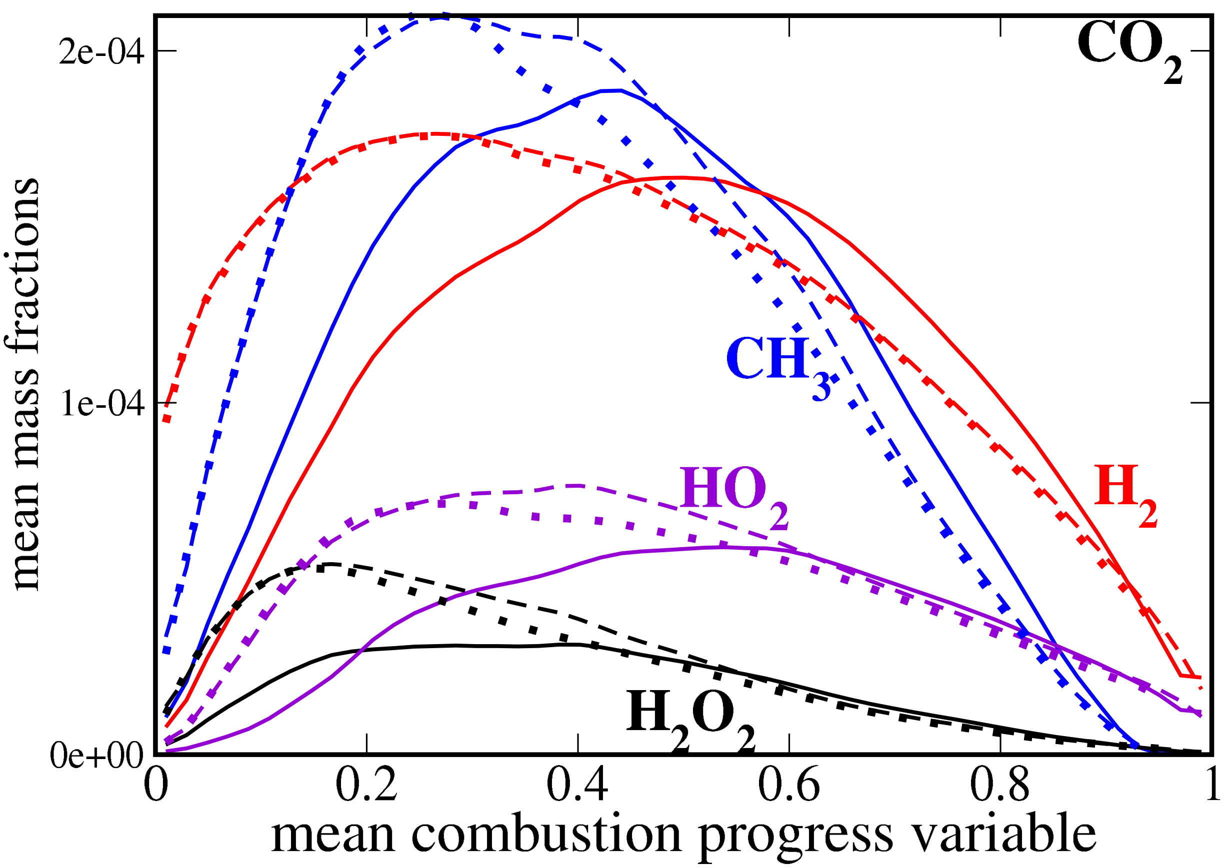
2e-04
1e-04
0e+00
0
0.2
0.4
0.6
0.8
1
mean mass fractions
mean combustion progress variable
CO2
CH3
H2
HO2
H2O2

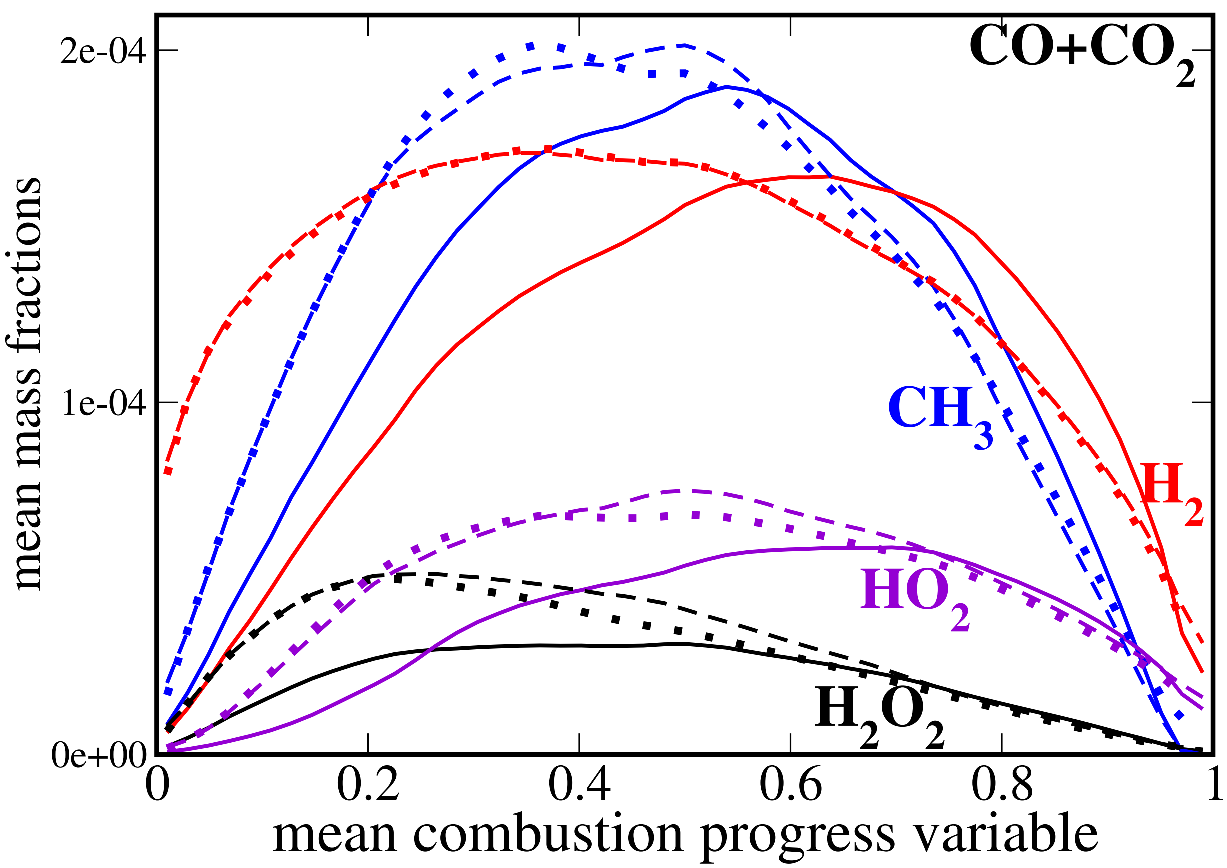
CO+CO2
CH3
H2
HO2
H2O2
2e-04
1e-04
0e+00
0
0.2
0.4
0.6
0.8
1
mean mass fractions
mean combustion progress variable

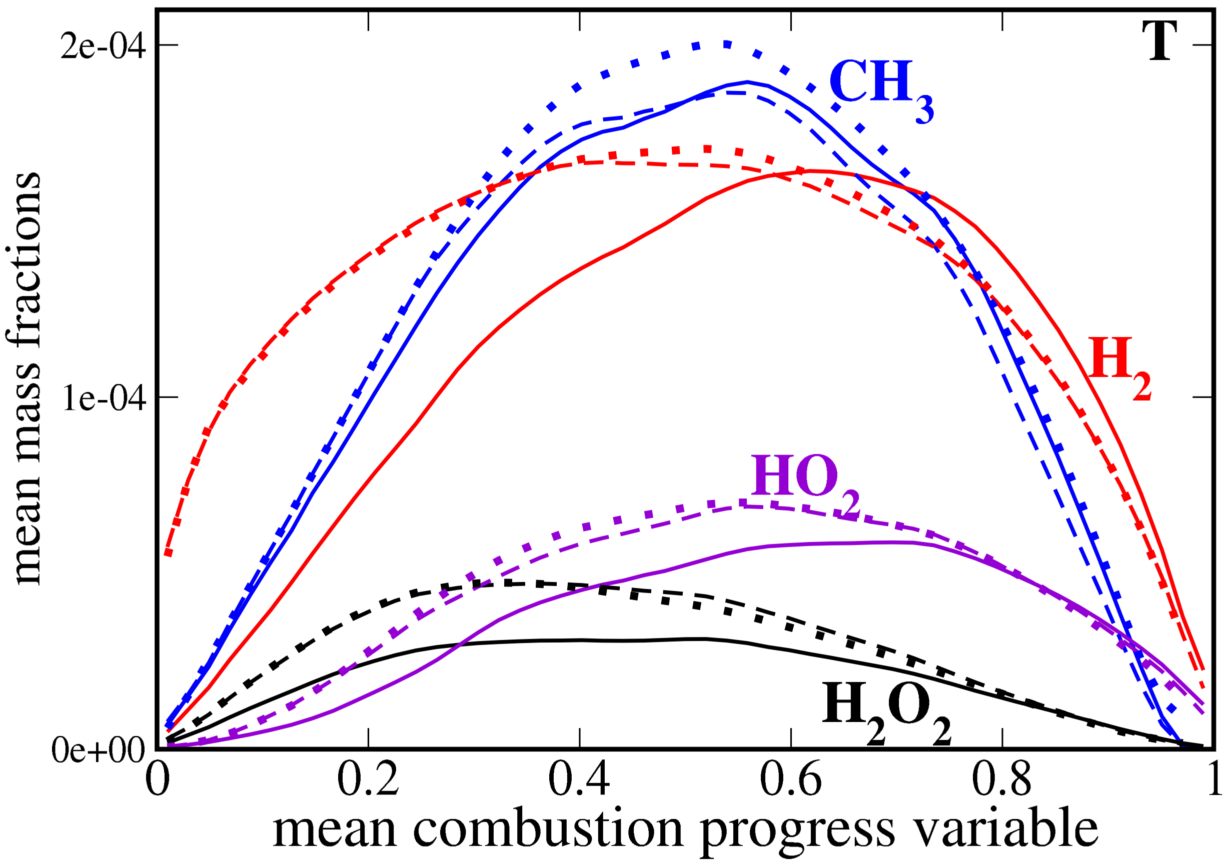
T
CH3
H2
HO2
H2O2
2e-04
1e-04
0e+00
0
0.2
0.4
0.6
0.8
1
mean mass fractions
mean combustion progress variable

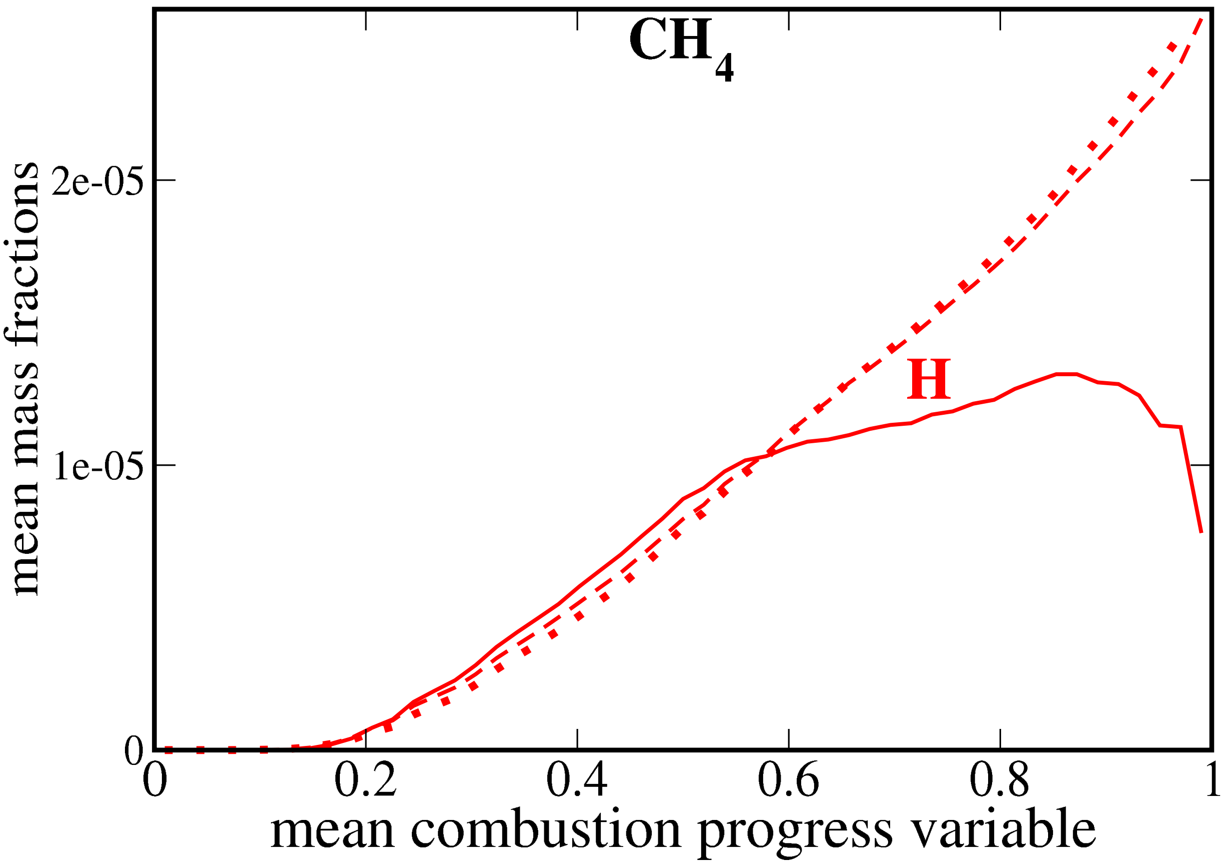
CH4
H
mean mass fractions
2e-05
1e-05
0
0
0.2
0.4
0.6
0.8
1
mean combustion progress variable

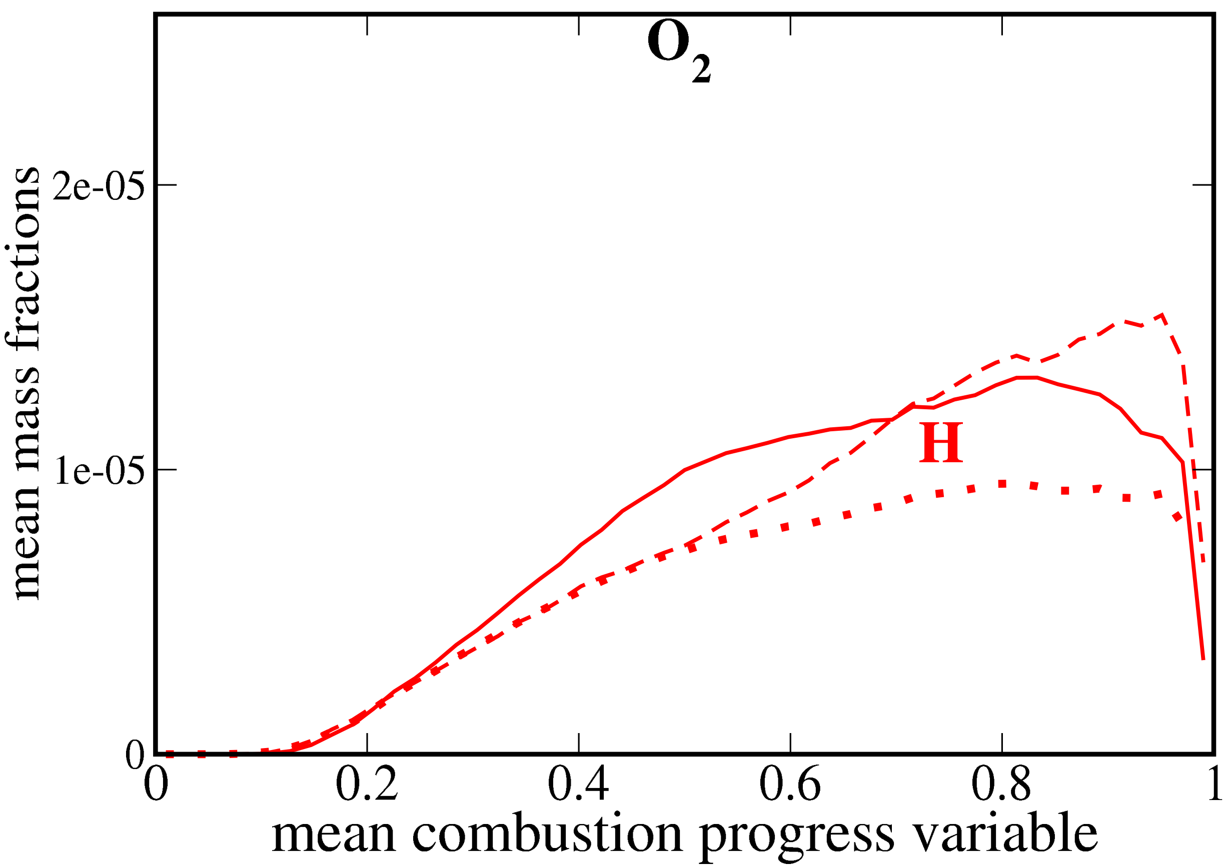
O_2
H
mean mass fractions
2e-05
1e-05
0
0
0.2
0.4
0.6
0.8
1
mean combustion progress variable

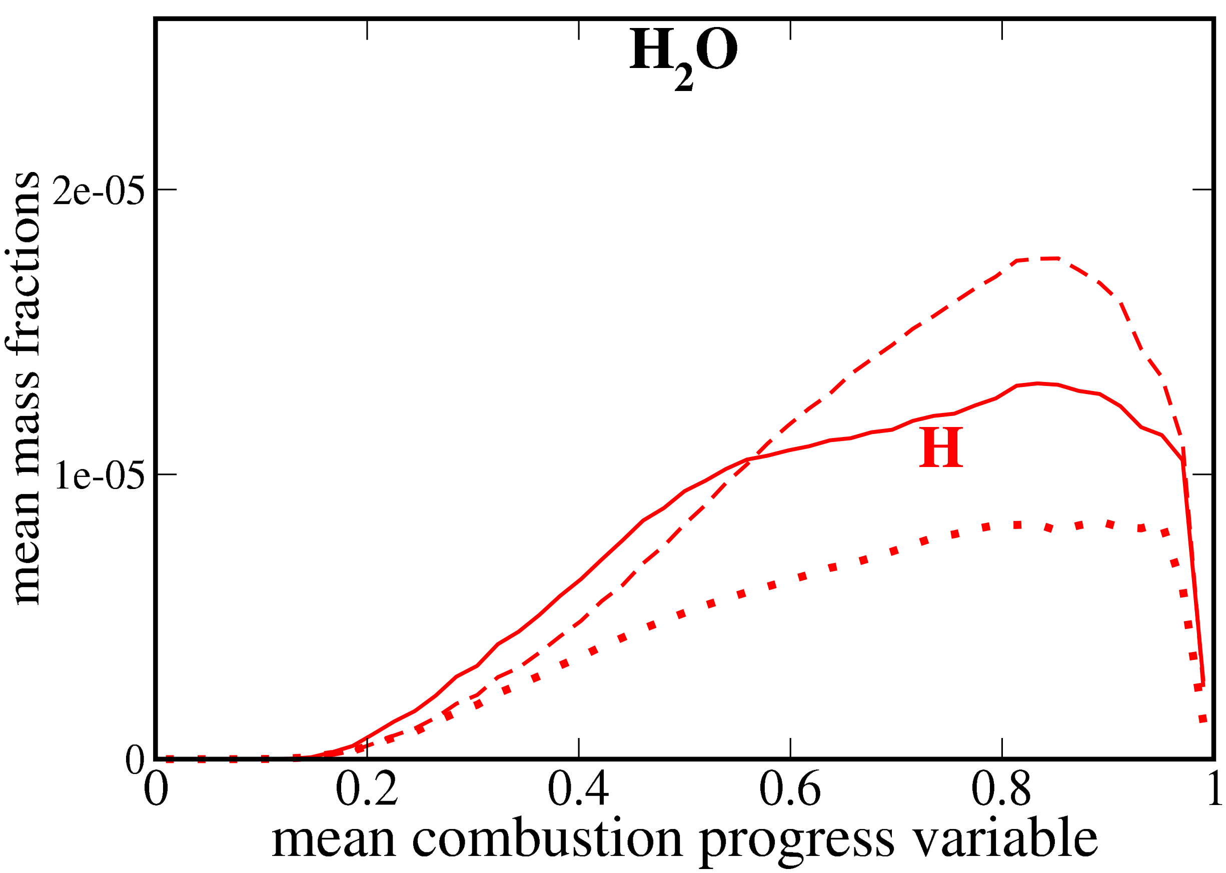
H_2O
H
mean mass fractions
2e-05
1e-05
0
0
0.2
0.4
0.6
0.8
1
mean combustion progress variable

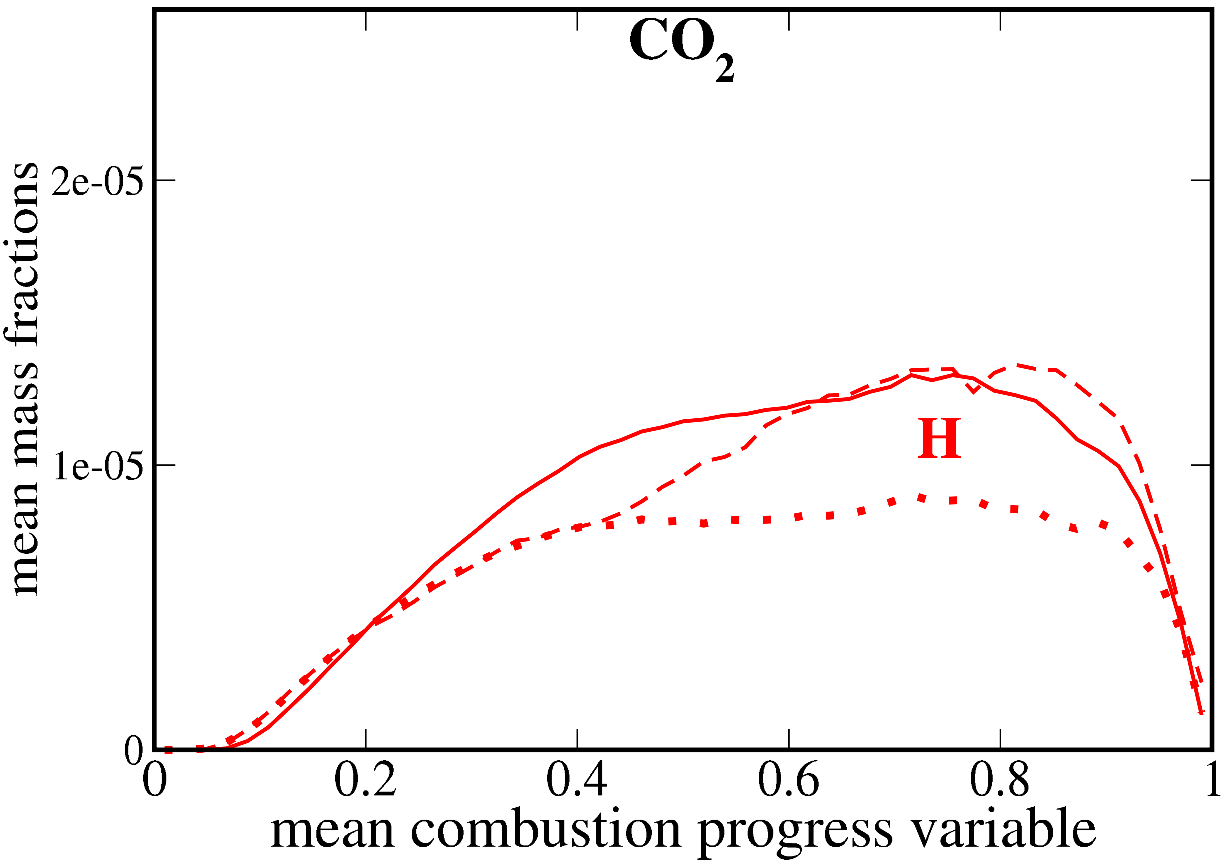
CO_2
H
mean mass fractions
2e-05
1e-05
0
0
0.2
0.4
0.6
0.8
1
mean combustion progress variable

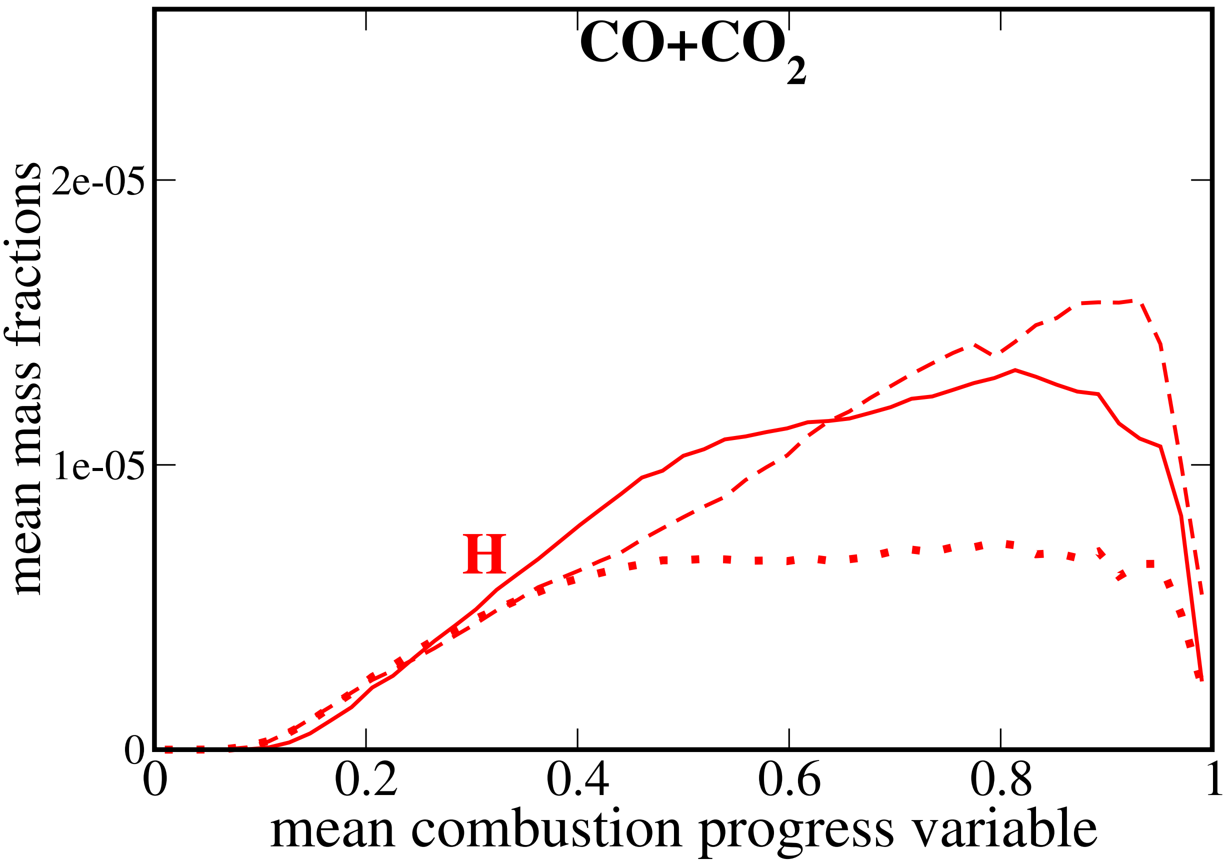
CO+CO2
H
2e-05
1e-05
0
0
0.2
0.4
0.6
0.8
1
mean mass fractions
mean combustion progress variable

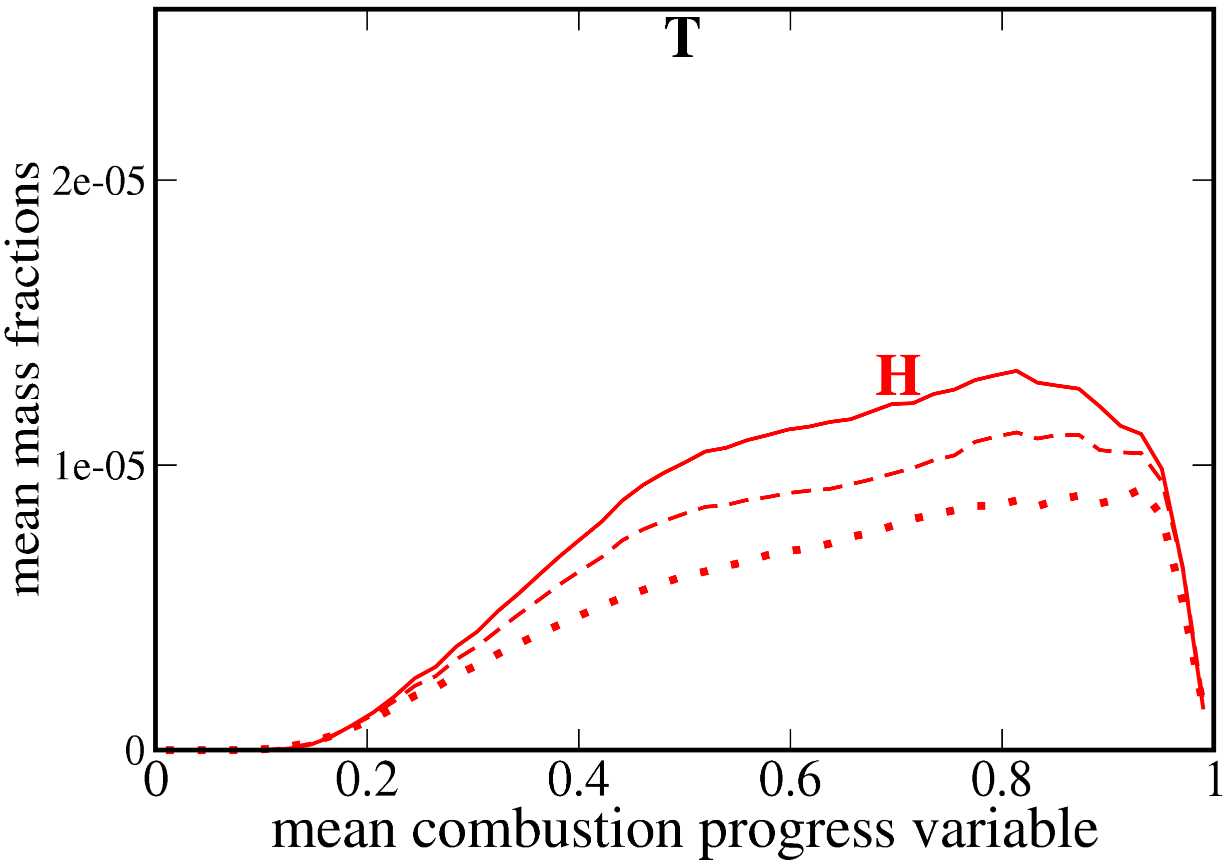
T
H
mean mass fractions
2e-05
1e-05
0
0
0.2
0.4
0.6
0.8
1
mean combustion progress variable

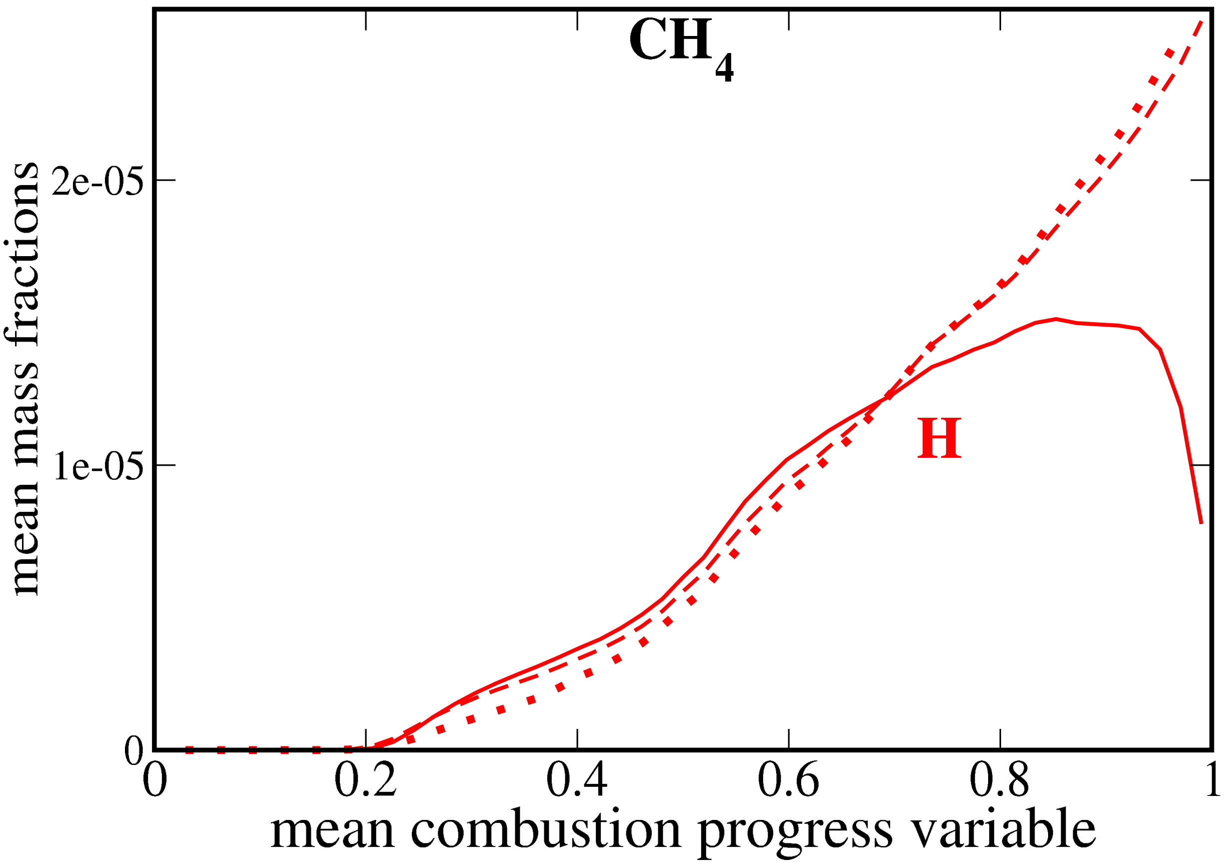
CH4
H
mean mass fractions
2e-05
1e-05
0
0
0.2
0.4
0.6
0.8
1
mean combustion progress variable

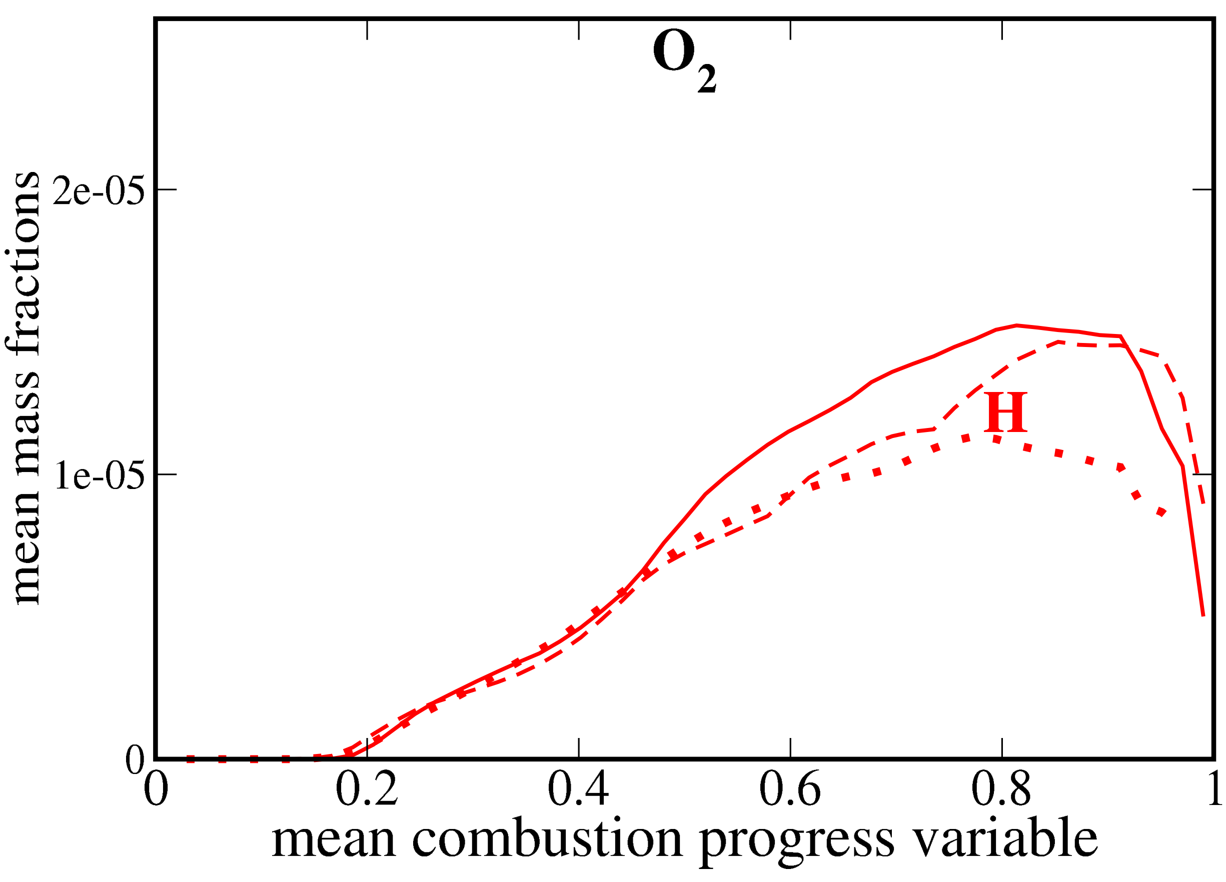
O_2
H
mean mass fractions
2e-05
1e-05
0
0
0.2
0.4
0.6
0.8
1
mean combustion progress variable

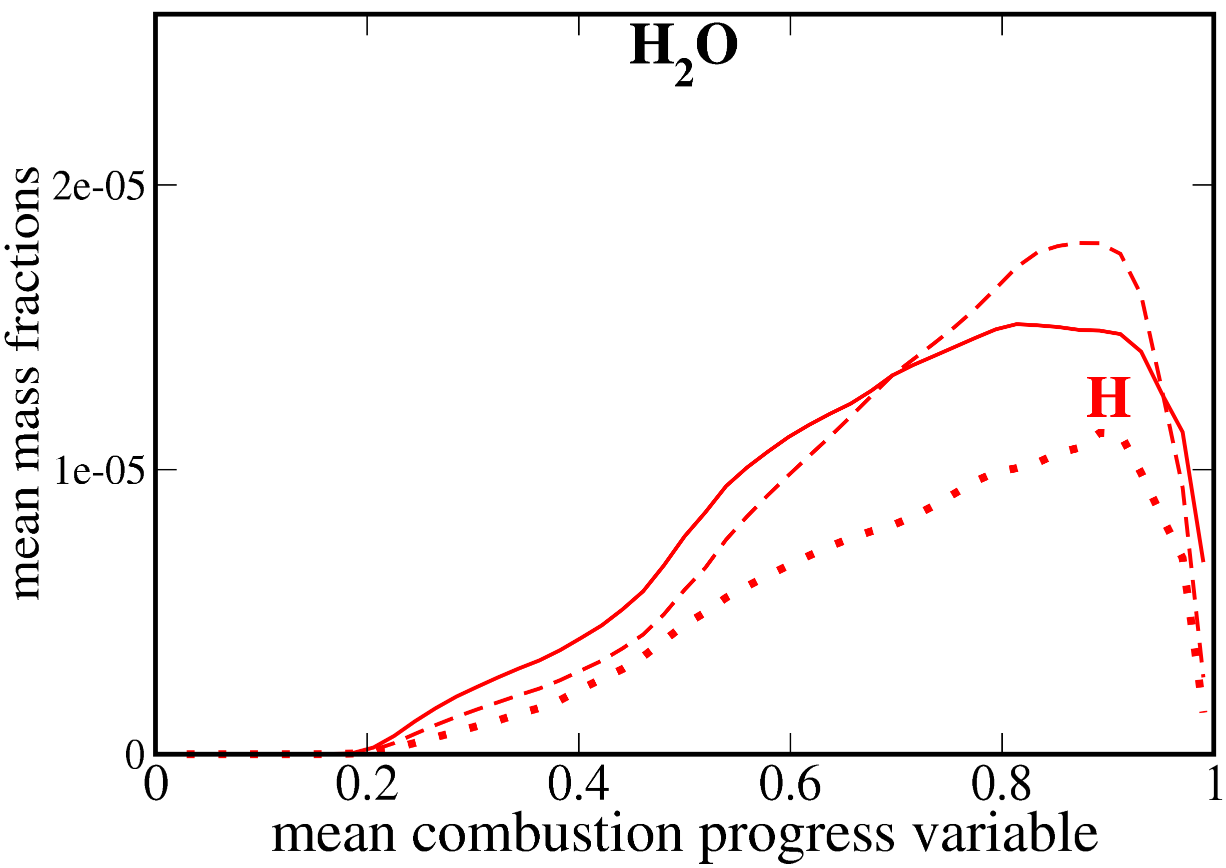
H2O
H
mean mass fractions
2e-05
1e-05
0
0
0.2
0.4
0.6
0.8
1
mean combustion progress variable

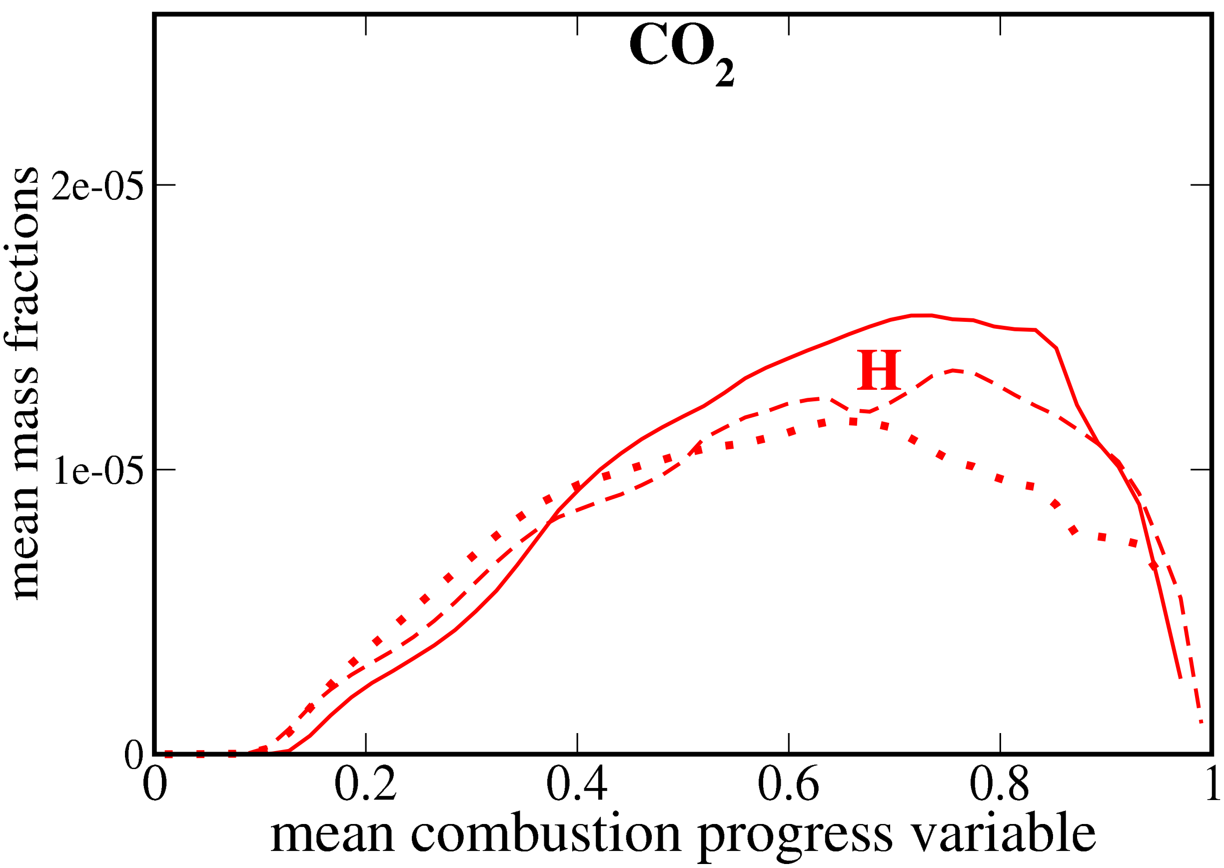
CO2
H
2e-05
1e-05
0
mean mass fractions
0
0.2
0.4
0.6
0.8
1
mean combustion progress variable

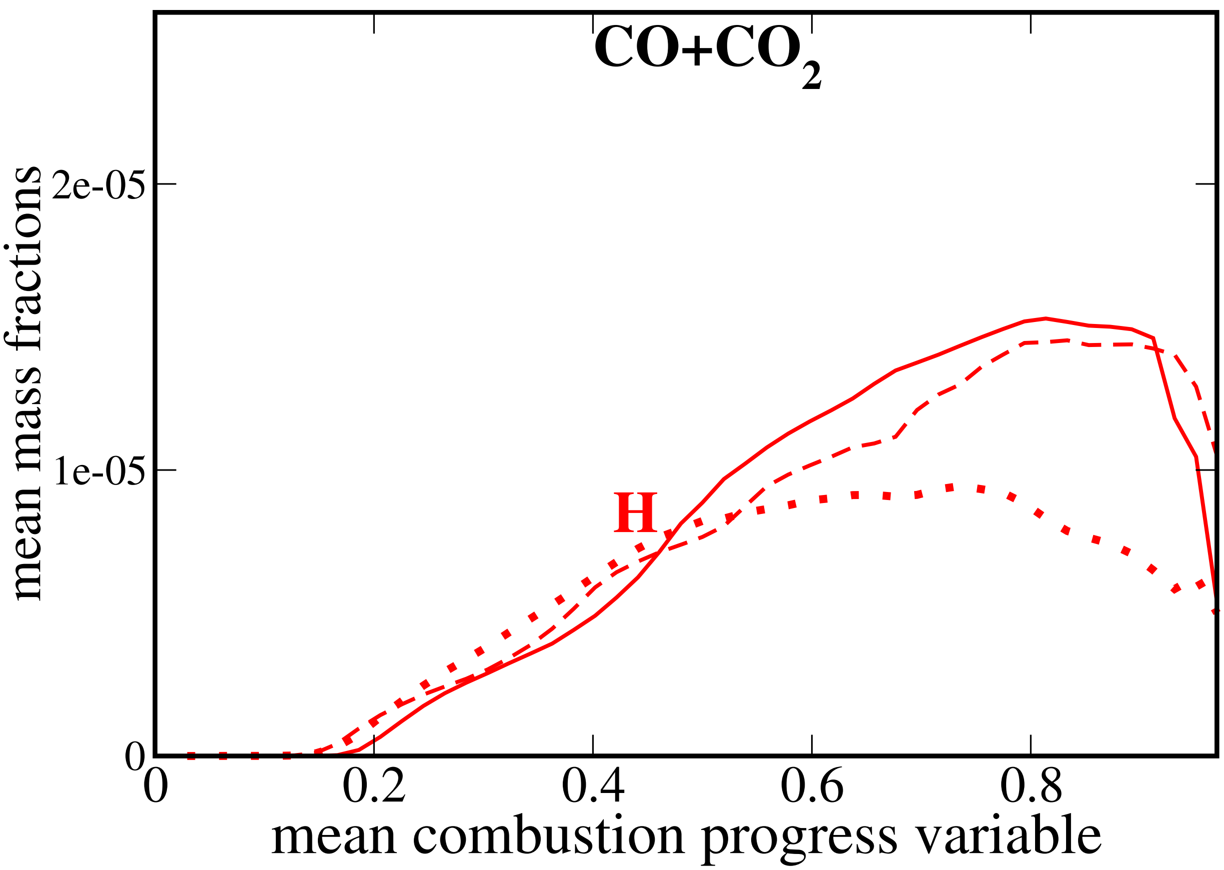
CO+CO2
H
mean mass fractions
2e-05
1e-05
0
0
0.2
0.4
0.6
0.8
mean combustion progress variable

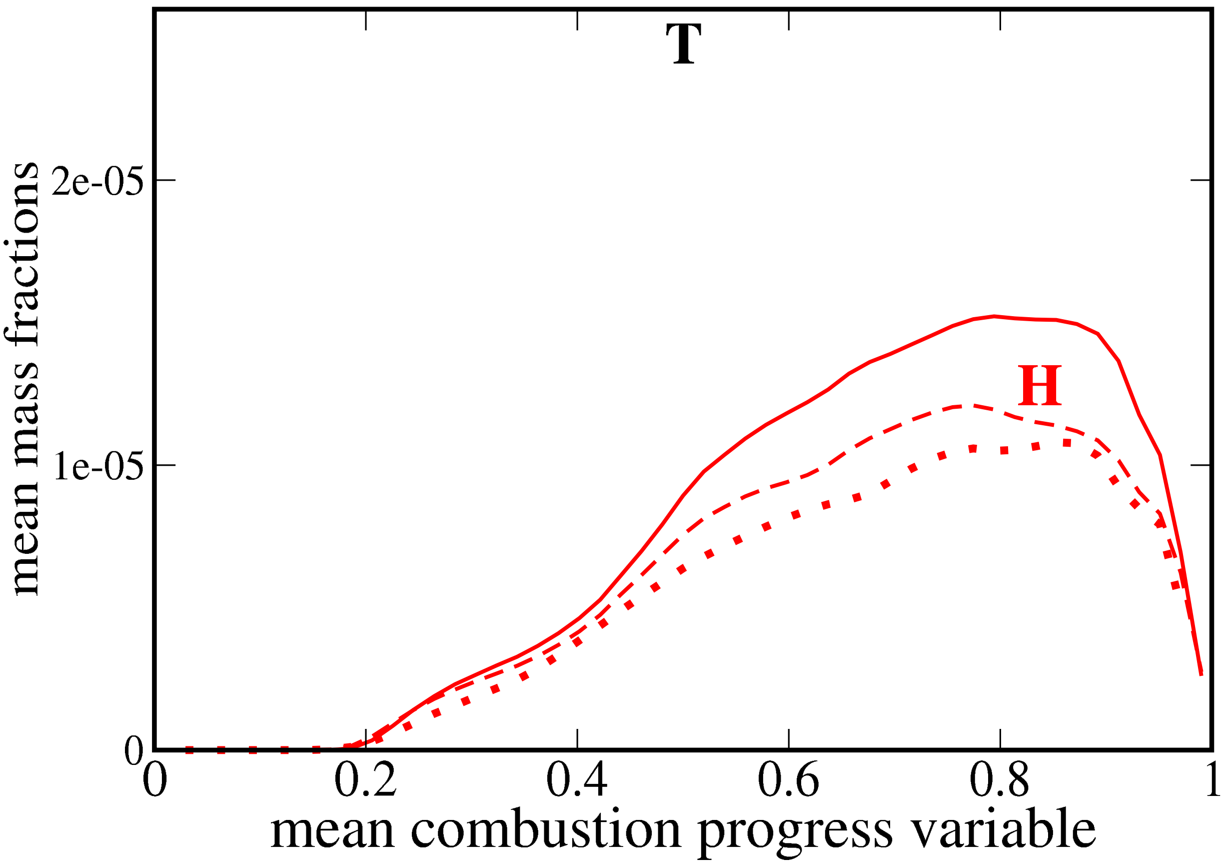
T
H
2e-05
1e-05
0
0
0.2
0.4
0.6
0.8
1
mean mass fractions
mean combustion progress variable

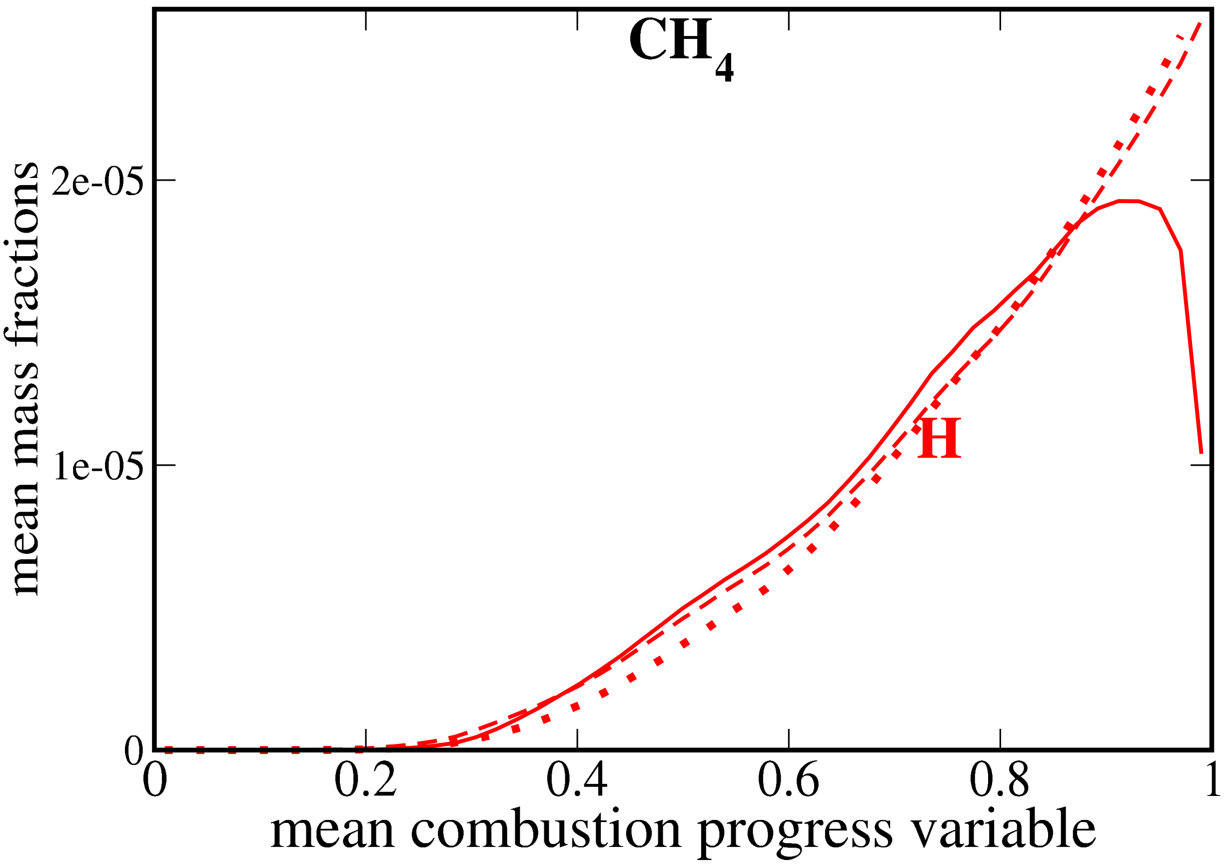
CH4
H
mean mass fractions
2e-05
1e-05
0
0
0.2
0.4
0.6
0.8
1
mean combustion progress variable

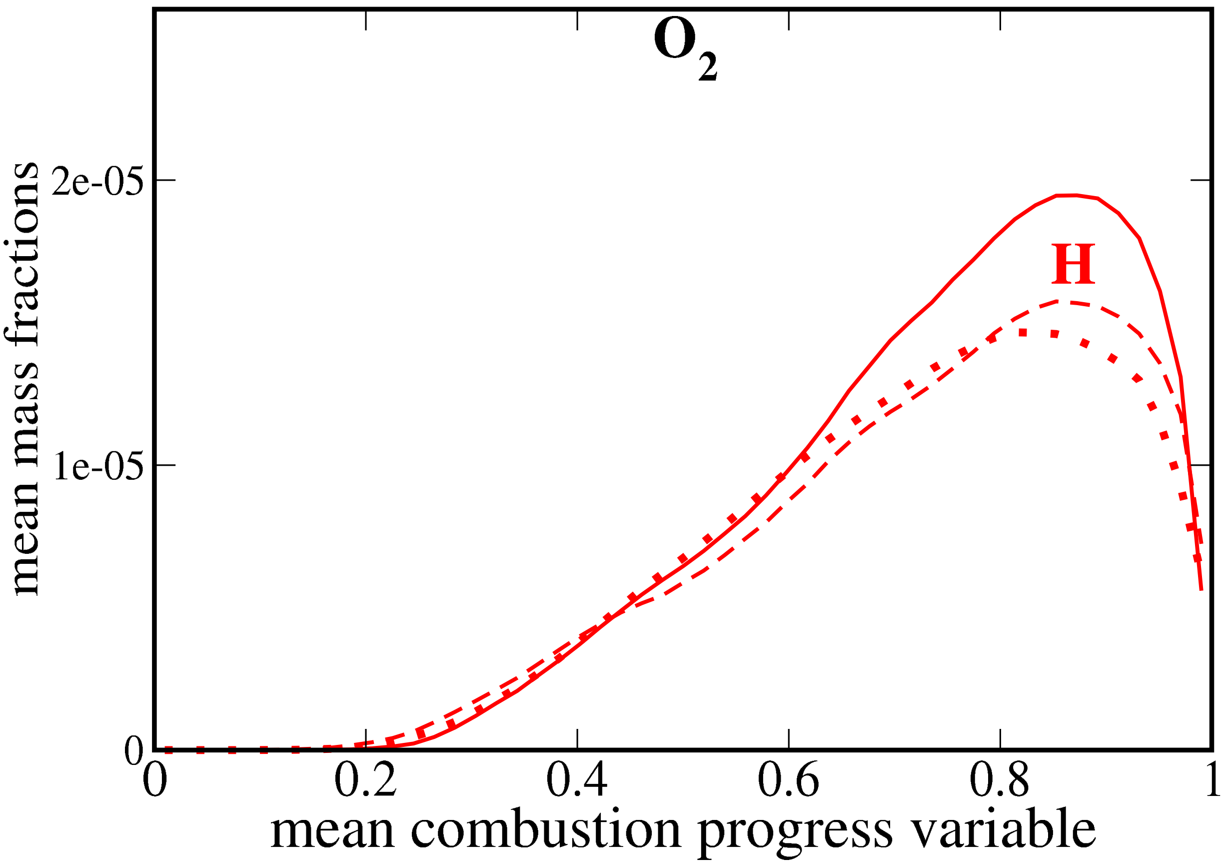
O_2
H
mean mass fractions
2e-05
1e-05
0
0
0.2
0.4
0.6
0.8
1
mean combustion progress variable

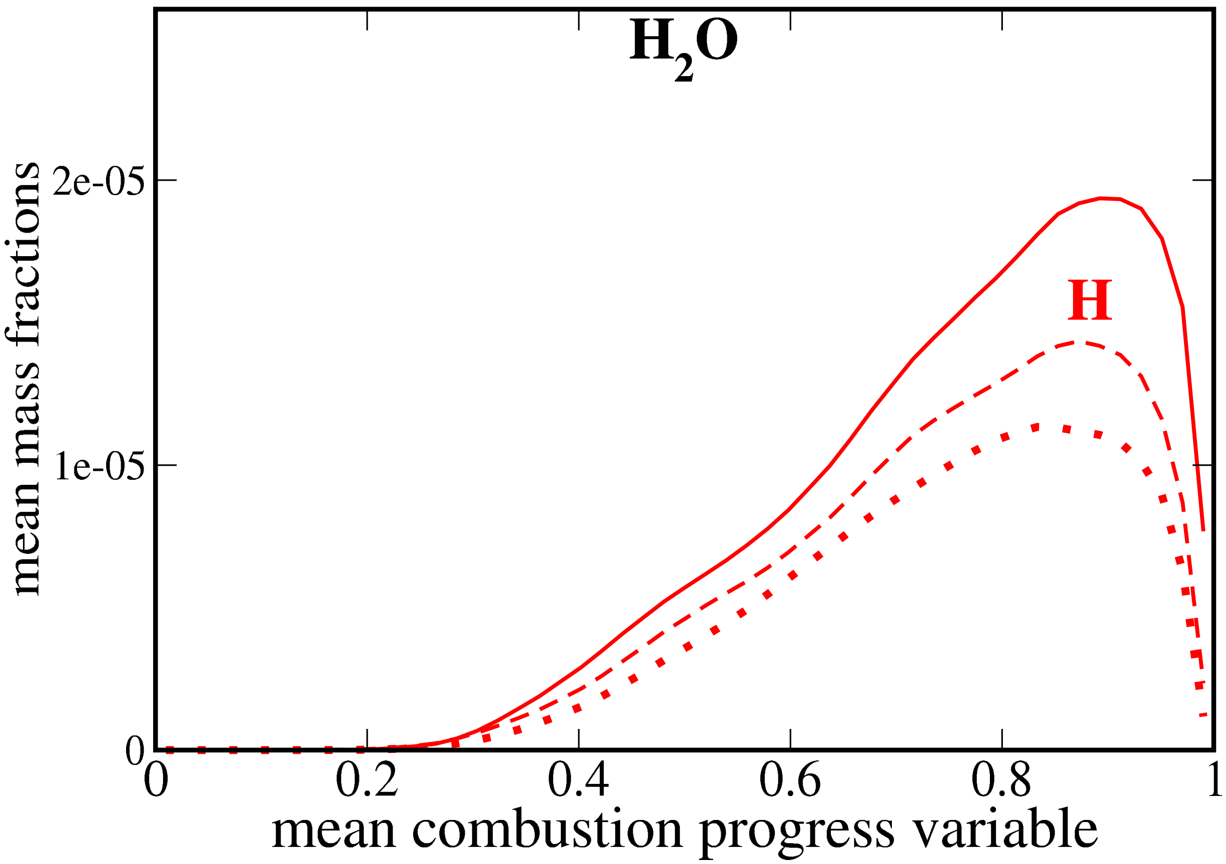
H_2O
H
mean mass fractions
mean combustion progress variable
0
1e-05
2e-05
0
0.2
0.4
0.6
0.8
1

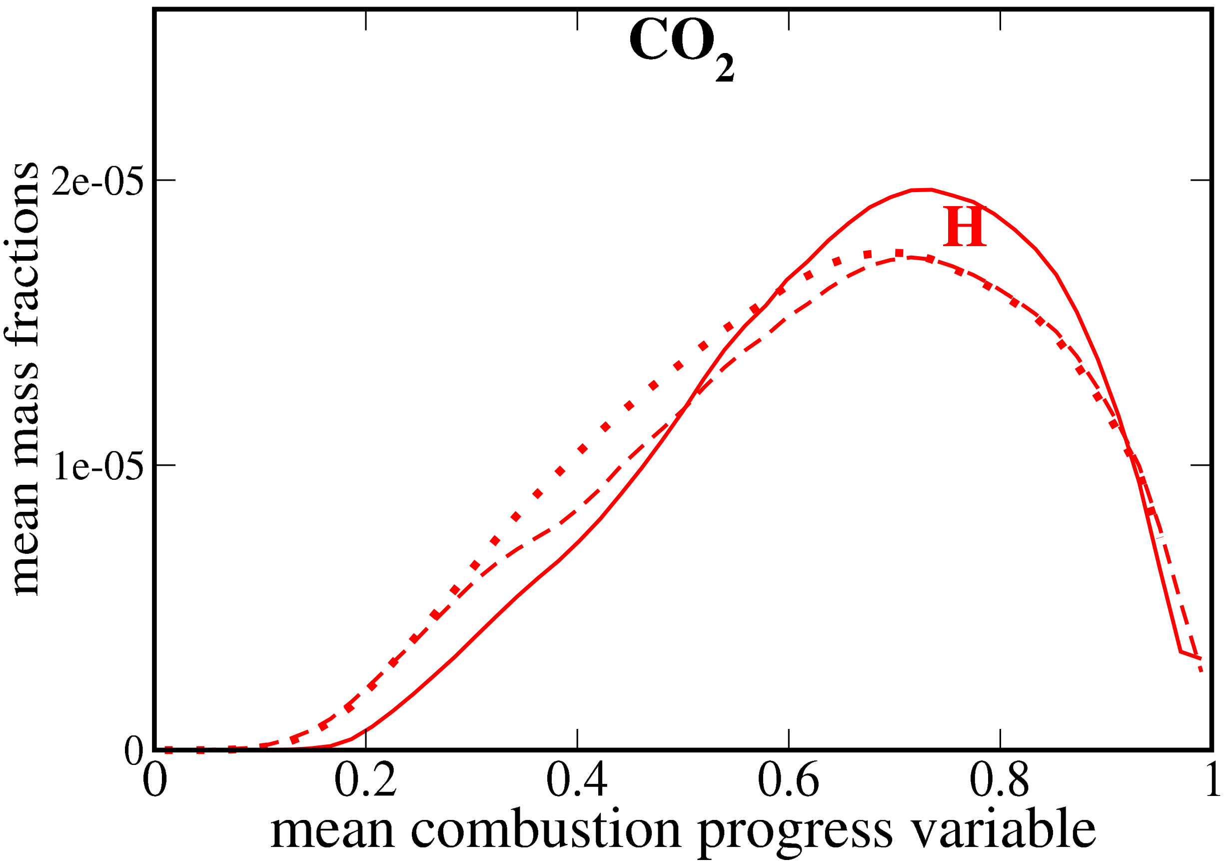
CO_2
H
mean mass fractions
2e-05
1e-05
0
0
0.2
0.4
0.6
0.8
1
mean combustion progress variable

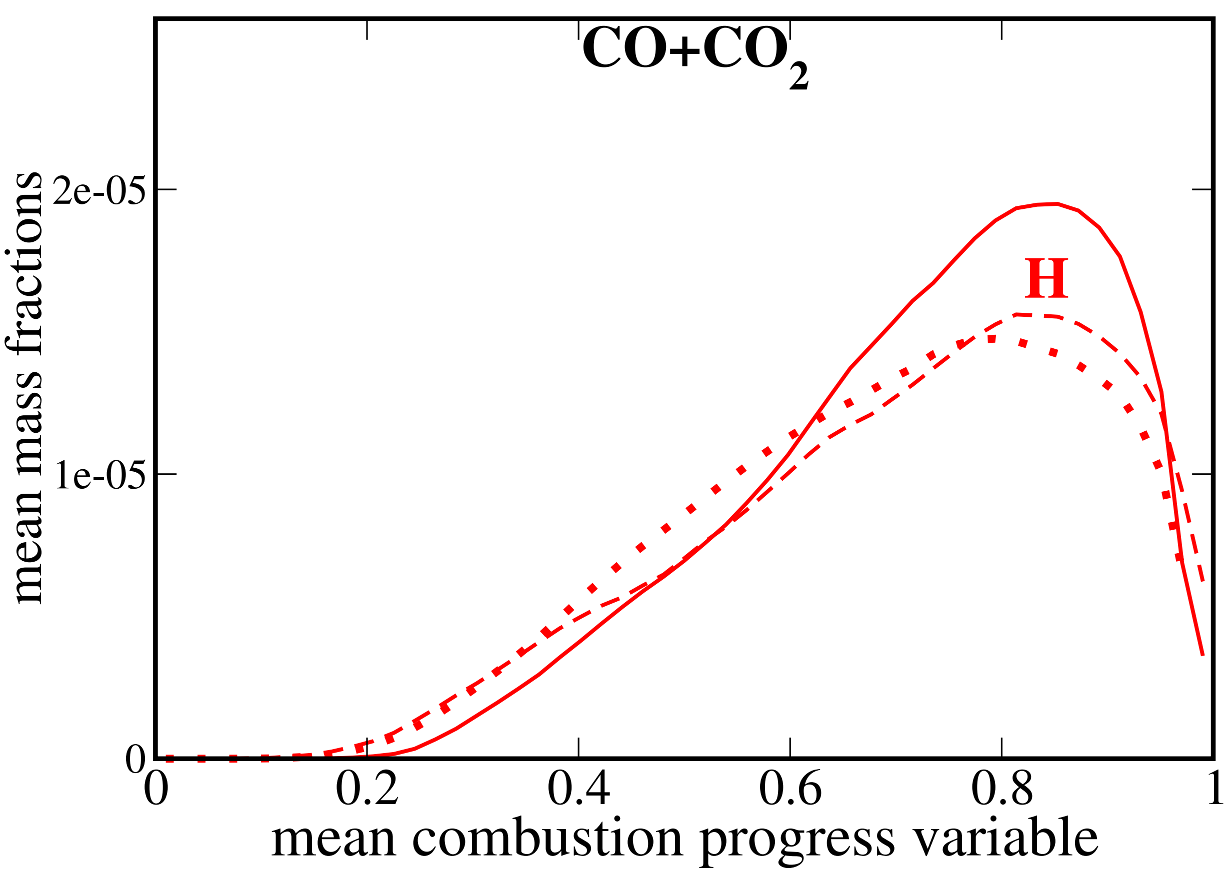
CO+CO2
H
mean mass fractions
2e-05
1e-05
0
0
0.2
0.4
0.6
0.8
1
mean combustion progress variable

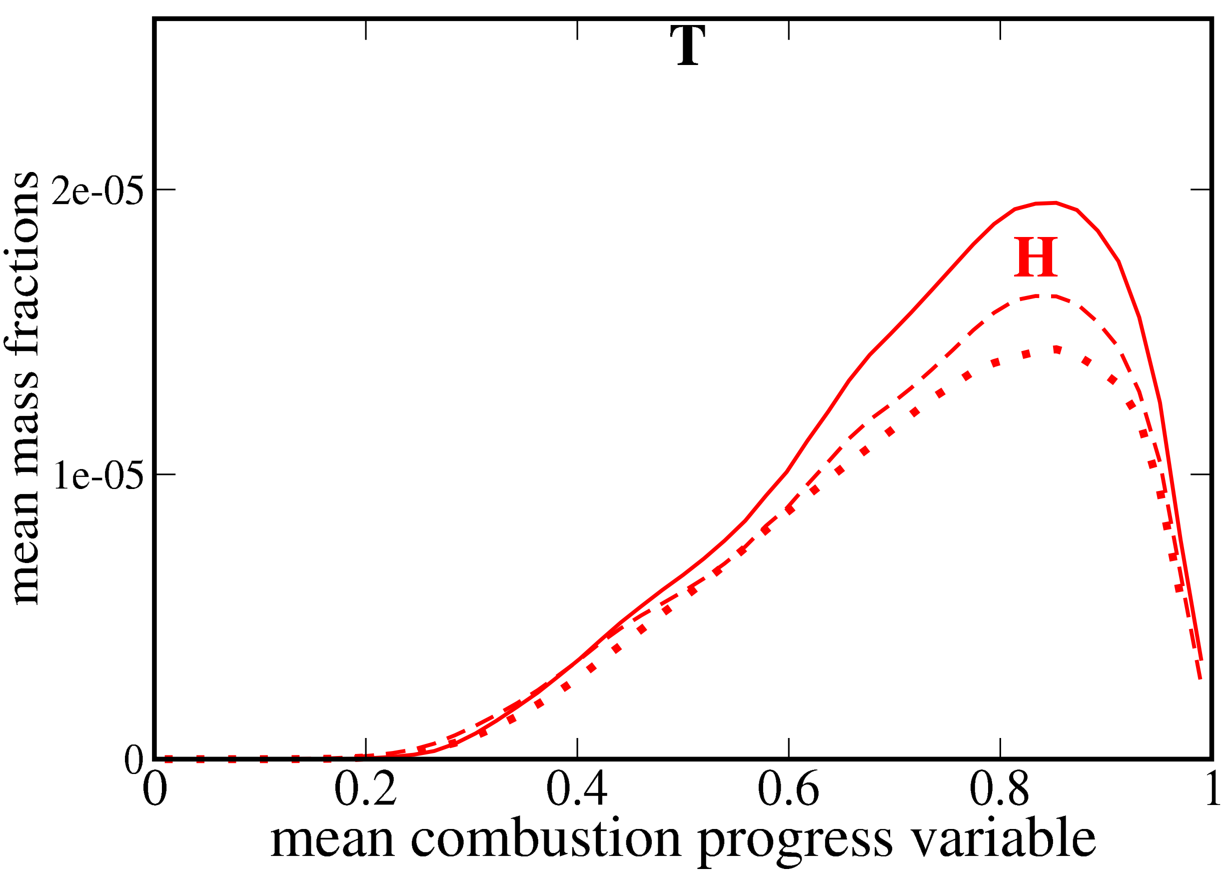
T
H
mean mass fractions
2e-05
1e-05
0
0
0.2
0.4
0.6
0.8
1
mean combustion progress variable

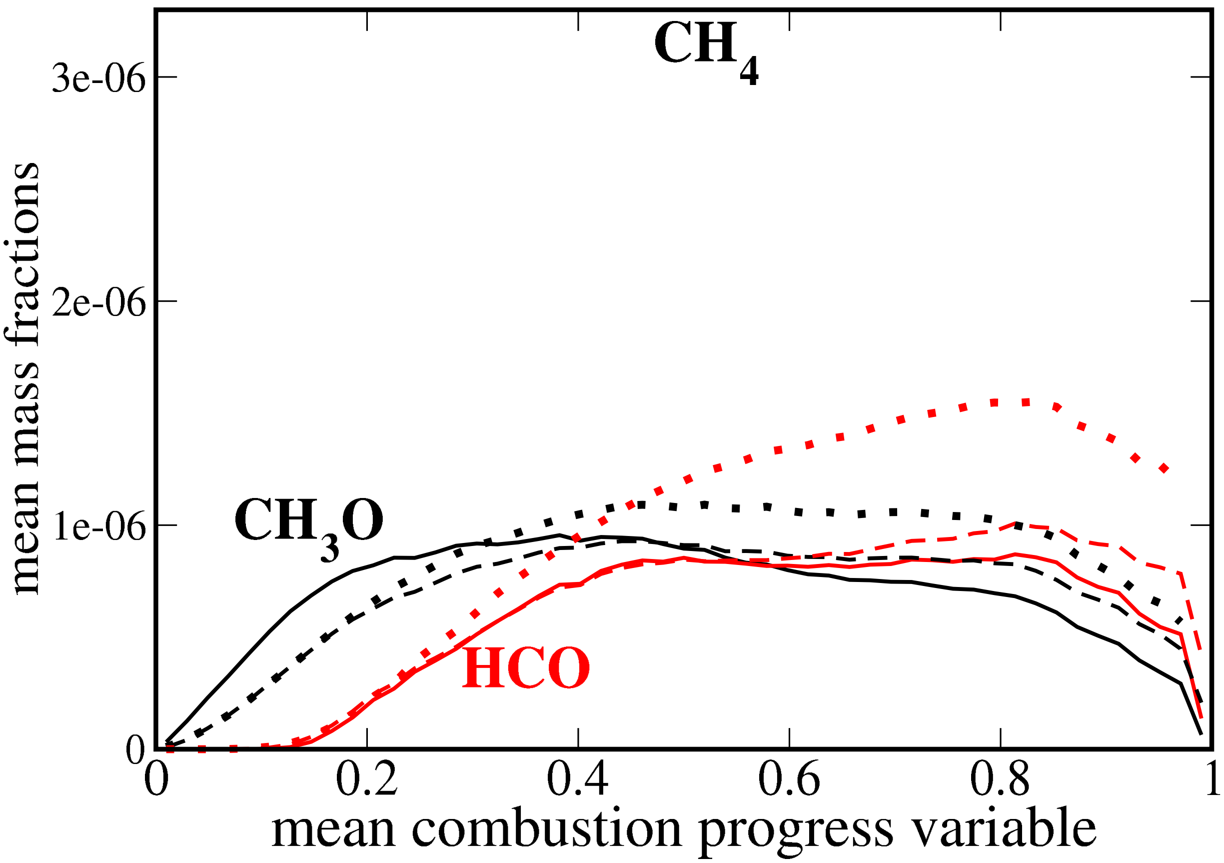
CH4
CH3O
HCO
3e-06
2e-06
1e-06
0
0.2
0.4
0.6
0.8
1
mean mass fractions
mean combustion progress variable

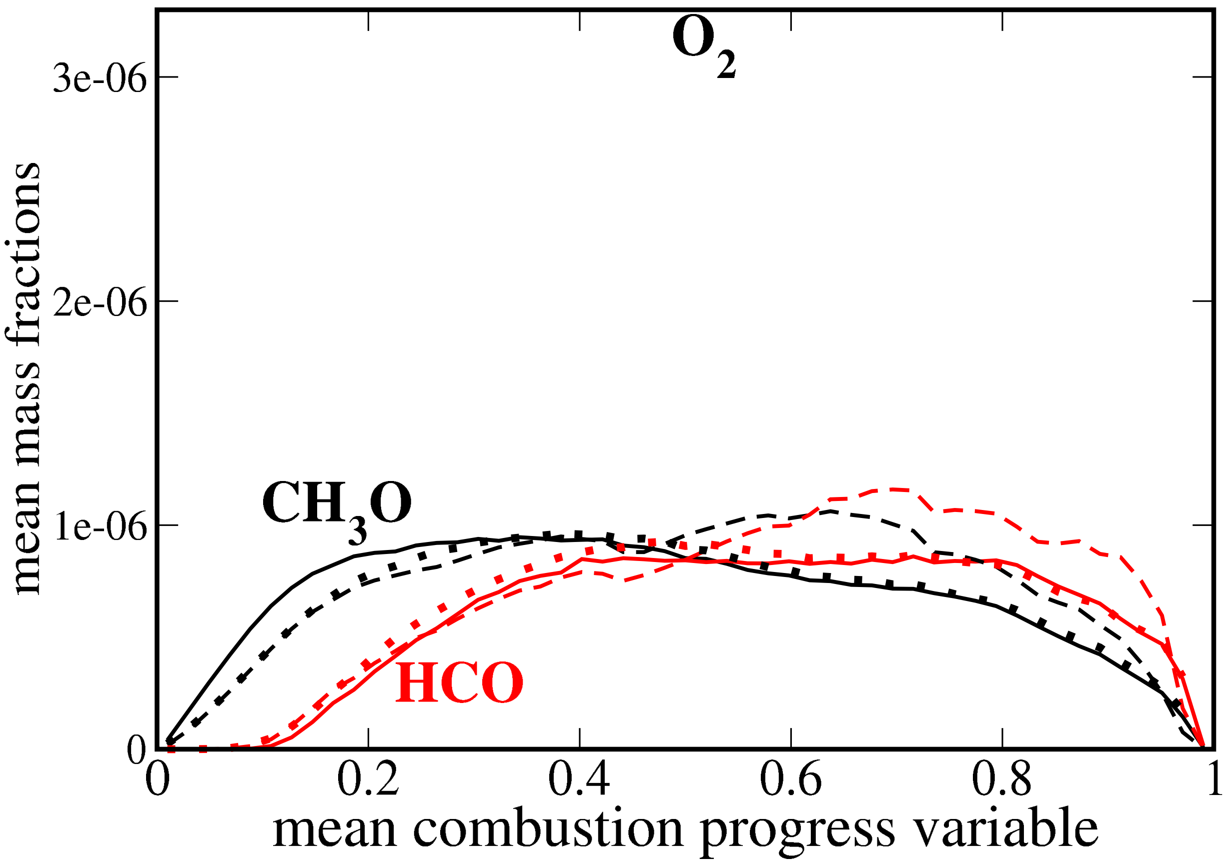
O2
3e-06
2e-06
1e-06
0
mean mass fractions
CH3O
HCO
0
0.2
0.4
0.6
0.8
1
mean combustion progress variable

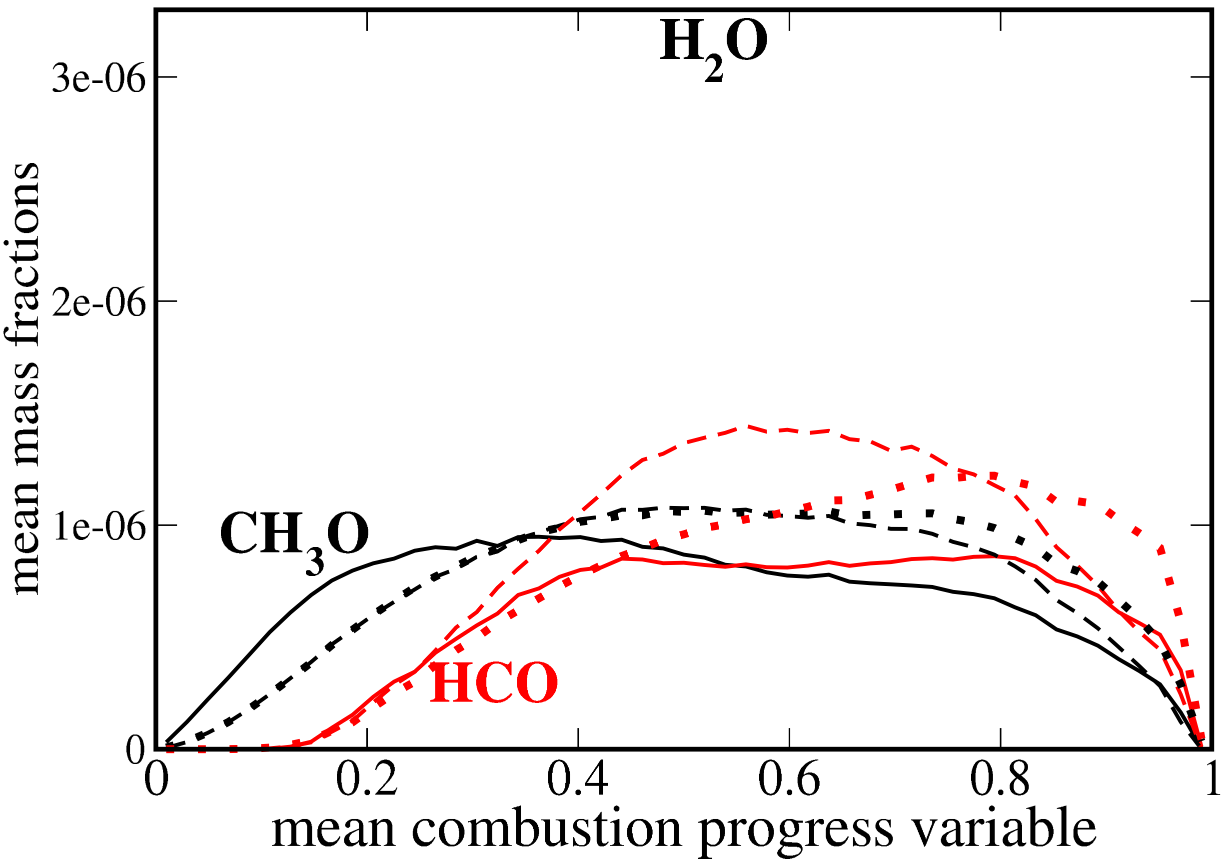
H2O
CH3O
HCO
3e-06
2e-06
1e-06
0
0
0.2
0.4
0.6
0.8
1
mean mass fractions
mean combustion progress variable

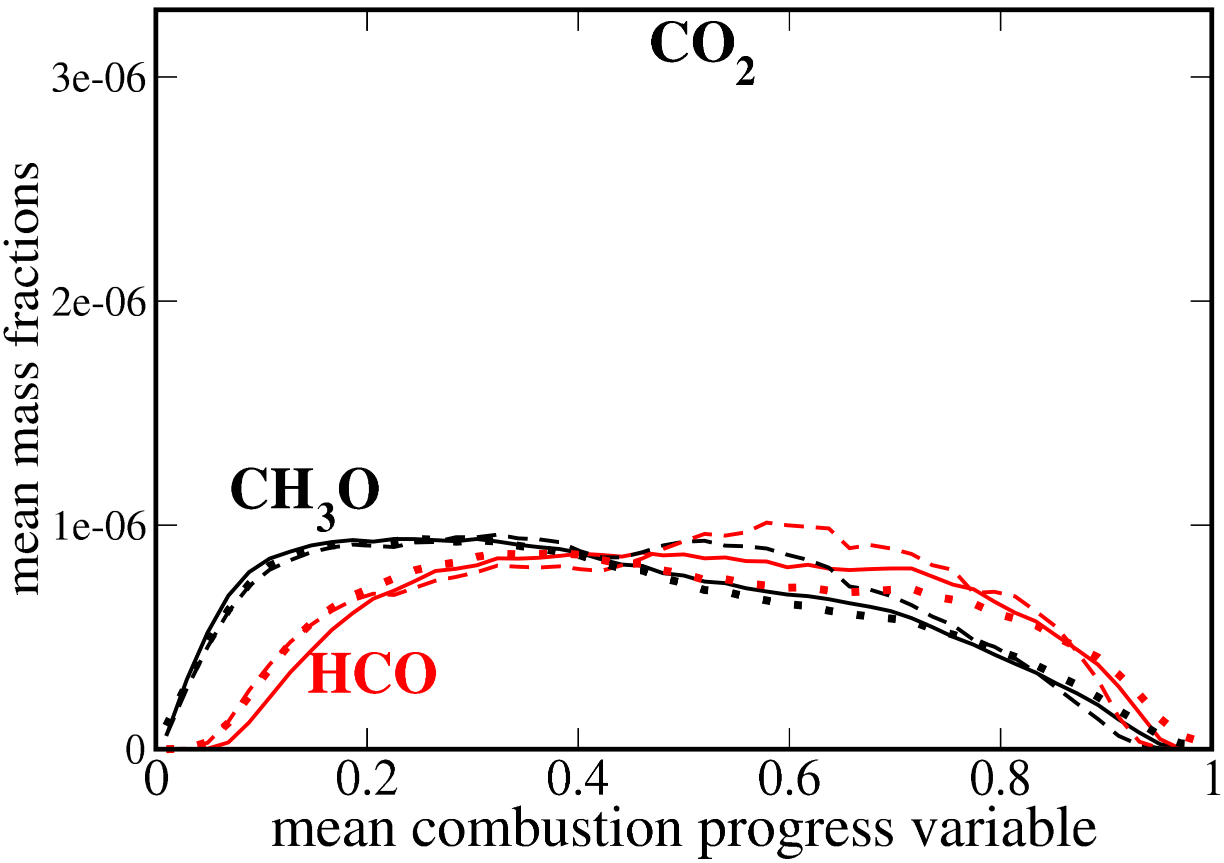
CO2
CH3O
HCO
mean mass fractions
3e-06
2e-06
1e-06
0
0.2
0.4
0.6
0.8
1
mean combustion progress variable

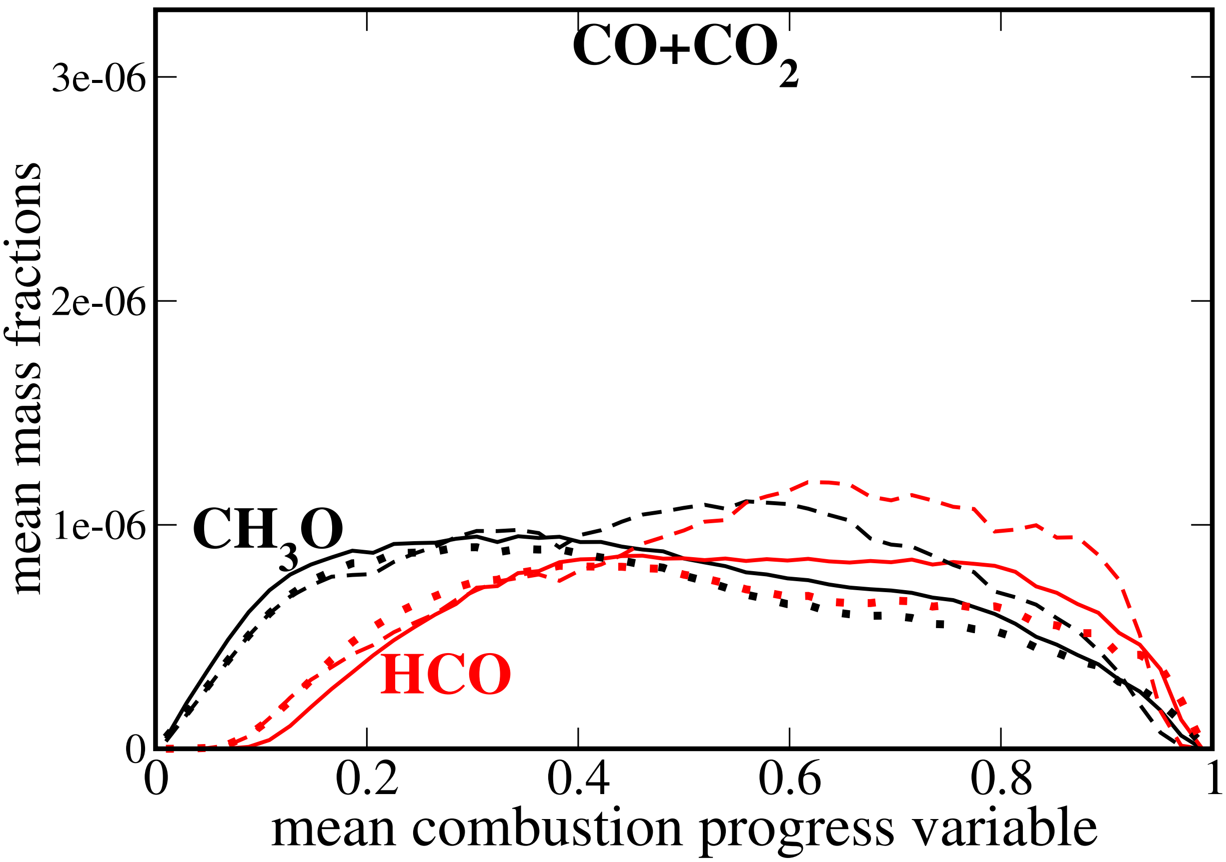
CO+CO2
CH3O
HCO
mean mass fractions
mean combustion progress variable
3e-06
2e-06
1e-06
0
0.2
0.4
0.6
0.8
1

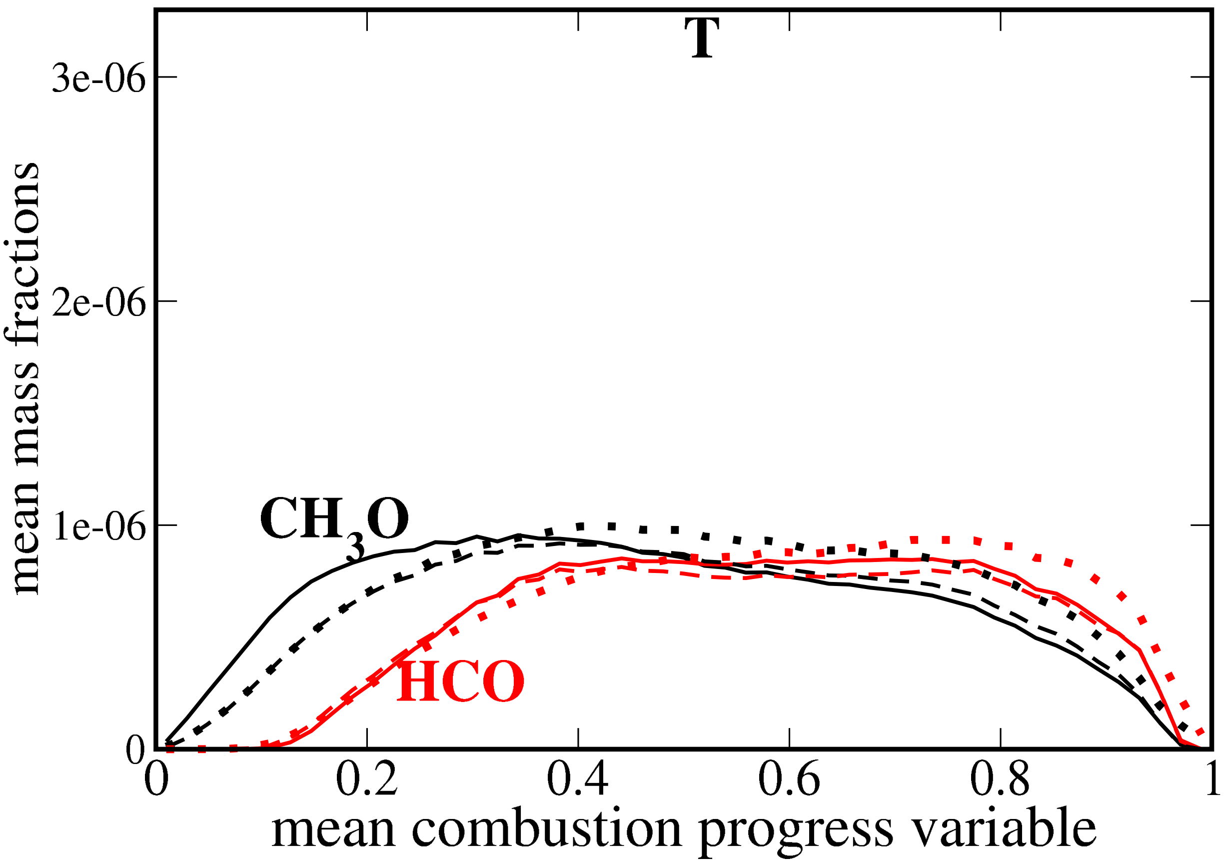
T
CH3O
HCO
mean mass fractions
mean combustion progress variable
3e-06
2e-06
1e-06
0
0
0.2
0.4
0.6
0.8
1

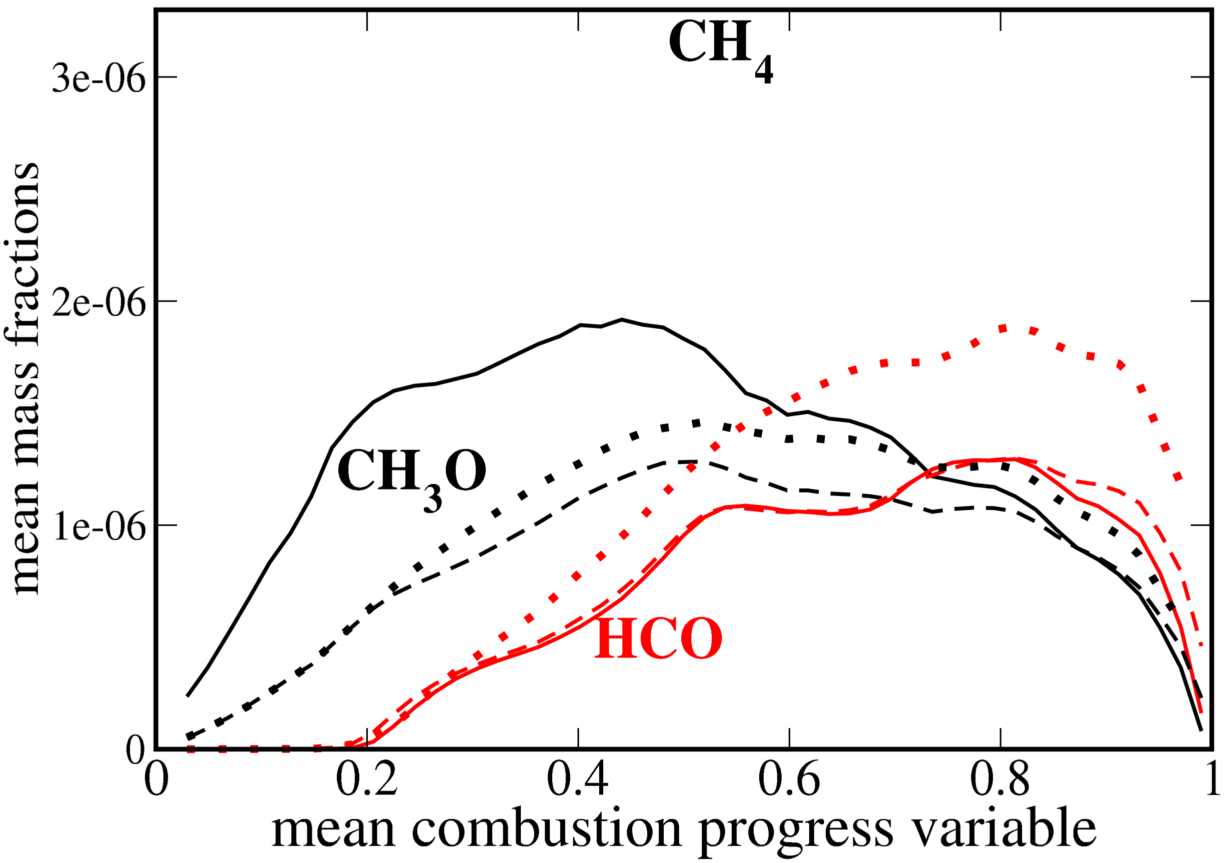
CH4
CH3O
HCO
3e-06
2e-06
1e-06
0
0.2
0.4
0.6
0.8
1
mean mass fractions
mean combustion progress variable

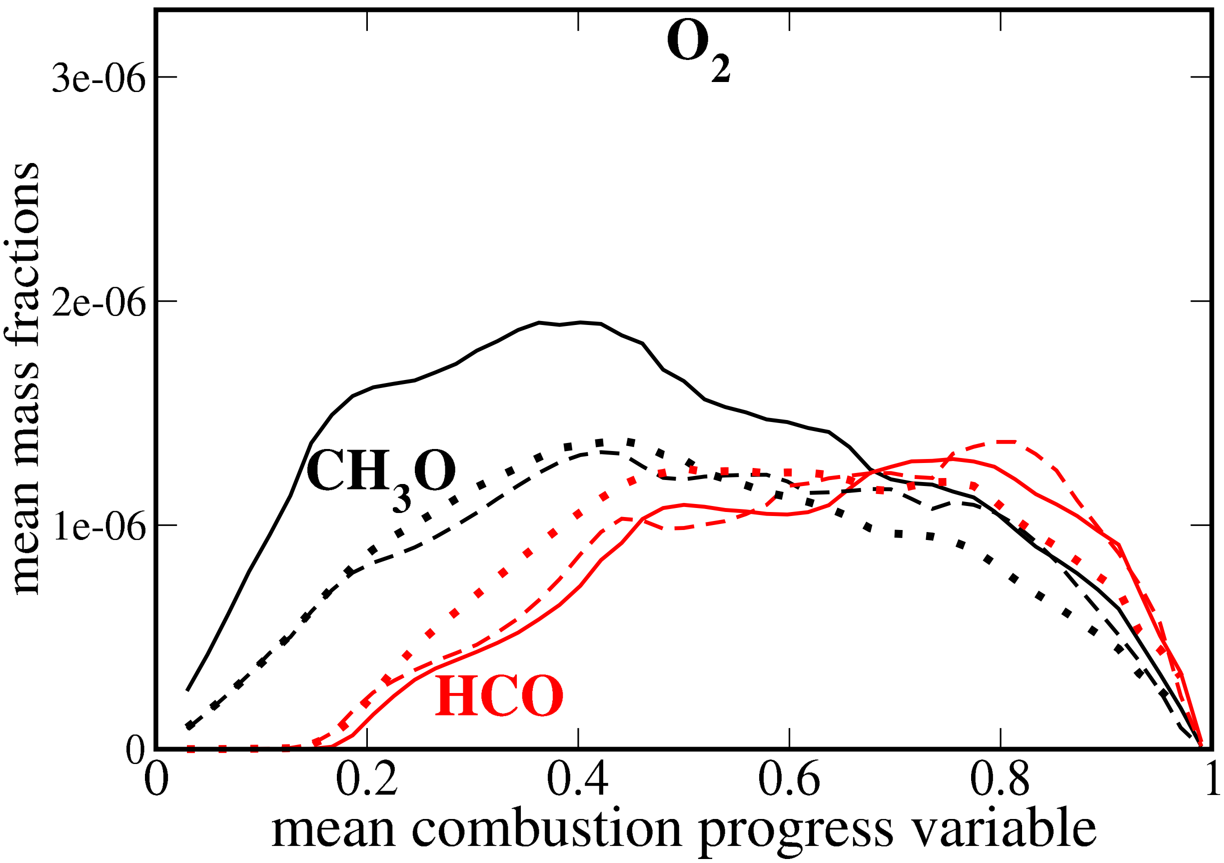
O2
CH3O
HCO
mean mass fractions
3e-06
2e-06
1e-06
0
0.2
0.4
0.6
0.8
1
mean combustion progress variable

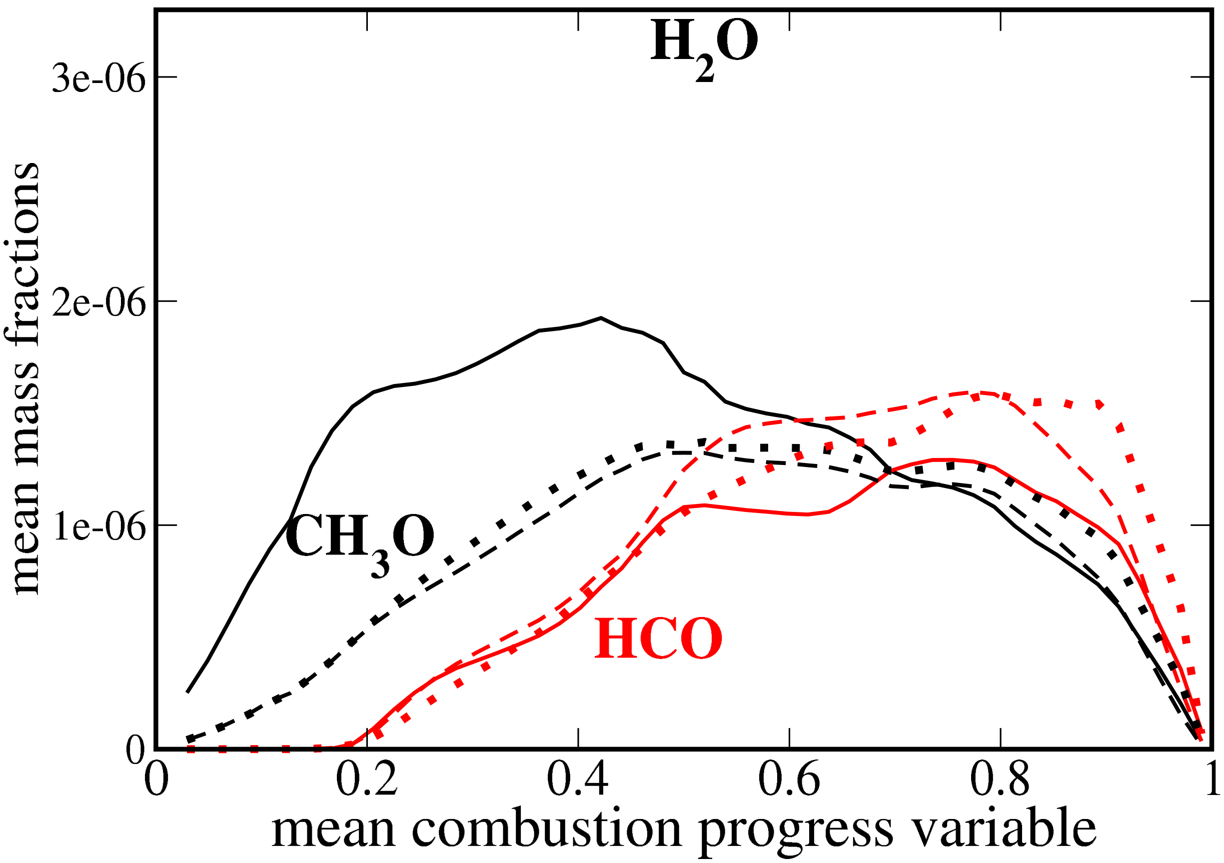
H_2O
CH_3O
HCO
3e-06
2e-06
1e-06
0
0
0.2
0.4
0.6
0.8
1
mean mass fractions
mean combustion progress variable

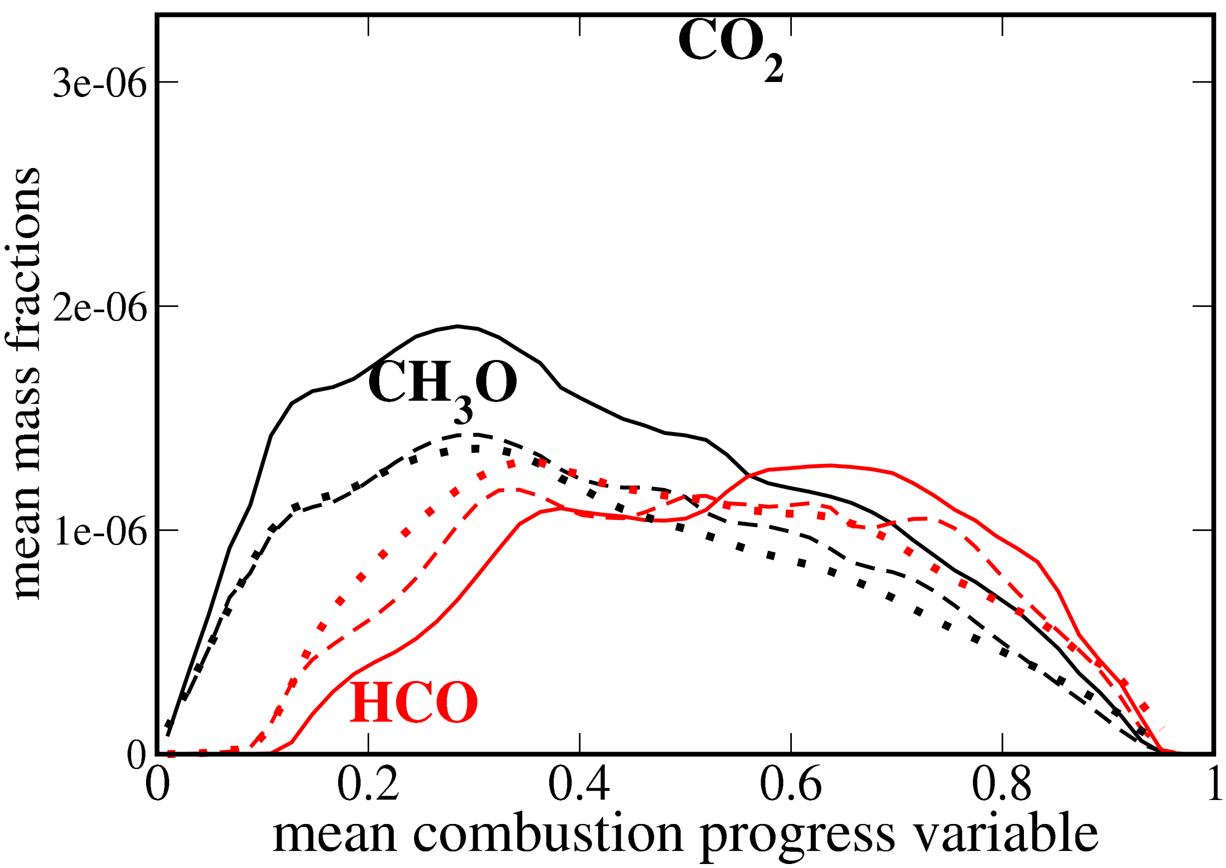
CO2
CH3O
HCO
3e-06
2e-06
1e-06
0
0.2
0.4
0.6
0.8
1
mean mass fractions
mean combustion progress variable

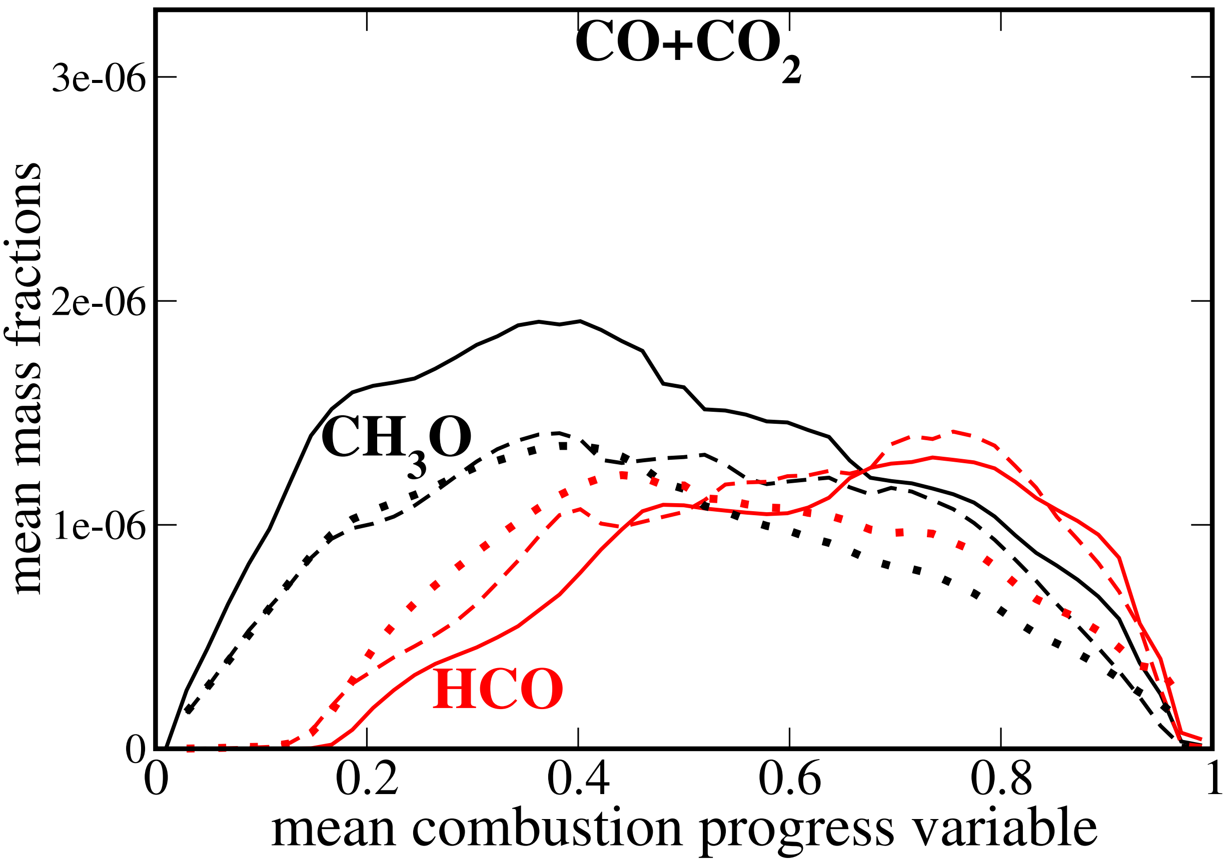
CO+CO2
CH3O
HCO
mean mass fractions
3e-06
2e-06
1e-06
0
0.2
0.4
0.6
0.8
1
mean combustion progress variable

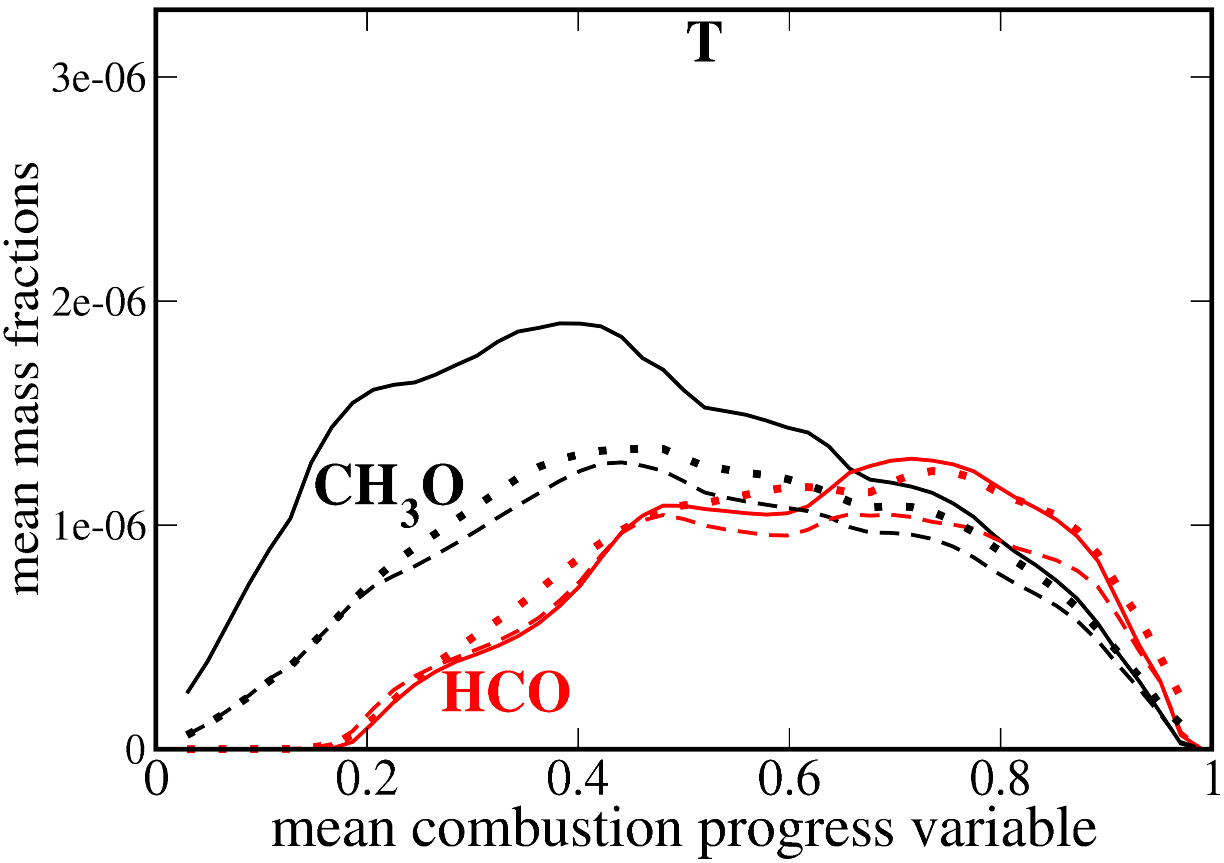
T
CH3O
HCO
mean mass fractions
mean combustion progress variable
3e-06
2e-06
1e-06
0
0
0.2
0.4
0.6
0.8
1

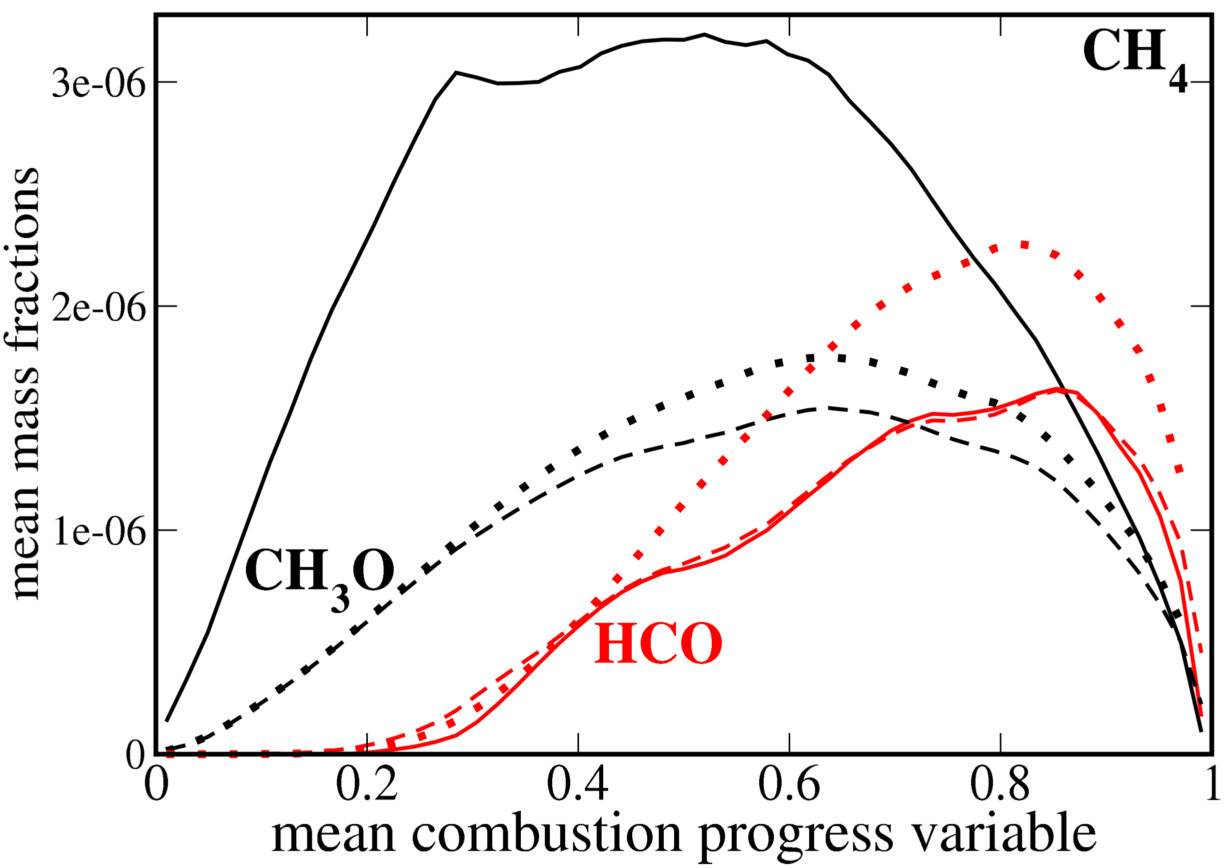
CH4
CH3O
HCO
3e-06
2e-06
1e-06
0
0.2
0.4
0.6
0.8
1
mean mass fractions
mean combustion progress variable

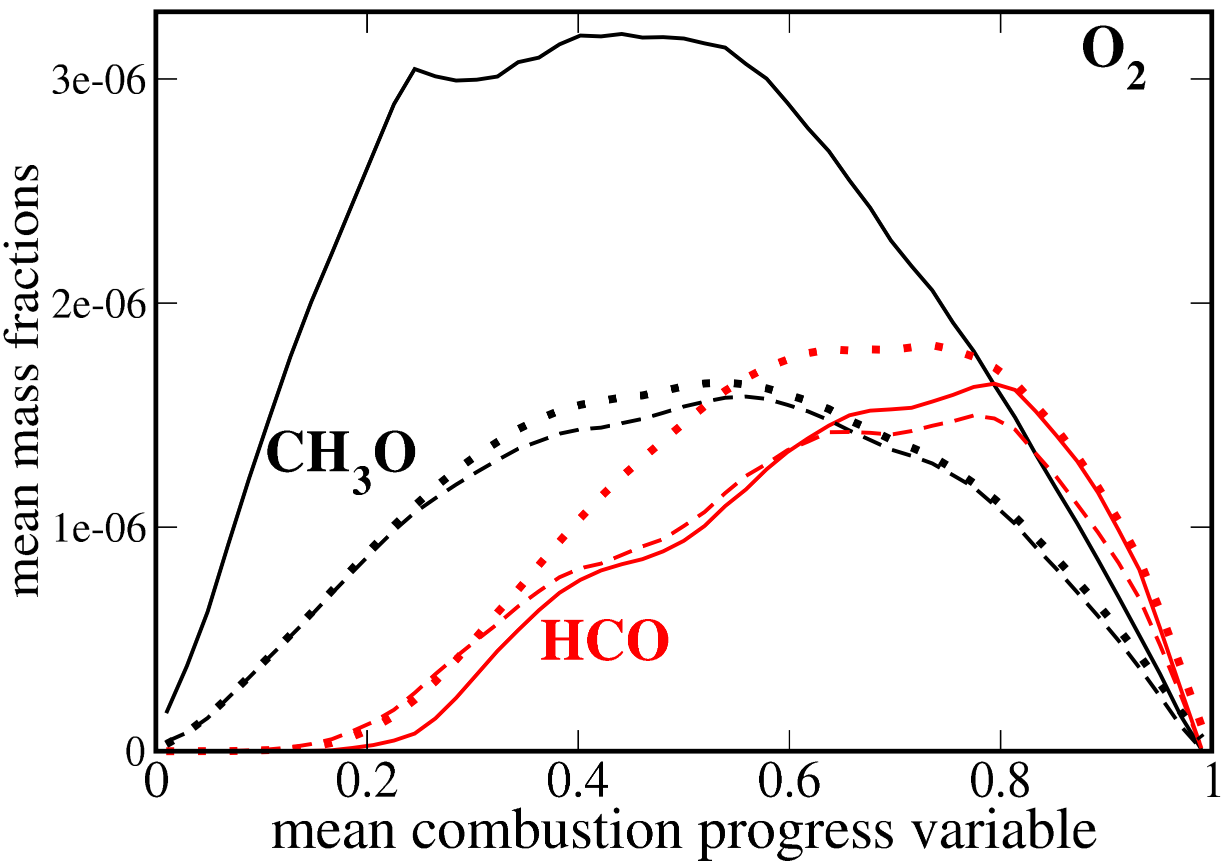
O2
CH3O
HCO
3e-06
2e-06
1e-06
0
0.2
0.4
0.6
0.8
1
mean mass fractions
mean combustion progress variable

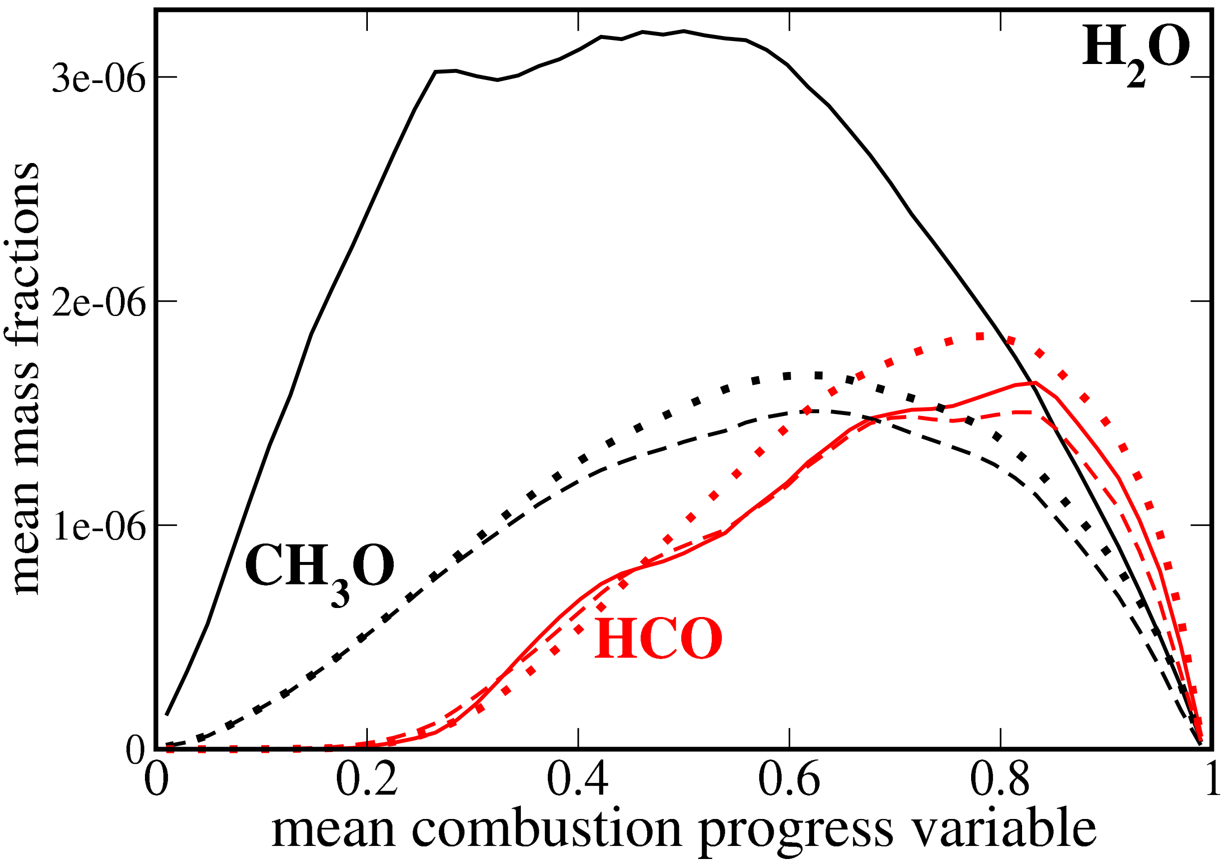
H$_2$O
CH$_3$O
HCO
3e-06
2e-06
1e-06
0
0.2
0.4
0.6
0.8
1
mean mass fractions
mean combustion progress variable

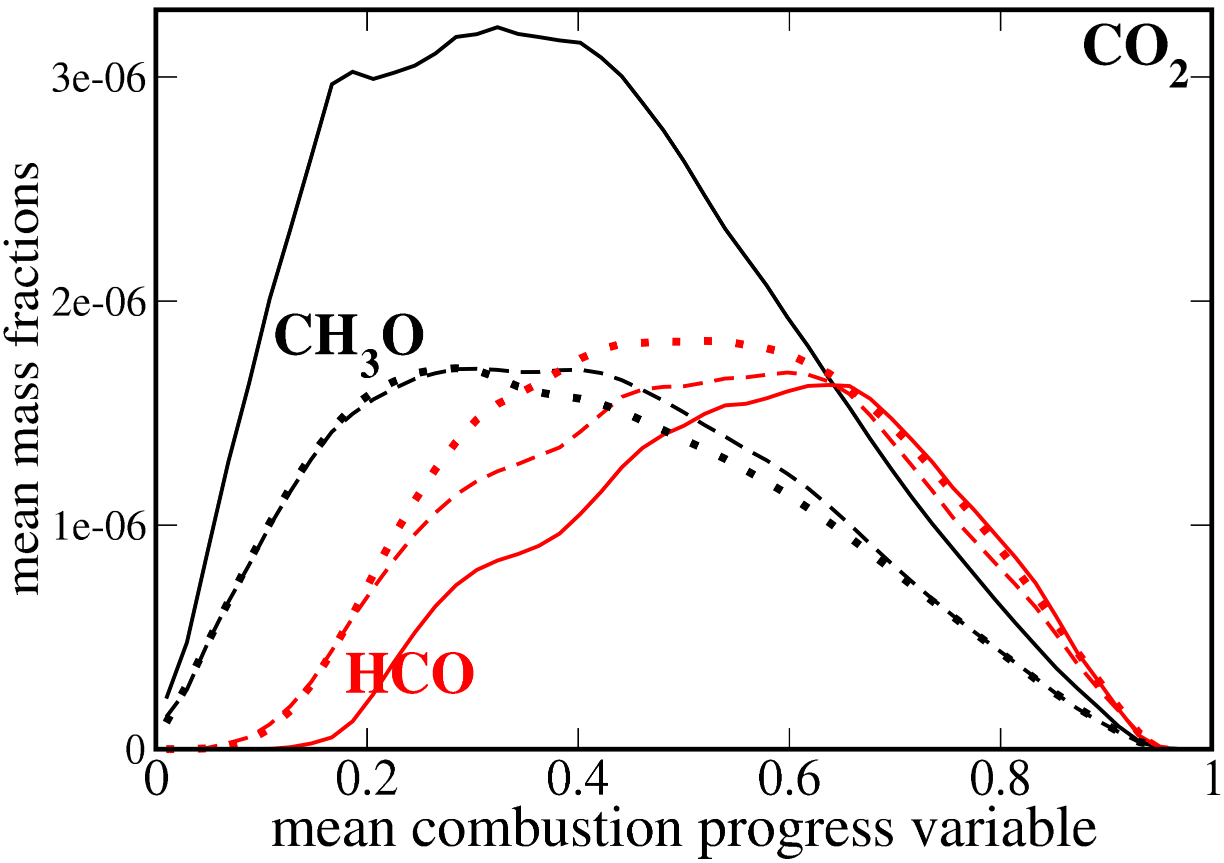
CO2
CH3O
HCO
3e-06
2e-06
1e-06
0
0
0.2
0.4
0.6
0.8
1
mean mass fractions
mean combustion progress variable

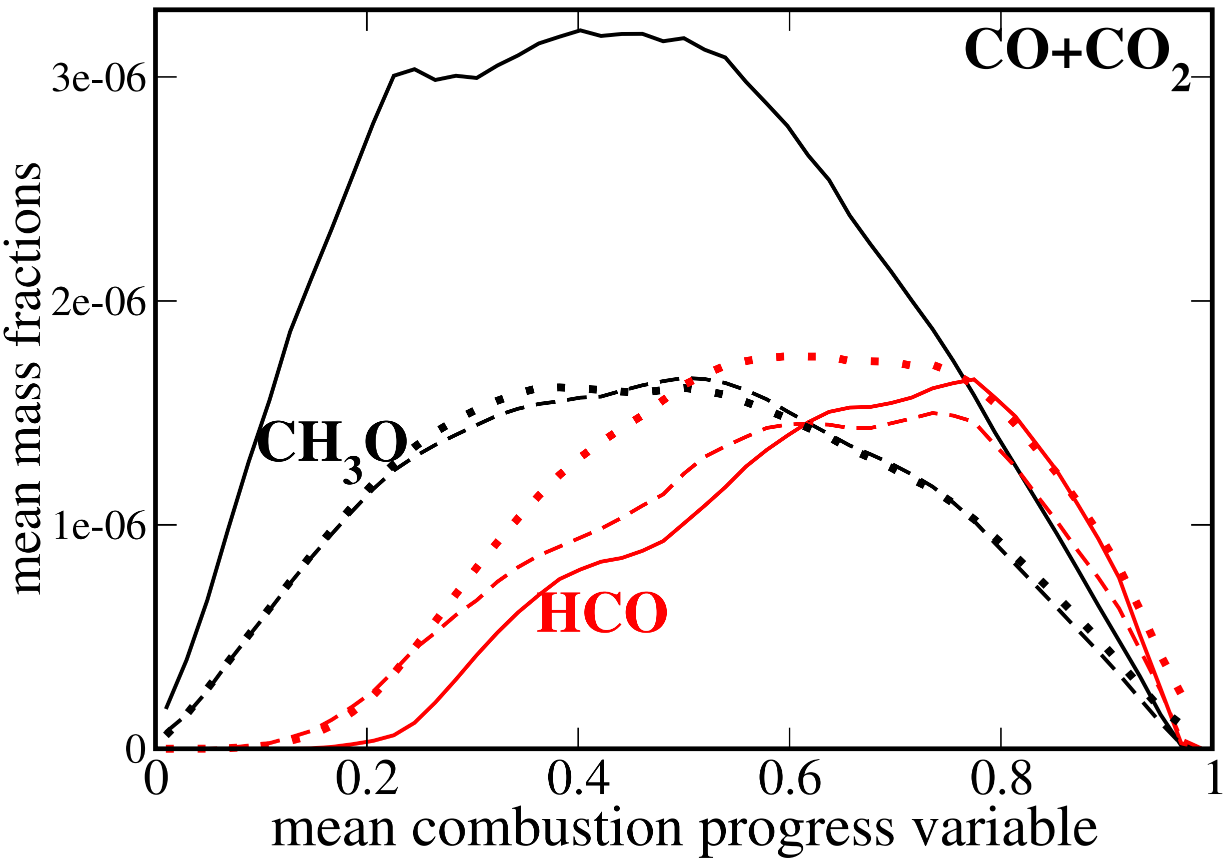
CO+CO2
CH3O
HCO
3e-06
2e-06
1e-06
0
0
0.2
0.4
0.6
0.8
1
mean mass fractions
mean combustion progress variable

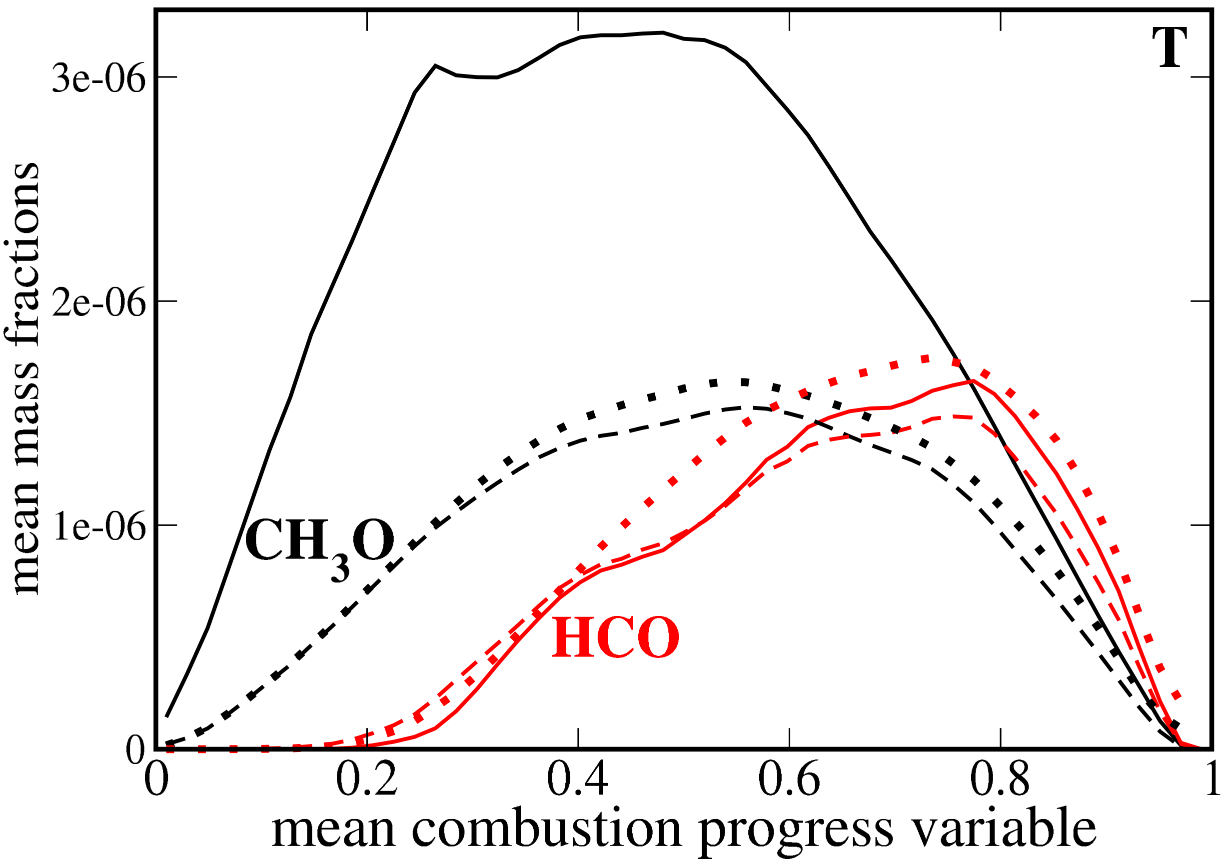
T
3e-06
2e-06
1e-06
0
mean mass fractions
CH3O
HCO
0
0.2
0.4
0.6
0.8
1
mean combustion progress variable

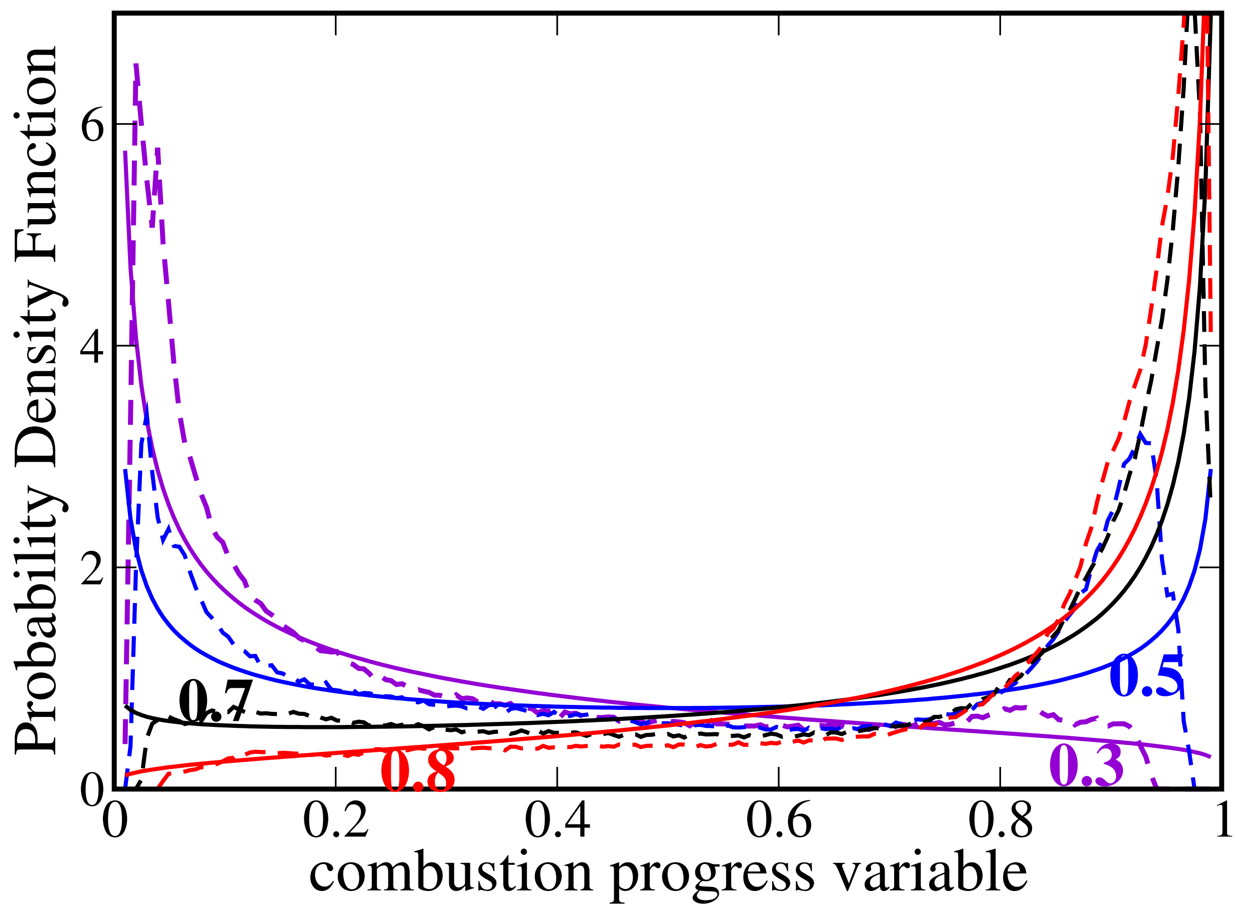
Probability Density Function
combustion progress variable
0
2
4
6
0
0.2
0.4
0.6
0.8
1
0.7
0.8
0.5
0.3

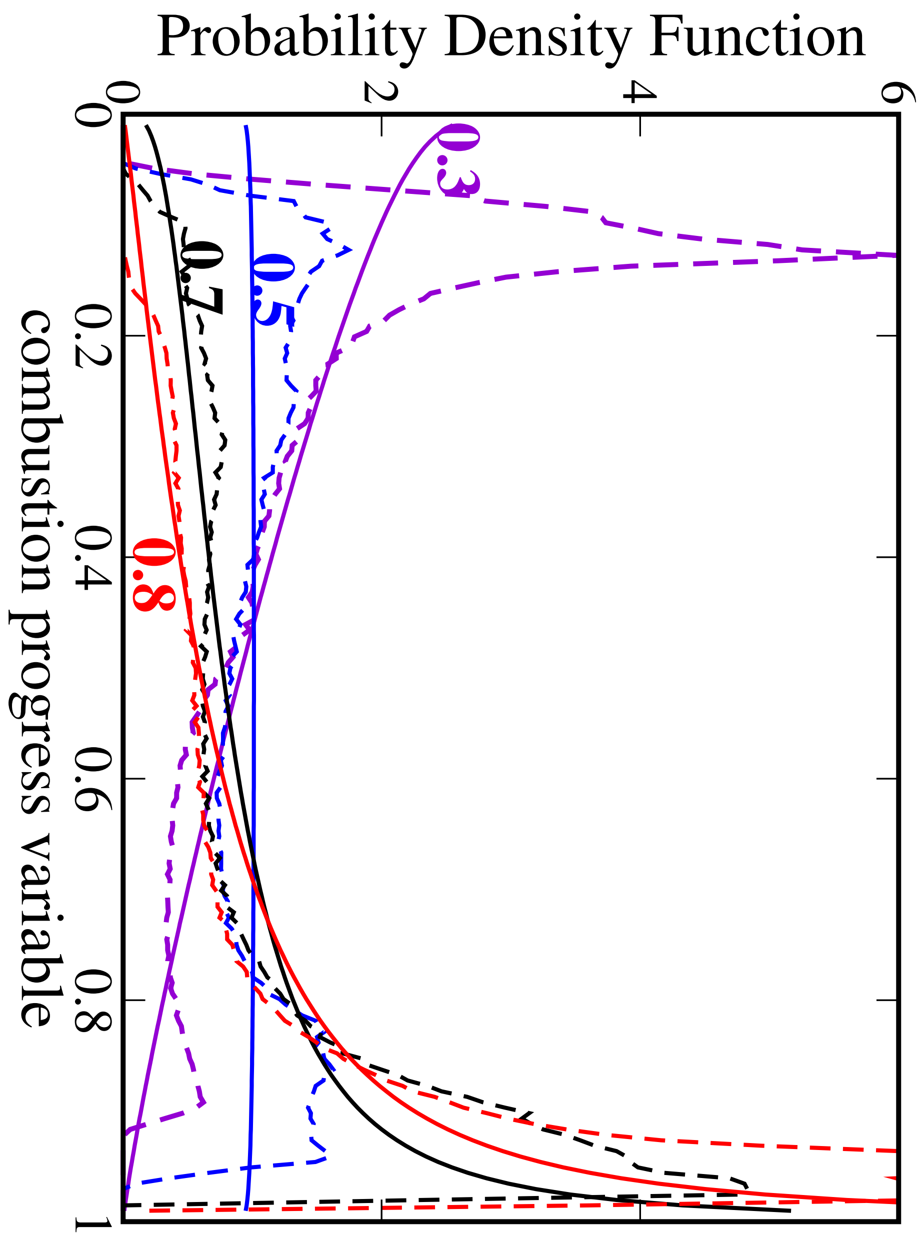
Probability Density Function
combustion progress variable
0
2
4
6
0
0.2
0.4
0.6
0.8
1
0.3
0.5
0.7
0.8

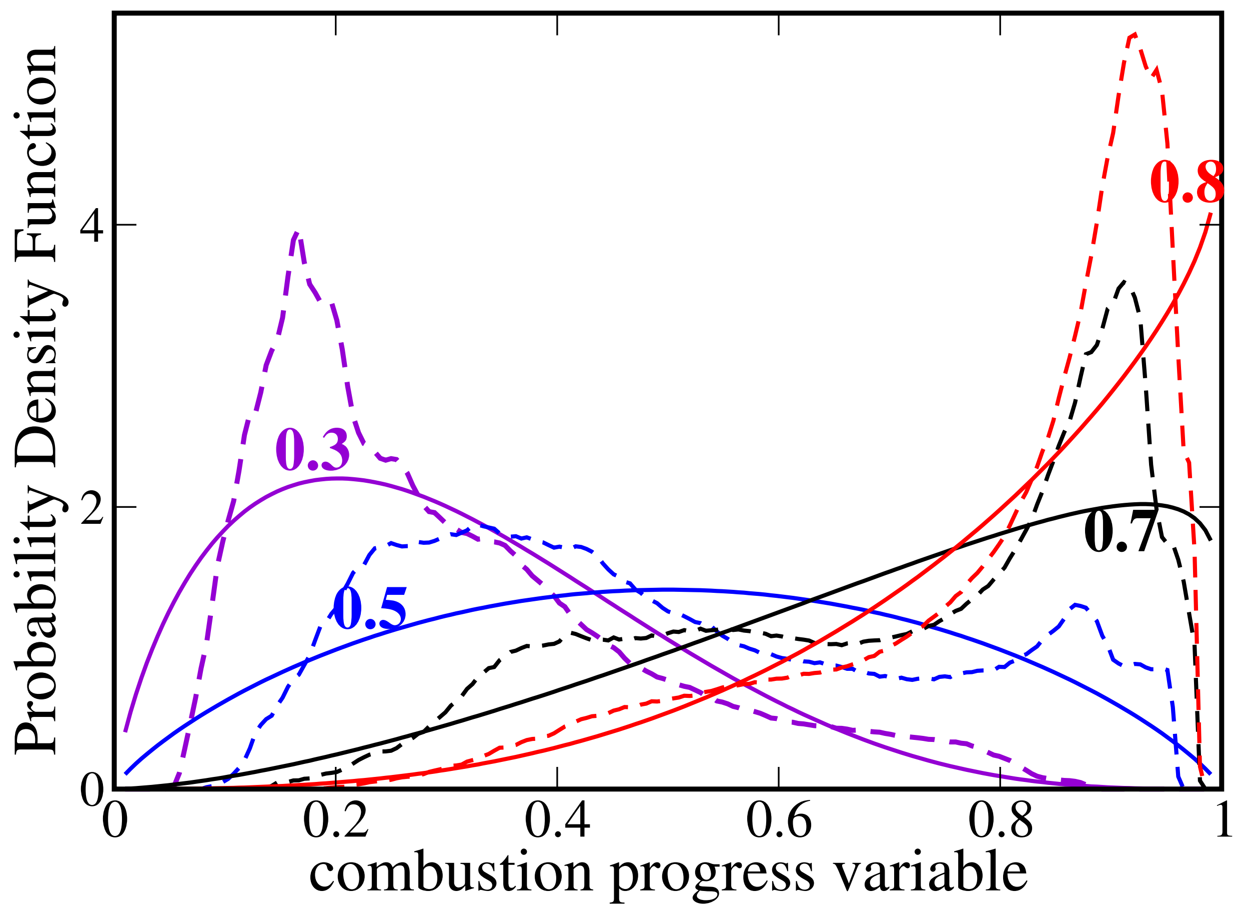
Probability Density Function
combustion progress variable
0
2
4
0
0.2
0.4
0.6
0.8
1
0.3
0.5
0.7
0.8

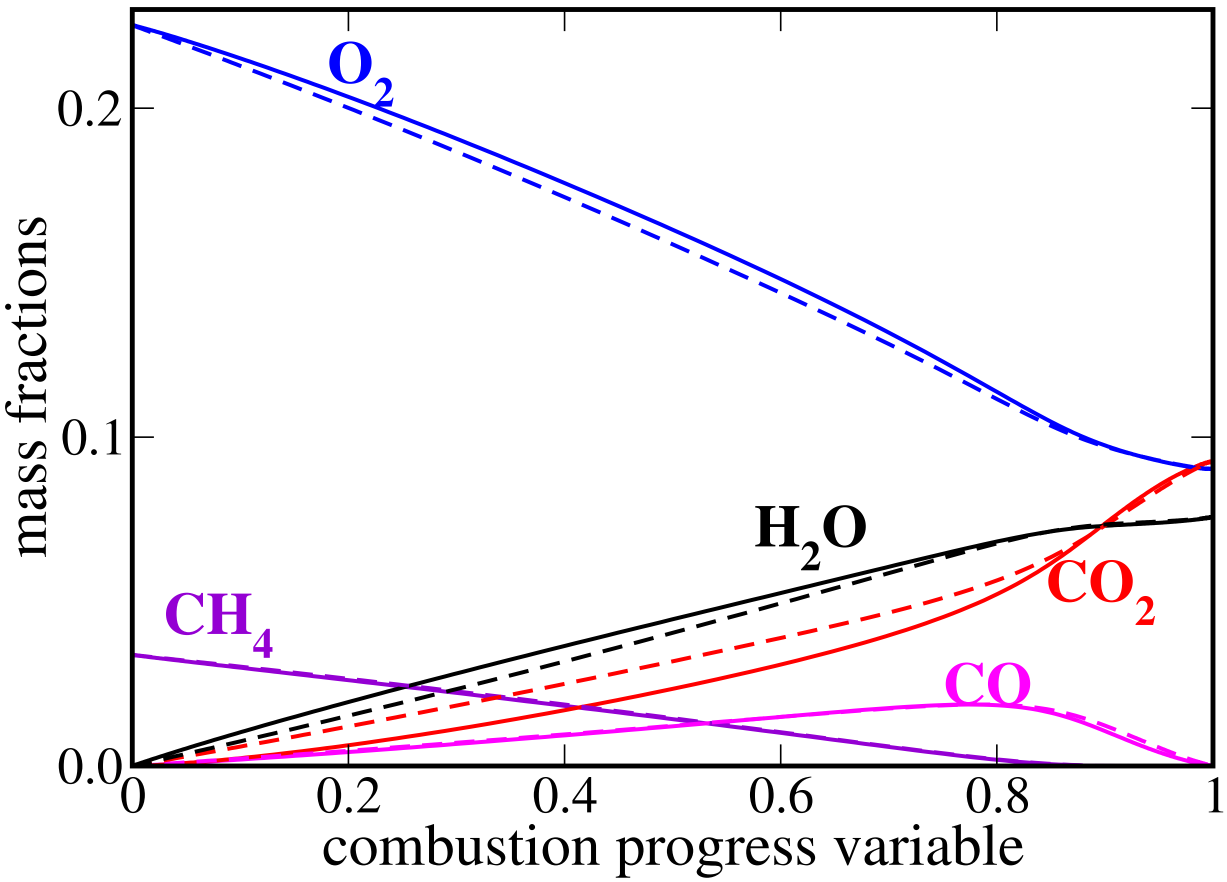
mass fractions
combustion progress variable
0.0
0.1
0.2
0
0.2
0.4
0.6
0.8
1
O2
H2O
CO2
CH4
CO

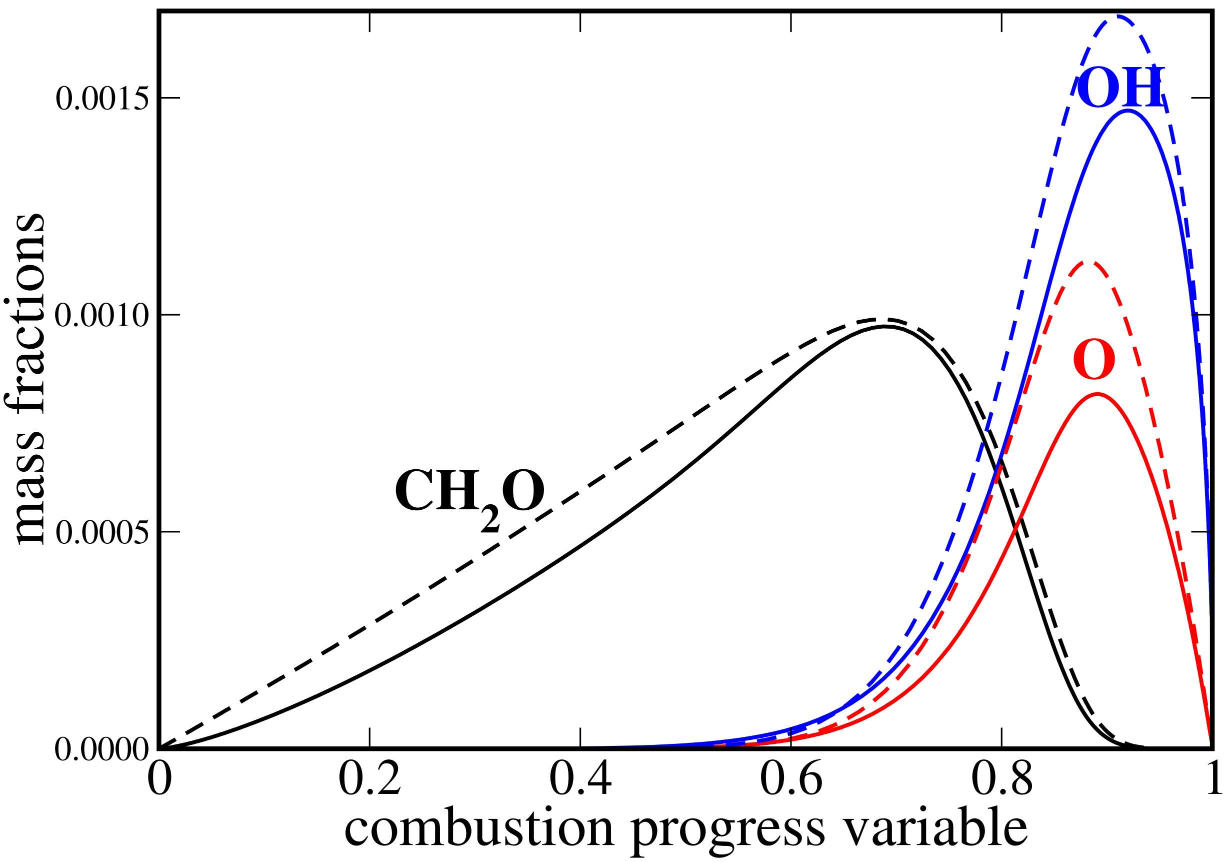
OH
O
CH_2O
mass fractions
0.0000
0.0005
0.0010
0.0015
0
0.2
0.4
0.6
0.8
1
combustion progress variable

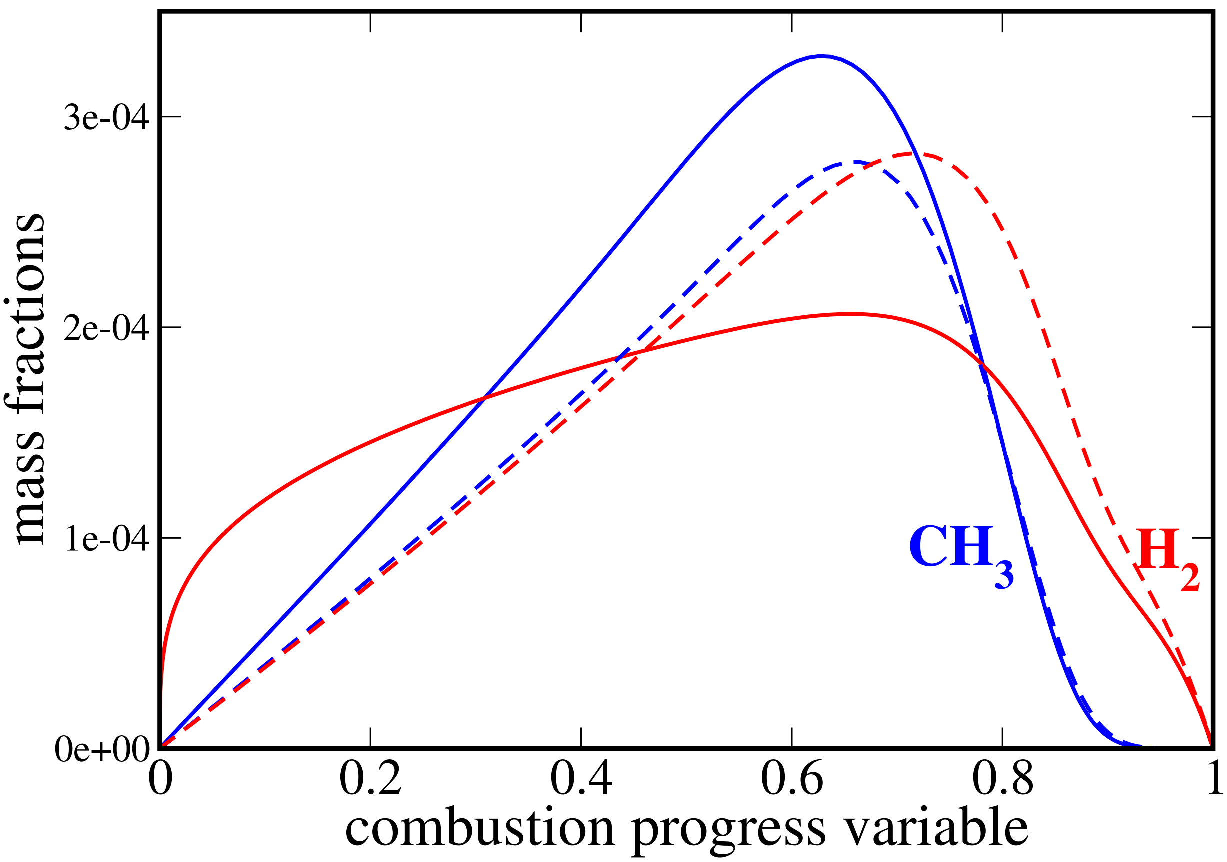
mass fractions
3e-04
2e-04
1e-04
0e+00
0
0.2
0.4
0.6
0.8
1
combustion progress variable
CH_3
H_2

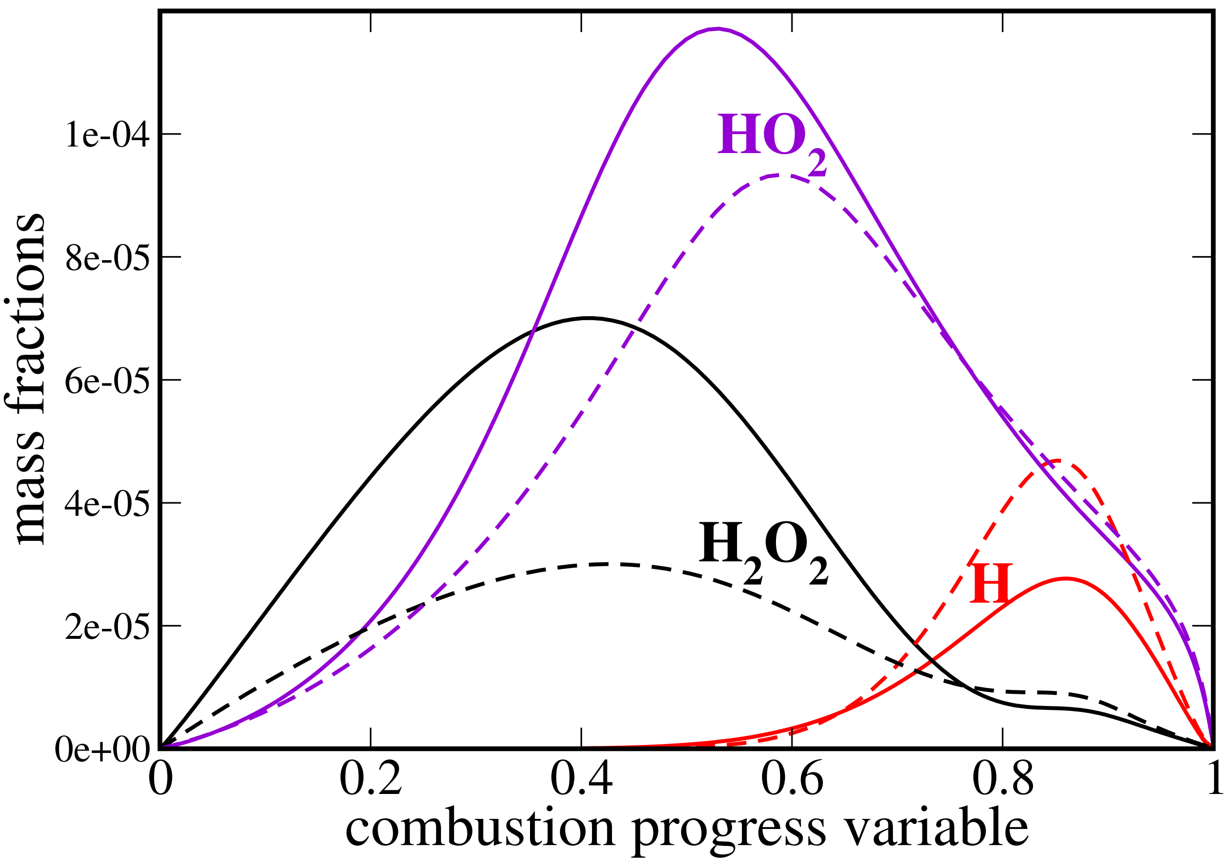
mass fractions
1e-04
8e-05
6e-05
4e-05
2e-05
0e+00
0
0.2
0.4
0.6
0.8
1
combustion progress variable
HO_2
H_2O_2
H

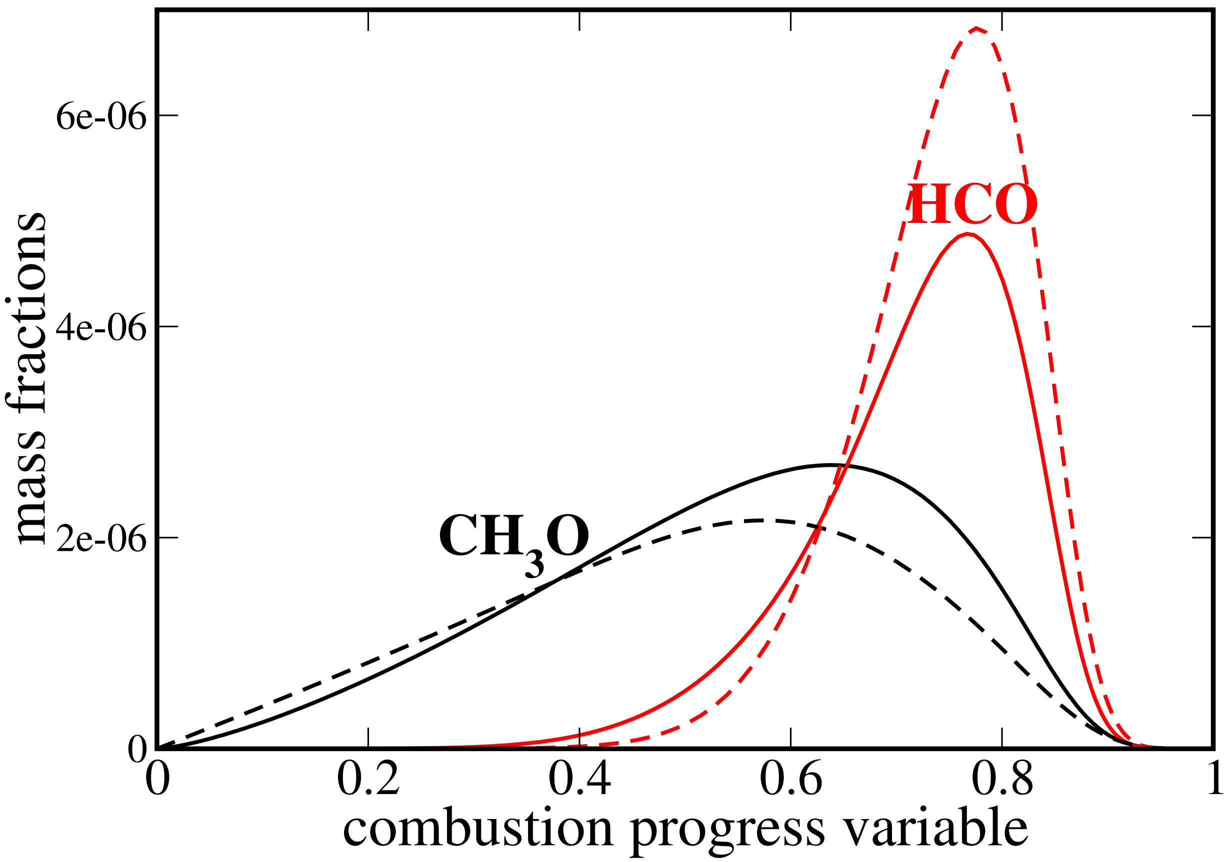
mass fractions
6e-06
4e-06
2e-06
0
0
0.2
0.4
0.6
0.8
1
combustion progress variable
HCO
CH_3O

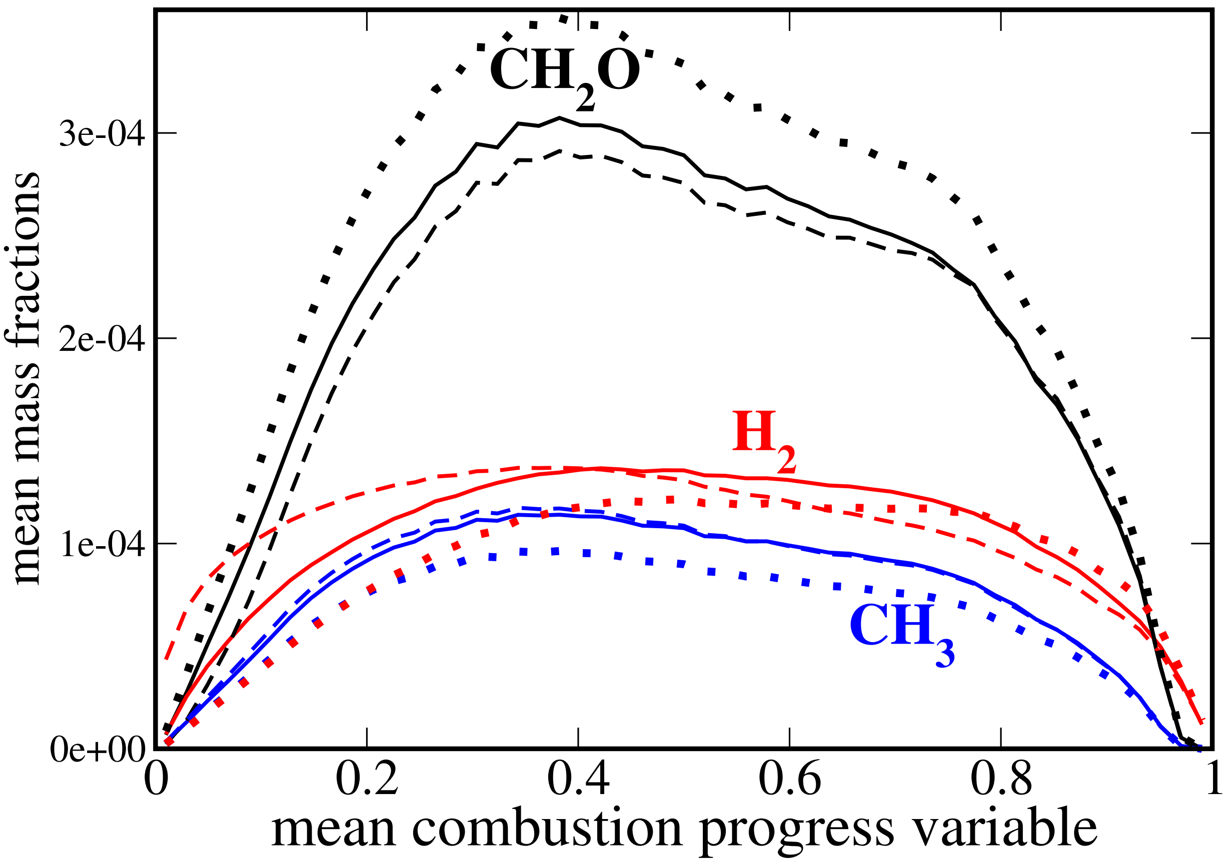
CH$_2$O
H$_2$
CH$_3$
mean mass fractions
3e-04
2e-04
1e-04
0e+00
0
0.2
0.4
0.6
0.8
1
mean combustion progress variable

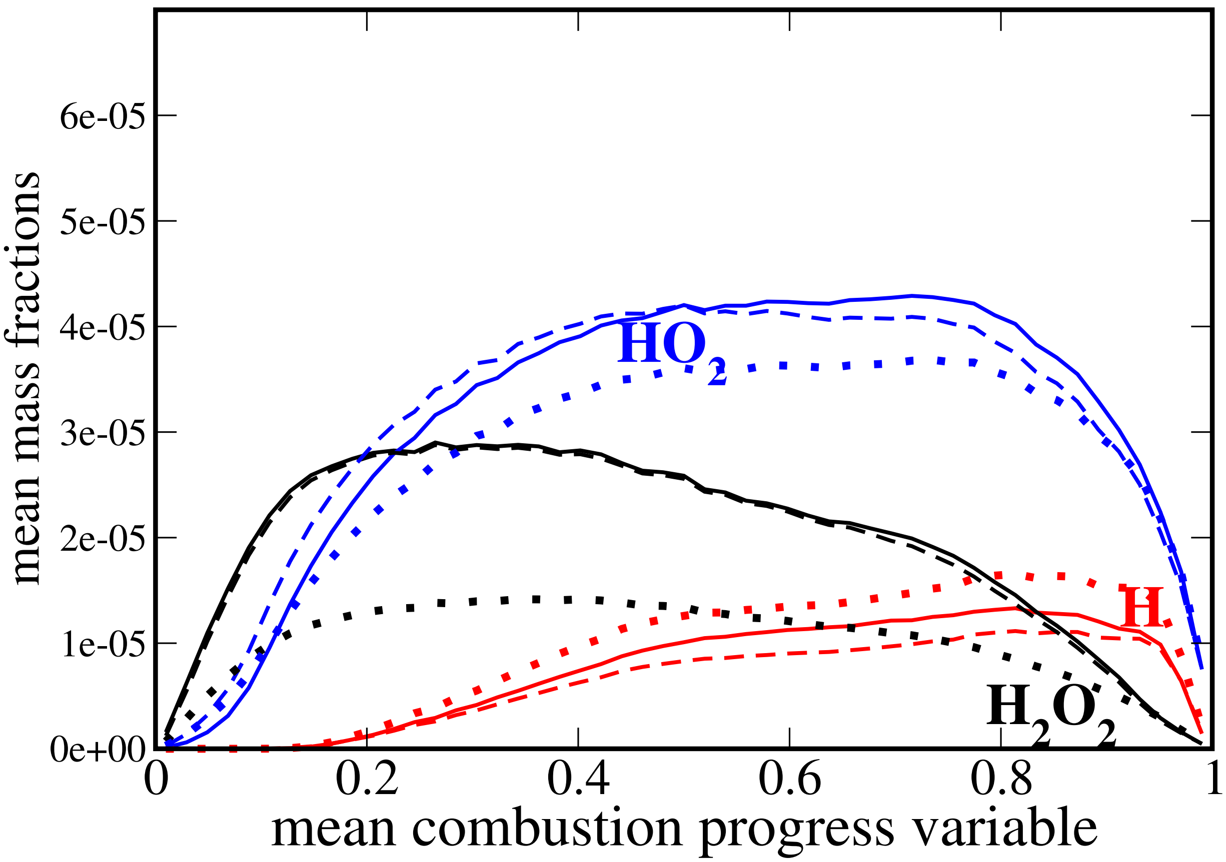
mean mass fractions
6e-05
5e-05
4e-05
3e-05
2e-05
1e-05
0e+00
0
0.2
0.4
0.6
0.8
1
mean combustion progress variable
HO2
H
H2O2

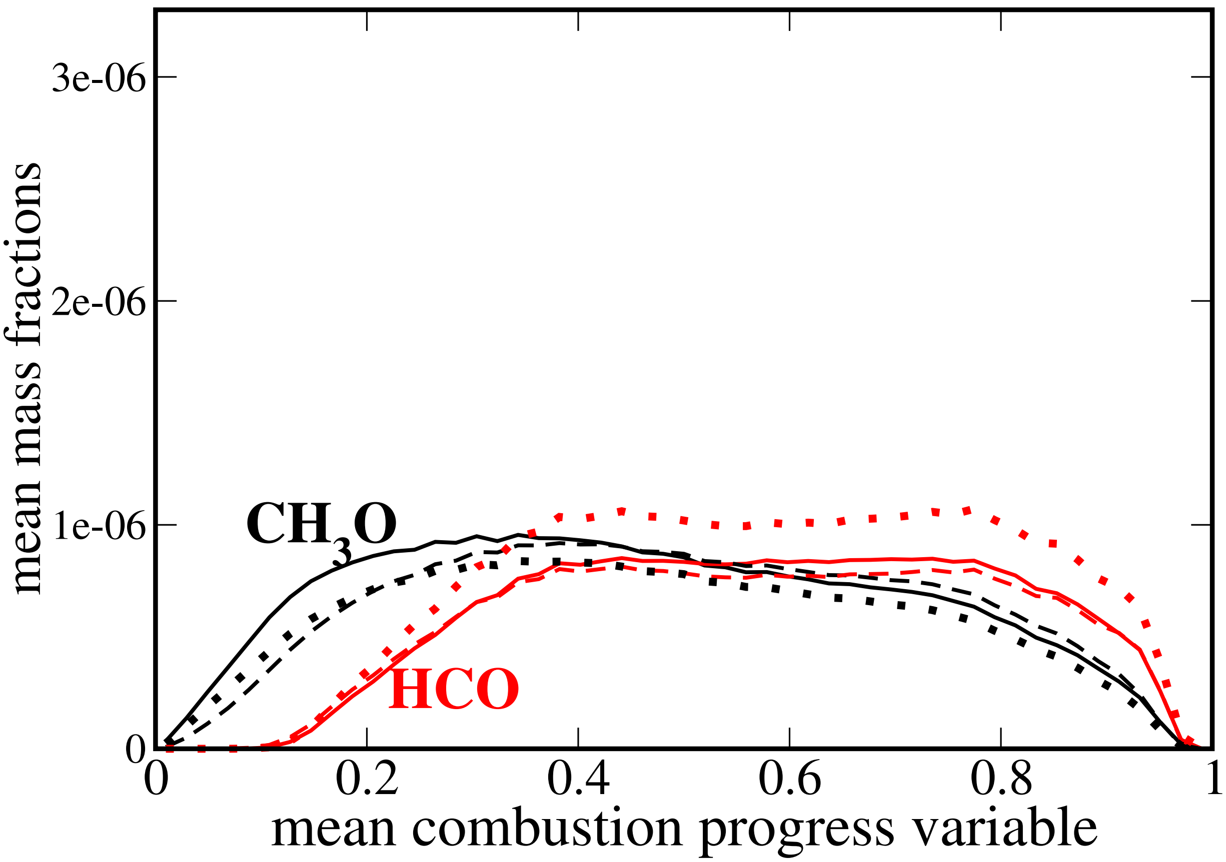
mean mass fractions
3e-06
2e-06
1e-06
0
0
0.2
0.4
0.6
0.8
1
mean combustion progress variable
CH_3O
HCO

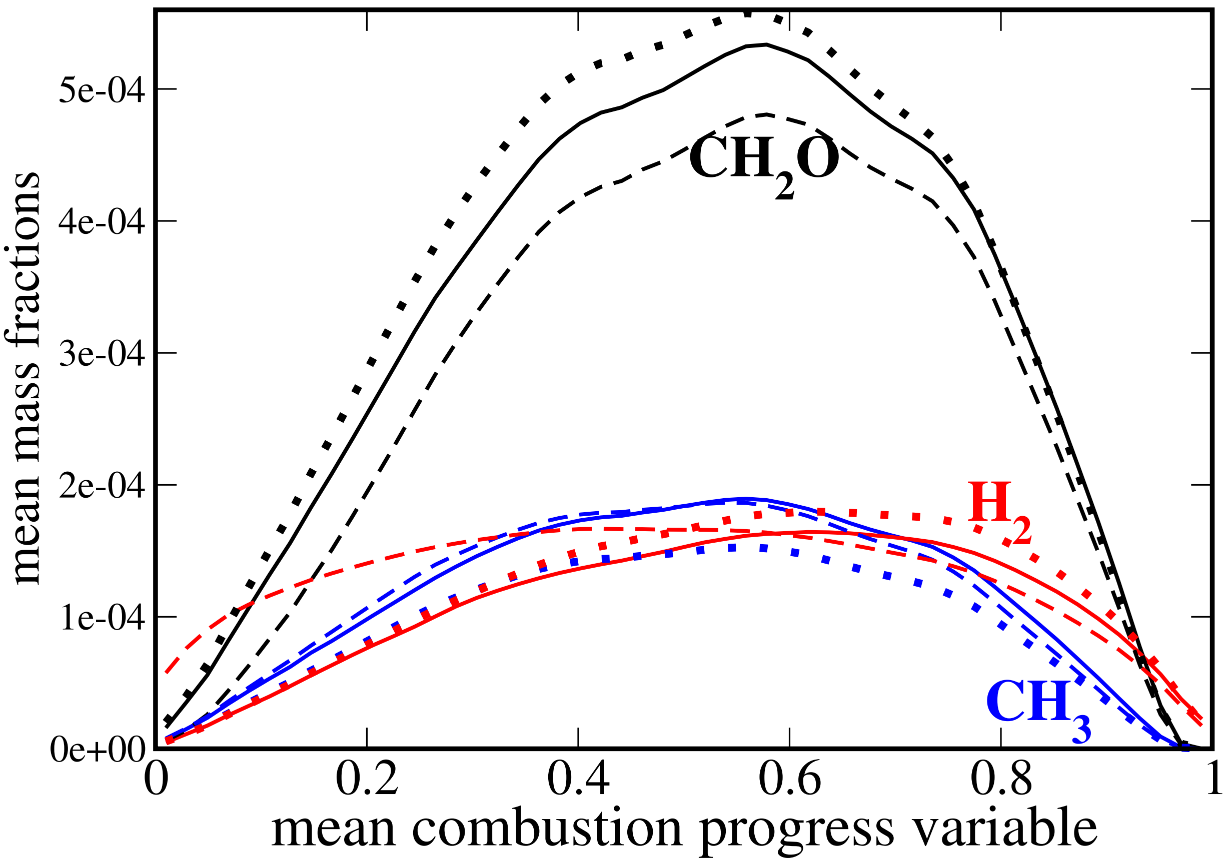
mean mass fractions
mean combustion progress variable
0e+00
1e-04
2e-04
3e-04
4e-04
5e-04
0
0.2
0.4
0.6
0.8
1
CH_2O
H_2
CH_3

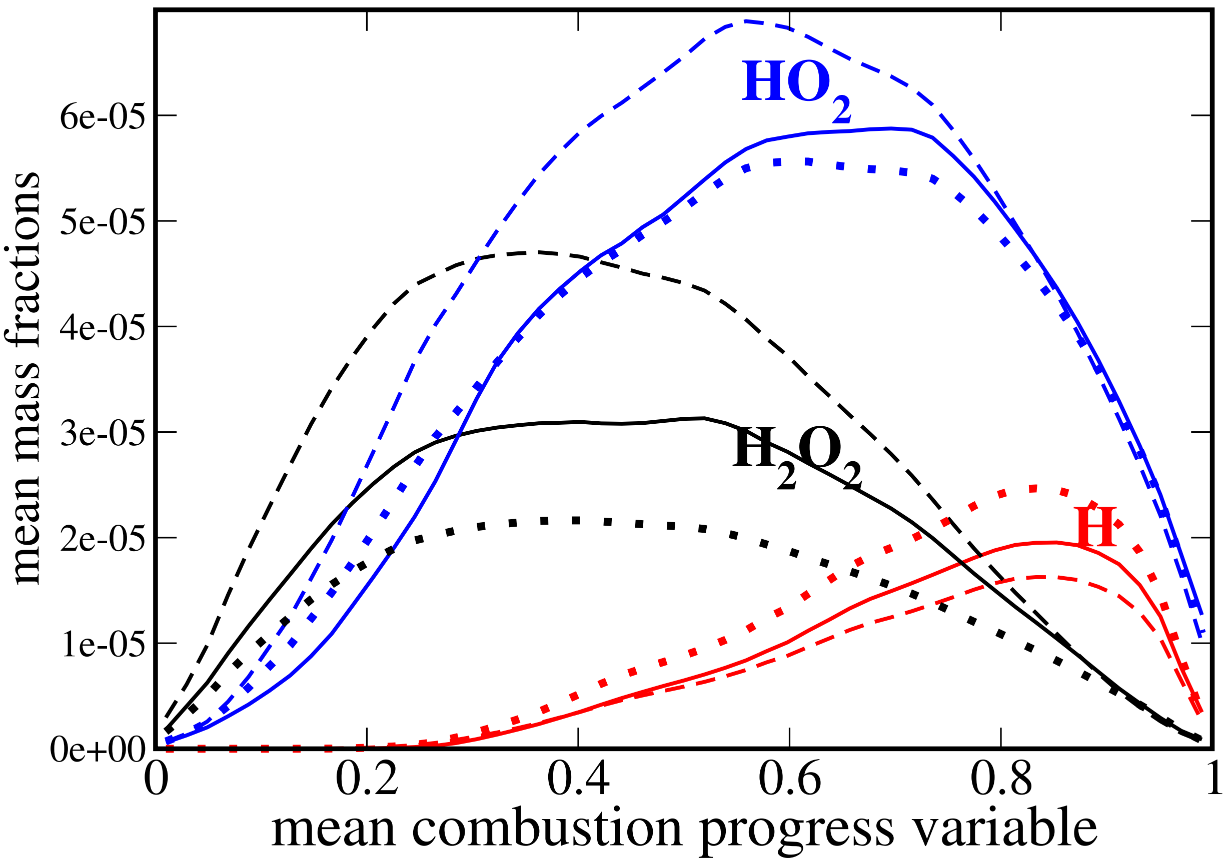
HO$_2$
H$_2$O$_2$
H
mean mass fractions
mean combustion progress variable
0e+00
1e-05
2e-05
3e-05
4e-05
5e-05
6e-05
0
0.2
0.4
0.6
0.8
1

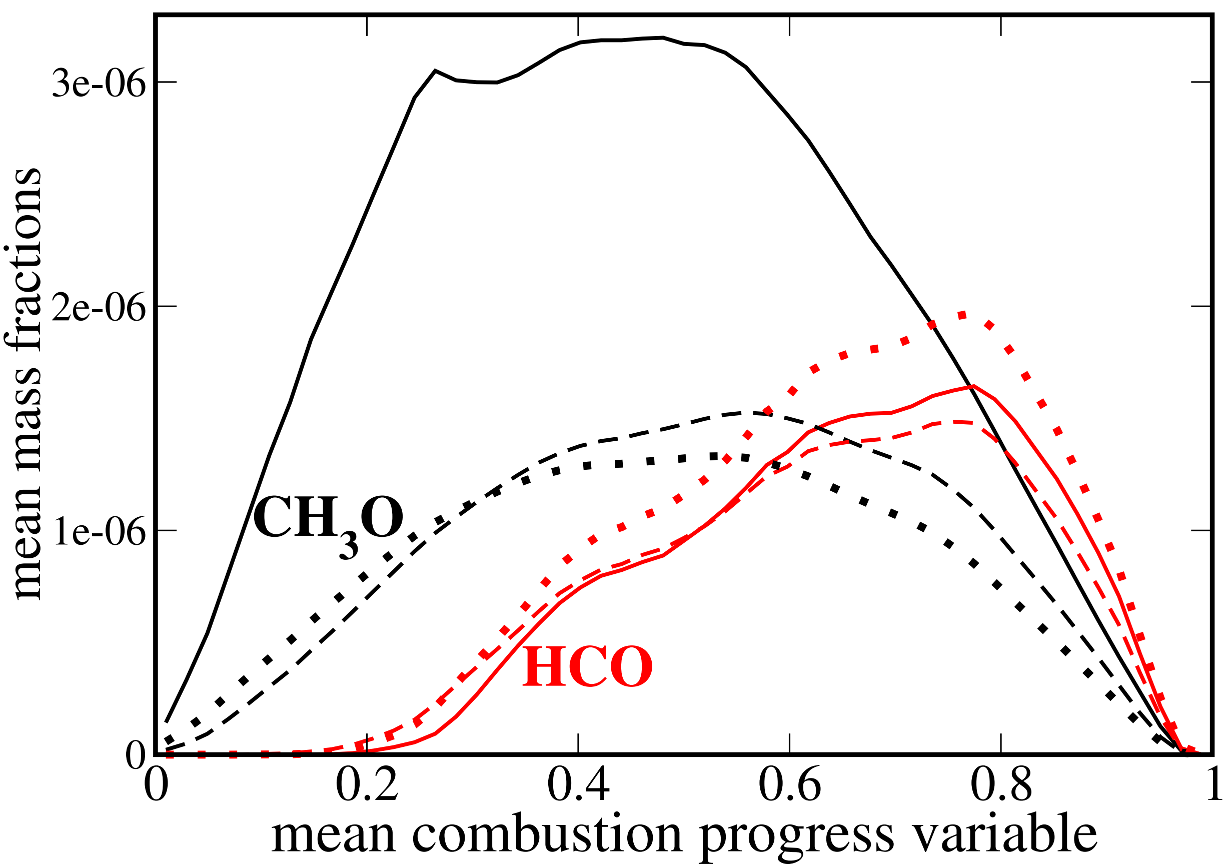
3e-06
2e-06
1e-06
0
mean mass fractions
0
0.2
0.4
0.6
0.8
1
mean combustion progress variable
CH3O
HCO

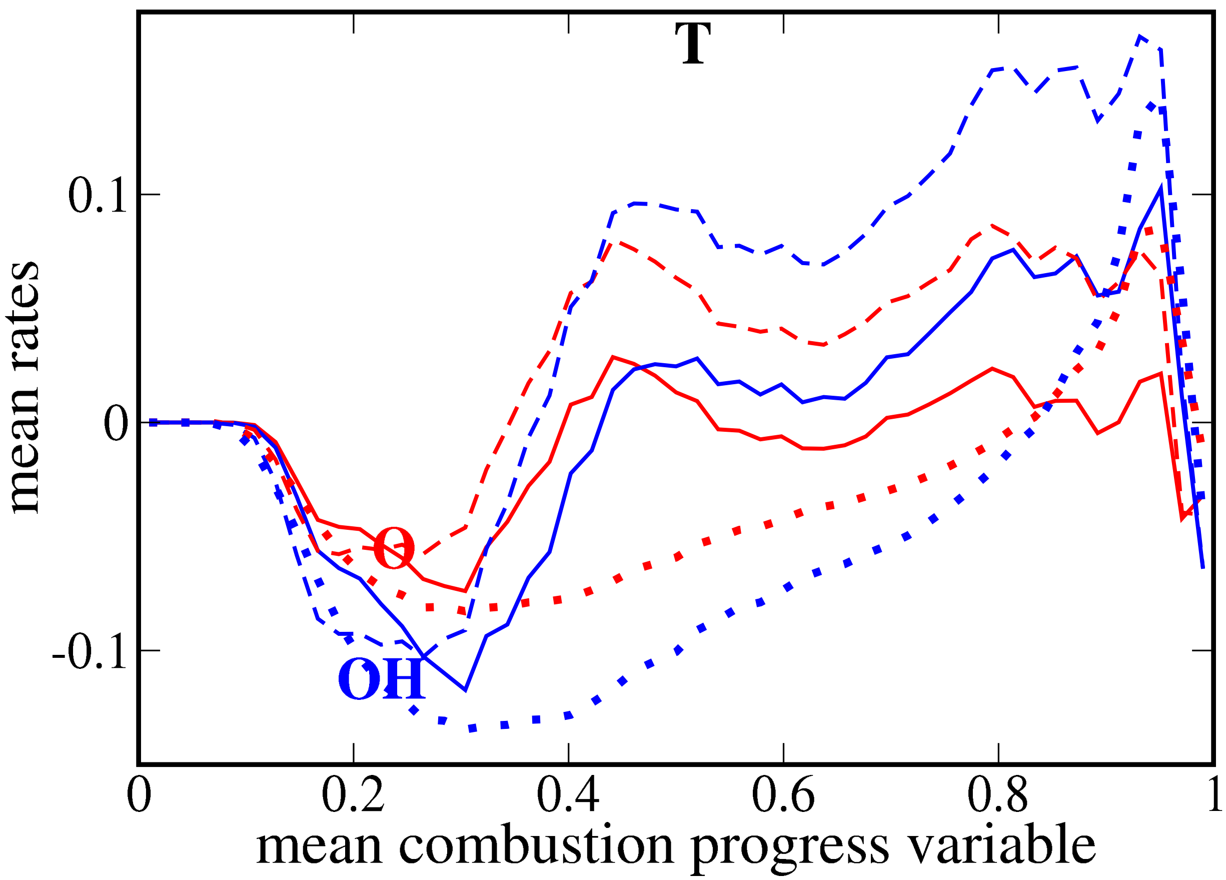
T
O
OH
0.1
0
-0.1
mean rates
0
0.2
0.4
0.6
0.8
1
mean combustion progress variable

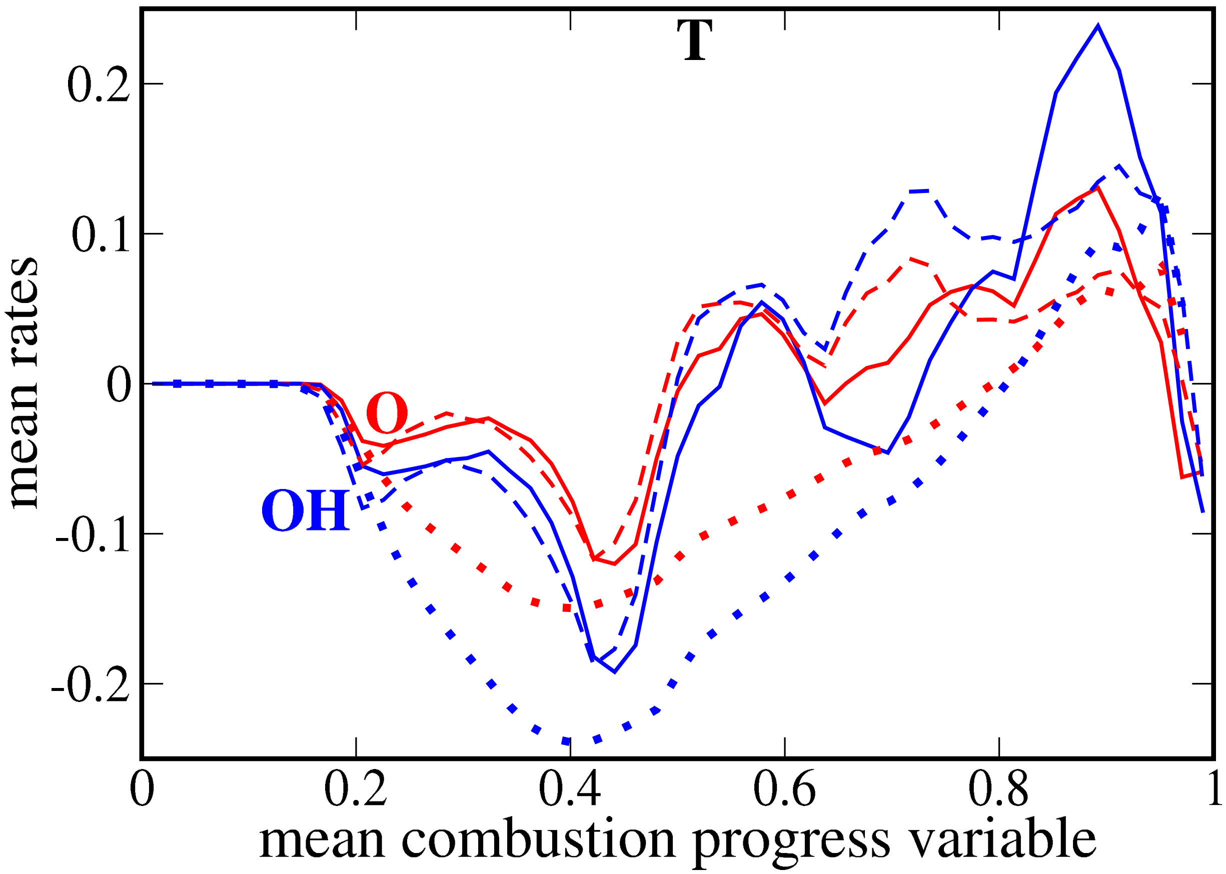
T
O
OH
0.2
0.1
0
-0.1
-0.2
mean rates
0
0.2
0.4
0.6
0.8
1
mean combustion progress variable

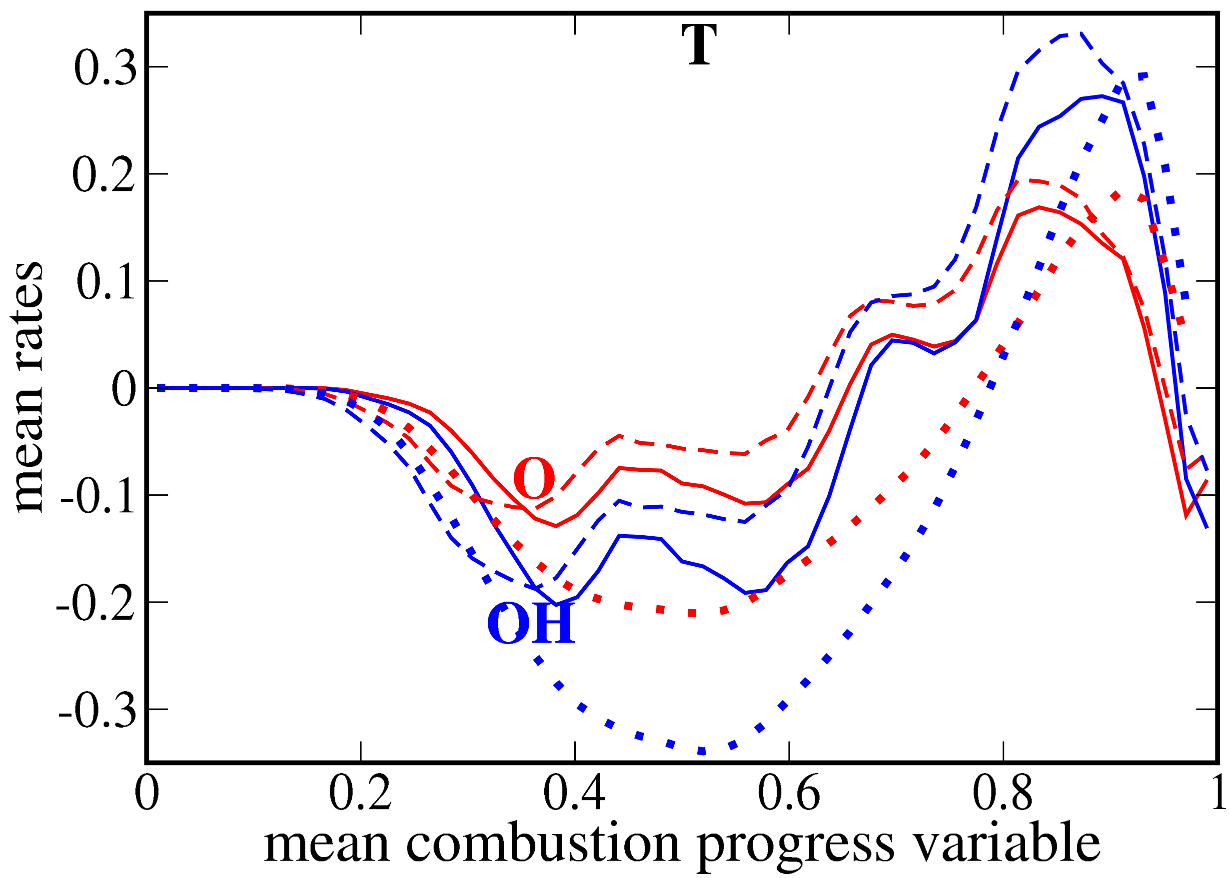
T
O
OH
mean rates
0.3
0.2
0.1
0
-0.1
-0.2
-0.3
0
0.2
0.4
0.6
0.8
1
mean combustion progress variable

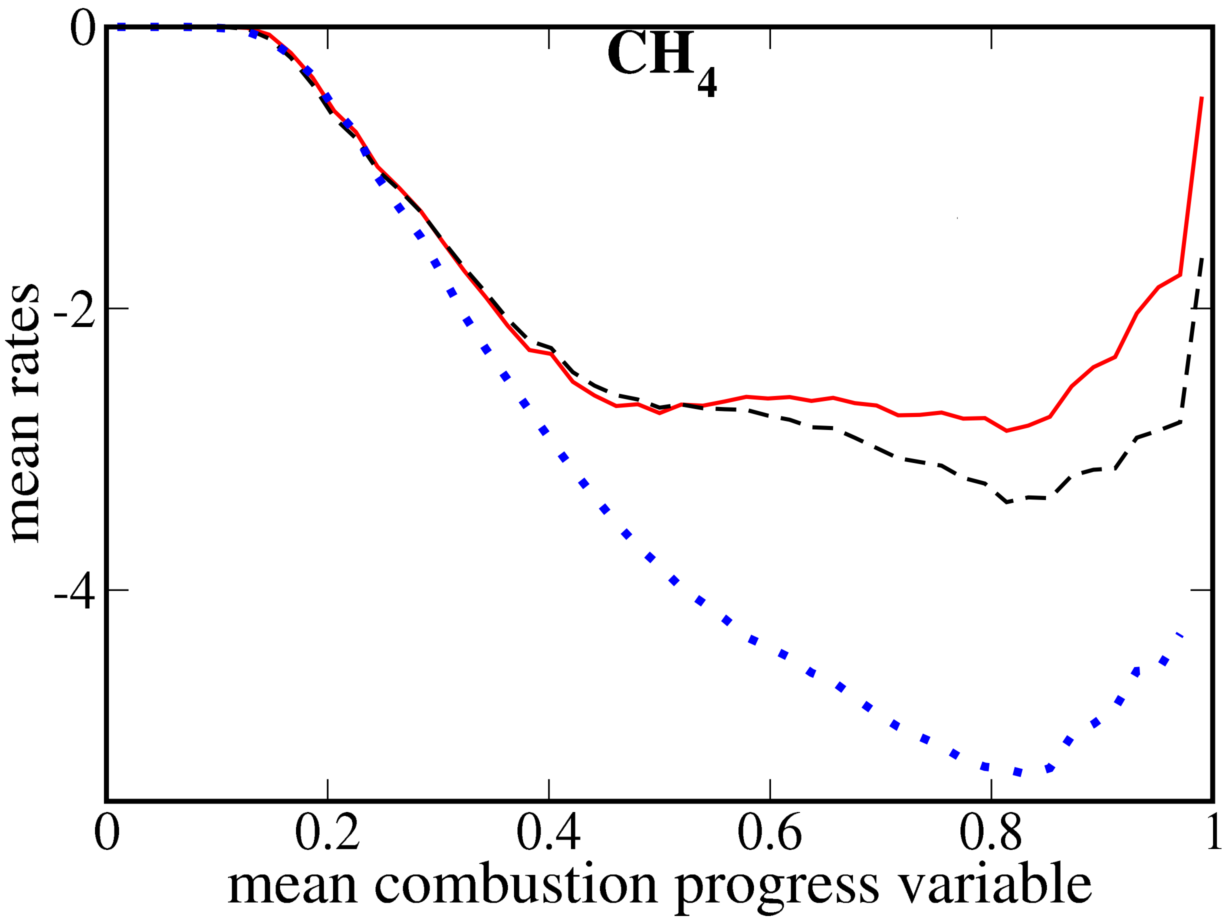
CH4
mean rates
mean combustion progress variable
0
-2
-4
0
0.2
0.4
0.6
0.8
1

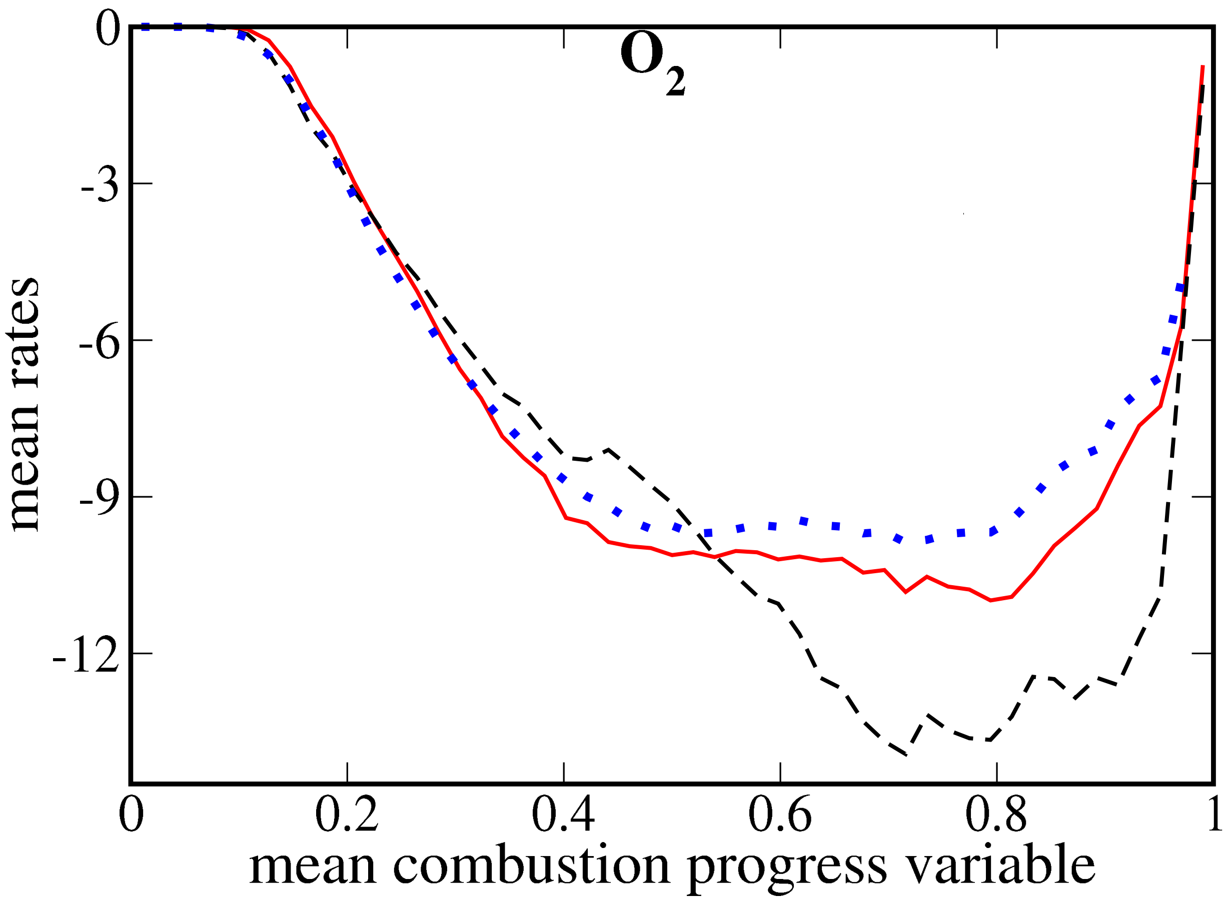
O2
0
-3
-6
-9
-12
mean rates
0
0.2
0.4
0.6
0.8
1
mean combustion progress variable

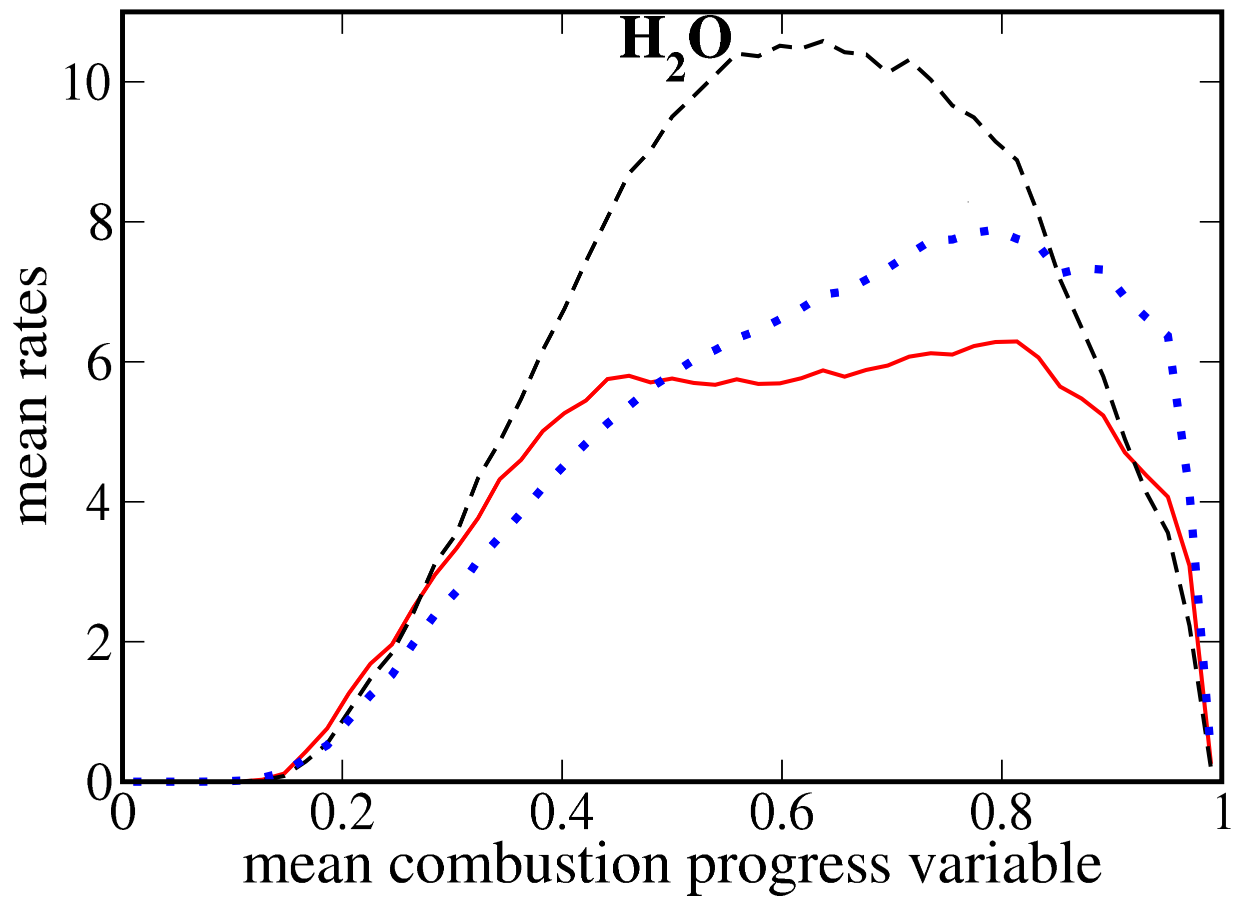
H_2O
mean rates
0
2
4
6
8
10
0
0.2
0.4
0.6
0.8
1
mean combustion progress variable

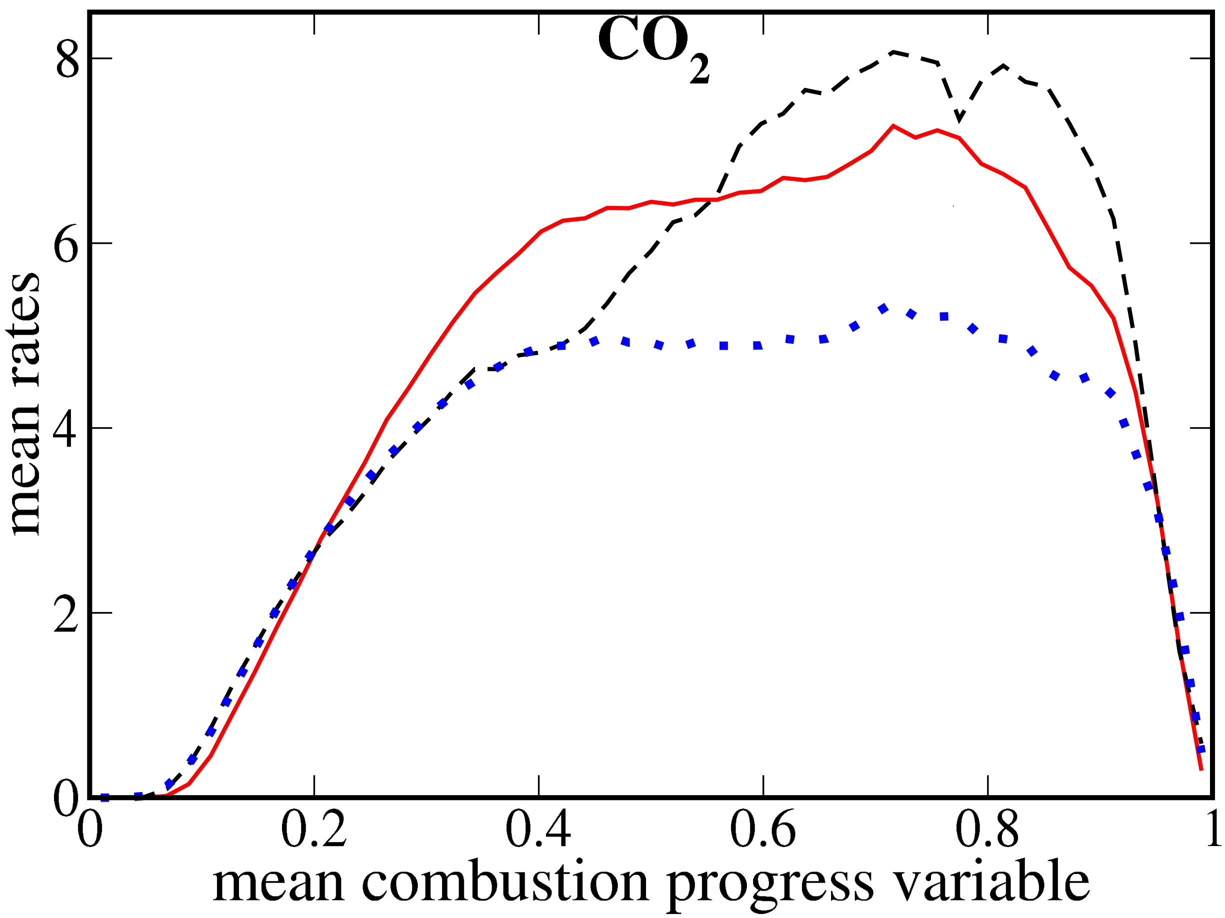
CO_2
mean rates
mean combustion progress variable
0
2
4
6
8
0
0.2
0.4
0.6
0.8
1

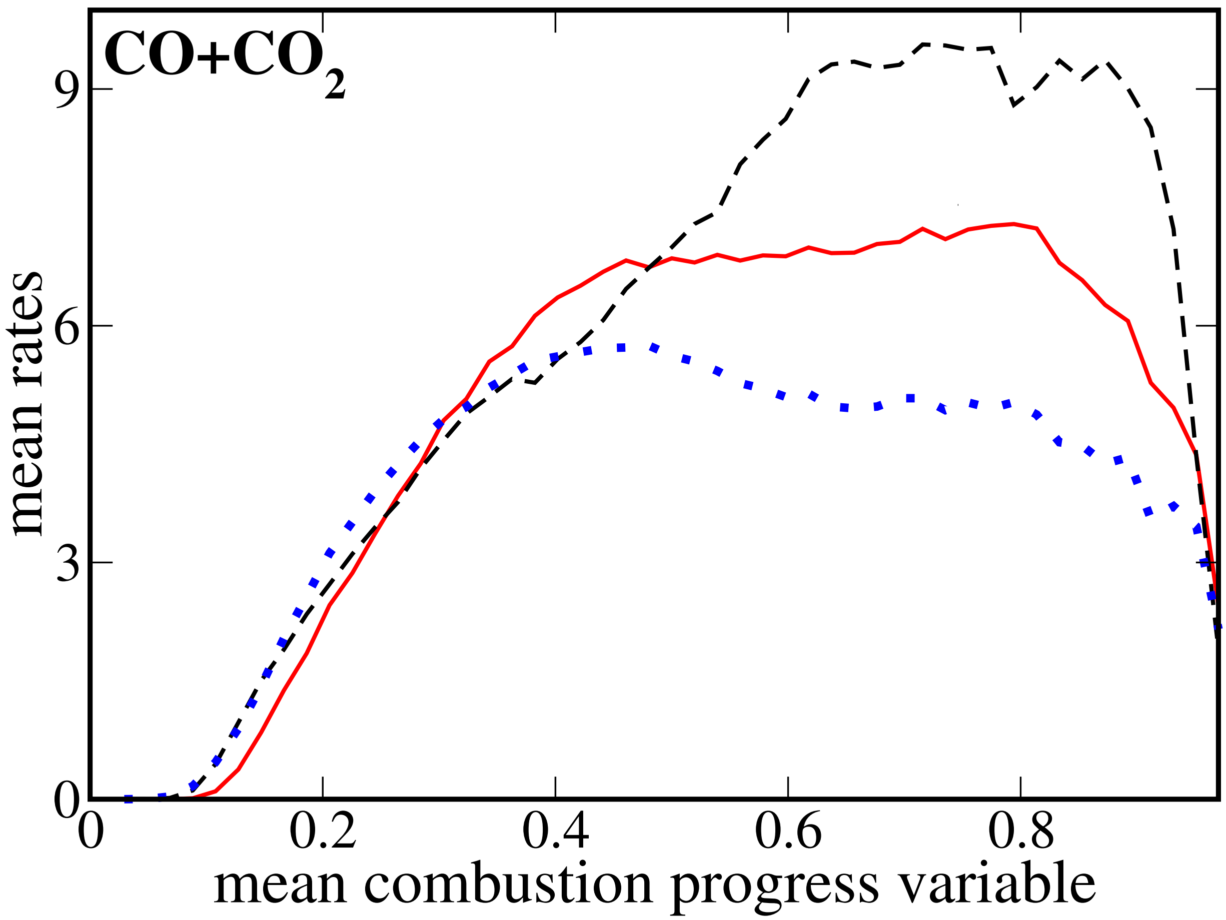
CO+CO2
mean rates
mean combustion progress variable
0
3
6
9
0
0.2
0.4
0.6
0.8

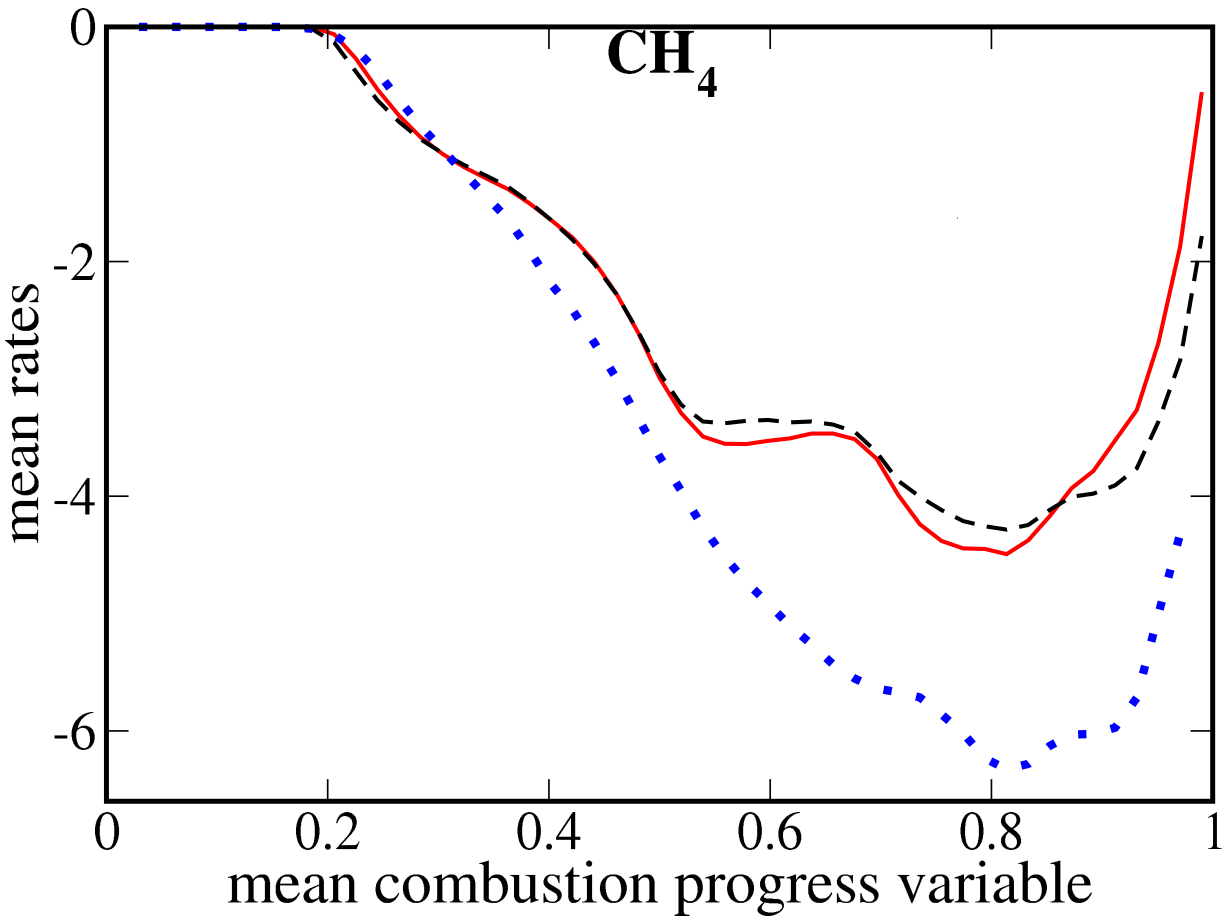
CH4
0
-2
-4
-6
mean rates
0
0.2
0.4
0.6
0.8
1
mean combustion progress variable

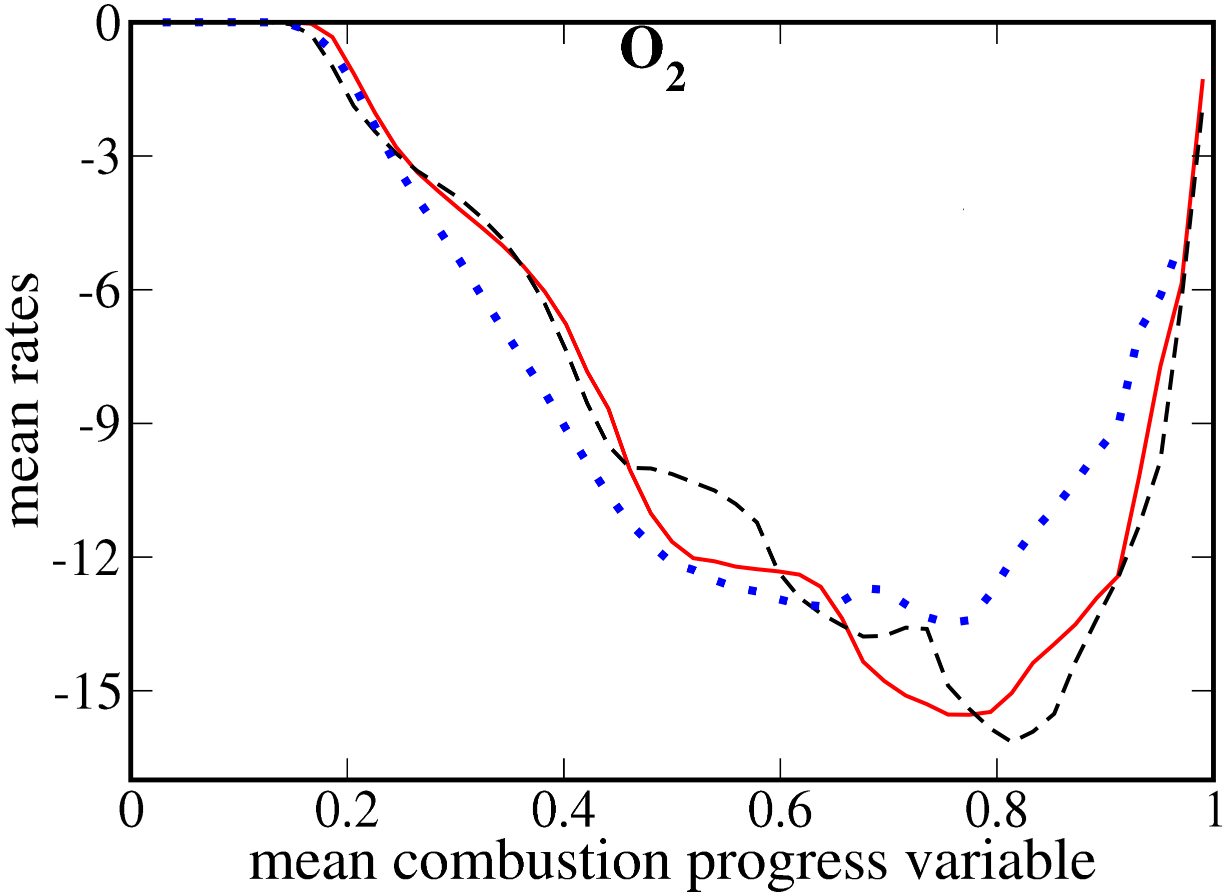
O2
mean rates
mean combustion progress variable
0
-3
-6
-9
-12
-15
0
0.2
0.4
0.6
0.8
1

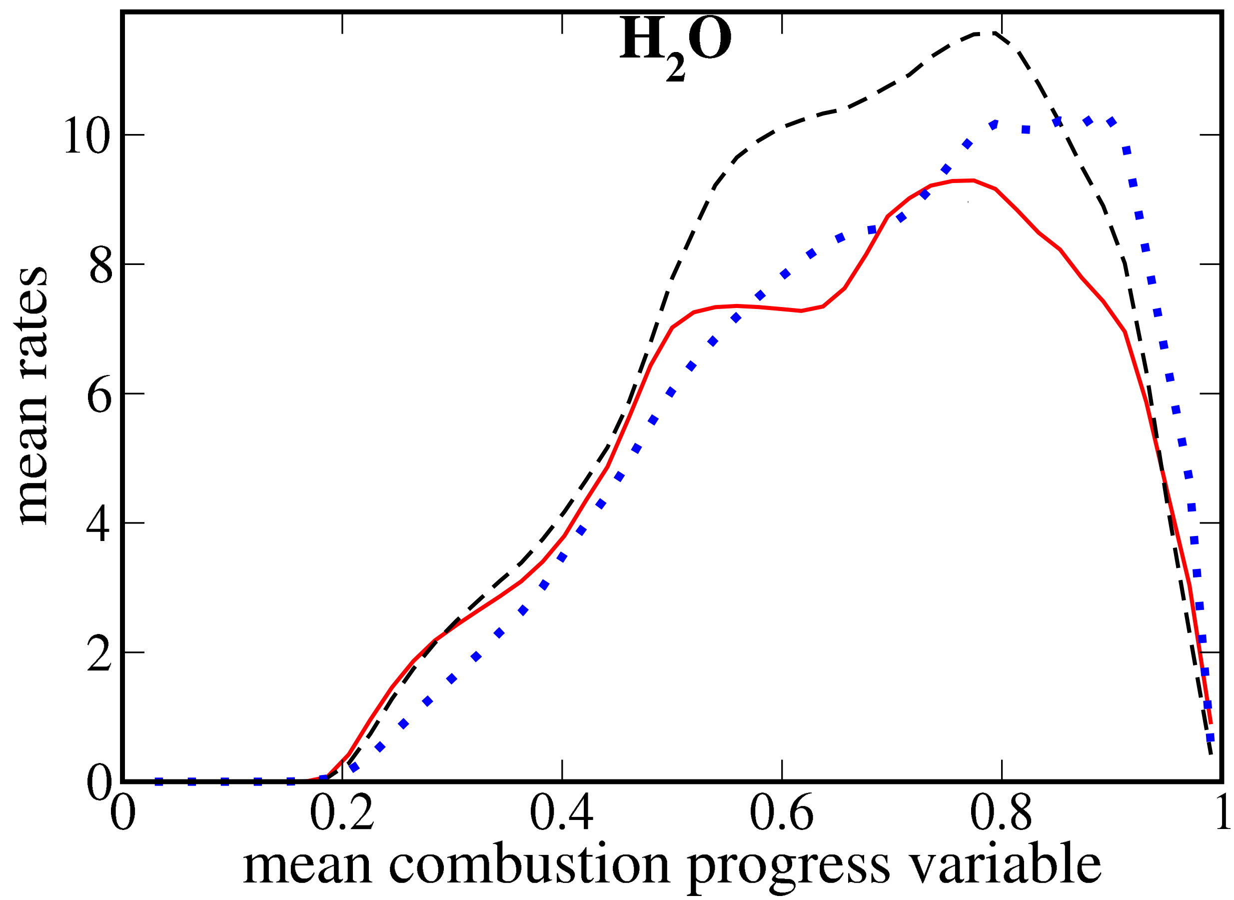
H_2O
mean rates
0
2
4
6
8
10
0
0.2
0.4
0.6
0.8
1
mean combustion progress variable

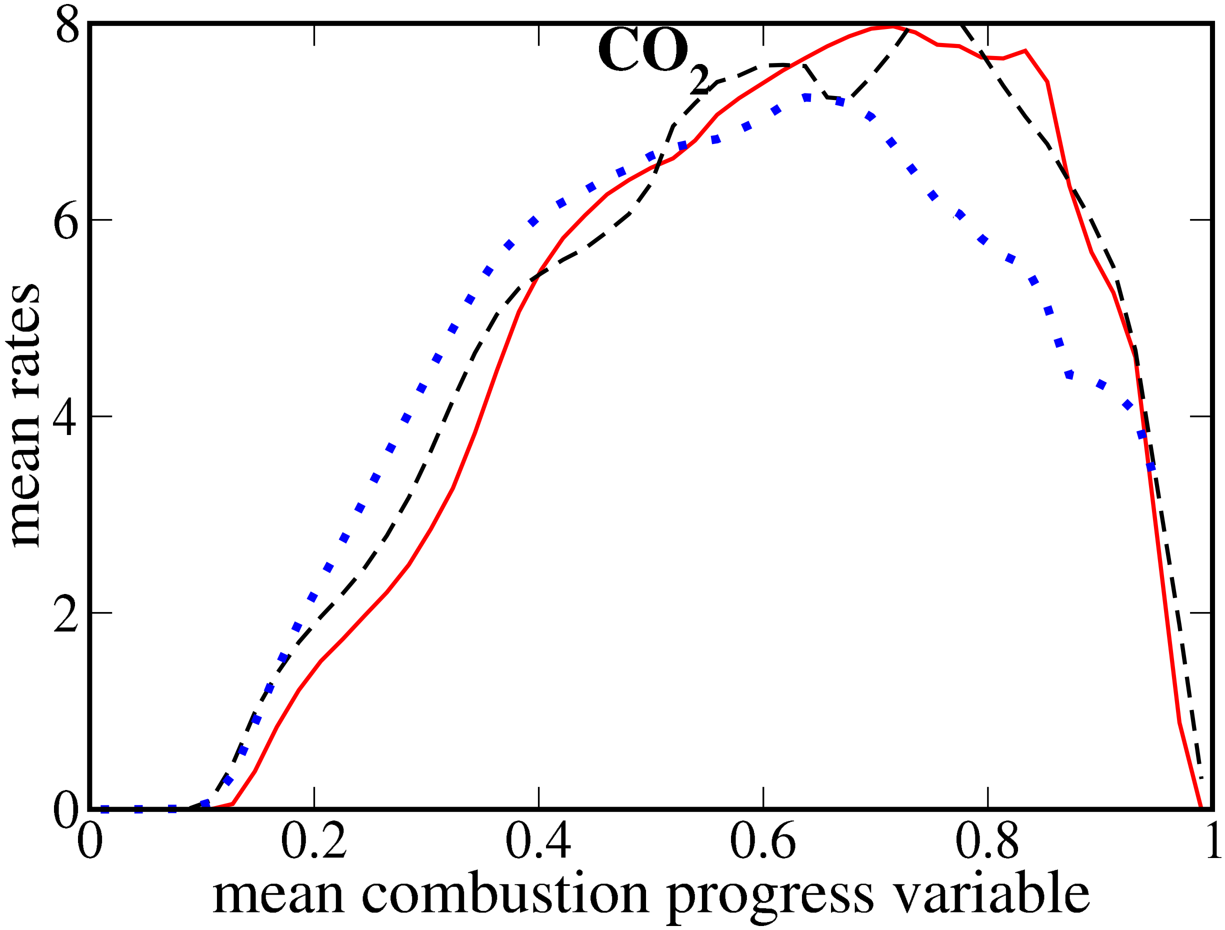
CO_2
mean rates
mean combustion progress variable
0
2
4
6
8
0
0.2
0.4
0.6
0.8
1

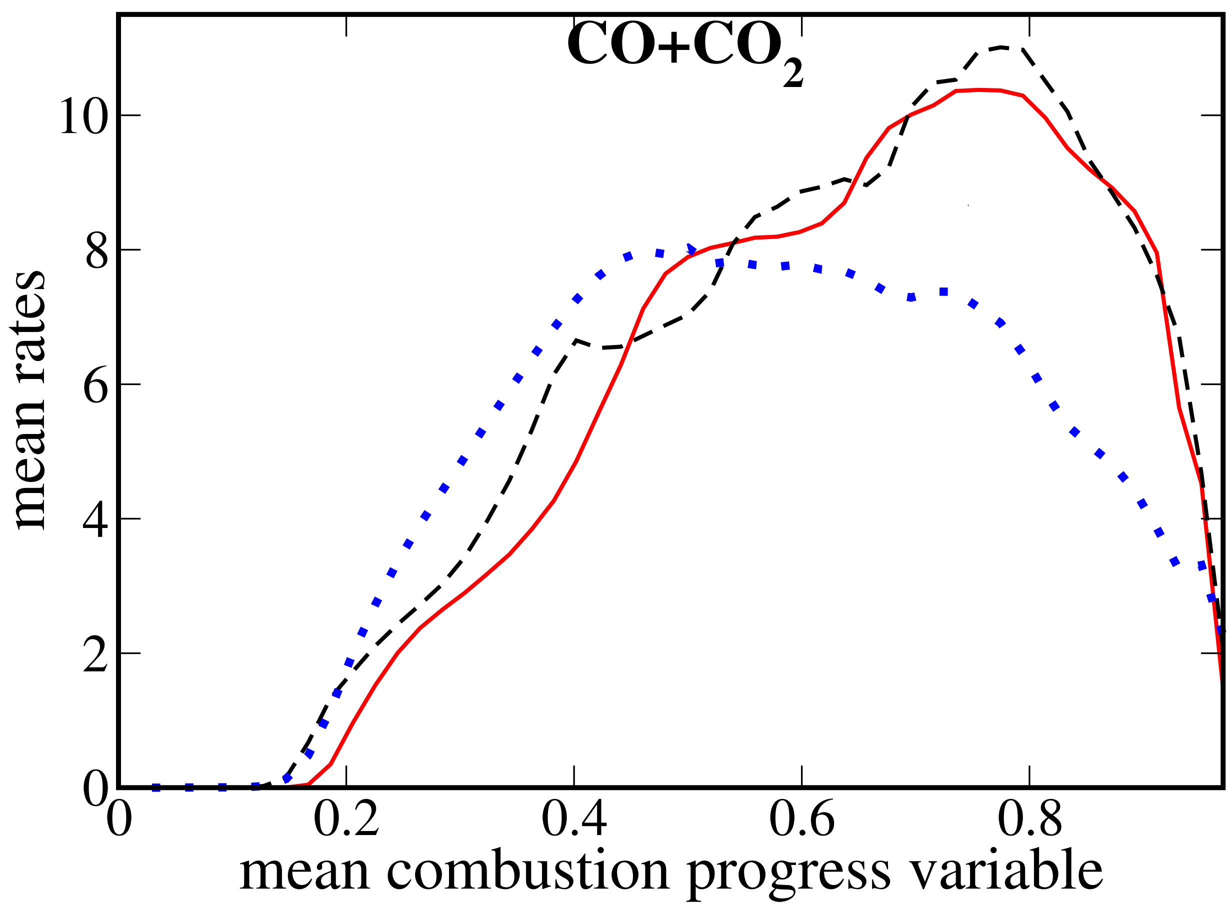
CO+CO2
mean rates
0
2
4
6
8
10
0
0.2
0.4
0.6
0.8
mean combustion progress variable

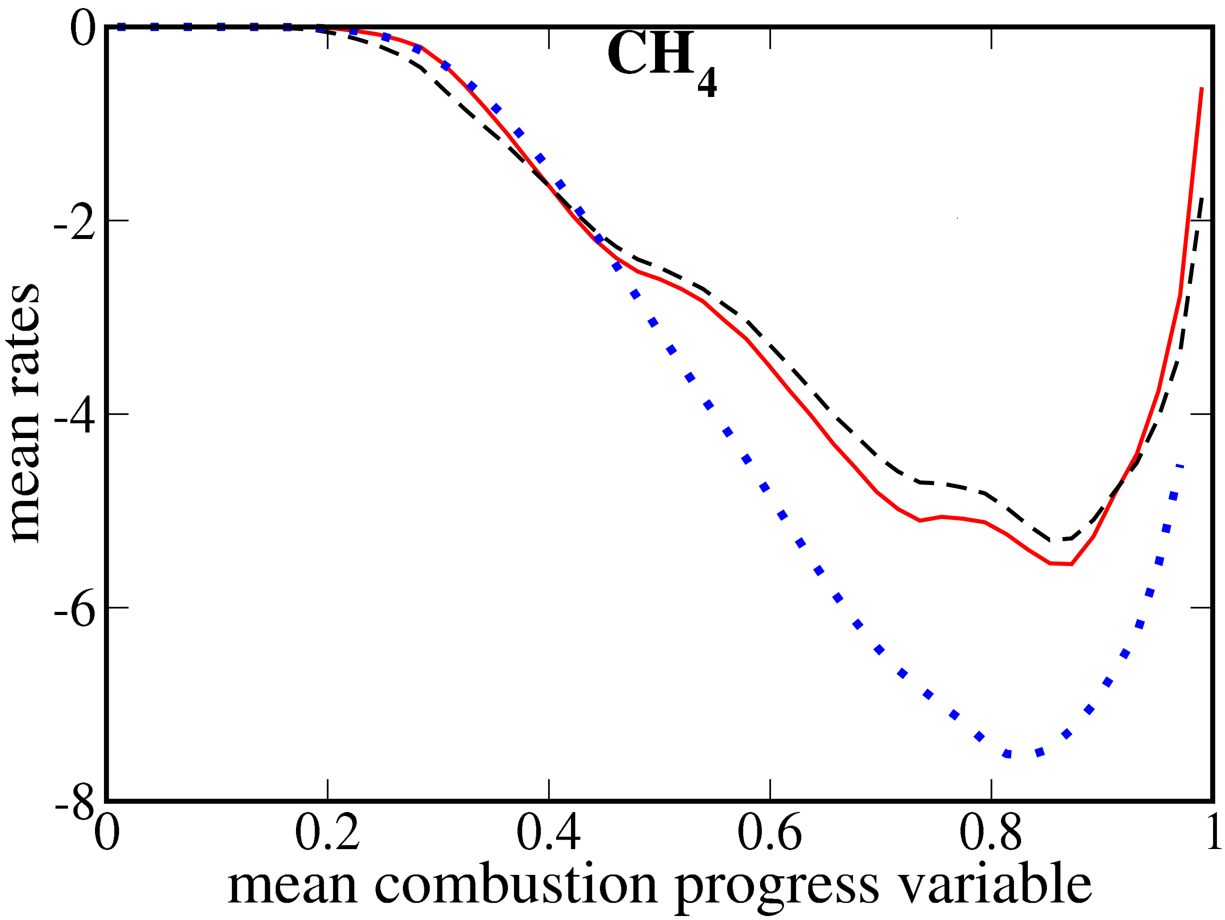
CH_4
mean rates
0
-2
-4
-6
-8
0
0.2
0.4
0.6
0.8
1
mean combustion progress variable

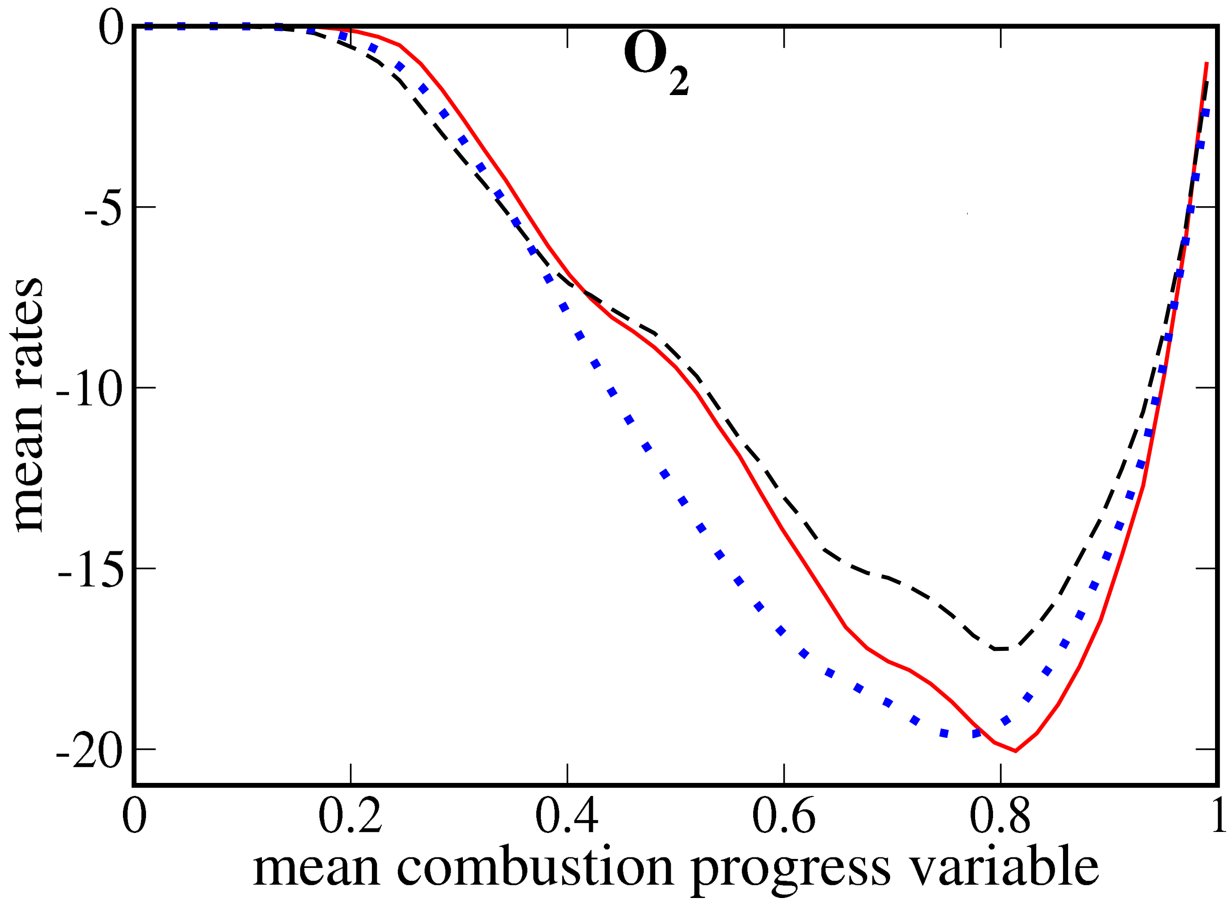
O_2
mean rates
mean combustion progress variable
0
-5
-10
-15
-20
0
0.2
0.4
0.6
0.8
1

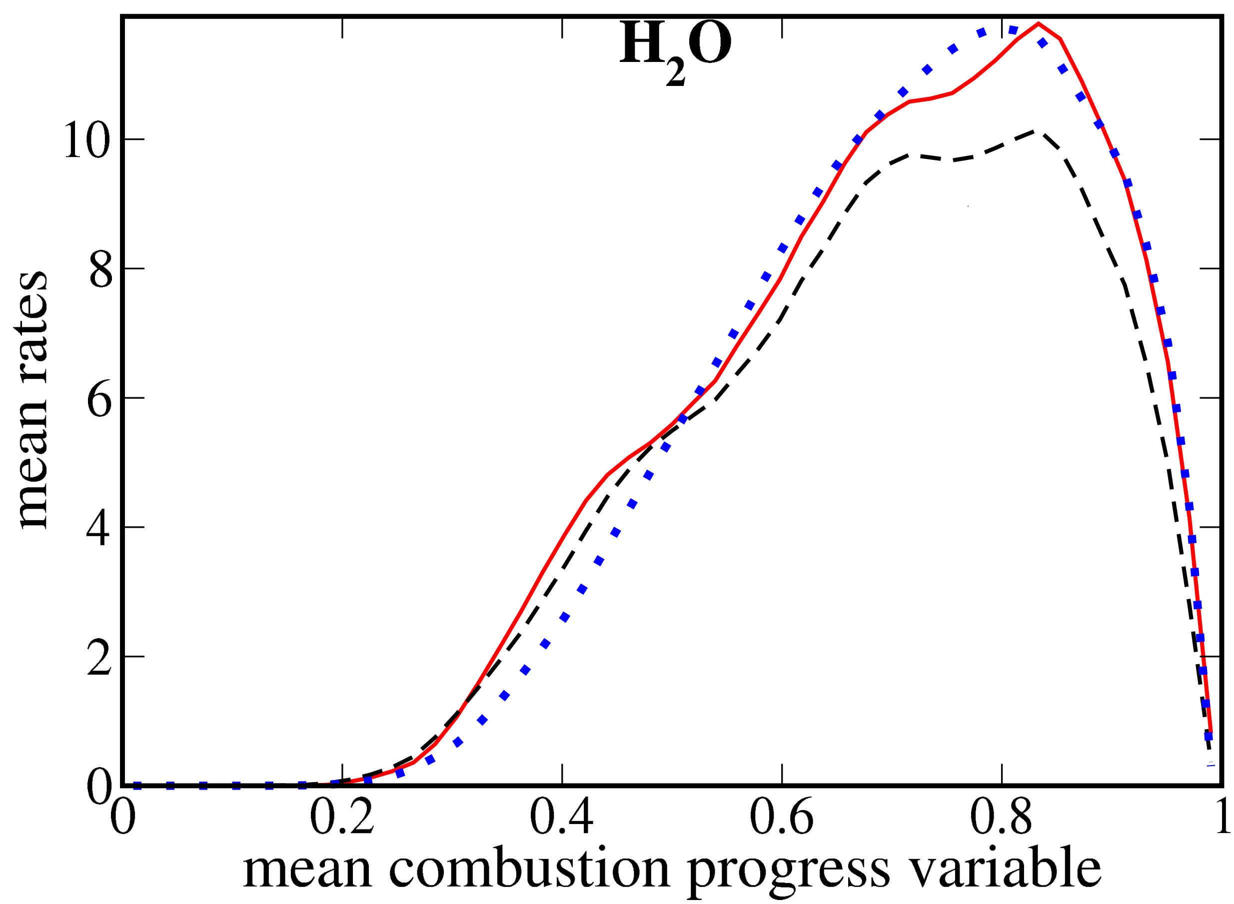
H_2O
mean rates
0
2
4
6
8
10
0
0.2
0.4
0.6
0.8
1
mean combustion progress variable

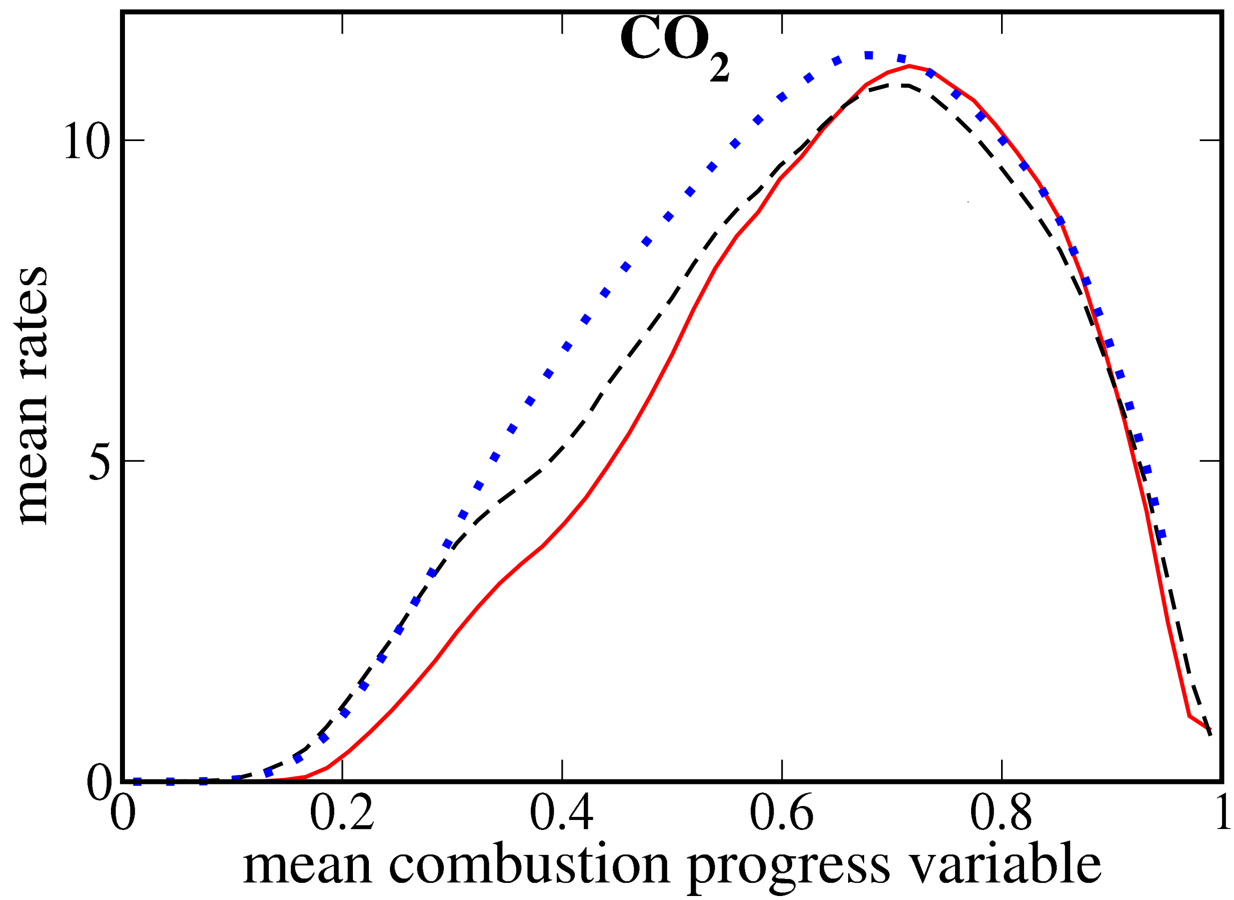
CO_2
mean rates
0
5
10
0
0.2
0.4
0.6
0.8
1
mean combustion progress variable

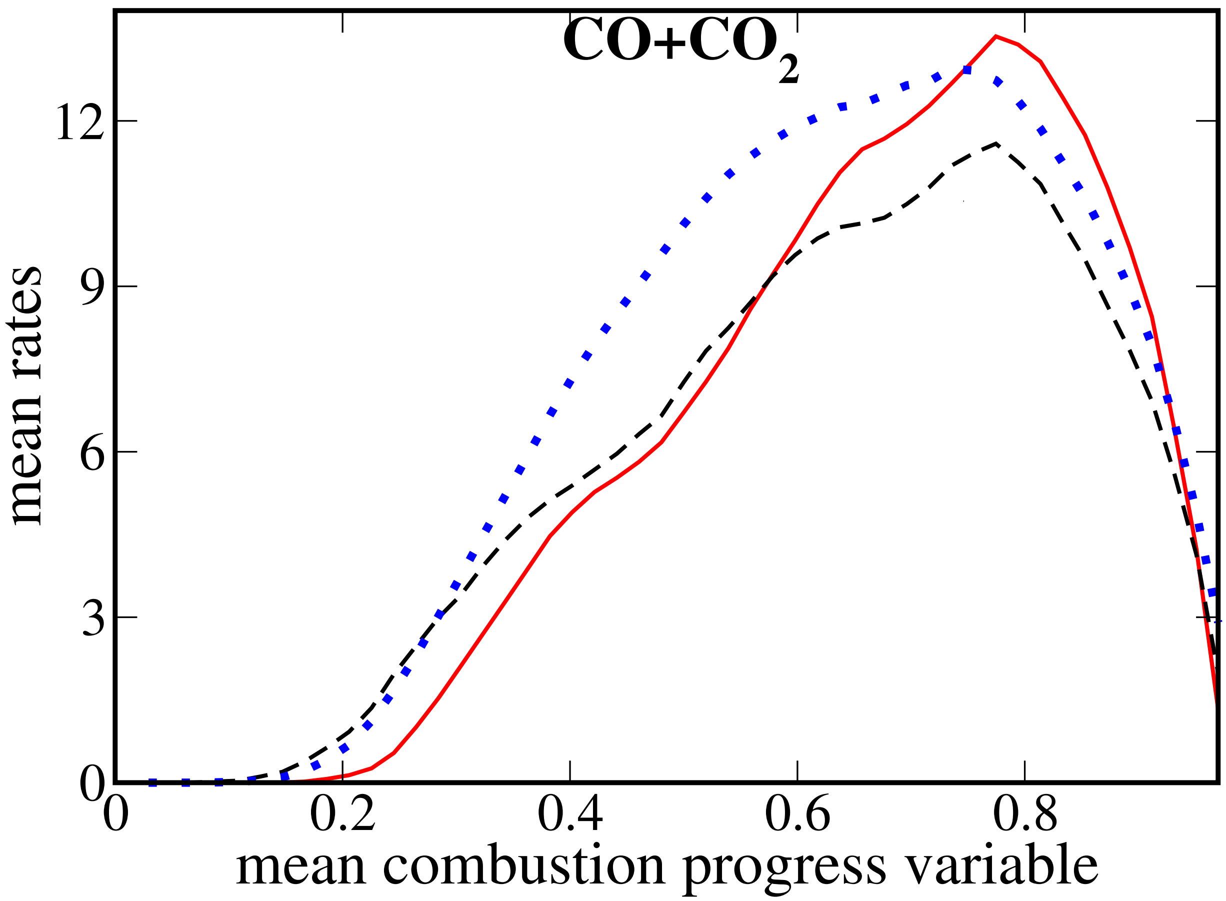
$CO+CO_2$
mean rates
0
3
6
9
12
0
0.2
0.4
0.6
0.8
mean combustion progress variable

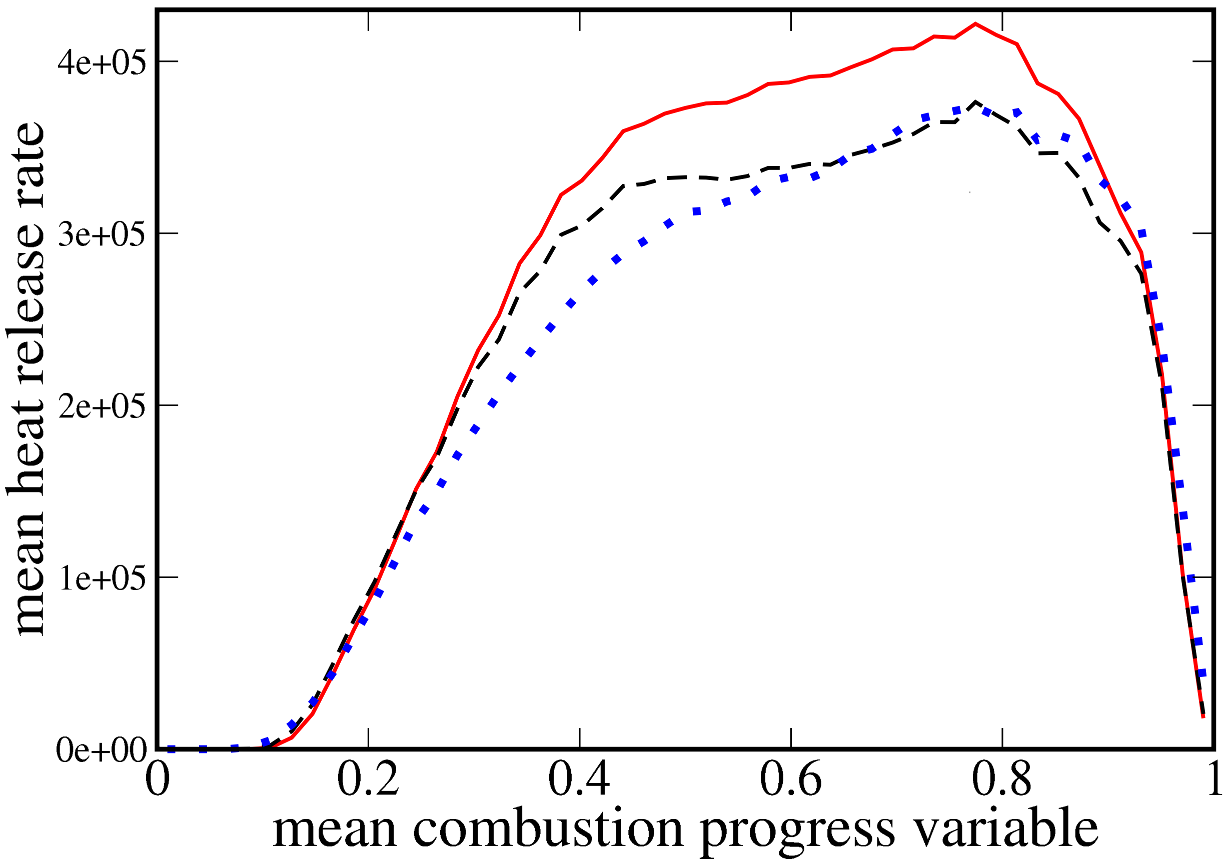
mean heat release rate
4e+05
3e+05
2e+05
1e+05
0e+00
0
0.2
0.4
0.6
0.8
1
mean combustion progress variable

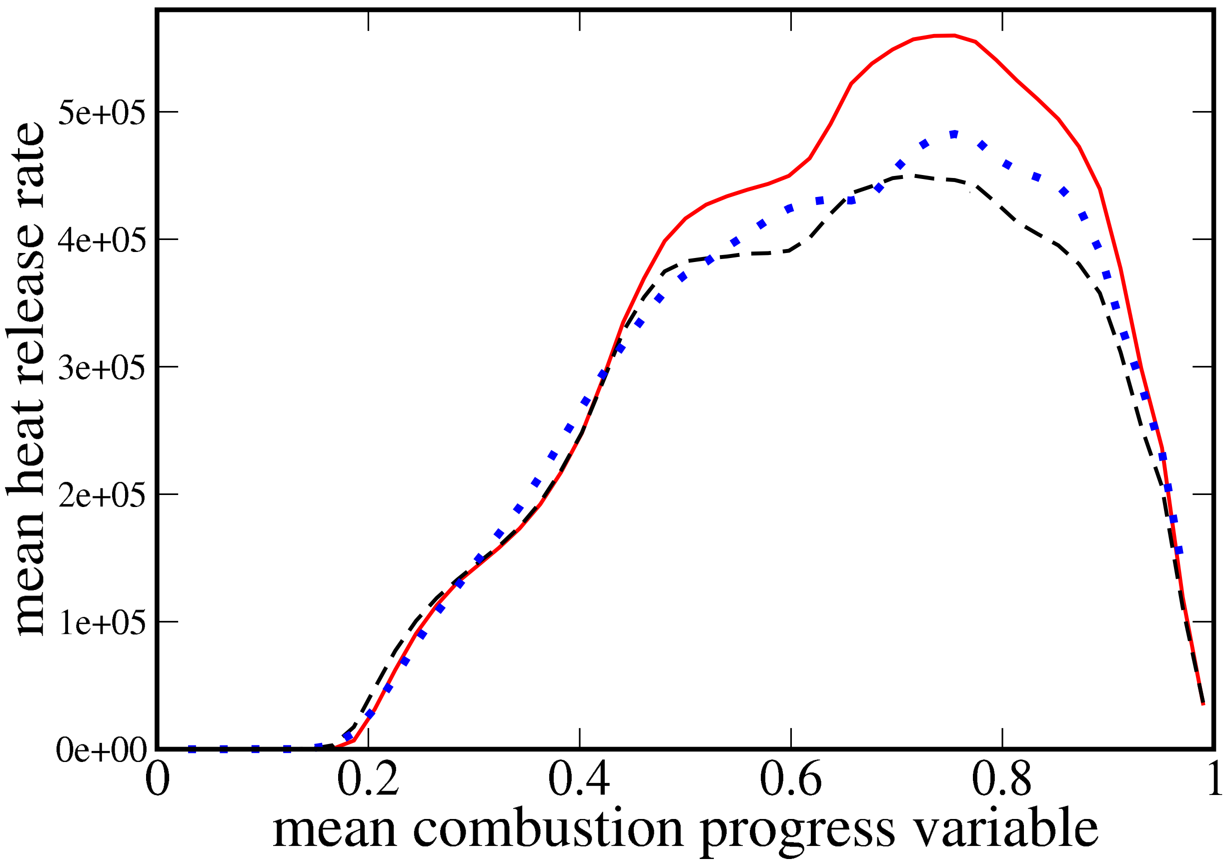
mean heat release rate
5e+05
4e+05
3e+05
2e+05
1e+05
0e+00
0
0.2
0.4
0.6
0.8
1
mean combustion progress variable

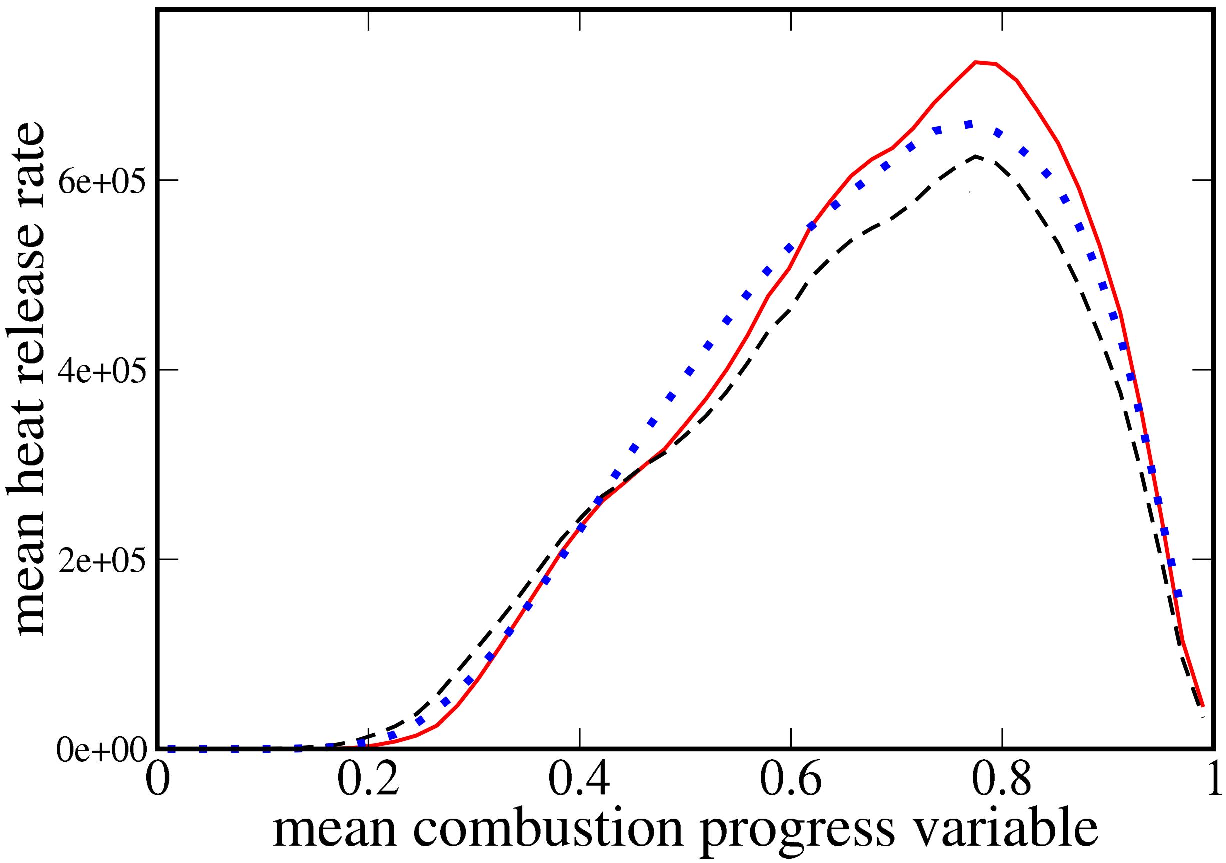
mean heat release rate
0e+00
2e+05
4e+05
6e+05
0
0.2
0.4
0.6
0.8
1
mean combustion progress variable

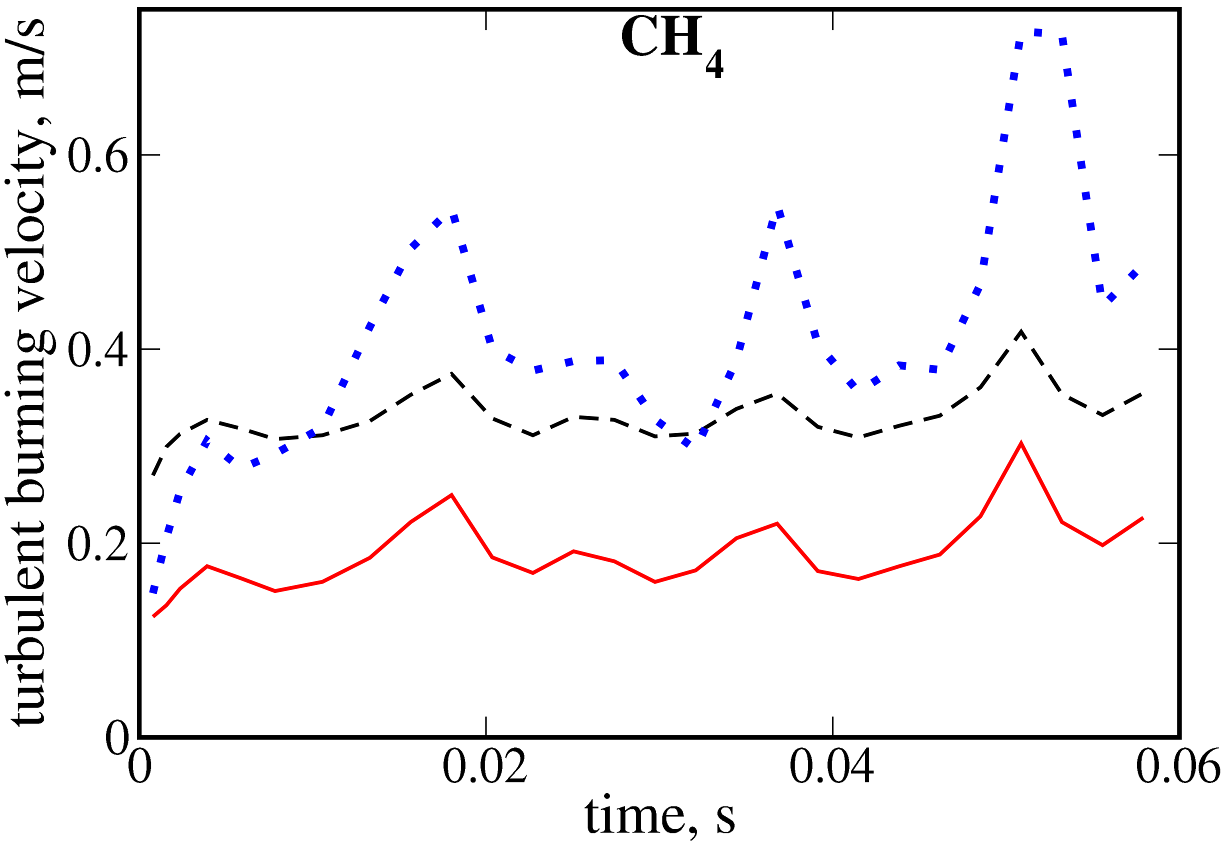
CH4
turbulent burning velocity, m/s
0
0.2
0.4
0.6
0
0.02
0.04
0.06
time, s

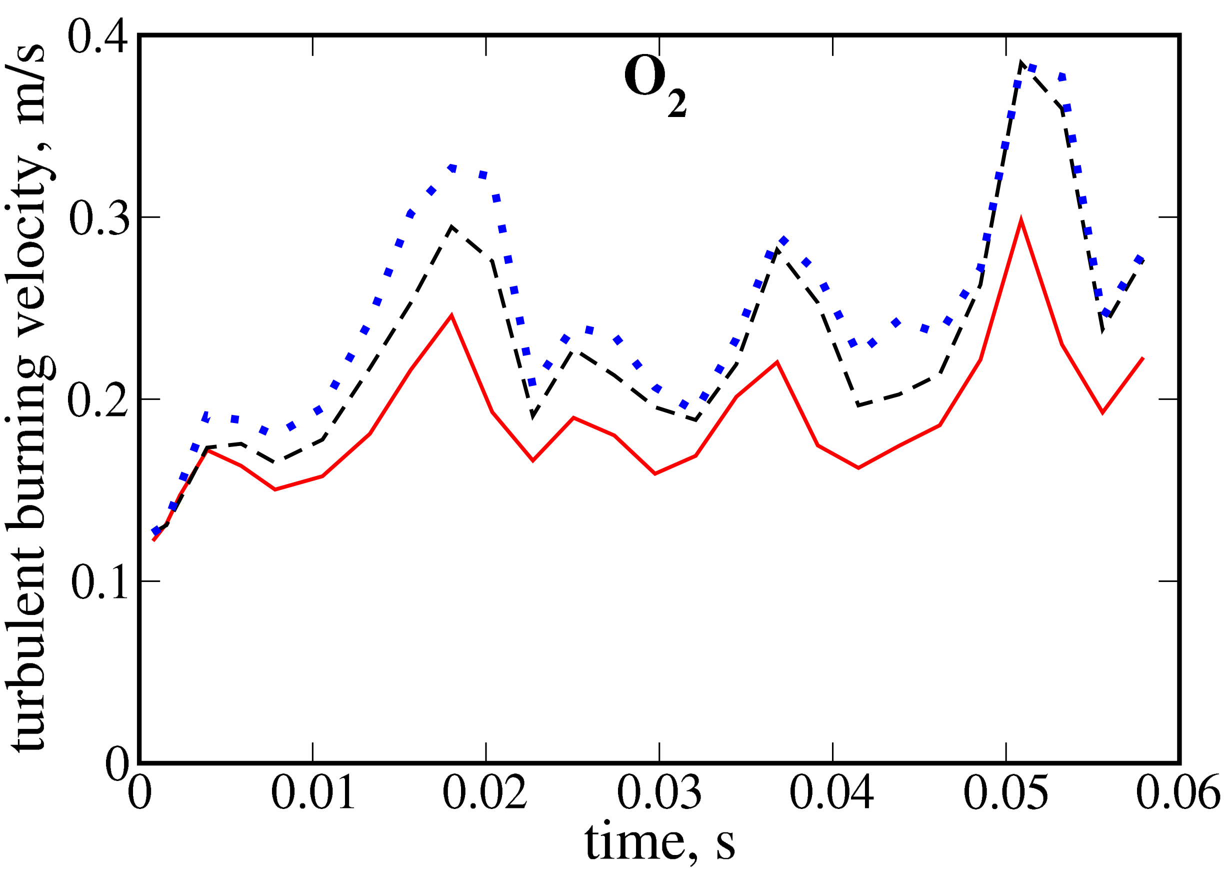
O_2
turbulent burning velocity, m/s
time, s
0
0.1
0.2
0.3
0.4
0.01
0.02
0.03
0.04
0.05
0.06

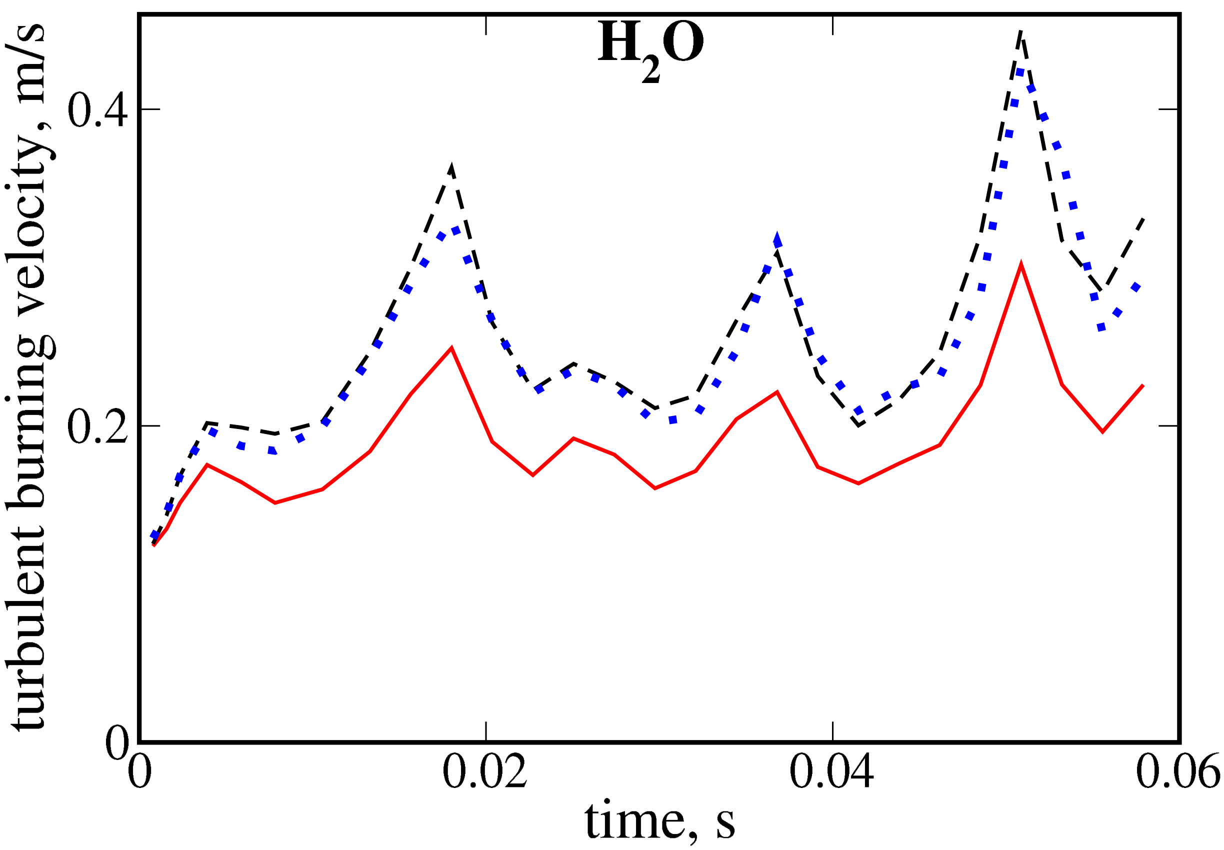
H2O
turbulent burning velocity, m/s
0
0.2
0.4
0
0.02
0.04
0.06
time, s

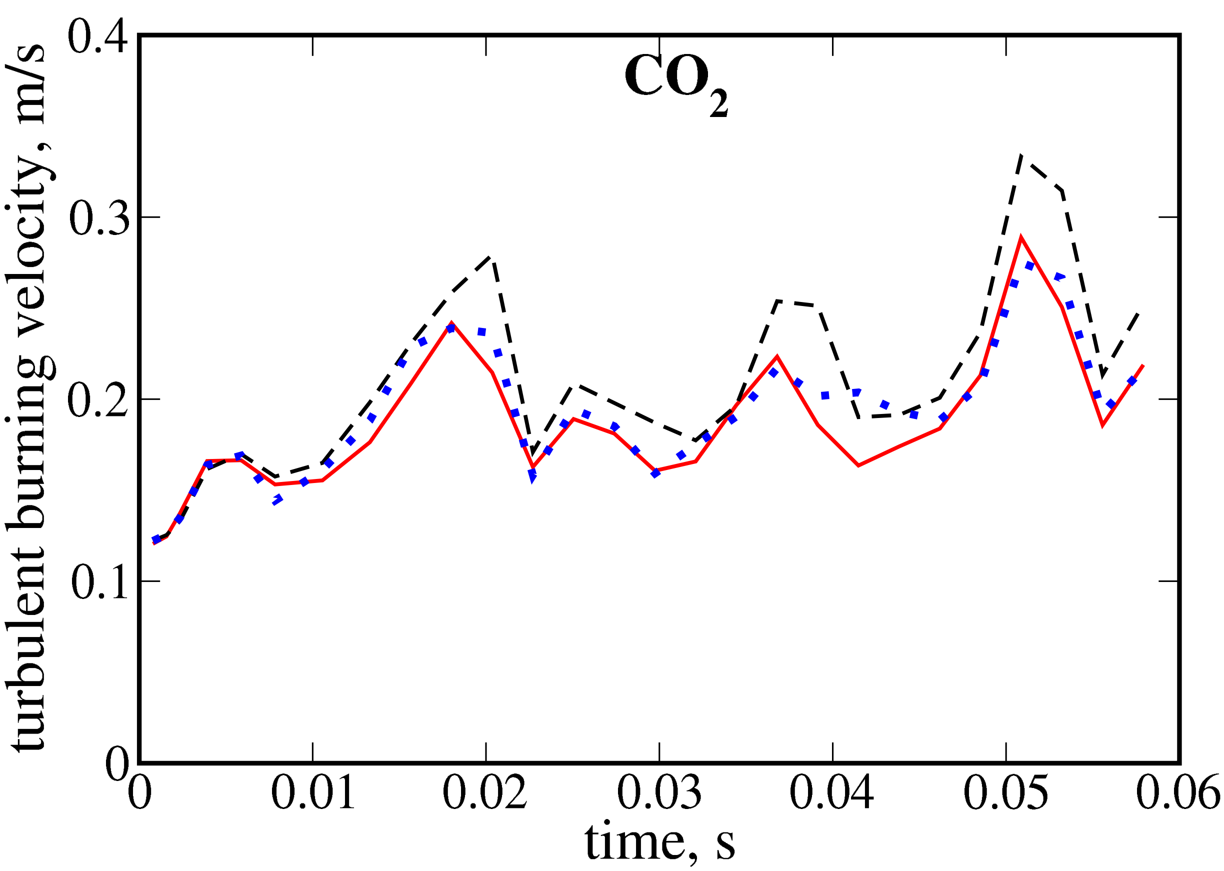
CO_2
turbulent burning velocity, m/s
time, s
0
0.1
0.2
0.3
0.4
0
0.01
0.02
0.03
0.04
0.05
0.06

Physics of Fluids

PLEASE CITE THIS ARTICLE AS DOI: 10.1063/5.0047500

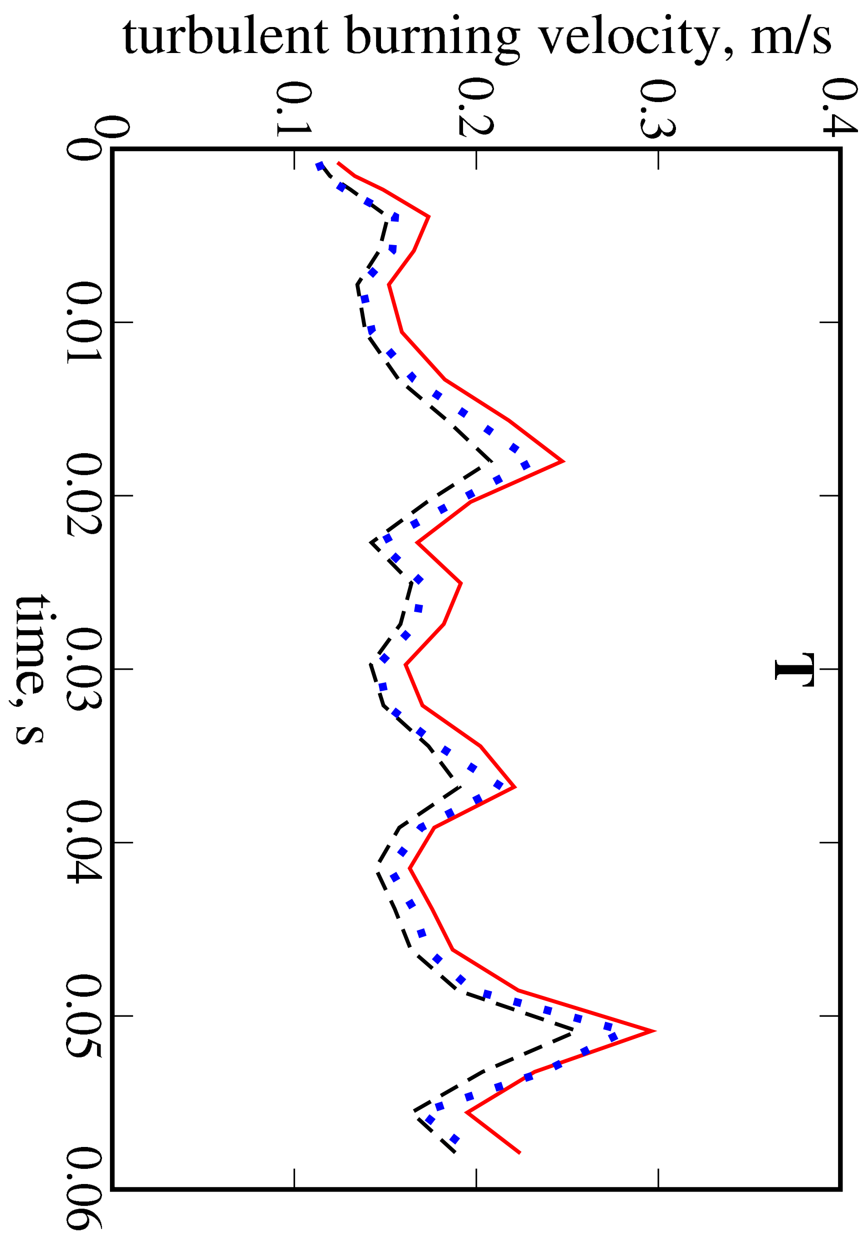

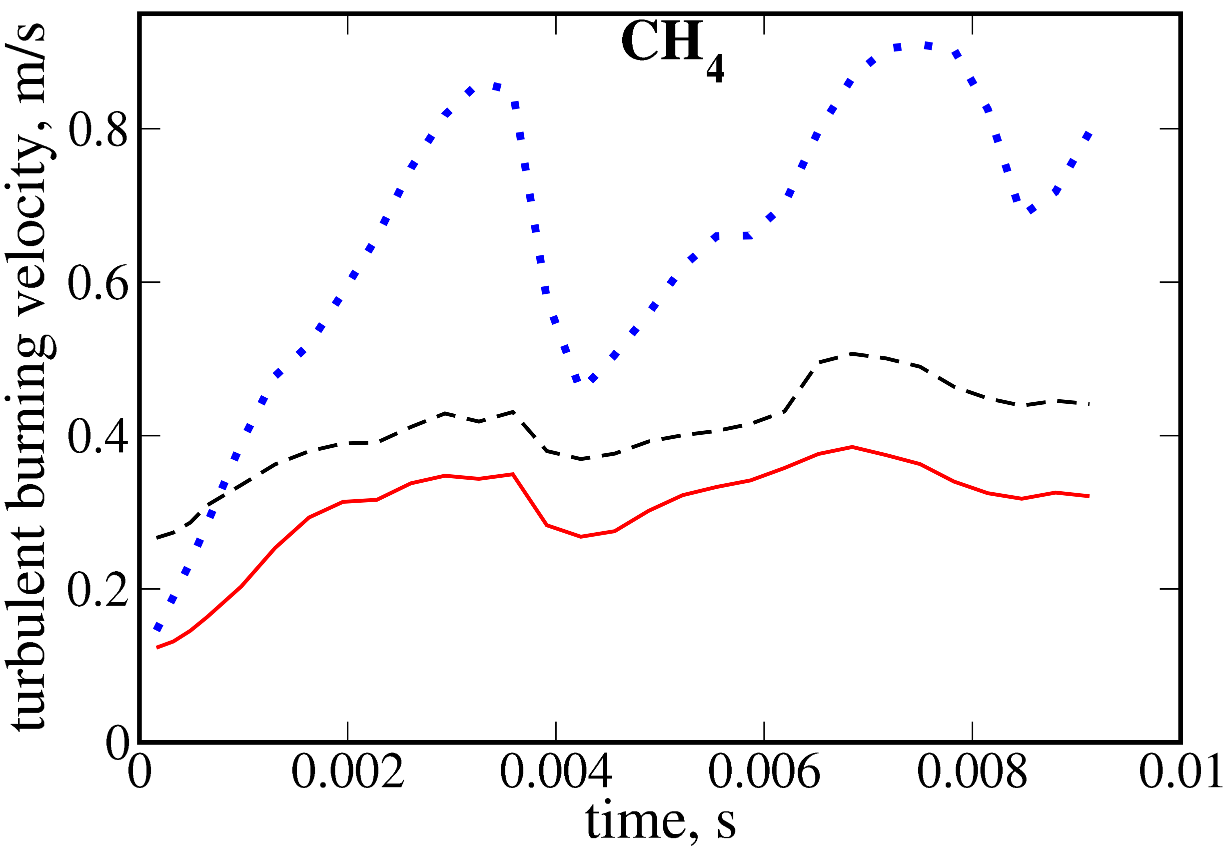
CH_4
turbulent burning velocity, m/s
0
0.2
0.4
0.6
0.8
0
0.002
0.004
0.006
0.008
0.01
time, s

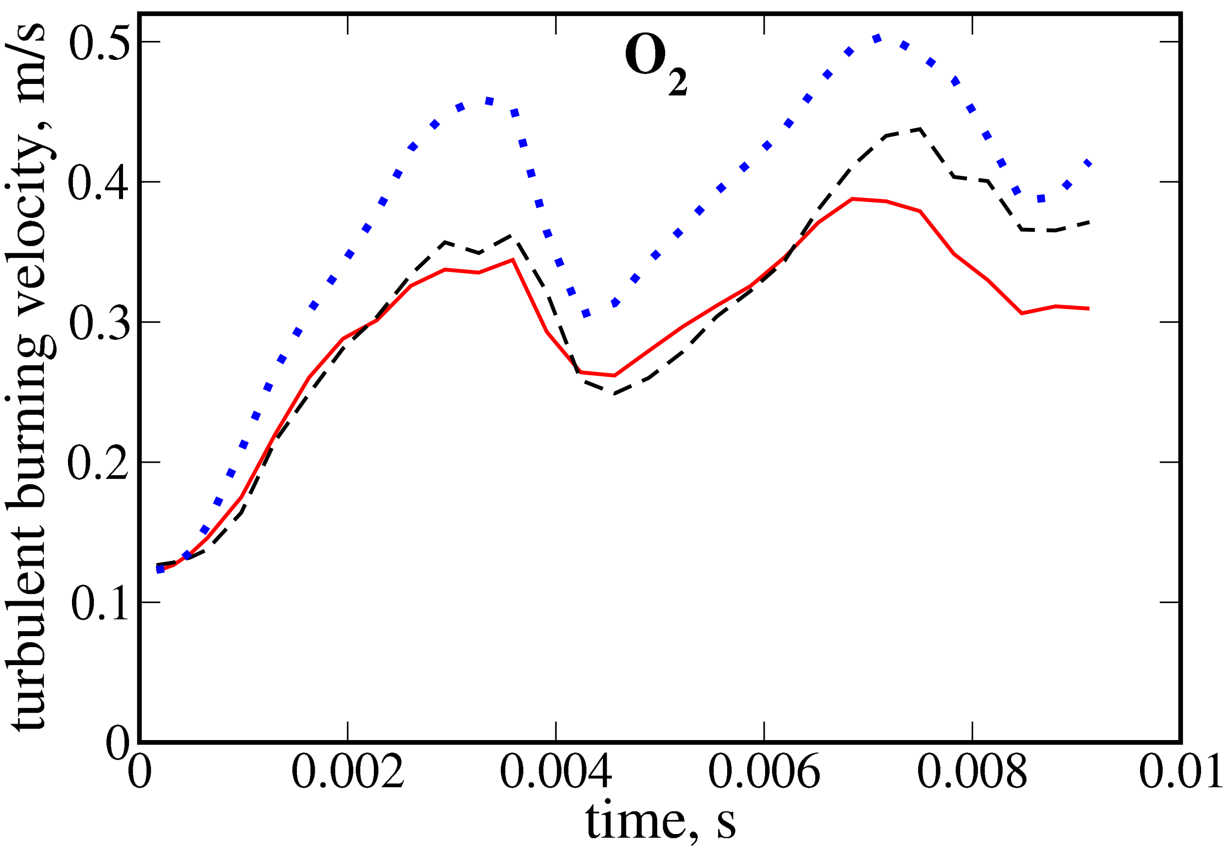
O_2
turbulent burning velocity, m/s
time, s
0
0.1
0.2
0.3
0.4
0.5
0.002
0.004
0.006
0.008
0.01

PLEASE CITE THIS ARTICLE AS DOI: 10.1063/5.0047500

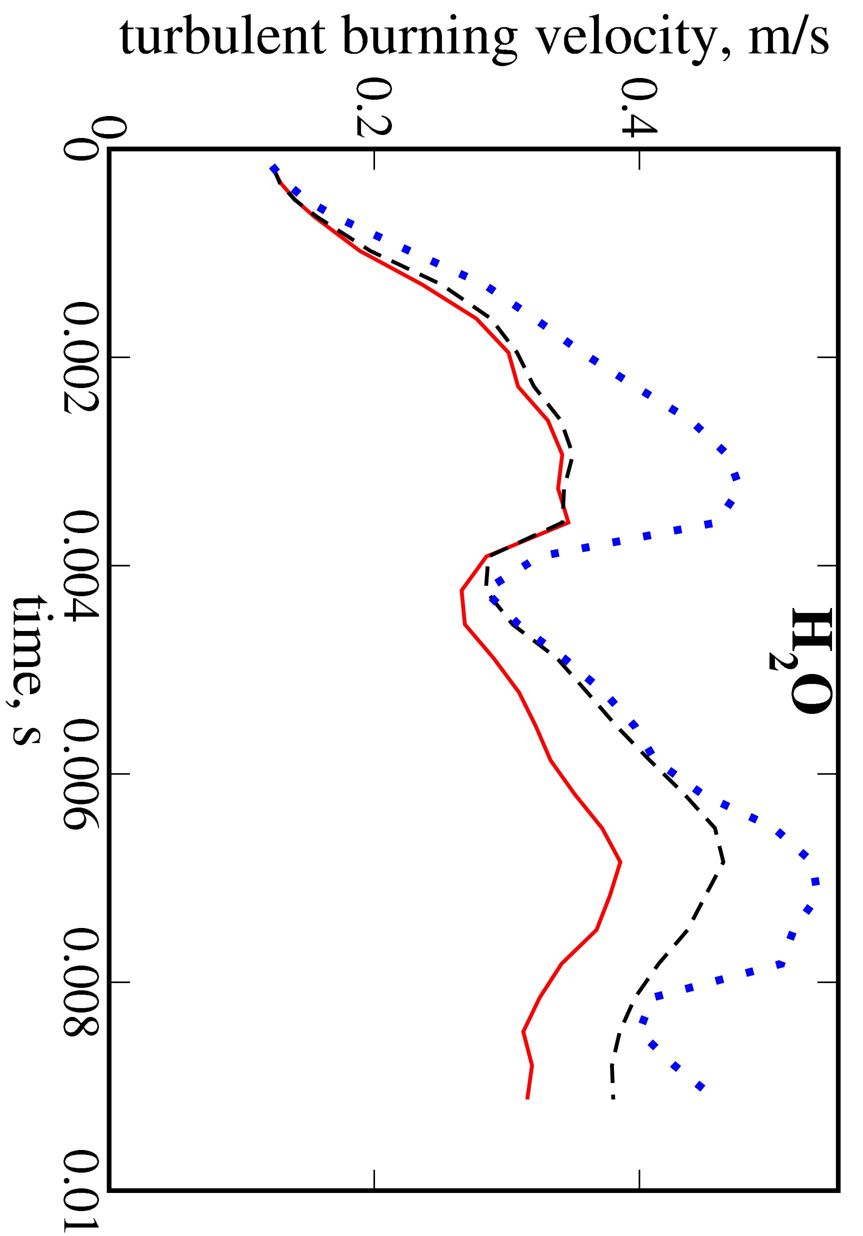

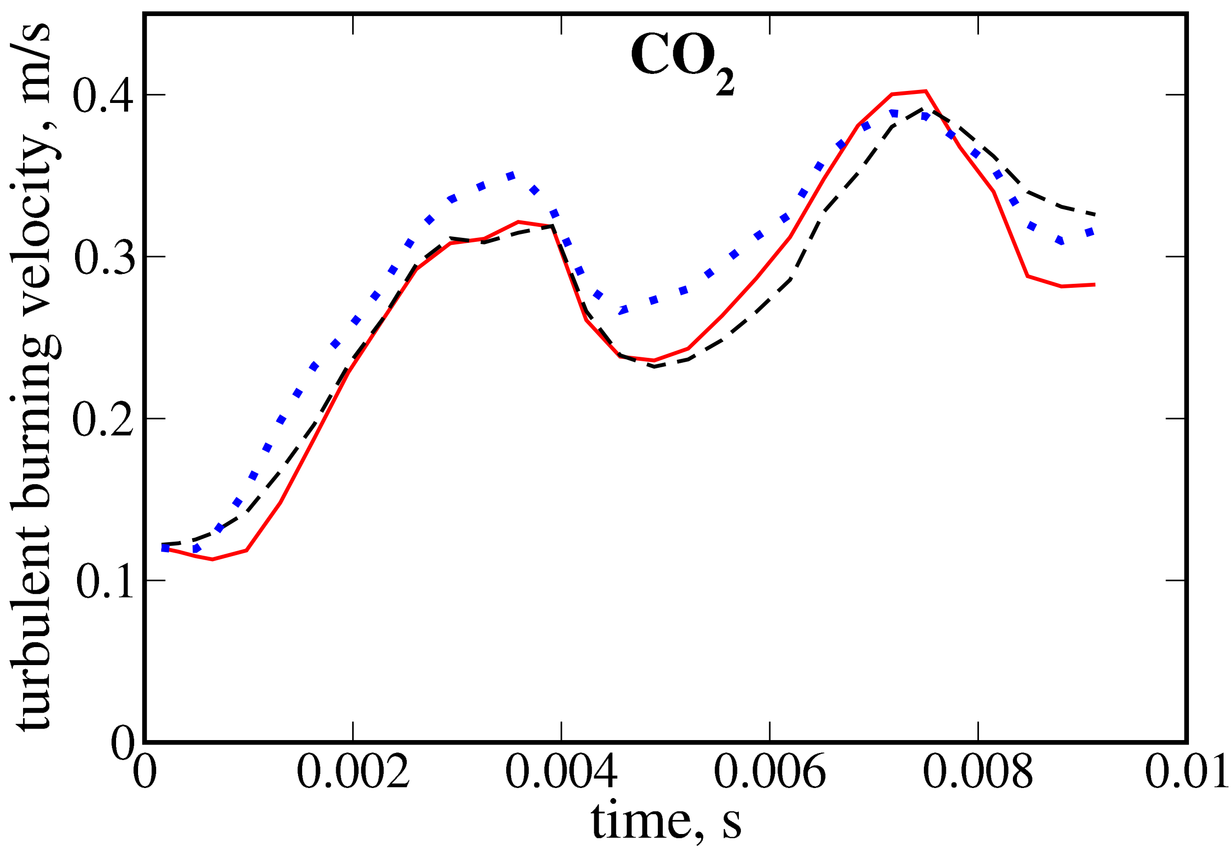
CO2
turbulent burning velocity, m/s
0
0.1
0.2
0.3
0.4
0
0.002
0.004
0.006
0.008
0.01
time, s

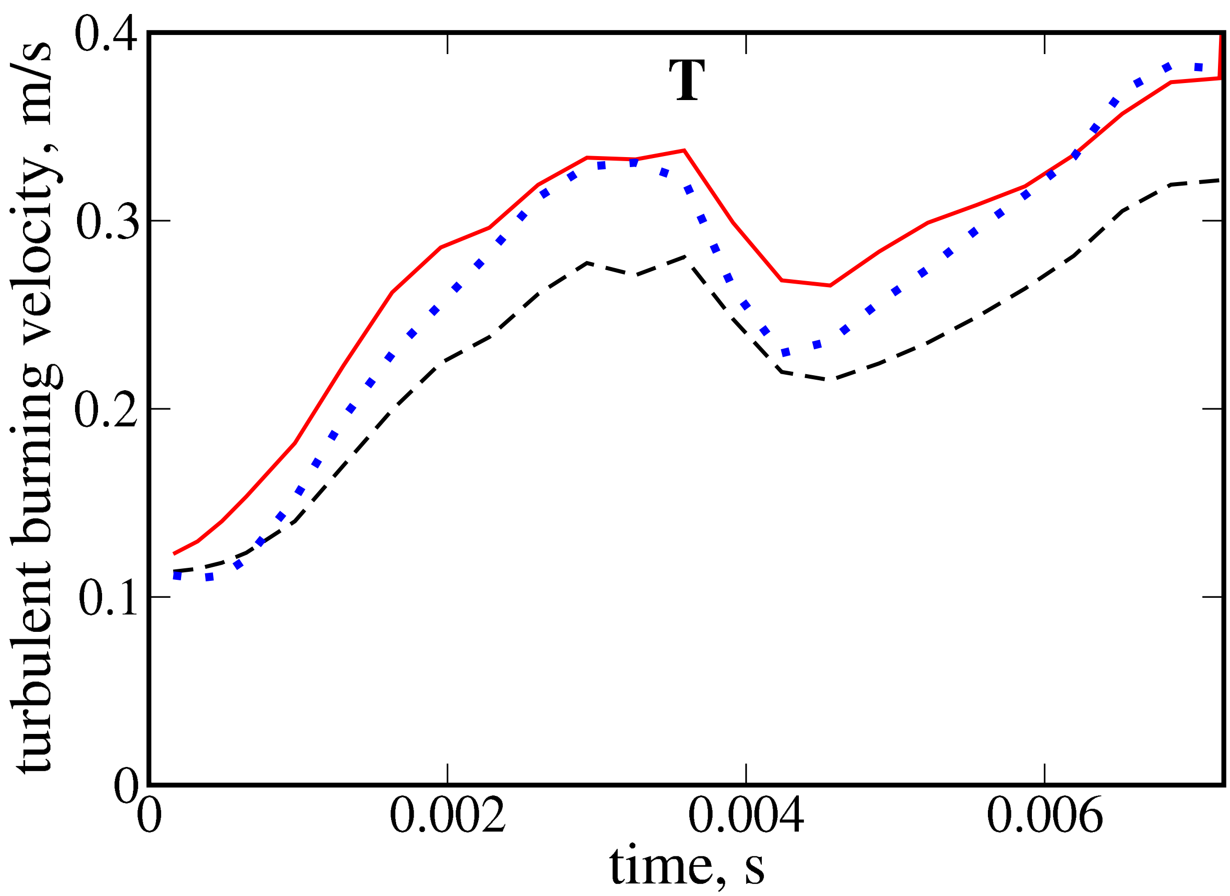
T
turbulent burning velocity, m/s
0.4
0.3
0.2
0.1
0
0
0.002
0.004
0.006
time, s

PLEASE CITE THIS ARTICLE AS DOI: 10.1063/5.0047500

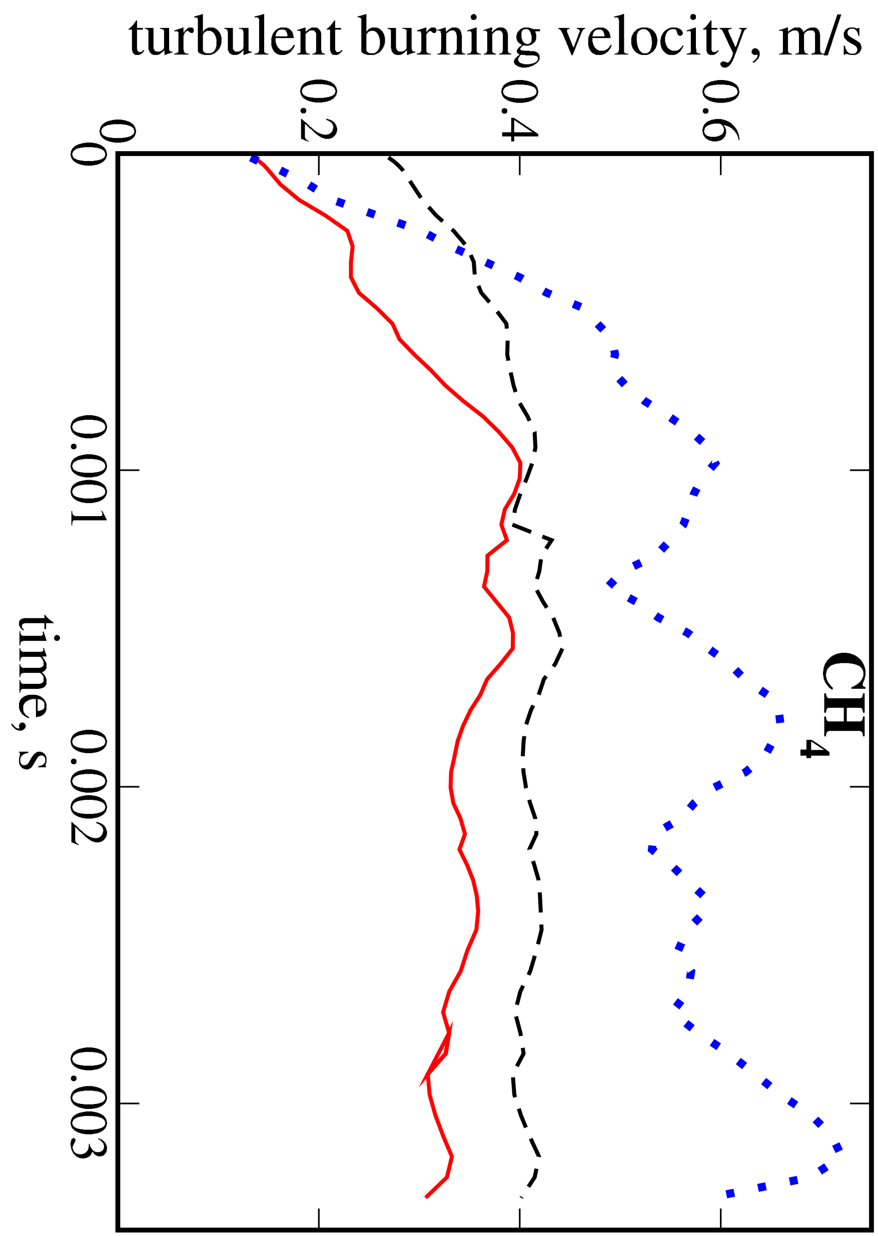

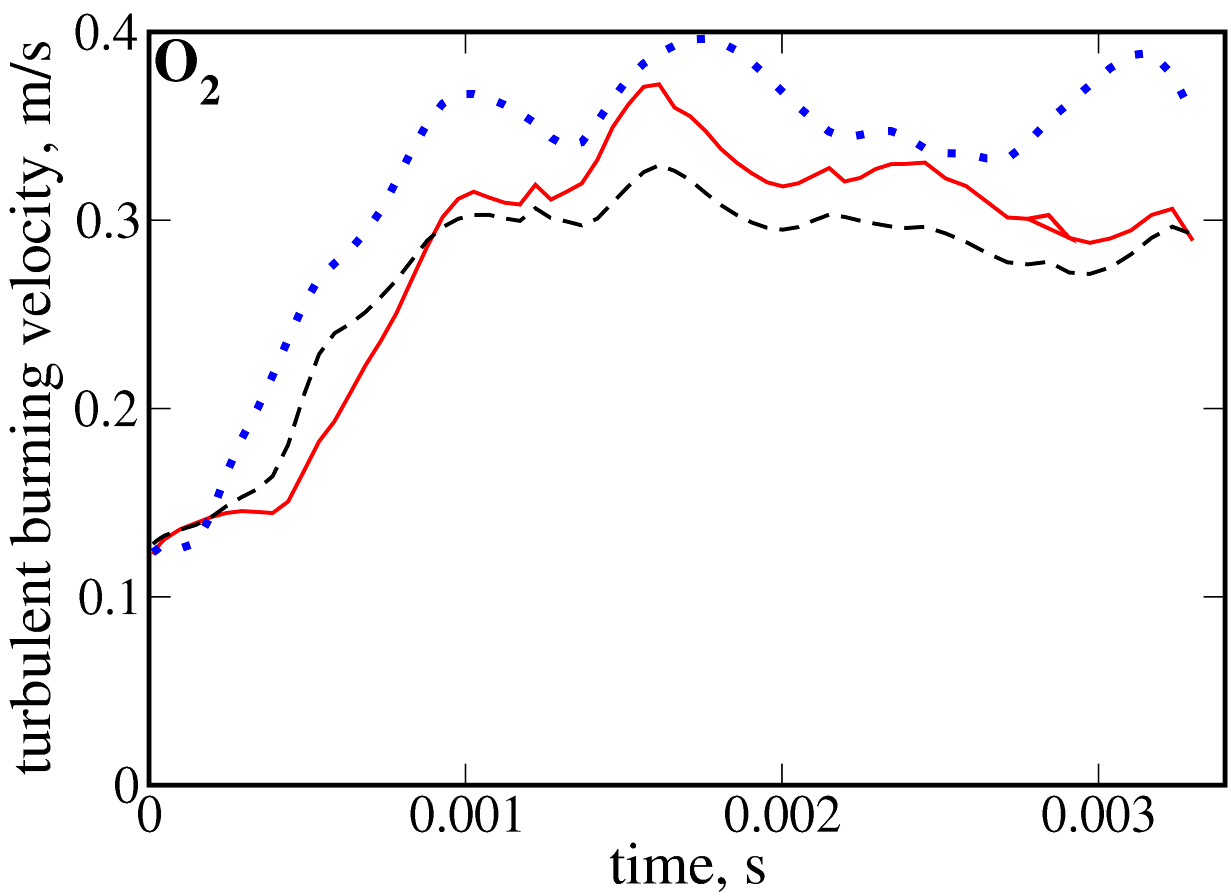
O2
turbulent burning velocity, m/s
0
0.1
0.2
0.3
0.4
0
0.001
0.002
0.003
time, s

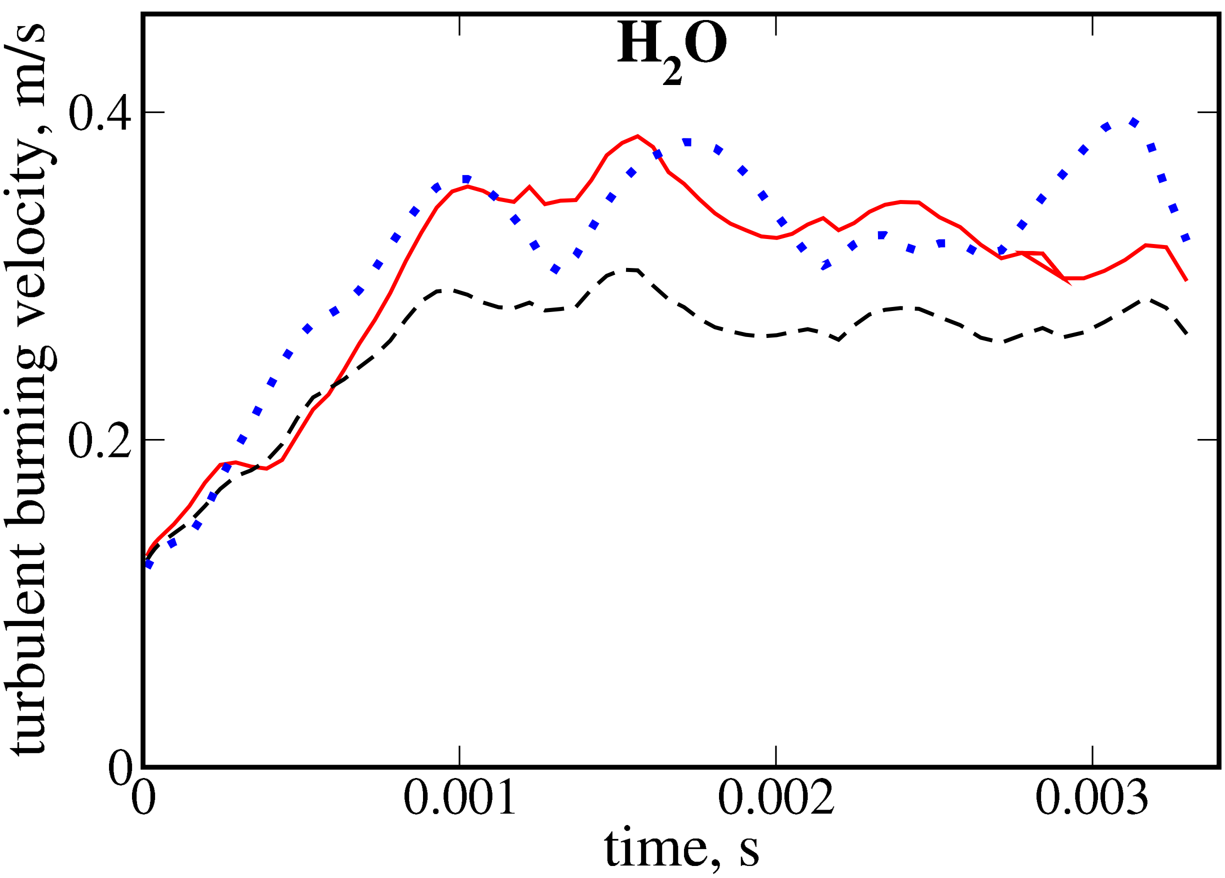
H_2O
turbulent burning velocity, m/s
0
0.2
0.4
0
0.001
0.002
0.003
time, s

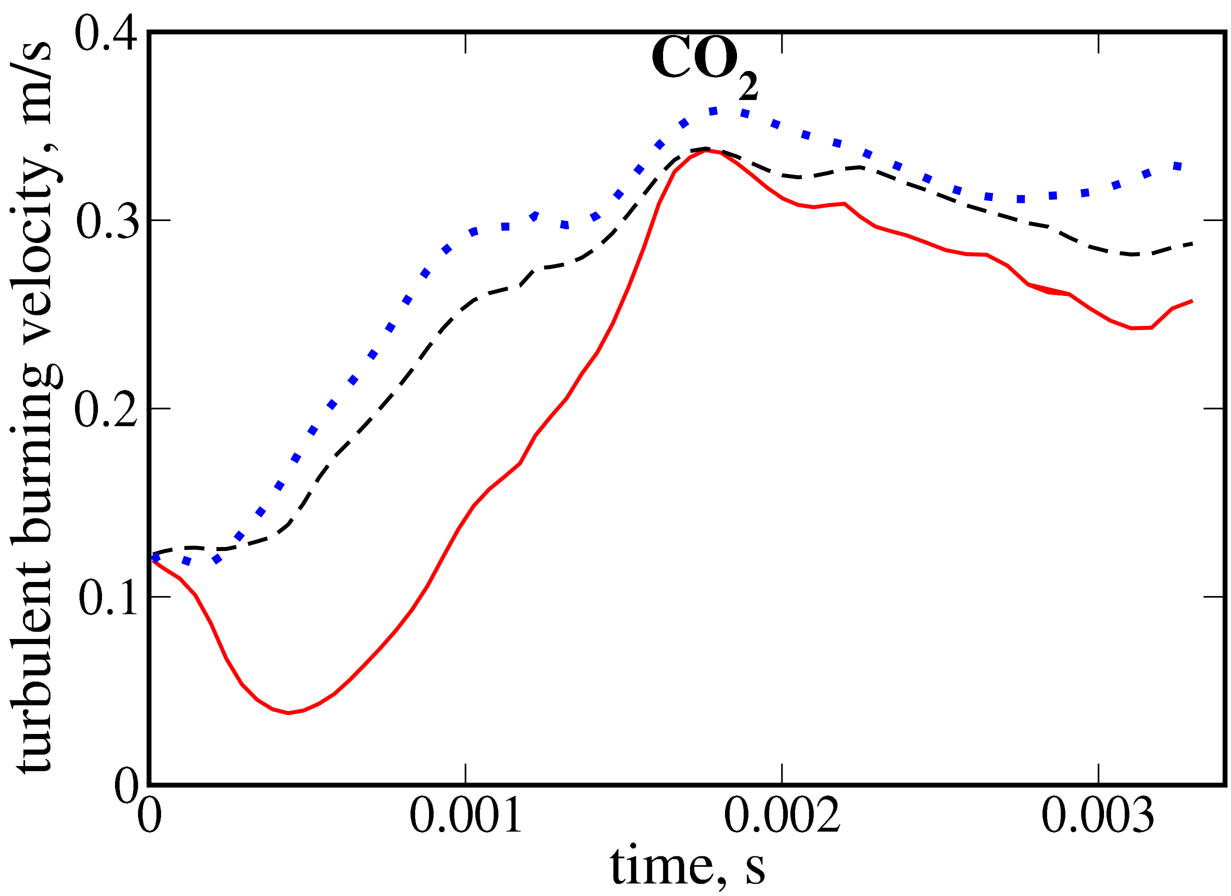
CO_2
turbulent burning velocity, m/s
time, s
0
0.1
0.2
0.3
0.4
0
0.001
0.002
0.003

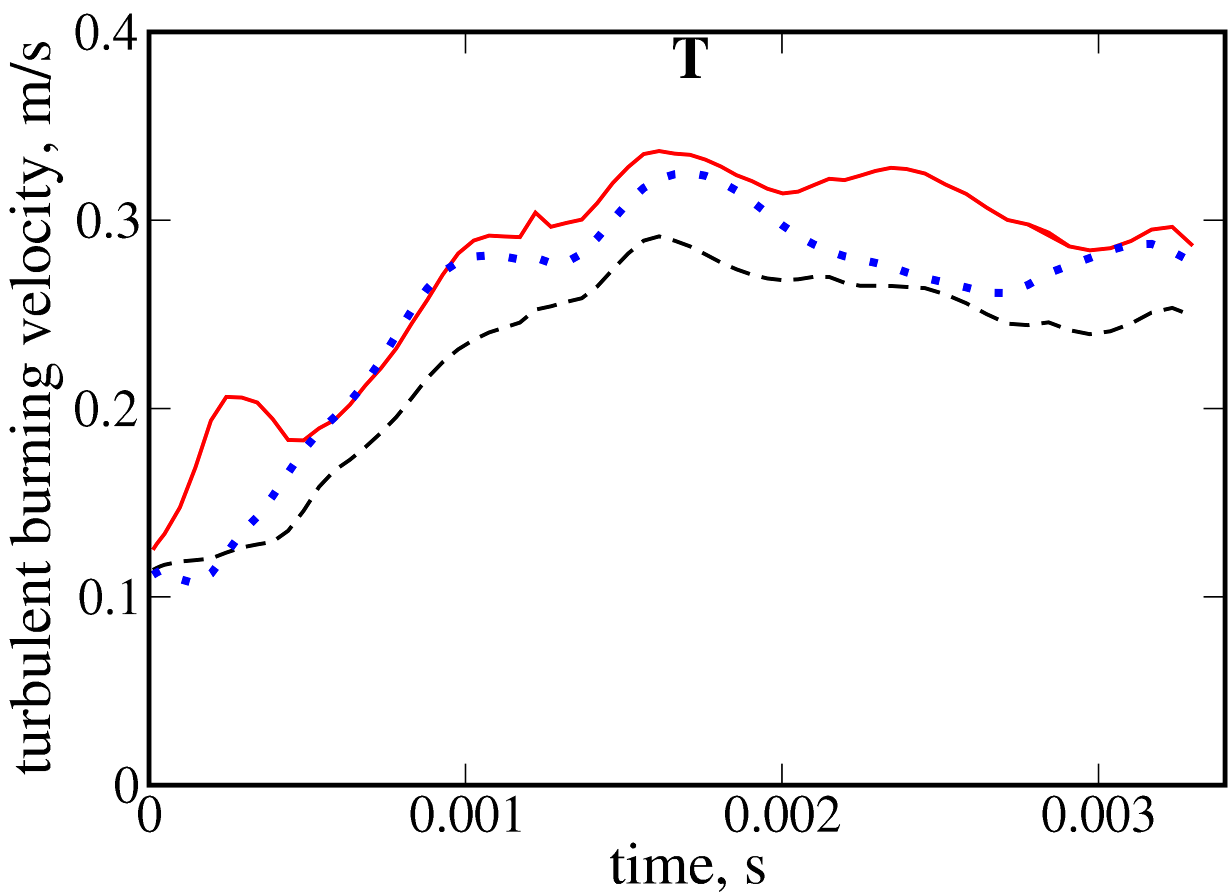
T
turbulent burning velocity, m/s
0.4
0.3
0.2
0.1
0
0
0.001
0.002
0.003
time, s